



<https://theses.gla.ac.uk/>

Theses Digitisation:

<https://www.gla.ac.uk/myglasgow/research/enlighten/theses/digitisation/>

This is a digitised version of the original print thesis.

Copyright and moral rights for this work are retained by the author

A copy can be downloaded for personal non-commercial research or study,
without prior permission or charge

This work cannot be reproduced or quoted extensively from without first
obtaining permission in writing from the author

The content must not be changed in any way or sold commercially in any
format or medium without the formal permission of the author

When referring to this work, full bibliographic details including the author,
title, awarding institution and date of the thesis must be given

Enlighten: Theses

<https://theses.gla.ac.uk/>
research-enlighten@glasgow.ac.uk

**AN AUTOMATED EXPERIMENTAL SYSTEM FOR THE
MEASUREMENT OF MEMBRANE TRANSPORT PARAMETERS
USING PULSED AND OSCILLATORY SOURCES.**

Thesis submitted to the University of Glasgow

for the degree of Ph.D.

by

Samuel M^cFadzean

FACULTY OF SCIENCE
CHEMISTRY DEPARTMENT

October 1998

© S. M^cFadzean 1998

ProQuest Number: 10992310

All rights reserved

INFORMATION TO ALL USERS

The quality of this reproduction is dependent upon the quality of the copy submitted.

In the unlikely event that the author did not send a complete manuscript and there are missing pages, these will be noted. Also, if material had to be removed, a note will indicate the deletion.



ProQuest 10992310

Published by ProQuest LLC (2018). Copyright of the Dissertation is held by the Author.

All rights reserved.

This work is protected against unauthorized copying under Title 17, United States Code
Microform Edition © ProQuest LLC.

ProQuest LLC.
789 East Eisenhower Parkway
P.O. Box 1346
Ann Arbor, MI 48106 – 1346

GLASGOW
UNIVERSITY
LIBRARY

11449 (copy 1)

I dedicate this thesis to my Mother and Father.

Everything I am, I owe to them.

Abstract

The development and use of membrane science and its related membrane processes have increased dramatically over the last twenty years or so. Although there has been a long history in the development of this field there remains a great deal more research and development to be done. One particular problem is in the testing and evaluation of new or modified membranes. Methods and methodologies for testing exist but they require the use of highly specific equipment and very highly skilled and knowledgeable operators in order to obtain data of any quality.

Investigation of the fundamental transport properties has been conducted using concentration (or pressure) steps and oscillations in the source (feed side) and to monitor the resultant response of the test membrane in the collecting volume (down stream). By using such methods it suggested that after initial investigation, multiple determinations of the transport properties could be made within a single experiment.

The construction and development of the hardware elements (measurement cells etc.) alone was insufficient to provide a routine method of testing. The methods used for the data analysis also required to be routine but still rigorous in their treatment of the experimental data. It was the combination of these two component parts that made the system both powerful and flexible.

One of the objectives of this current work was to produce a measurement system which would be simple and flexible to operate and

also allow semi-skilled personnel to obtain accurate and precise membrane transport data on a routine basis.

A completely automated computer controlled system was designed and built in conjunction with membrane simulation software to optimise the measurement cell designs. The control hardware system was developed around a commercial modular interface system, Biodata MICROLINK™. Using only the commercial device driver supplied, all of the necessary software for the control, display and processing of the experimental information was written specifically for the tasks at hand.

Two systems were developed around the same hardware/software configuration (a) a system for testing gaseous transport in membranes and (b) a system for liquid (solution) based transport.

There is a substantial literature of gaseous transport in membrane systems, particularly using polymeric membranes. It was one of the main objectives of this work to study new porous ceramic membranes and to attempt to determine the transport properties of the thin active layers explicitly, both for gaseous and liquid based transport.

The performance of the systems have been thoroughly tested to ensure that the generated step and oscillatory concentration waveforms are as close to ideal as practically possible.

The performance of the systems have also been tested using model membrane systems to ensure the accuracy and precision of the transport data obtained for known systems prior to testing new ceramic membranes.

This has been possible, as ceramic membranes are produced in a step by step fashion and by measurement at each stage in the preparation and at the final (composite) membrane stage, the effect due only to the active layer can be determined by the data analysis methods used.

Using these measurement systems it has been possible for the first time to determine the transport properties of the active layer of a ceramic membrane both accurately and routinely.

The systems are of course suitable for the testing of more conventional membrane types such as polymeric and charged membrane systems and examples of these are also given to show the general scope and application of the system.

In conclusion, measurement systems have been produced that allow for the totally automated and repeated determination of the fundamental transport properties of membranes on a routine basis without the need for highly skilled personnel.

Acknowledgements

I would like to thank the Faculty of Science and the Department of Chemistry for affording me the opportunity to carry out this research at the University of Glasgow. I would also like to thank the highly skilled staffs of the various departmental workshops who assisted me during my period of research. In particular I am indebted to Messers A. Hood and B. Robb of the mechanical workshop who between them managed to convert my various drawings and designs into real and effective devices.

As part of a E.U sponsored Jummelage (Twinning) with ENSC Montpellier I am especially grateful to Professors L.Cot, J. Sarrazin, A. Larbot and Dr. J. Etienne for the production and supply of the many and various ceramic membrane samples used throughout this research. Thanks are also due to the numerous members of the Glasgow research group for their stimulating and often humorous debates and discussions. I would like to single out Donald Young for his contribution to the development of software and in particular for his efforts in constructing a Graphic Kernal System (GKS) that allowed for greatly increased software functionality. I must also thank Dr P.P Mardilovich for his expertise in the development of the preparation methods for the anodic alumina membranes used in this work.

I must thank my father for his continuous support and who has met all of the costs associated with the production and submission of this thesis. I thank my wife for her unwavering support and I must

congratulate her on her patience and tolerance at being effectively reduced to a single parent family particularly during the writing of this thesis.

Finally, I would like to express my thanks to Dr Russell Paterson for providing me with a world class research facility in which to work. For the last eighteen years he has been "The Boss", the last portion of which as my Ph.D supervisor. I will be eternally grateful to him for his guidance and much advice over many years, it has been both a pleasure and an honour to work with such a creative and innovative spirit.

Without him I would not be in the position I now find myself and I only hope that he is as proud of this work as I am.

Declaration

The material presented in this thesis is a record of the work carried out by myself at the Chemistry Department, University of Glasgow. The entire contents are original and have never before been presented for a higher degree at any other institution.

Some of the contents of Chapter 7 have been presented previously in a poster form, Determination of Diffusion Coefficients and Permeabilities of Ceramic Membranes Using a Concentration Oscillator Technique, Proceedings of 2nd International Conference on Inorganic Membranes, Montpellier 1991, Trans Tech Publications.

Samuel Mc Fadzean

October 1998

LIST OF SYMBOLS

Alphabetical Symbols

a_A	activity of ion A
A	Surface Area (m^2)
A_o	Surface area covered by single molecule (m^2)
c_i	concentration of substance i ($mol\ cm^{-3}$)
C	Molar concentration ($mol\ dm^{-3}$)
d	gas molecule diameter (m)
D_i	Diffusion coefficient of substance i (cm^2s^{-1})
D_s	Surface diffusion coefficient (m^2s^{-1})
G	Electrolyte conductivity ($\Omega^{-1}\ m^{-1}$)
I	Ionic strength
J_i	Flux density of substance i across unit membrane area
l	experimental membrane thickness (cm)
L_{ij}	Phenomenological coefficients
M	Molecular weight of a substance ($kg\ mol^{-1}$)
n	number of moles
N_A	Avogadro's constant ($6.022 \times 10^{23}\ mol^{-1}$)
p	Pressure (Pa)
P	Gas permeability as described in Chapter 5 ($mol\ s^{-1}\ m^{-2}\ Pa^{-1}$)
P	Solution permeability as described in Chapter 7 ($cm\ s^{-1}$)
P_{ab}	Experimental permeability of a composite membrane
P_b	Experimental permeability of a backing layer
P_a	Calculated permeability of an active layer
Q	Quantity of material (mol)

r	Mean pore radius (m)
R	Gas constant ($8.314 \text{ J mol}^{-1} \text{ K}^{-1}$)
S	Entropy ($\text{J mol}^{-1} \text{ K}^{-1}$)
t	Time (s)
T	Temperature (K)
V	Volume (m^3)
x	Generalised membrane thickness (cm)
X	Generalised driving force

Greek Symbols

α	Distribution coefficient
α_k	Knudsen separation factor (Chapter 5)
γ_{\pm}	Mean ionic activity coefficient
ε	Membrane porosity
Λ	Molar conductivity ($\Omega^{-1} \text{m}^2 \text{mol}^{-1}$)
Λ_0	Molar conductivity at infinite dilution
Φ	Dissipation function
η	Gas viscosity (Pa s)
μ_i	Ionic mobility ($\text{cm s}^{-1} / \text{Vcm}^{-1}$)
μ_p	Pore tortuosity factor
ρ	apparent density (kg m^{-3})
φ_i	Electrical (diffusion) potential of substance i (V)
v	Gas velocity (m s^{-1})

v_A	Electrical stoichiometry coefficient of ion A
λ_{\max}	Wavelength of maximum absorbance (nm)
τ	Timelag value (s)
τ_{ab}	Experimental timelag of a composite membrane (s)
τ_b	Experimental timelag of a backing layer (s)
τ_a	Calculated timelag for an active layer (s)

TABLE OF CONTENTS

Abstract

Acknowledgements

Declaration

List of Symbols

Chapter 1 GENERAL INTRODUCTION

1.1 Historical Summary

1.2 Future Needs

1.3 Aims and Objectives

1.3.1 Methods Employed

1.3.2 Aerosol Spray

1.3.3 Flow Systems

1.3.4 Closed Pumped Loop System

1.4 Advantages of Current System.

1.4.1 Speed of Analysis

1.4.2 Comparison to Other Test Methods

1.5 References

Chapter 2 THEORETICAL CONSIDERATIONS

2.1 Diffusion Controlled Processes

2.2 Non-Equilibrium Thermodynamics

2.3 Numerical Solutions

2.3.1 Phase shift Analysis

2.3.2 Determination of Peak Maxima/Minima

2.3.3 Determination of Permeability and Diffusion Coefficient

2.4 Oscillator Theory and Predictive Models

2.4.1 Bond Graph Modelling of Oscillator System

2.4.2 Timelag Analysis

2.4.3 Permeability Relationships

2.5 References

Chapter 3 CONTROL & DISPLAY SOFTWARE

3.1 Internal Communication

3.2 Device Preconditioning & Data Collection

3.2.1 Timelag Experiment

3.2.2 Oscillator Experiment

3.3 Display Outputs to System Operator

3.3.1 Timelag Experiment Output

3.3.2 Oscillator Experiment Output

3.4 Data Manipulation and Processing

3.4.1 Calculation of Cell Concentration from Absorbance Values

3.4.2 Calculation of Cell Concentration from Conductivity Values

3.4.3 Display of Concentration versus Time

3.4.4 Data Export Facilities

3.5 References

Chapter 4 Experimental Measurement of Gaseous Systems

4.1 General Description

4.2 Cell Design and Tests

4.2.1 Gas Diffusion Cell Assembly

- 4.2.2 Determination of Cell Volume
- 4.2.3 Testing for Collecting Volume Error
- 4.3 Cell Components
 - 4.3.1 Pressure Transducers
 - 4.3.2 Calibration of Transducers
 - 4.3.3 Tubular Connections and Fittings
 - 4.3.4 Solenoid Valves
- 4.4 Generation of a Gas Pressure Step
 - 4.4.1 General Procedure for the Production of a Gas Step.
 - 4.4.2 Pressure Step Calibration Test
- 4.5 References

Chapter 5 Membrane Characterisation by the Gas Permeation System

- 5.1 Background
 - 5.1.1 Poiseuille (Viscous) Flow
 - 5.1.2 Knudsen Flow
 - 5.1.3 Surface Diffusion
 - 5.1.4 Determination of a Suitable Transport Mechanism
 - 5.1.5 Membrane Structural Considerations
- 5.2 Experimental Data Treatment
- 5.3 Experimental
- 5.4 Results and Discussion of the Gas Permeability System
 - 5.4.1 Anodic Alumina Membranes
 - 5.4.2 Ceramic Disc Membranes
 - 5.4.3 Ceramic Tube Nanofiltration Membranes

5.4.4 'Dense' Polymer Films

5.5 Pore Size Estimation

5.6 Conclusions

5.7 References

Chapter 6 Experimental Measurement of Liquid Based Systems

6.1 General Description

6.2 Measurement Cell Design

6.2.1 The Support Frame

6.2.2 The Detector Block

6.2.3 Stirrer Housing Block

6.2.4 Screw Cap Seal

6.2.5 Solution Delivery Head

6.2.6 Measurement of the Cell Volume

6.3 Measurement Equipment

6.3.1 Temperature

6.3.2 Solution (Electrolytic) Conductivity

6.3.3 Optical Density (Absorbance) Measurement

6.4 Measurement System and Instrument Calibration

6.4.1 Calibration of Thermistors

6.4.2 Ultra-Violet/Visible Spectrophotometer

6.4.3 Conductivity Bridge Measurements

6.5 The Generation of a Concentration Step

6.5.1 System Assembly and Layout

6.5.2 Solution Flow to the Test Cell (Switch Logic)

6.5.3 Pumped Solution Flow Rates

6.5.4 Calibration Test for an Imposed Concentration Step

6.6 'Null' Cell Tests

6.7 References

Chapter 7 Membrane Characterisation by the Liquid Permeation System

7.1 Background

7.1.1 NT Analysis of Cell Volume Effects

7.1.2 Experimental Data Treatment

7.2 System Validation

7.2.1 Test of Daynes ($l^2/6D$) Law

7.2.2 Preparation of Membranes

7.2.3 Experimental Procedure

7.3 Results and Discussion of Membranes Investigated

7.3.1 Anodic Alumina Membranes

7.3.2 Ceramic Disc Membranes

7.3.3 Tubular Ceramic Nanofiltration Membranes

7.3.4 Oscillator Experiments

7.3.5 Charged Membranes

7.3.6 Enhanced Transport

7.3.7 Coupled Flows

7.4 Conclusions and Future Research

7.5 References

Annex 1 Preparation of Anodic Alumina Membranes

1.1 Introduction

1.2 Anodisation System

1.3 Preparation of Anodic Alumina Films

1.4 Electrochemical Treatments

1.5 References

TABLE OF FIGURES

Chapter 1

- 1.1 Representation of a Modified Stokes Diaphragm Cell

Chapter 2

- 2.1 Schematic representaiton of flow through a membrane to aid Fick's second law
- 2.2 Simulated Membrane Phase Concentration Profiles for Daynes Classical System.
- 2.3 Simulation of the Accumulated Concentration Profile in the Collecting Volume after an Imposed Step.
- 2.4 Simulated Membrane Phase Concentration Profile for an Applied Steady State Condition.
- 2.5 Simulated Accumulation in the Collection Volume with Initial Steady State Conditions
- 2.6 Simulated Membrane Phase Concentration Profiles After a Switch Down from a Steady State Condition.
- 2.7 Simulated Accumulation in the Collecting Volume after a Concentration Switch Down from a (Pseudo) Steady State Condition.
- 2.8 Simulated Accumulation in the Collecting Volume after a Concentration Switch Down to a Lower Concentration Value.
- 2.9 Combined Outputs from the Simulated Concentration Profiles in the Collecting Volume. The Linear Intercepts are Shown in Dotted Lines and Coincide at Time τ .
- 2.10 Simulated Concentration Profile in the Collecting Volume for an

Asymmetric Oscillator.

Chapter 3

- 3.1 Schematic Diagram of the Software Command and Control Structure.
- 3.2(a) Screen Capture of the Timelag Program Parameter Input Section.
- 3.2(b) Screen Capture of the Timelag Program Cell Heating Period Showing the Current Cell Temperature.
- 3.3(a) Screen Capture of the Timelag Program at the Run Initiation.
- 3.3(b) Screen Capture of the Timelag Program a Short Time into the Baseline Data Collection Period.
- 3.4(a) Screen Capture of the Timelag Program Shortly after the Concentration Step has been Imposed.
- 3.4(b) Screen Capture of the Timelag Program the Screen has been Toggled to Display the Cell Temperature.
- 3.5 Beer's Law Plot of Absorbance versus Concentration for the Calibration of DL-Phenylalanine.
- 3.6 Specific Conductivity for Potassium Chloride solutions of known Concentrations at 298 K.
- 3.7(a) Screen Capture of Raw Data Display from Timelag Processing Program.
- 3.7(b) Screen Capture of Plotting Options from Timelag Processing Program.
- 3.8(a) Screen Capture of Y-Axis Display Options from Timelag Processing Program.
- 3.8(b) Screen Capture of Input Section of Conversion to Concentration

Routine from the Timelag Processing Program.

3.9 Screen Capture of the Baseline Selection During the Process Option (P).

3.9 Screen Capture after the Slope Selection (Option P) and the Display of the Calculated Timelag.

Chapter 4

4.1 A Schematic Diagram of the Gas Testing System

4.2 Comparison Tests For Nitrogen Flow through a Polycarbonate Track-Etched membrane(0.015 μm) with Two Different Cell Volumes.

4.3 Comparison Tests for Nitrogen Flow through a Polycarbonate Track-Etched membrane (0.015 μm) with Two Different Cell Volumes and after Applying a Volume Correction.

4.4 Plot of the Collecting Volume Pressure Transducer Voltage Output versus the Displayed Pressure.

4.5 Measured Response of the Gas System to an Imposed Pressure Step.

4.6 Close-up view around the time of the applied pressure step.

Chapter 5

5.1 Schematic Representation of Possible Different Pore Geometries Present in Membranes.

5.2 Schematic drawing showing possible membrane gas transport mechanisms: (a) Poiseuille, (b) Knudsen (c) Surface diffusion.

5.3 Gas Permeation Tests of a Homogeneous Anodic Alumina Membrane (SAA1) with different gases.

- 5.4 Knudsen plot for the membrane (SAA1)
- 5.5 Gas Permeation Tests of a Homogeneous Anodic Alumina Membrane (SAA2) with different gases.
- 5.6 Knudsen plot for the membrane (SAA2)
- 5.7 Gas Permeation Tests of a Homogeneous Anodic Alumina Membrane (SAA3) with different gases.
- 5.8 Knudsen plot for the membrane (SAA3)
- 5.9 Gas Permeation Tests of an Asymmetric Anodic Alumina Membrane (LAA1) with different gases.
- 5.10 Knudsen plot for Bilayer membrane (LAA1)
- 5.11 Gas Permeation Tests of an Asymmetric Anodic Alumina Membrane (LAA2) with different gases.
- 5.12 Knudsen plot for Bilayer membrane (LAA2)
- 5.13 Hydrogen gas permeation through an Anodic Alumina membrane, 60 μm thick and with a nominal pore size of 0.2 μm .
- 5.14 Comparison in relative hydrogen flow between an Anodic Alumina membrane, 60 μm thick and with a coated layer of AlN (0.5 μm).
- 5.15 Hydrogen permeation through AlN coated Anodic Alumina membrane. The estimated τ value was 1125 s.
- 5.16 Gas Permeation Tests of a Homogeneous ceramic 'support' disc (ZrSup) with different gases.
- 5.17 Gas permeation tests of an asymmetric ceramic membrane (ZrAL1) with different gases.
- 5.18 Knudsen plot for support disc (ZrSup)

- 5.19 Knudsen plot for ceramic membrane (ZrAl₂)
- 5.20 Comparison between a support tube and the 5nm membrane, response to a +1bar nitrogen pressure step.
- 5.21 Gas Permeation Tests of a tubular ceramic membrane (TLa1) with different gases. Imposed step was +1 bar.
- 5.22 Gas Permeation Tests of a tubular ceramic membrane (TLa1) with different gases. Imposed step was +2 bar.
- 5.23 Gas Permeation Tests of a tubular ceramic membrane (TLa1) with different gases. Imposed step was +3 bar.
- 5.24 Knudsen plot for a 5nm tube membrane (TLa1) with +3 bar pressure step.
- 5.25 Relative gas flows for a Bayer Macrofoil KG Polycarbonate film (10µm thick) with +5 bar applied pressure steps.
- 5.26 Pore size estimation test plot using a Millipore VSWP 0.025µm membrane filter.

Chapter 6

- 6.1 A Schematic of the Pumped Liquid Flow System Showing the Major System Components.
- 6.2 Engineering Drawing for the Support Frame.
- 6.3 Engineering Drawing for the Detector Block.
- 6.4 Engineering Drawing for the Stirrer Housing.
- 6.5 Engineering Drawing for the Liquid System Test Cell Solution Delivery Head.
- 6.6 Drawings of the Assembled Liquid System.
- 6.7 Calibration Profile for the n.t.c Thermistor Bead Encapsulated in

- the Screw Cap Assembly of the Membrane Test Cell.
- 6.8 Wavelength Accuracy Calibration Test Using a Didymium Coated Optical Glass Slide.
 - 6.9 Diffraction Grating Calibration Test Using a Narrow Band Filter.
 - 6.10 A schematic representation of the Liquid Flow System Layout and Valve Configuration.
 - 6.11 Flow Control Logic for Membrane Test Cell. Example shows a Full Oscillator Cycle.
 - 6.12 Measured Response of the Liquid System to a Series of Imposed Concentration Steps using Brilliant Blue FCF Dye with the Optical Detection System.
 - 6.13 Three Concentration Step Cycles Superimposed.
 - 6.14 A Null Test Experiment in which 0.0001M KCl is used as both the low and the high Concentration Solution.
 - 6.15 Comparison of the Null test to an Experiment in which 0.01M KCl was used as the High Concentration Solution.

Chapter 7

- 7.1 Simulated Data (Q versus t) for Various Collecting Volume Values
- 7.2 Simulated Data (Conc. versus t) for Various Collecting Volume Values
- 7.3 Timelag Experiment with Visking Dialysis Membrane of Thickness 0.0149cm. The Resultant τ value was 11.28 seconds.
- 7.4 Timelag Experiment with Visking Dialysis Membrane of Thickness 0.0303cm. The Resultant τ value was 46.5 seconds.
- 7.5 Timelag Experiment with Visking Dialysis Membrane of Thickness

0.0453cm. The Resultant τ value was 102.5 seconds.

- 7.6 Timelag Experiment with a Symmetrical Anodic Alumina Support (48 μm thick).
- 7.7 Timelag Experiment with an Symmetrical Anodic Alumina Membrane (80 μm thick).
- 7.8 Timelag Experiment with an Asymmetrical Anodic Alumina Membrane (48 μm base with 9 μm Active Layer).
- 7.9 Timelag Experiment with an Asymmetrical Anodic Alumina Membrane (48 μm base with 22 μm Active Layer).
- 7.10 Time lag Experiment with Ceramic (Alumina) Support Disc of 0.0611cm Thickness.
- 7.11 Time lag Experiment with Ceramic (Alumina) Support Disc of 0.0936cm Thickness.
- 7.12 Time lag Experiment with Ceramic (Alumina) Support Disc of 0.199cm Thickness.
- 7.13 Time lag Experiment with Ceramic Membrane. The (Alumina) Support was 0.0648cm Thick and the Active Layer (Zirconia) was 4.2 μm thick.
- 7.14 Timelag Experiment with a Tubular Support of 0.168cm thickness.
- 7.15 Timelag Experiment with a Tubular Membrane. Support thickness was 0.1778cm and the Active Layer(γ -alumina) 2 μm .
- 7.16 Portion of the emergent wave from a stepped oscillator experiment with a Whatman AnoporeTM 0.02 μm pore size bilayer membrane.

- 7.17 Portion of the emergent wave from a stepped oscillator experiment with the anodic alumina bilayer membrane (LAA2).
- 7.18 Experimental Emergent Wave from an Oscillator Experiment with a Ceramic Bilayer Membrane.
- 7.19 Schematic of the Development of a Donnan Potential within a pore at an ion-exchanger/water interface.
- 7.20 A timelag experiment for a NAFION membrane in the Potassium form of thickness 0.0189cm.
- 7.21 Steady State profiles for a NAFION membrane in the Potassium form.
- 7.22 Steady State profiles for a NAFION membrane in the hydrogen form.
- 7.23 Steady State profiles for a NAFION membrane in the calcium form.
- 7.24 Timelag plots for 0.05M and 0.01M Phenylalanine solutions through a NAFION ion exchange membrane in the hydrogen form.
- 7.25 Timelag plots for 0.05M and 0.01M Phenylalanine solutions through a NAFION ion exchange membrane in the sodium form.
- 7.26 Comparison between a NAFION membrane in the hydrogen and sodium forms with Phenylalanine (0.05M)
- 7.27 The U.V/Visible Spectra for Phenylalanine and Sodium Citrate Solutions
- 7.28 Permeation Data for a Phenylalanine Solution through a NAFION membrane in the Hydrogen form.
- 7.29 Permeation Data for a tri-Sodium Citrate Solution through a

NAFION membrane in the Hydrogen form.

7.30 Permeation Data for a Phenylalanine /tri-Sodium Citrate mixture through a NAFION membrane in the Hydrogen form.

Annex 1

A1.1 Schematic Representation of the Anodisation System

A1.2 Schematic Representation of the Anodisation Cell

A1.3 Representation of an Anodic Alumina Film

A1.4 Flow-chart for the Preparation of Anodic Alumina Films

Chapter 1 General Introduction

- 1.1 Historical Summary
- 1.2 Future Needs
- 1.3 Aims and Objectives
- 1.4 System Advantages
- 1.5 References

1 General Introduction

1.1 Historical Summary

The first credited membrane experiments were by Frenchman Abbe Nolte (1748) who accidentally discovered the semi-impermeability of a membrane (water from ethanol)[1]. All of the early studies were involved with the phenomena due to membranes, it was not until later that the real science with membrane system began.

Thomas Graham (Glasgow) was probably the first true membrane scientist, his revolutionary work, mainly with gaseous diffusion through animal membranes lead to his discovery of the effect due to molecular weight on gas transfer rates(1829 and 1833)[2,3]. It was much later (1909) that Martin Knudsen really proved the geometrical considerations regarding Graham's earlier work on gases[4]. Graham is also credited with the first discussion of a solution-diffusion mechanism (1866)[5].

In all of these pioneering early studies only two basic membrane types existed, (a) animal membranes which were microporous and hydrophilic and (b) rubbery membranes(gum) which were homogenous and hydrophobic. In 1855 August Fick produced his paper "On Liquid Diffusion" [6] this probably for the first time established the physical/chemical nature of membrane science and showed (using Graham's original data) that liquid (and gas) diffusion was analogous to the diffusion of heat or electricity. In his paper Fick also mentioned the use of collodion (cellulose nitrate) membranes for

the first time. These were the first synthetic membranes produced that could compete with the natural membranes used previously such as pig bladder and parchment paper and they are still widely available today (membrane filters).

Parallel to the phenomena due to membranes there has also been a related development of possible membrane processes. The first commercial membranes were produced in Germany by Sartorius (1920) using the methods of Zsigmondy[7] for small scale laboratory filtration. Although dialysis had been known of since Graham's time it was not until the 1940's that Kolff [8] showed the application to hemodialysis and this really began the first widespread use of membrane technology. At about the same time highly secretive, and still classified, work was being conducted in the United States (Manhattan Project). This led to the development of 'inorganic' membranes for the gas separation of uranium isotopes and of course the birth of nuclear technology.

It was not until 1962 when Loeb and Sourirajan developed the first asymmetric membranes[9] that the full industrial scale use of membranes could be considered. This is due to the permeation rate being inversely proportional to the barrier layer thickness, hence thin top layers on 'support' structures have a much higher permeation rate than homogeneous (symmetrical) membranes of the same thickness. It was not until 1981 however that industrial scale gas separation became economically feasible, due to the work of Henis and

Tropodi[10]. At about this same time there was a large French effort in the development of improved inorganic (ceramic) membranes (using earlier information from their own nuclear industry) for more general use, although these membranes continue to be used in the nuclear industry for gas separation purposes. The technology developed by the French groups lead to the commercial release of microfiltration and ultrafiltration membranes (SCT and LeCarbone Lorraine). The work in particular of the group of L. Cot [11] has progressively refined these membranes to the position where nanofiltration membranes (pore sizes < 1nm) have been successfully and reliably produced[12].

1.2 Future Needs

Membrane research is currently a massive area. The technology is energy efficient, can be highly selective and is capable of being run in conjunction with existing industrial processes (hybrid systems). Ever smaller pore size membranes are being produced such as zeolitic membranes. This is perhaps a secondary consideration with the main thrust being the development of new technologies based around membranes such as membrane reactors (reaction and separation in a single module), fuel cells and battery technologies.

The rapid increase in the use of membrane processes appears to be continuing unabated. One estimate of the potential world market for inorganic (ceramic) membranes alone is over five hundred million US dollars per year by the year 2000[13] the large majority of this being in the food and beverage industry.

Although conventional (polymeric) membranes will continue to be used, ceramics have the potential to outperform and outlast these (polymeric) and purely on commercial reasoning will result in their less frequent use.

Much work however still needs to be done in the associated technology. One example is in the use of ceramic membranes for high temperature gas separations (>500°C). The membranes themselves have few problems functioning at such temperatures but producing suitable modules and seals that can make the systems economically attractive and with sufficient lifetime and throughput remain to be resolved.

1.3 Aims and Objectives

The primary aim of this work was to characterise the transport properties of new membranes using improved methods. In particular to investigate further [14] possible use of pulsed and oscillatory sources and using the response of the test membrane to deduce the fundamental transport (and solubility) parameters. The investigation by the use of concentration (or pressure) waves suggested that it could be possible to make multiple determinations of the membrane parameters within a single experiment.

The emphasis of this current study was to examine the porous type of membranes (microfiltration / ultrafiltration / nanofiltration) with respect to gas and liquid permeation, therefore, the rubbery/glassy classification of polymer membrane will be effectively ignored in this

work. The range in the type of membrane to be studied was wide ranging, from anodic alumina membranes to ceramic membranes of different pore sizes and geometries of the sol-gel type and also tube format membranes of nanofiltration pore size.

The equipment needed to perform these investigative experiments would require to be completely computer controlled as any appreciation of such methods requires this automated (and precise) control to accurately define the boundary conditions and the waveforms generated. Meanwhile the concentration changes downstream of the membrane would be detected by the chosen sensors to be collected and displayed to the end user. The collected data analysis also required to be performed by the computer.

The hardware and software required for all these tasks had to be developed. As a consequence this thesis is primarily concerned with the design, development and operation of this new equipment for application to both gas and liquid diffusion processes. Wherever possible application in relation to new membranes, particularly ceramic membranes, prepared in Glasgow and other leading innovative research laboratories in the European Union, Japan and Brazil will be given.

1.3.1 Methods Employed

Concentration (and pressure) steps have been generated at one exposed face of a test membrane. Using this method the downstream membrane response can be followed and the

transport parameters determined. The actual methods used to produce these sudden changes have evolved over several years and these will be briefly discussed here.

1.3.2 Aerosol Spray

Two (or three) artist air brushes were used originally to produce a concentration step[14]. Solution reservoirs were sprayed at one exposed face of a test membrane. This was very efficient in terms of the actual concentration switchover times but had several other problems. The first was temperature variation. Maintaining a near constant spray temperature (at the membrane surface) was extremely difficult. Additionally, due to the expansion effect a large temperature drop of the solution occurred. Typically, to maintain approximately 25°C at the membrane surface, the solution reservoirs required to be heated to approximately 45°C. There were also problems with mist the sprays produced and the entire system required to be enclosed. Finally, very large quantities of solution were required and these were discharged to the public drains. The combination of these problems severely restricted the use of the system and the choice of permeant material for investigation although it did prove the effectiveness of the method.

1.3.3 Flow Systems

This major design change replaced the sprays with gravity fed

solution reservoirs. These were delivered to the membrane surface through tubing connected to syringe (luer) fitted ends at either edge of the exposed test membrane and was removed by sucking off the solution on the opposite edge of the exposed face using a water vacuum pump to apply the slight negative pressure. This again suffered from the problem of discharge to the mains and the need for a mains water supply.

1.3.4 Closed Pumped Loop System

This is the current (liquid) system to be described later in some detail (Chapter 6). In essence a closed solution loop is pumped across the exposed membrane surface and this is switched to produce the concentration step. In conjunction with completely new cell designs and improved detection methods available, vast improvements in the system sensitivity and applications have been made. In particular, the use of the pumped loop allows for the choice of permeant material to be almost limitless, provided it can be in a liquid form. Finally, for the first time using almost identical hardware, gaseous diffusion systems can also be investigated, this single advancement massively improves the flexibility and application of the system, this is discussed in Chapter 4.

1.4 System advantages

It will not (and cannot) be claimed that this current system is the best possible for the determination of all membrane transport (and

solubility) properties. What will be shown is that compared to the conventional testing systems that this newly developed system has a great many advantages and benefits which together make these measurements both precise and routine.

1.4.1 Speed of Analysis

The basic 'speed' of any analysis will be physically dependant upon the test membrane thickness, permeability and the test area. This current system employs a small effective test area as the methods of production used today have reached such high degrees of reproducibility that a representative test area is not difficult to obtain. Whether a single or multiple tests are to be made, the system design allows a rapid turnover between experiments. It is therefore possible that the testing of a series of membrane sections can be quickly and easily achieved. The raw experimental data is saved directly on computer and is available for immediate processing, no intermediate data input is needed. The system is dynamic with measurements in real time and hence rogue or erroneous experiments can be quickly identified and terminated, reducing lost time.

1.4.2 Comparison with Other Test Methods

The characterisation of membranes can be split into two main areas (a) their physical characterisation and (b) their transport and solubility properties. Several methods exist for the physical characterisation of membrane structures such as

SEM/TEM/AFM for visual inspection of morphology, bubble point measurements, mercury intrusion analysis, gas and liquid displacement methods and a great many variants of these, for pore size and pore size distribution analysis. Care is needed with these (liquid) displacement methods due to possible errors caused by swelling and other possible effects. In this current work, only with the gaseous system will any physical characterisation be attempted i.e. pore size estimation from gas flow rates (Section 5.5). The characterisation of the transport properties of a membrane (porous or non-porous) is much more difficult and few methods exist.

1.4.2.1 Stokes Diaphragm Cell

The use of a diaphragm type cell for the measurement of liquid transport parameters originated in 1929 when introduced by Northrop and Anson[15] and was much improved upon by Stokes[16] as shown in Figure 1.1. These cells were used for the measurement of free solution diffusion parameters but by modification of such cell types the glass diaphragm can be replaced by a membrane holder and clamped to hold the test cell together.

This is a relative method and requires a cell calibration to be performed with a suitable test permeant for example potassium chloride. Once calibrated the diffusion

coefficients of test systems can be obtained. There are some disadvantages to such systems. Single experiments can take between 1-3 days and require sampling for analysis (at known times), temperature must be maintained over the period of the experiments.

With the greatest of care, this type of cell can generate data with an accuracy of better than 0.5% in the calculated concentration averaged diffusion coefficient (\bar{D}). This type of cell however, is only suitable for passive diffusion (Fickian) systems.

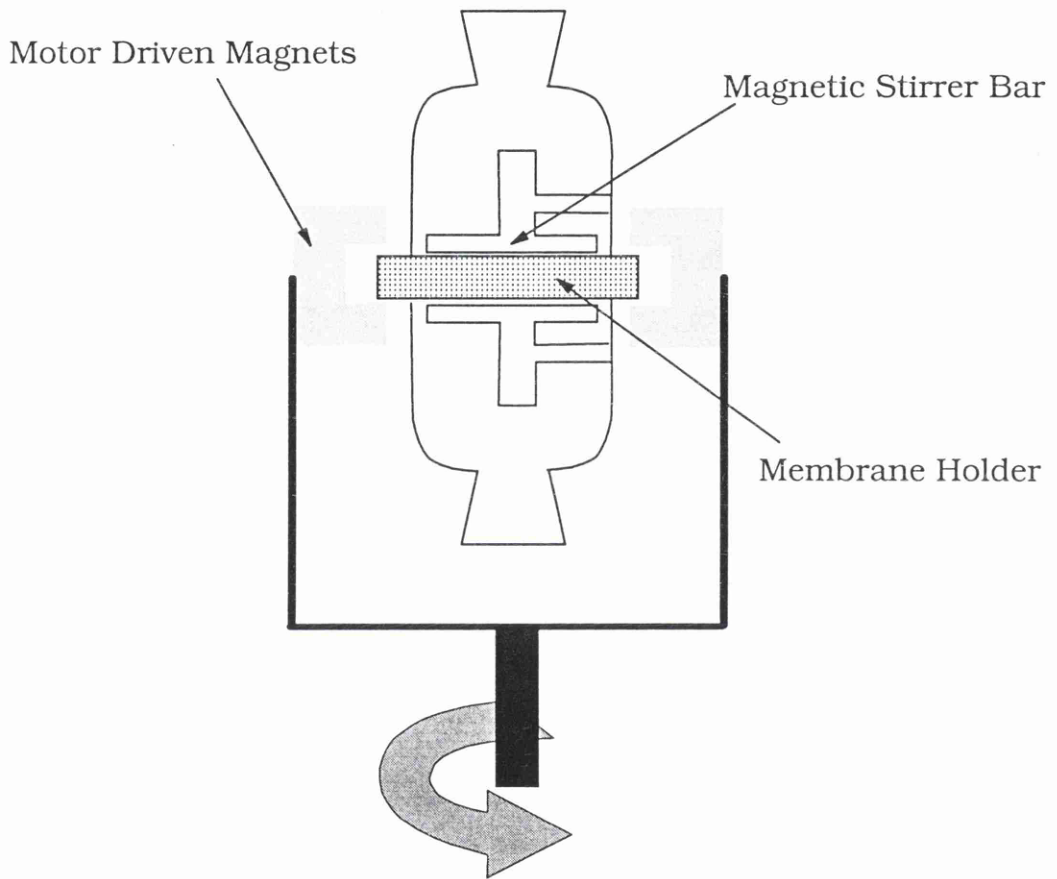


Figure 1.1 Representation of a Modified Stokes Diaphragm Cell

1.4.2.2 Dead End Filtration

The transport rate of pure water through a membrane is used routinely to establish both pore size and effective transport rates. This is usually performed in the 'dead-end' filtration mode and allows for the water flow versus applied pressure to be observed. Although this is an extremely simple method it is impractical as a general method for other liquid permeants. This is due to concentration polarisation and ultimately to the formation of fouling (cake) layers at the membrane surface. Even with systems modified to reduce these effects, great care is needed to minimise concentration polarisation. This normally means working with very dilute solutions which have their own associated problems such as flux variation due to changes in the ionic strength and sensitivity to pH changes or by working at very low applied pressures. These are conditions which are not normally encountered in practical applications.

1.4.2.3 Permeation Methods

This is the method most commonly used for transport studies, especially with gaseous systems. It basically involves the application of a driving force and monitoring the response of the system to the applied force. The method is also applicable to liquid systems but is much less

commonly used.

These steady state methods make for accurate and precise measurements. The main problems tend to be technical based, such as large and unwieldy testing systems, poor monitoring methods (for example bubble flow meters) and lengthy and complicated analysis of data.

This is the method chosen for this current study. It will be shown that with the developments in the test cell designs combined with the improved and simplified data analysis and treatments, that the test systems described in this current work now allow the routine and repeated determination of membrane transport properties and also for the first time the contribution of the active layers.

1.5 References

- [1] Nollet, J.A., Recherches sur les causes du Bouillonnement des Liquides, Histoire de l'Académie Royal des Sciences, Année MDCCXLVIII, Paris 1752, 57-104
- [2] Graham, T., Notice of the Singular Inflation of a Bladder, Quarterly Journal of Science, No II (1829) 88-89
- [3] Graham, T., On the Law of Diffusion of Gases, The London and Edinburgh Magazine and Journal of Science, Vol.II (1833) 175-190
- [4] Knudsen, M., The Laws of Molecular Flow and of Inner Friction Flow of Gases Through Tubes, Annalen der Physik, 28 (1909) 75-130
- [5] Graham, T., On the Absorption and Dialytic Separation of Gases by Colloid Septa. Part I: Action of a Septum of Caoutchouc, The London, Edinburgh and Dublin Philosophical Magazine and Journal of Science, Vol. XXXII (1866) 401-420
- [6] Fick, A., On Liquid Diffusion, The London, Edinburgh and Dublin Philosophical Magazine and Journal of Science, Vol. X (1855) 30-39
- [7] Zsigmondy, R., and Bachmann, W., About a New Filter, Z. Anorg. Chem., 103, (1918) 119
- [8] Kolff, W.J., Berk, H.T., terWelle, M., Van der Ley, J.W., van Dijk, E.C. and van Noordwijk, J., The Artificial Kidney: A Dialyser with a Great Area, Acta Med. Scand. 117 (1944) 121

- [9] Loeb, S. and Sourirajan, S., Sea Water Demineralization by Means of an Osmotic Membrane, *Adv. Chem. Ser.* 38, 1962, 117
- [10] Henis, J.M.S and Tripodi, M.K., Composite Hollow Fibre Membranes for Gas Separation: The Resistance Model Approach, *J. Mem. Sci.*, 8, 1981, 233
- [11] Cot, L., New Developments in Inorganic Membranes: Fundamentals and Application Aspects. Proceedings of the Third International Conference on Inorganic Membranes, Worcester, Massachusetts, 1994, Ed. Y.H. Ma
- [12] Larbot, A., Alami-Younssi, S., Persin, M., Sarrazin, J. and Cot, L., Preparation of a γ -alumina Nanofiltration Membrane. *J. Mem. Sci.*, 97, 1994, 167-173
- [13] Hsieh, H.P., Inorganic Membranes for Separation and Reaction, Section 12.2 Potential Markets, *Science and Technology Series 3*, Elsevier, ISBN 0-444-81677-1, 1996
- [14] Paterson, R. and Doran, P., A Spray Technique for the Determination of Membrane Diffusion and Distribution Coefficients by the Timelag Method, *J. Mem. Sci.*, 26, 1986 289-301
- [15] Northrop, J.H and Anson, M.L, A Method for the Determination of Diffusion Constants and the Calculation of the Radius and Weight of the Hemoglobin Molecule, *J. Gen. Physiol.*, 12, 1929 543

- [16] Stokes, R.H, An Improved Diaphragm-cell for Diffusion Studies
and some Tests of the Method. J.Amer. Chem. Soc., 72 (1950) 76

Chapter 2 Theoretical Considerations

Introduction

- 2.1 Diffusion Controlled Processes
- 2.2 Non-Equilibrium Thermodynamics
- 2.3 Numerical Solutions
- 2.4 Oscillator Theory and Predictive Models
- 2.5 References

2 Theoretical Considerations

Introduction

In this chapter the more theoretical aspects of this current work will be considered and discussed. A comparison between the data processing methods used here and the methods that have been used previously will also be given. The use of computer modelling and the benefits that this has generated will also be briefly discussed.

2.1 Diffusion Controlled Processes

The process of (chemical) diffusion can be described as the general transport of matter whereby molecules (or ions) mix through normal thermal agitation. This description is valid for both liquid and gaseous systems. The first mathematical approach to this topic was by A. Fick [1] who in 1855 showed that the diffusion of salts in liquid systems was analogous to the diffusion of heat in conducting bodies (Fourier) and the diffusion of electricity in conductors (Ohm). Fick showed that the transfer of salt in solution could be described by

$$J_i = -D_i \left(\frac{\delta c_i}{\delta x} \right) \quad \text{Equation 2.1}$$

In terms of transport through a membrane, J_i is the flow of substance i ($\text{mol}\cdot\text{s}^{-1}\cdot\text{cm}^{-2}$) perpendicular to the plane of the membrane, $\left(\frac{\delta c_i}{\delta x} \right)$ is the concentration gradient across the thickness of the membrane, x and D_i is the proportionality constant (Diffusion coefficient) of the substance i ($\text{cm}^2\cdot\text{s}^{-1}$), this is a statement of Fick's first law of diffusion, for one dimension. As a direct consequence of this and if flow across a membrane is to be considered then it must also hold true for more

than one dimension. Fick's first law is localised and describes the flow at a single point only. If we now consider a plane within the solid body of a membrane (x) with a concentration difference across that plane, a net flux will be generated across the plane. The penetrating front will move through the plane, x , with a velocity, v , but there will be an equalising movement of solvent in the opposite direction, to maintain a mass balance. Under these conditions the only nett transport is that due to the solute (salt) and its concentration can be estimated. If we consider a second plane a very small distance from the first ($x + \delta x$) then the quantity of material entering the plane (at position x) will be $(J_1 \cdot \delta t)$ and the quantity of material leaving the second plane (at $x + \delta x$) will be $(J_1 + \frac{\delta J_1}{\delta x} \delta x) \delta t$, this is shown schematically in Figure 2.1.

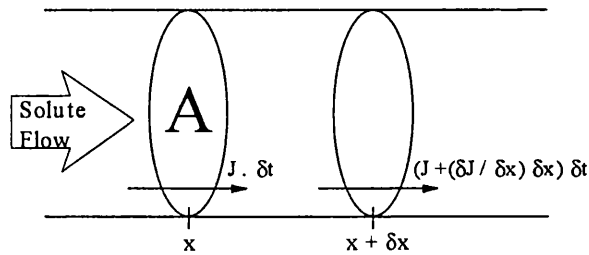


Figure 2.1 Schematic representation of solute flow through a membrane with no convective flow to aid Fick's second law

From this representation, the change in concentration in the volume between the two planes defined by x and $x + \delta x$ will be

$$\delta c_i = \frac{J_i \delta t - (J_i + \frac{\delta J_i}{\delta x} \delta x) \delta t}{\delta x} \quad \text{Equation 2.2}$$

and so

$$\delta c_i = -\left(\frac{\delta J_i}{\delta x}\right)\delta t \quad \text{Equation 2.3}$$

for an infinitely small section ($x \rightarrow 0$) and an infinitely small time ($t \rightarrow 0$)

$$\frac{\delta c_i}{\delta t} = -\left(\frac{\delta J_i}{\delta x}\right) \quad \text{Equation 2.4}$$

As we have already defined J_i (Equation 2.1) by substitution we obtain

$$\frac{\delta c_i}{\delta t} = \frac{\delta}{\delta x}\left(D\frac{\delta c_i}{\delta x}\right) \quad \text{Equation 2.5}$$

if we assume that the diffusion coefficient (D) remains constant over such a small distance and time period then

$$\frac{\delta c_i}{\delta t} = D\left(\frac{\delta^2 c_i}{\delta x^2}\right) \quad \text{Equation 2.6}$$

This is a statement of Fick's second law and shows that the change in concentration is a function of both distance and time. It is these two laws of diffusion (Fick's 1st and 2nd laws) that represent the basis of all of the transport studies in this current research and are vital to the validity of the data treatments and computer models that will be used for the experimental work (Chapters 5 & 7).

It has been assumed that in all cases the diffusion process was being driven by a concentration driving force. This is of course not always the case as there are other possible driving forces such as pressure or electrical potentials and these do play an important part in the diffusion/transport process.

Whenever electrical driving forces are present, either by externally applied fields or by the diffusion process itself, the flow due to the electrical component can be described in exactly the same manner as

the diffusion of salt in solution when arriving at Fick's first law. In electrical terms this can be represented by

$$J_i^{elect} = c_i \mu_i \left(-\frac{\delta \psi}{\delta x} \right) \quad \text{Equation 2.7}$$

where c_i is the concentration (mol cm^{-3}), $\left(\frac{\delta \psi}{\delta x} \right)$ is the electrical gradient across the membrane of thickness x and μ_i is the ionic mobility ($\text{cm s}^{-1}/\text{Vcm}^{-1}$), this is in fact a statement of Ohm's law.

The total ionic flow across the membrane is therefore simply the sum of the two components, i.e. concentration and electrical gradients present

$$J_i^{total} = J_i^{conc} + J_i^{elect}$$

and is more fully represented by

$$J_i = D_i \left(-\frac{\delta c_i}{\delta x} \right) + c_i \mu_i \left(-\frac{\delta \psi}{\delta x} \right) \quad \text{Equation 2.8}$$

this is the Nernst-Planck equation [2][3]. There are some further inter-relationships between the component parts of this equation but these will not be discussed here.

As a considerable quantity of the work in this study made use of electrolyte solutions we must be capable of assuming that both electrolytes and non-electrolytes behave in the same manner under our experimental conditions. In order for this to be the case we must be able to reduce the electrodiffusion equation to a Fickian form. From previous studies in this area by Doran [4] we know that for the experimental conditions used this constraint is satisfied, i.e.

$$J_{salt} = -D \text{grad } C_{salt} \quad \text{Equation 2.9}$$

2.2 Non-Equilibrium Thermodynamics

The transport of material(s) through a membrane is a thermodynamic non-equilibrium process. This means that for an adequate description of the process it is necessary to make use of the thermodynamics of irreversible processes. This in fact is something of a unifying theory governing all transport processes.

The basic foundation of this application is that for a constant driving force, free energy will be dissipated continuously and hence entropy will be produced. The rate of this entropy production caused by the process is the summation of all of these irreversible processes and is termed the dissipation function (Φ).

$$\Phi = (-gradT)X_q + (-gradP)X_p + (-gradV)X_{el} + (-gradC)X_c \dots \geq 0$$

Equation 2.10

where each of the individual processes can be described as the product of the flux and its corresponding force.

$$\Phi = T \left(\frac{\delta S}{\delta t} \right) = \sum J_i X_i$$

Equation 2.11

When the system is close to equilibrium it can be assumed that each flux can be expressed as a linear function of the forces in the system.

$$J_i = \sum L_{ij} \cdot X_j$$

Equation 2.12

where L_{ij} are the (constant) phenomenological coefficients and X_j the driving forces for the process.

For a two component system (1 and 2) we would obtain two flux equations but with four coefficients (L_{11} , L_{22} , L_{12} and L_{21}). There are some basic constraints that must be observed;

$L_{12} = L_{21}$ i.e. Onsager reciprocal rule holds true [5]

L_{11} (and L_{22}) are always positive and greater than zero.

$$L_{11} \cdot L_{22} \geq L_{12}^2$$

The coupling coefficient L_{12} (L_{21}) can be positive or negative.

Network thermodynamics and Bond graph theory are extensions to the basic principles of the thermodynamics of irreversible processes. They could (and have been) the subject of a Ph.D thesis in their own right but in this current work these methods have been applied purely as design and predictive tools for the experimental systems. These topics are covered in far greater detail elsewhere [6,7,8,9] and will not be discussed further in this work. The use of the computer models (as a predictive tool) will be made use of further and the information generated will also be discussed.

2.3 Numerical Solutions

Over the evolution to this current system, several different numerical methods have been used in order to extract the transport characteristics of test membranes. Of those methods described, only the final one was used in this current work but the others show the evolution of the analysis methods and their increased suitability for routine use.

2.3.1 Phase Shift Analysis

In the first attempt at an experimental system based upon generating concentration waves Paterson and Doran devised a system based around aerosol sprays[10]. When a membrane

was exposed to a series of regular square concentration waves it has been shown that the phase shift between the input (square) wave and the detected (sine) wave could be used to estimate the diffusion coefficient [10]. There were several disadvantages to this method however. Only the diffusion coefficient could be determined and this was done by an iterative numerical method that required an initial over estimate for D and took several hours to process. Although this was a significant step it was not considered suitable for routine use.

2.3.2 Determination of Peak Maxima/Minima

A further development from 2.3.1 above was the use of the experimental peak maxima and minima for the determination of the diffusion coefficient. It was shown that provided the switch period was significantly longer than was necessary to achieve a steady state condition the peak maxima and minima occurred at times, $\tau = (l^2 / 7.2D)$ after the switch [11]. This was greatly superior to arbitrarily selecting the maxima/minima. Due to experimental scatter and the very small amplitude of the detected waves this maxima/minima selection was very difficult to do with great confidence or precision.

2.3.3 Determination of Permeability and Diffusion Coefficient

In a further significant development of this symmetrical oscillator system, the permeability could be determined from

the linear portions of the waves and the diffusion coefficients from the intersection of the two linear portions [12]. Although this was effectively a near ideal system with no net accumulation due to the symmetrical waveform, the amplitude of the emergent wave remained a huge problem for practical application.

Using the numerical methods described above the current system overcomes the emergent wave amplitude problem completely. This for the first time has allowed the generation of concentration waves to be used as a routine method for membrane characterisation. In conjunction with the other analytical methods that have been devised, particularly for multi-layer membranes, the current system has allowed for far greater concentration changes in the collecting volume. This has enhanced the number of different possible detection methods available, for example spectrophometric or electrochemical sensors and has increasing the overall scope of the system.

2.4 Oscillator Theory & Predictive Models

The experimental detection cells used in this work are 'closed' systems in which a concentration difference across a test membrane is generated effectively instantaneously. This causes transport of material across the membrane under the force of the applied concentration difference, this was the method devised by Daynes [13].

By the conservation of mass, the total number of moles of a component present in a closed system must be constant and will be made up of the sum of all contributions.

$$n_{total} = n_1 + n_2 + \dots n_n \quad \text{Equation 2.13}$$

and so this must also be true for concentrations

$$c_{total} = c_1 + c_2 + \dots c_n \quad \text{Equation 2.14}$$

and so

$$grad c_{total} = grad c_1 + grad c_2 + \dots grad c_n \quad \text{Equation 2.15}$$

therefore for Fickian systems with constant diffusion coefficients (Equation 2.1)

$$-D grad c_{total} = -D grad c_1 - D grad c_2 \dots \quad \text{Equation 2.16}$$

and similarly for the flows

$$J_{total} = J_1 + J_2 + \dots J_n \quad \text{Equation 2.17}$$

This at first sight might appear somewhat simplistic. It has been shown by Crank [14] that the change in concentration within the membrane from the imposition of a concentration step to the onset of the steady state condition to be complex, shown by Equation 2.18.

$$C = C_1 + (C_2 - C_1) \frac{x}{l} + \frac{2}{\pi} \sum_{n=1}^{\infty} \frac{C_2 \cos n\pi - C_1}{n} \sin \frac{n\pi x}{l} \exp\left(-Dn^2\pi^2 t/l^2\right) \\ + \frac{4C_0}{\pi} \sum_{m=0}^{\infty} \frac{1}{2m+1} \sin \frac{(2m+1)\pi x}{l} \exp\{-D(2m+1)^2\pi^2 t/l^2\} \quad 2.18$$

where C_1 is the concentration at the external face ($x=0$), C_2 the concentration at the internal face ($x=l$), C_0 is the initial uniform membrane equilibrium concentration, l is the membrane thickness and D is the diffusion coefficient.

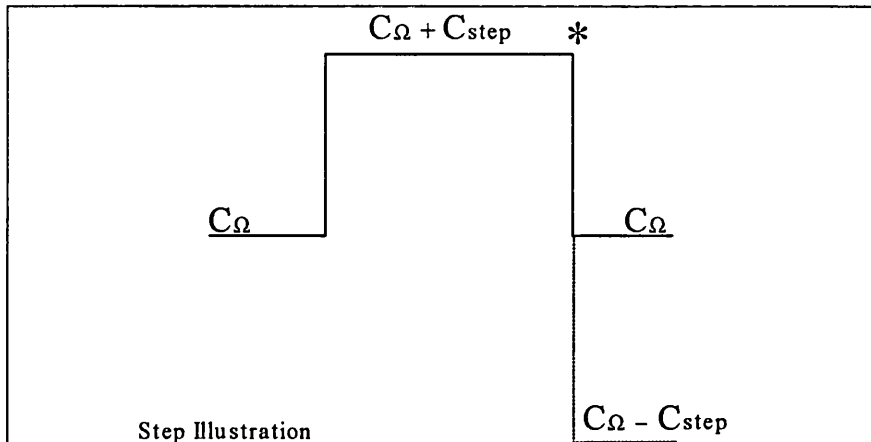
Use of these relationships (Equations 2.13 to 2.17) indicate that solutions to the diffusion equation can be obtained by a linear combination of existing solutions. Such linear combinations of these existing, well defined solutions of the diffusion equations provide relationships which can be used for step wave oscillators. This will be described below.

2.4.1 Bond Graph Modelling of Oscillator System

The use of the bond graph models provides us with information regarding the flux into the collecting volume. In addition, the predicted concentrations within the membrane phase are also available and hence concentration profiles within the membrane can be obtained. The bond graph models have been used to demonstrate both the validity and the ease of use of the data analysis routines.

In the first instance, the classical Daynes system was modelled. The imposition of a concentration step generated a concentration difference across the membrane and this in turn generated an accumulation of material within the membrane phase, these profiles are shown in Figure 2.2. The subsequent flow into the collecting volume is shown in Figure 2.3. This clearly shows the build-up from an initial non-steady state condition to the beginning of the (linear) steady state period, labelled B. The model parameters are listed in Table 2.1. If we now consider a system initially in a pseudo steady state

condition at time zero. The membrane and collecting volume



concentration profiles from this model are shown in Figures 2.4 and 2.5 respectively. In Figure 2.5 the concentration profile is labelled A and is in fact parallel to the steady state portion of curve B in Figure 2.3.

For a symmetrical oscillator in a pseudo steady state with a step (c_{step}) applied, then (at the position * in the illustration above) is switched down to the original level (c_Ω), this produces a concentration profile in the membrane (Figure 2.6) and in the collecting volume shown in Figure 2.7 and labelled C. This curve represents the solution for (A-B).

If a similar system is switched down but now to the lower level ($c_\Omega - c_{step}$) the concentration profile produced is shown in Figure 2.8, labelled D. This curve passes through a maximum and it can be shown that the intersection of curve A (Figure 2.5) and the steady state portion of curve D, which has a solution of (A-2B), occurs at $\tau = l^2/6D$. These solution relationships are

shown graphically in Figure 2.9.

For continuous symmetrical oscillations of this type, oscillating for equal times above and below the mean (equilibrium concentration) of the collection volume, provided steady state conditions have been obtained, this provides the simple repetitive evaluation of $\tau = l^2/6D$ and so the diffusion coefficient, D .

It is well known that from the mathematical solutions [14] the flow from a simple step experiment is exactly half the steady state flow at the time $\tau^* = l^2/7.2D$.

At this time (τ^*), the slope of curve B, is half the steady state value, curve A. Consequently for the curve labelled D, (A-2B), τ^* corresponds to the maximum concentration in the collection volume oscillation and by a similar argument also the minimum.

This appears to be an even simpler method for determination of D but in practice the exact locations of maxima and minima are impossible to choose with confidence due to random small errors in concentration detector systems.

The preferred method therefore was to use the intersection of the steady state portions of the detected wave. This method being graphical is extremely simple and avoids the lengthy calculations as described earlier in Section 2.3.

With the asymmetrical oscillator a consecutive series of

timelag experiments are performed repeatedly. Concentration square waves were generated at one face of the test membrane but in this case the lower concentration used was equal to that initially in the collecting volume.

By using such boundary defining conditions the accumulation of material in the collecting volume followed an increasing 'staircase' concentration profile with a much greater amplitude than for a symmetrical oscillator (about a mean concentration). An example of simulated output using these boundary conditions is shown in Figure 2.10 and the simulation parameters are given in Table 2.2.

At much later times in such an experiment there will be significant back diffusion from the collecting volume and although the slopes from the originally horizontal portions will become negative, the intercepts can still be described in exactly the same manner. These simulation results show that the basic assumptions made earlier regarding the linear combinations of solutions to the diffusion equations are indeed true and show the validity of the method.

Number of Layers	1
Layer Thickness l (cm)	0.015
Distribution Coefficient α	0.19
Diffusion Coefficient D (cm^2s^{-1})	3.29×10^{-6}
Number of Lumps in Model	30
Source Volume V_s (cm^3)	100
Collection Volume V_c (cm^3)	1.752
Exposed Membrane Area A (cm^2)	0.569
Max. Source Concentration (M)	0.1
Source Period (s)	100
Initial Sink Concentration (M)	0
Set up Steady State Conditions	No
Initial Concentration in Layer 1	0
Total Simulation Time (s)	250
Number of Membrane Profiles	50
Stepsize (s)	0.1
Number of Integrations / stepsize	10

Table 2.1 List of the Conditions Used for Computer Models for the Data Analysis Proofs.

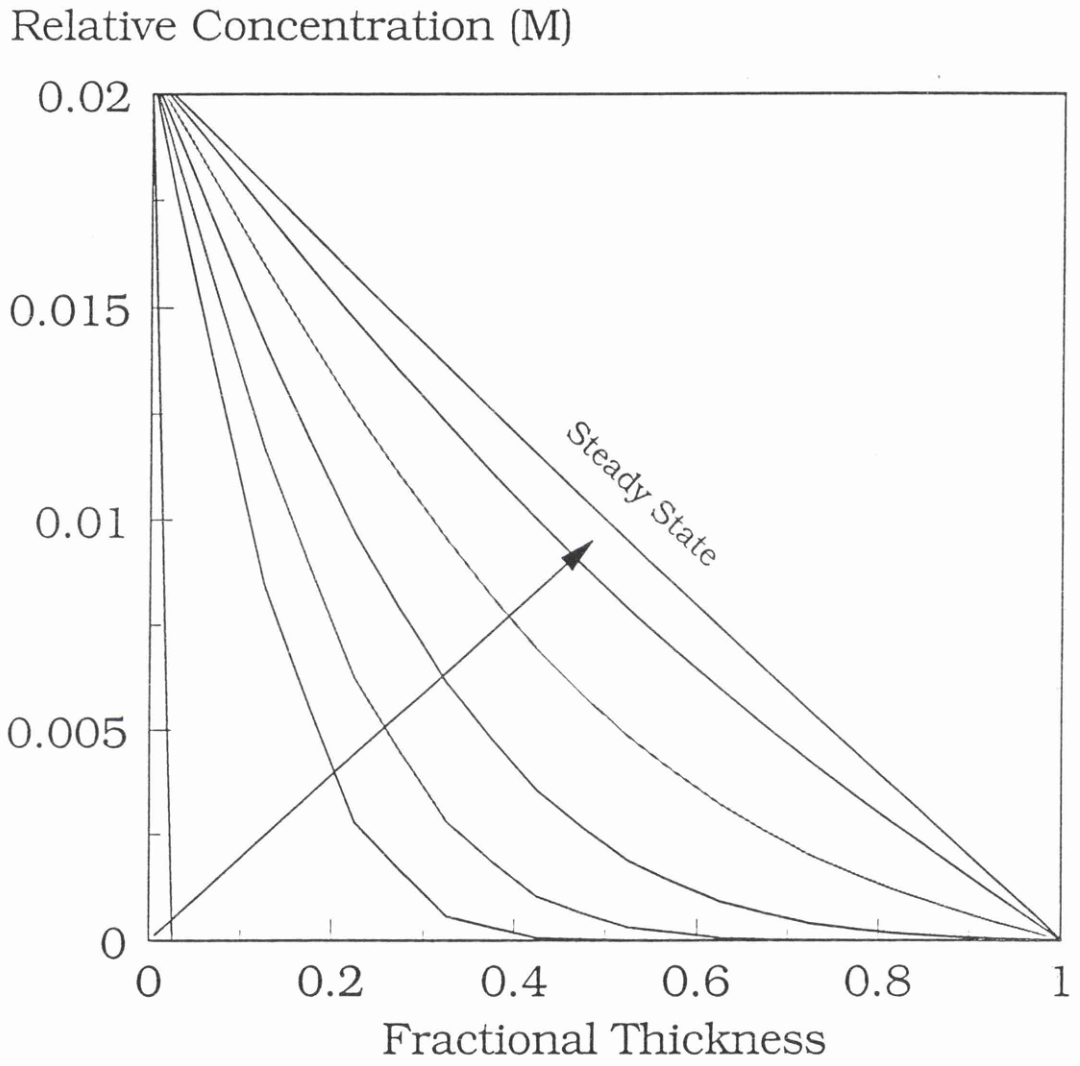


Figure 2.2 Simulated Membrane Phase Concentration Profiles for Daynes Classical System.

Relative Concentration (M)

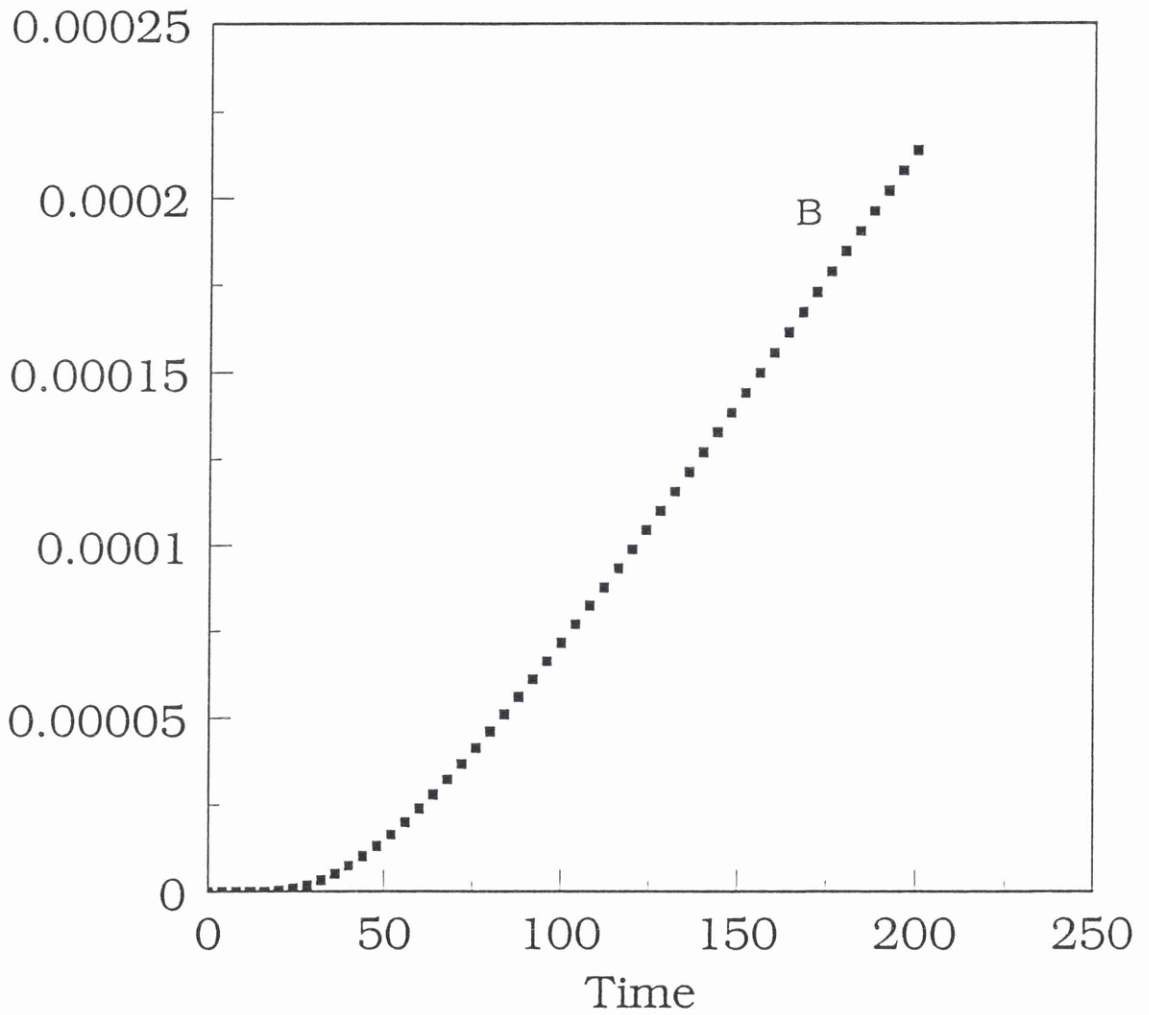


Figure 2.3 Simulation of the Accumulated Concentration Profile in the Collecting Volume after an Imposed Step.

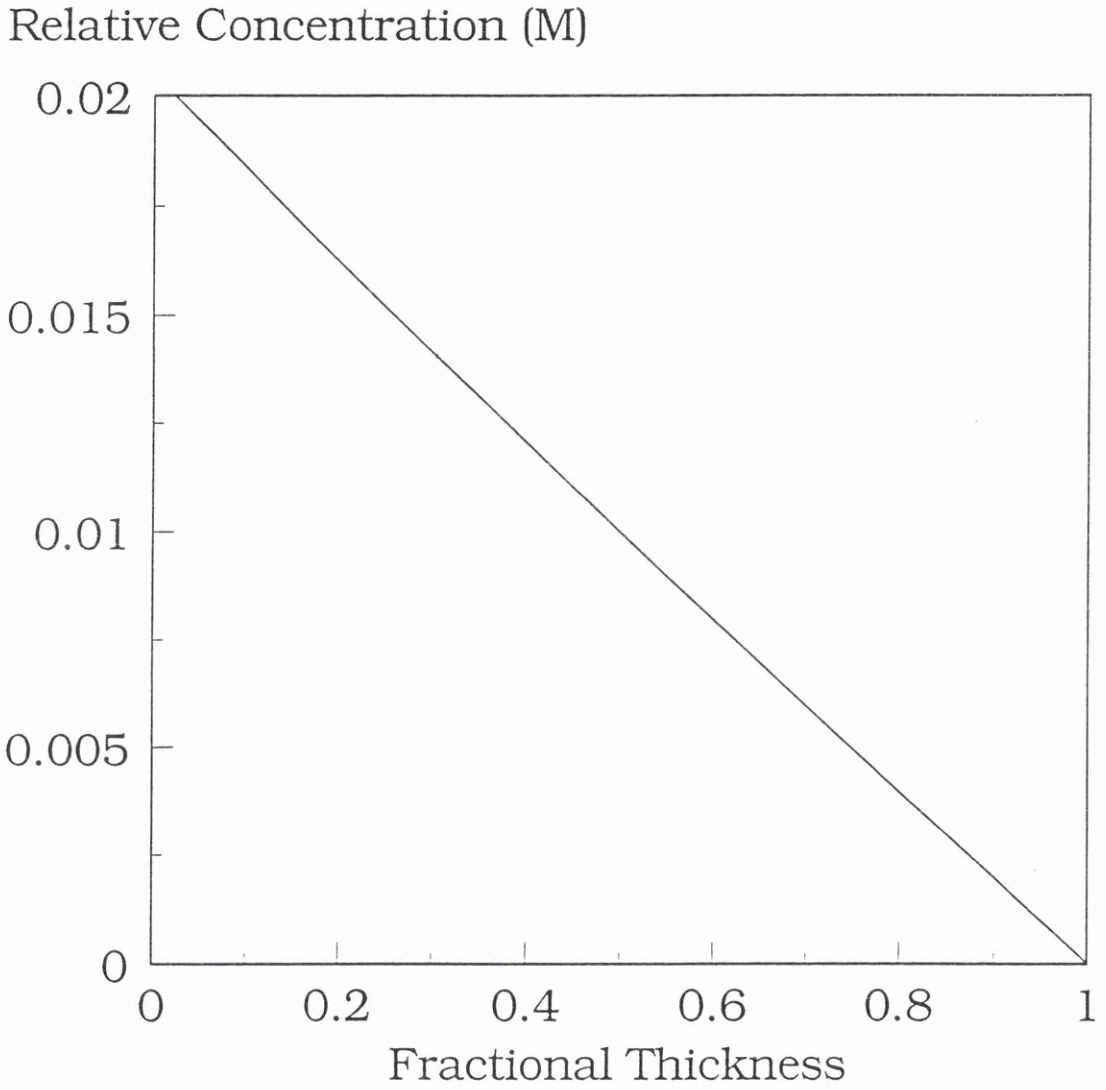


Figure 2.4 Simulated Membrane Phase Concentration Profile for an Applied Steady State Condition.

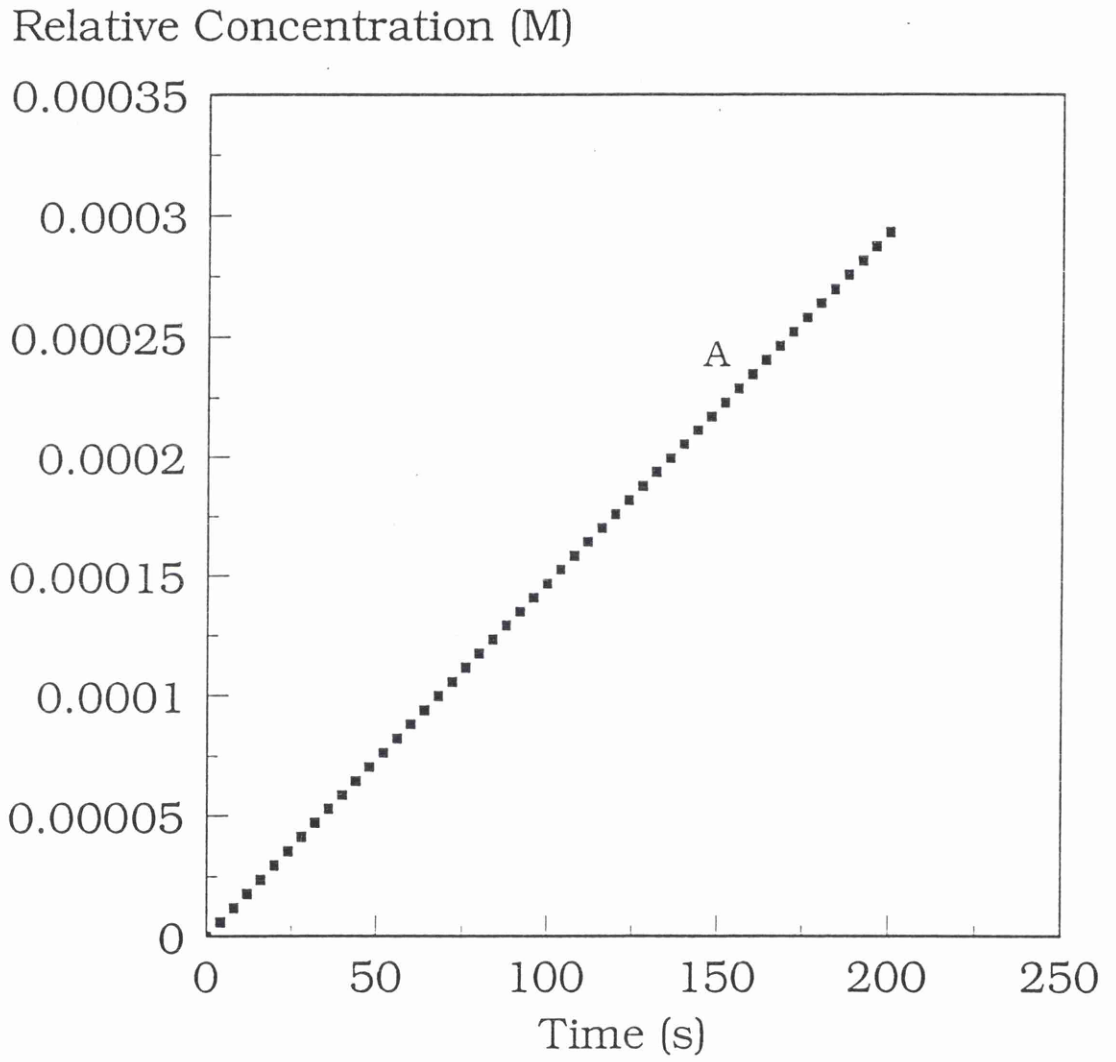


Figure 2.5 Simulated Accumulation in the Collection Volume with Initial Steady State Conditions

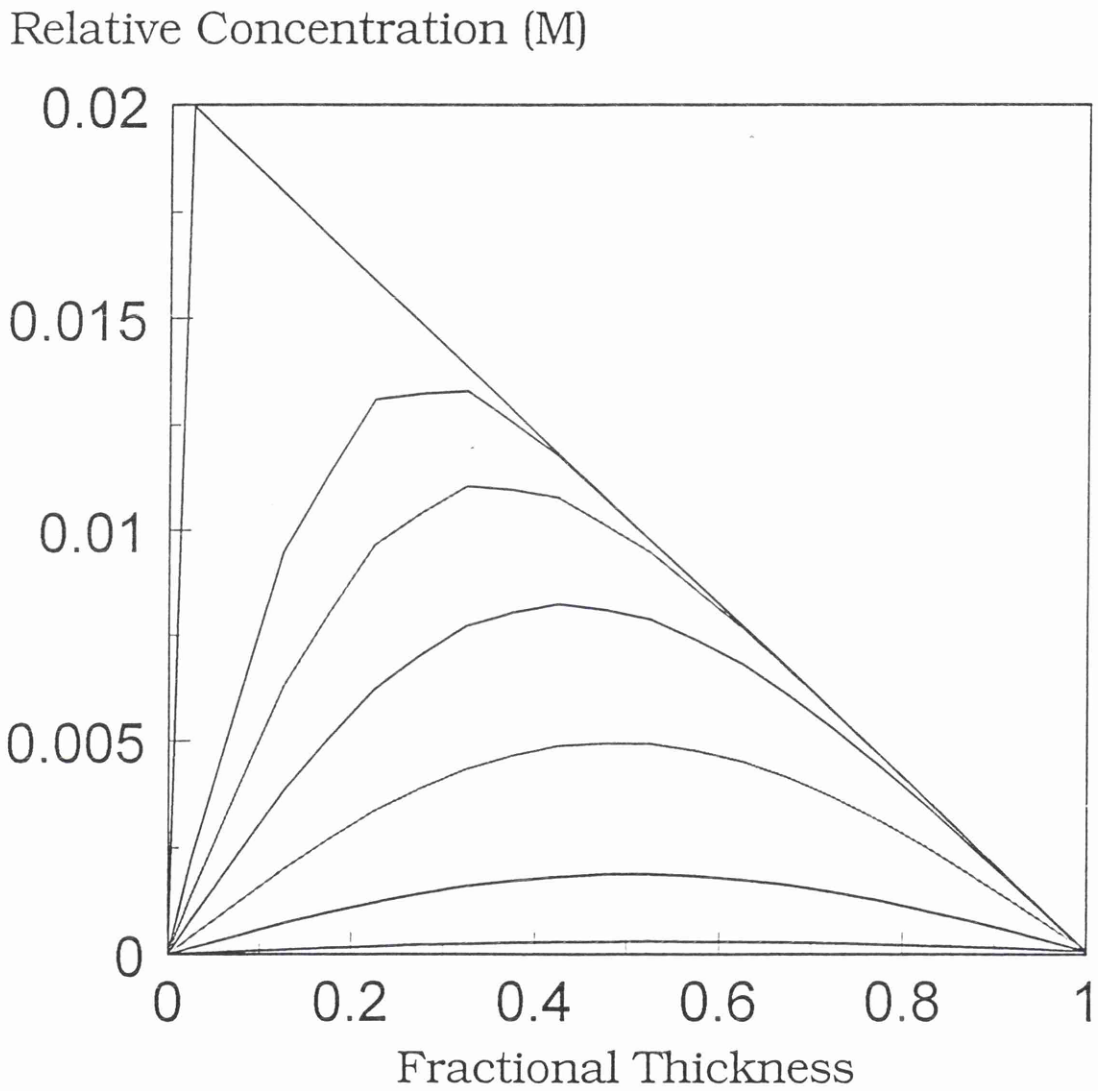


Figure 2.6 Simulated Membrane Phase Concentration Profiles After a Switch Down from a Steady State Condition.

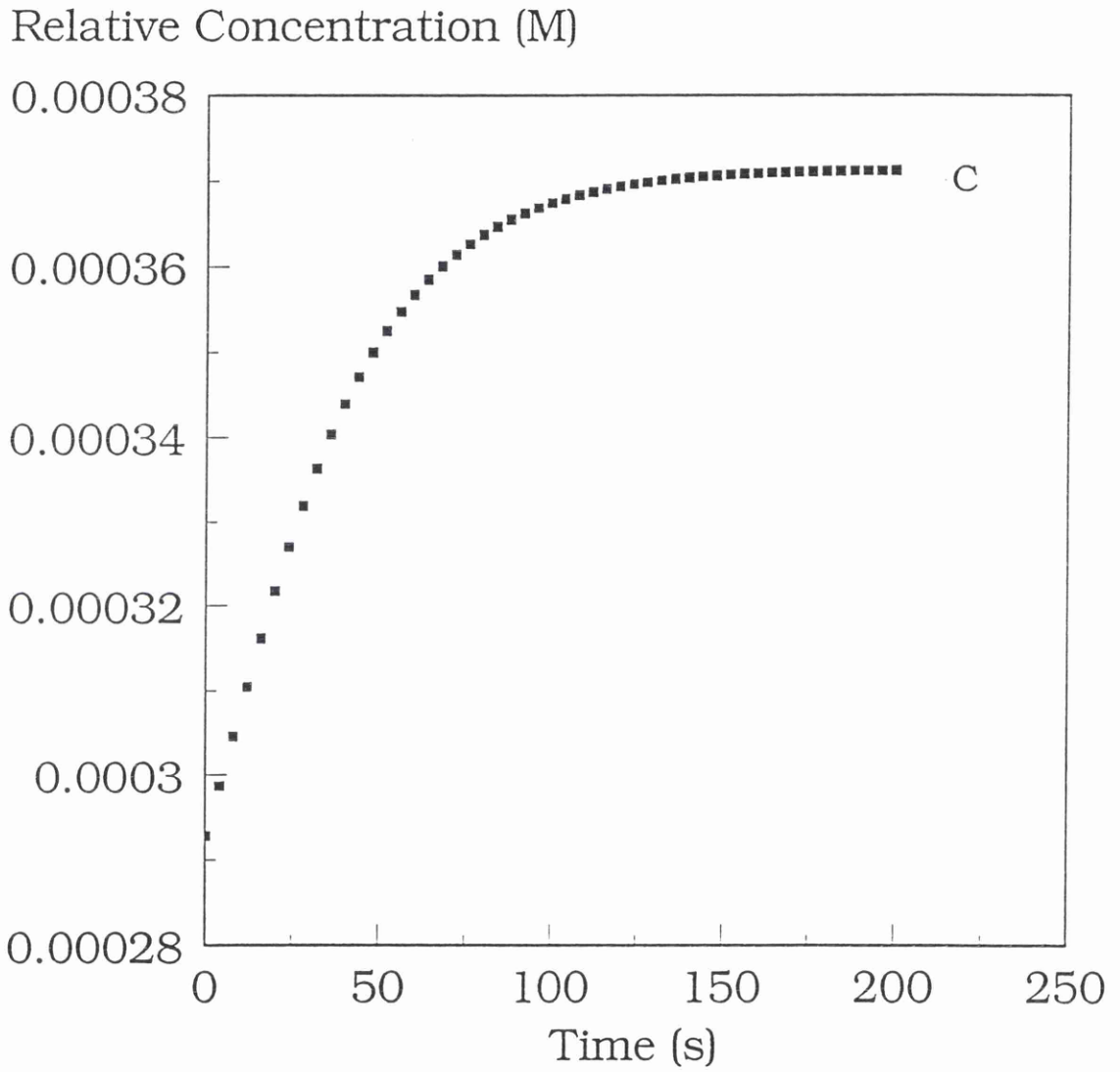


Figure 2.7 Simulated Accumulation in the Collecting Volume after a Concentration Switch Down from a (Pseudo) Steady State Condition to the Original Level.

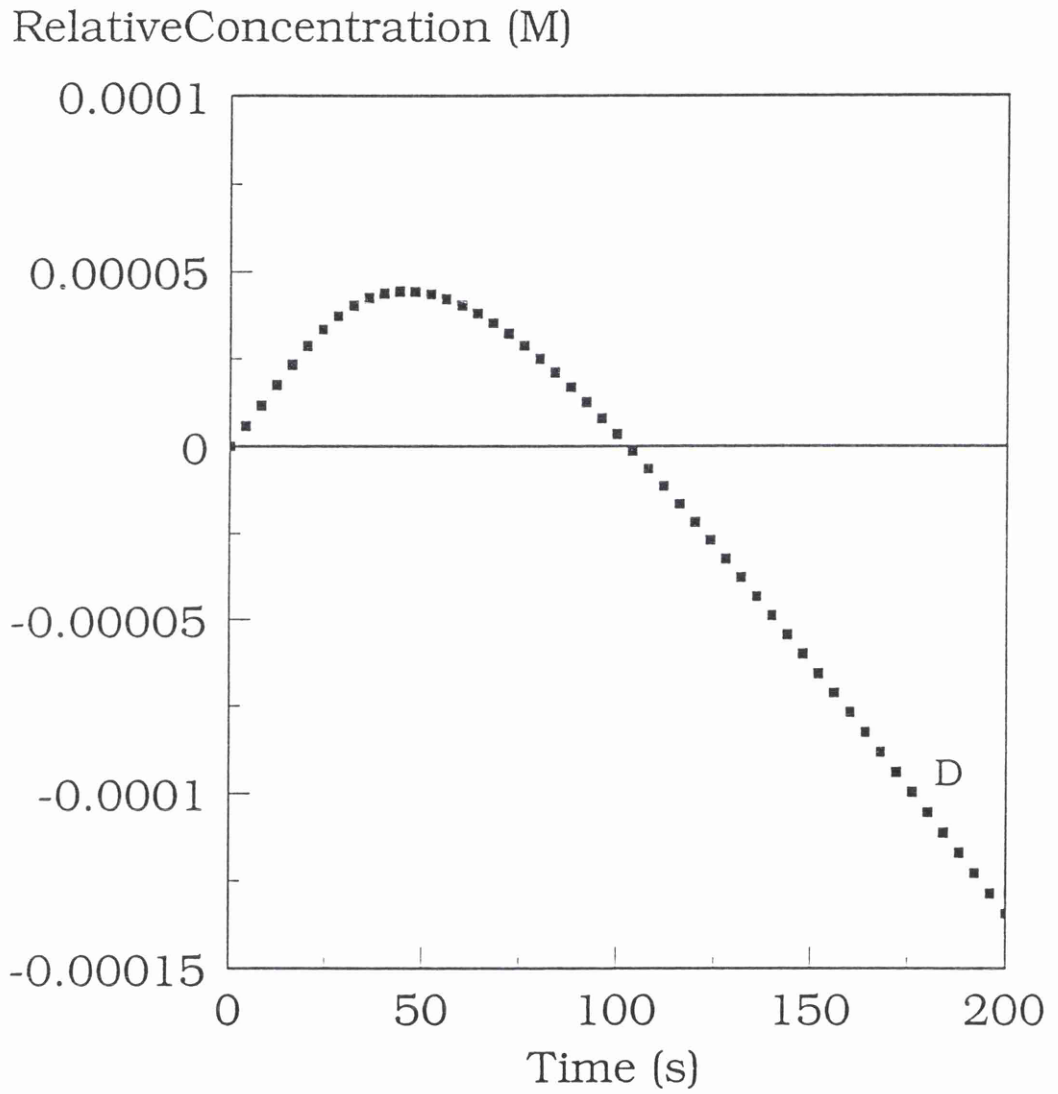


Figure 2.8 Simulated Accumulation in the Collecting Volume after a Switch Down from a (Pseudo) Steady State Condition to a Lower Concentration.

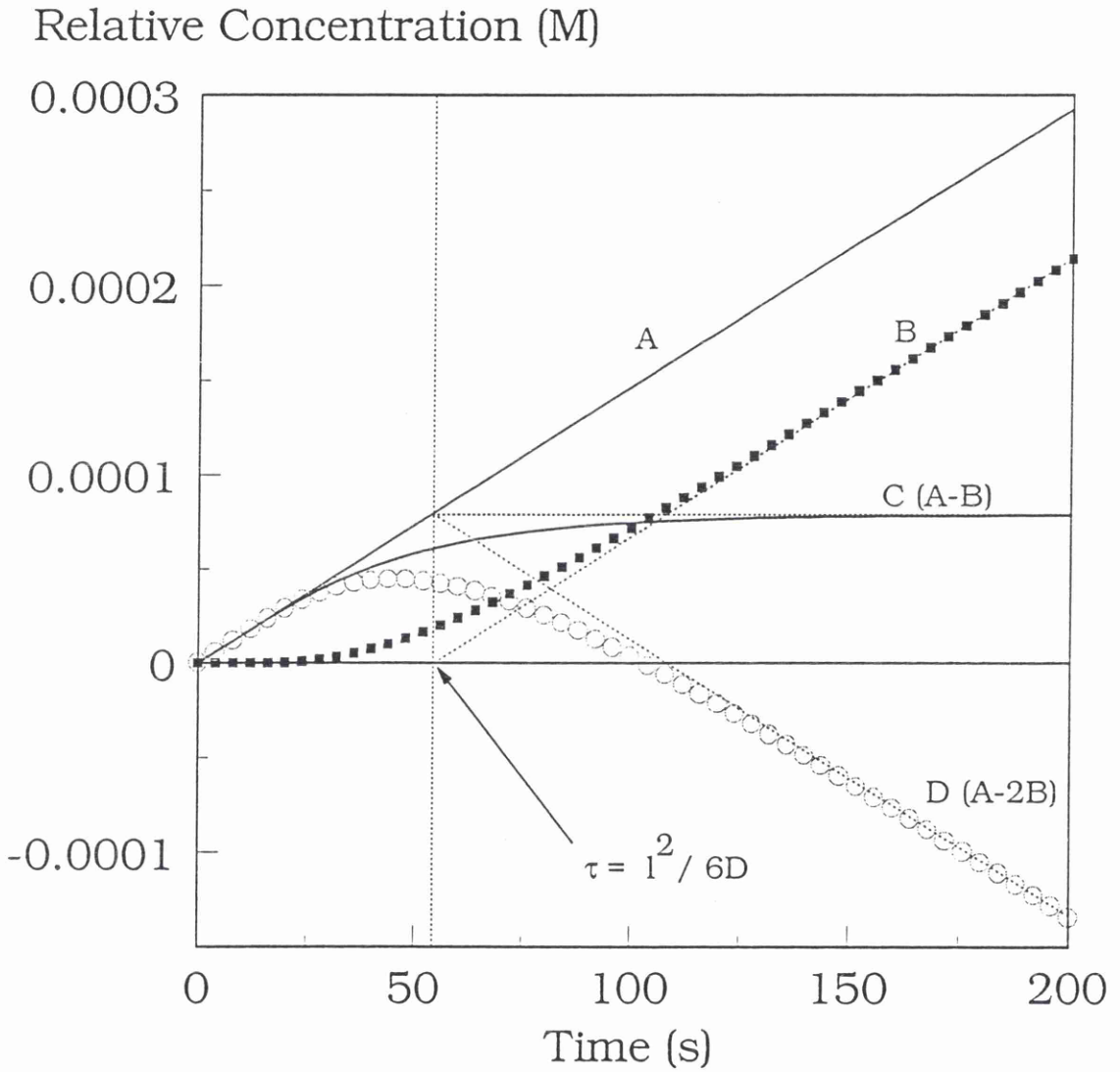


Figure 2.9 Combined Outputs from the Simulated Concentration Profiles in the Collecting Volume. The Linear Intercepts are Shown in Dotted Lines and Coincide at Time τ .

Theoretical Considerations

Number of Layers	1
Layer Thickness l (cm)	0.048
Distribution Coefficient α	1
Diffusion Coefficient D (cm^2s^{-1})	1.71×10^{-6}
Number of Lumps in Model	30
Collection Volume V_c (cm^3)	1.752
Exposed Membrane Area A (cm^2)	0.569
Source Waveform	Square
Max. Source Concentration (M)	0.1
Source Amplitude (M)	0.05
Source Period (s)	100
Initial Sink Concentration	0
Set up Steady State Conditions	No
Initial Concentration in Layer 1	0
Total Simulation Time (s)	300
Number of Membrane Profiles	50
Step time (s)	0.1
Number of Integrations / step time	10

Table 2.2 List of the Conditions Used for Computer

Model of an Asymmetric Oscillator Experiment.

Relative Concentration(M)

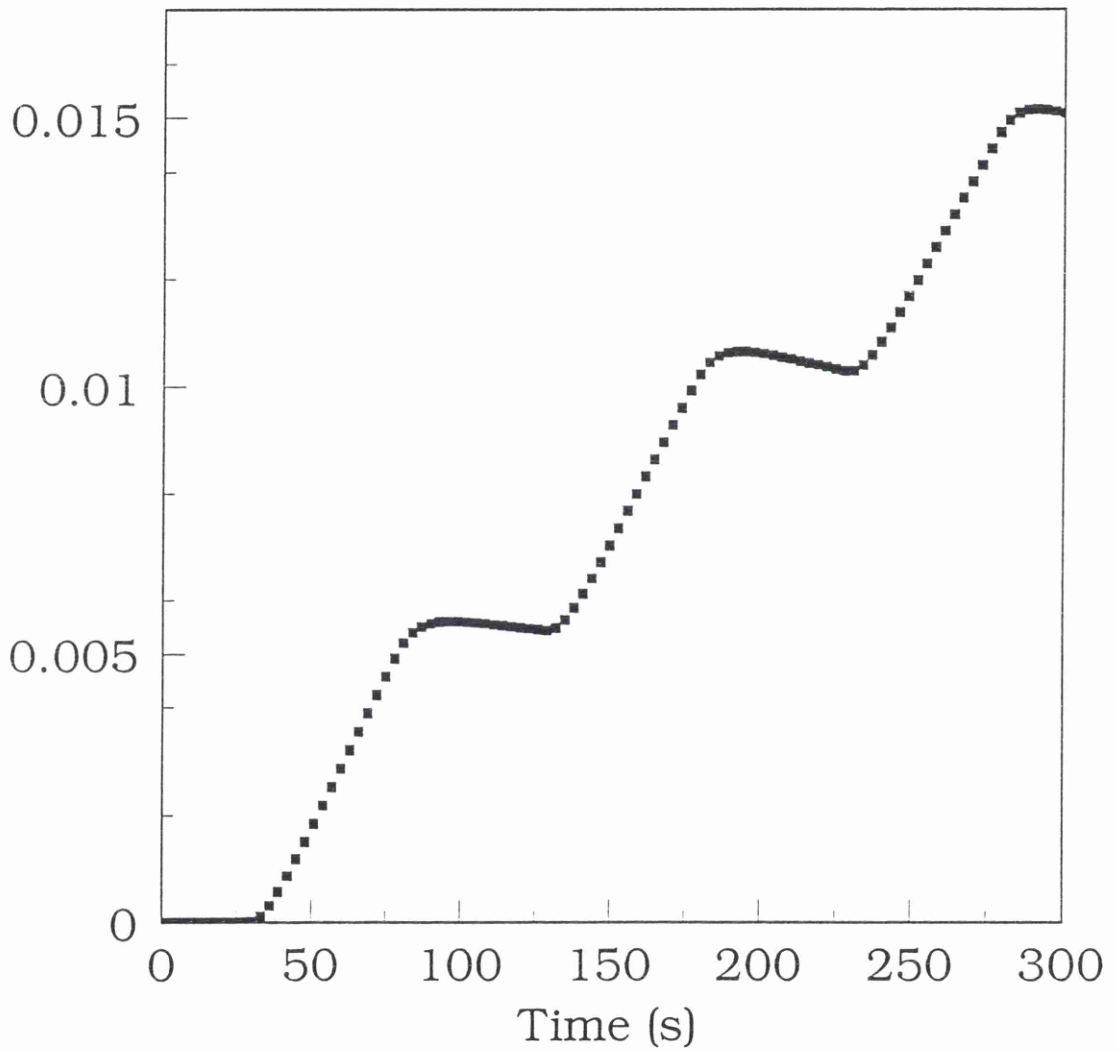


Figure 2.10 Simulated Concentration Profile in the Collecting Volume for an Asymmetric Oscillator.

2.4.2 Timelag Analysis

The simplest experiment is a single timelag where only one concentration step is made above the initial equilibrium value. The extrapolated intercept of the linear section of the concentration profile with the x-axis is known as the timelag (τ) which can be related directly to the membrane phase diffusion coefficient (D). Just how these data are treated is discussed in Chapter 7. The permeability can also be obtained from the linear portion of the concentration profile, this again will be discussed in Chapter 7. There has been some discussion about at which point this linearity begins and where in the concentration profile is a suitable point for the analysis. Jenkins et al.[15] reported that the onset of linearity was at a value equal to 3τ but Paterson and Doran [16] showed that by using a linear extrapolation between $3-6\tau$ the error in the permeability determination could be significantly reduced, from -4% to -1.7% based upon an infinite volume calculation. In all of the experimental results quoted in this work the later method has been used for the determination of permeability values.

2.4.3 Permeability Relationships

It is normal to define the permeability, P, of a membrane by

$$J = P\Delta c \quad \text{Equation 2.19}$$

where Δc is the external concentration difference across the

membrane in the liquid (or gaseous) phase interface . For Fickian systems

$$P = \frac{DA\alpha}{l} \quad \text{Equation 2.20}$$

where D is the Diffusion coefficient (cm^2s^{-1}), A the membrane area (cm^2) and l the membrane thickness (cm). The distribution coefficient (α) defines the concentration ratio between the membrane and the external solution (or gas) phase.

In the bond graph notation system used for the computer modelling the generalised description of a flow, f, is given as an effort, e, divided by a resistance, R.

$$f = \frac{e}{R} \quad \text{Equation 2.21}$$

by comparing Equation 2.19 to 2.21 this shows the Fickian bond graph resistance to be the reciprocal of the permeability.

$$R = \frac{1}{P} = \frac{l}{DA\alpha} \quad \text{Equation 2.22}$$

Composite Membranes

If we now consider a bilayer membrane system, a and b, as shown in Figure 2.11, the permeability of the composite will be P_{ab} . Under steady state conditions the steady state flow (J) is

$$J = P_{ab}(c' - c'') \quad \text{Equation 2.23}$$

Let the permeabilities of the individual layers a & b be P_a and P_b . If one imagines a vanishingly thin layer between a and b (which provides no barrier to diffusion) and this is in

equilibrium with both layers simultaneously, then the flows will remain the same

$$J = P_a(c' - c^*) \quad \text{and} \quad J = P_b(c^* - c'') \quad \text{Equation 2.24}$$

and since $(c' - c'') = (c' - c^*) + (c^* - c'')$

$$\frac{1}{P_{ab}} = \frac{1}{P_a} + \frac{1}{P_b} \quad \text{Equation 2.25}$$

Typically a bilayer membrane consists of a thin active layer coating, "a" and the backing layer, "b". If the permeabilities of the composite membrane "ab" and that of the backing layer, "b" are measured experimentally, then the permeability of the active layer alone can be estimated by rearrangement of Equation 2.25.

In practice with ceramic membranes the backing layer is available before coating. With organic membranes it would be necessary to remove the (thinner) active layer, possibly by abrasion. The form of Equation 2.25 could be extended to cover any number of layers.

$$\frac{1}{P_{abc..n}} = \frac{1}{P_a} + \frac{1}{P_b} + \frac{1}{P_c} + \dots + \frac{1}{P_n} \quad \text{Equation 2.26}$$

This relationship will be used later in the experimental sections, Chapter 5 (for gaseous systems) and Chapter 7 (for liquid systems) for the calculation of the permeability due explicitly to the active layer in multilayer systems.

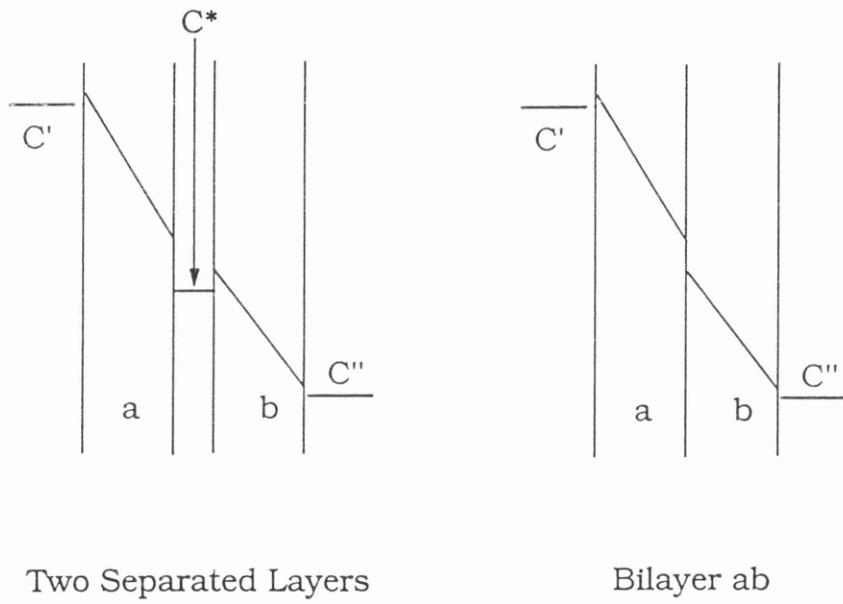


Figure 2.11 Diagram for the Explanation of the Permeability of a Bilayer.

2.5 References

- [1] Fick, A., The London, Edinburgh and Dublin Philosophical Magazine and Journal of Science, Vol. X (1855), 30-39
- [2] Nernst, W., Z. Physik Chem., 2, (1888), 613
- [3] Plank, M., Ann. Physik Chem., 39, (1890), 161
- [4] Doran, P., Ph.D Thesis, University of Glasgow, 1985
- [5] Onsager, L., Ann. Physical Review, 37, (1931), 405
- [6] Paterson, R., : Network Thermodynamics, Ch. 1 in "Membranes Structure and Function" Ed. E.E Bittar, J. Wiley, New York, 1980
- [7] Paterson, R., Swiss Chem., 1988, 10Nr3a,17
- [8] Paynter, H., "Analysis and Design of Engineering Systems", MIT, Cambridge, Mass., 1961
- [9] Katchalsky, A. and Curran, P. F., Non-Equilibrium Thermodynamics in Biophysics, Harvard University Press, Cambridge, Mass., 1965
- [10] Paterson, R., and Doran, P., J. Mem. Sci., 27 (1986) 105
- [11] Young, D., and Paterson, R., Proc. Vth World Filtration Congress (Nice), 1, (1990), 261.
- [12] Young, D., and Paterson, R., Proc. 1st International Conference on Inorganic Membranes, Montpellier, 443-447, Eds. Cot and Charpin, ENSCM Press (1989)
- [13] Daynes, H. A., Proc. Roy. Soc. Series A, 97, 286 (1920)
- [14] Crank, J., "The Mathematics of Diffusion", Clarendon Press, Oxford, 1959

- [15] Jenkins, R. C., Nelson, P.M. and Sirer, L., Trans Faraday Soc., 66 (1970) 1391
- [16] Paterson, R., and Doran, P., J. Mem. Sci., 26 (1986) 289-301

Chapter 3 Control & Display Software

Introduction

- 3.1 Internal Communication
- 3.2 Device Preconditioning & Data Collection
- 3.3 Display Outputs to System Operator.
- 3.4 Data Manipulation and Processing.
- 3.5 References.

3 Control and Display Software

Introduction

All of the computing systems described in this study refer to the International Business Machines (IBM) family of personal computers (PC's). These computers have evolved significantly since their introduction some fifteen or so years ago. They have been since the earliest days of an 'open' architecture with well defined hardware, software and input/output sub-systems. This has allowed for the third party development of several interfacing options to enable the computer to communicate with and to control external electronic devices. From these, now many options, three have become commonly used for interfacing IBM PC's (and their clones) to external devices of many types, these are the serial and parallel ports and the GPIB (IEEE-488).

A great many programming languages were available such as C++, Pascal, Fortran and more recently the 'Visual' languages for use with Microsoft Windows™ to name but a few. These all had their own merits and disadvantages but on balance it was decided to use Microsoft QuickBASIC as the language of choice. The version used for all of the systems described here was Microsoft QuickBASIC Version 4.5.

This was a highly structured form of the language with a great many in-built functions. It also had the ability to easily access IBM PC systems addresses, such as input/output ports, control of the VDU/monitor attributes and could be used to link to external program modules such as the NAG mathematical routines and so on. To give even greater

control and flexibility to the finished programs, QuickBASIC 4.5 was used to write and debug the programs but at the final stage of compilation (to executable code) the full Microsoft Basic Compiler Version 6.0a was used. The programs written in this way made the maximum use of the available computer systems resources.

To describe in detail all of the software written and used in the course of this study would take far too much space, it would also detract from the overall description and use of the experimental systems for which they were written. For this reason only a brief overview of the software systems is given here. All of the software could be divided into one of four main subject areas;

- (1) Internal communication & actions
- (2) Device preconditioning & data collection
- (3) Display output for the system operator.
- (4) Data handling & manipulation .

These four subject areas will now be briefly described.

3.1 Internal Communication

The software code which actually allowed for the controlling computer to communicate with the individual measurement devices was extremely complex. It consisted of a large series of modules or subroutines which were written in such a manner as to allow a person who was reasonably computer literate to make use of the system. By chaining together the relevant subroutines, data could be passed across the system quickly and easily. These routines were linked to a

device driver (commercial) which was loaded automatically each time the computer was switched on and allowed these routines to be used with different hardware options. Some of the tasks that these routines handled were for example; (a) ensuring that a selected measurement device actually existed and was properly configured, if this was not the case, warning messages were passed back to the system user; (b) ensuring that the sequence of data requests were in a 'sensible' order i.e. that all fast data collection routines were placed together and not astride a subroutine that would require a longer time to return values; (c) ensuring that instrument commands, for example, the change of measurement range, were not confused with data being passed back across the interface. A data/command flow diagram of this control system is shown in Figure 3.1.

3.2 Device Preconditioning & Data Collection

In this section two different experimental methods are described, they are (a) a timelag experiment and (b) an oscillator experiment. The latter experiment was essentially a consecutive series of timelag experiments but it did require some additional software control systems.

3.2.1 Timelag Experiment

The user was first required to select the method of detection to be used, conductivity or UV-Visible spectrophotometer. There then followed a series of questions, the answers to which were input and these formed the program variables. These passed

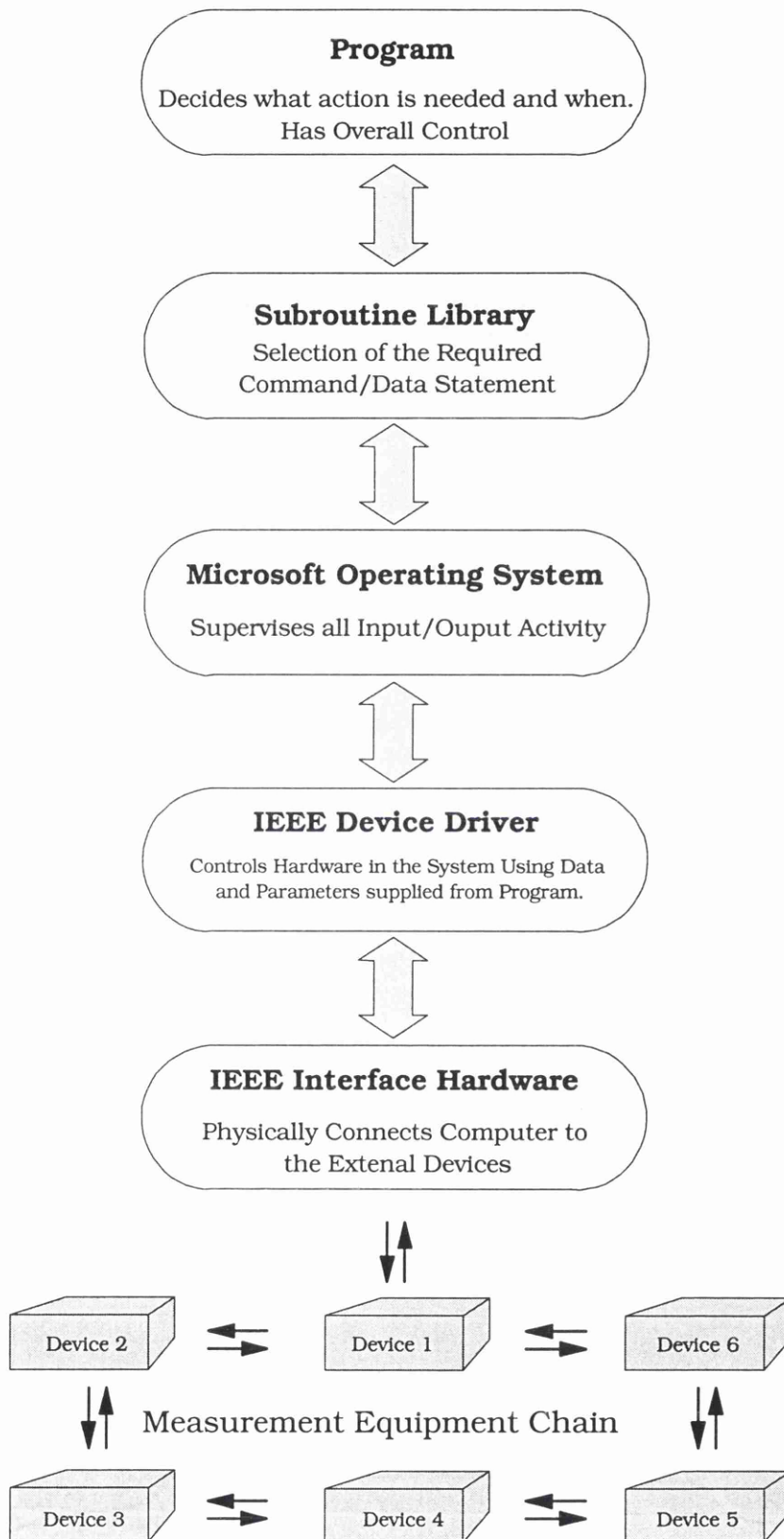


Figure 3.1 Schematic Diagram of the Software Command and Control Structure.

system dependant information as well as general information to help at the later stage of data processing. The sort of information prompted for was ; the type of membrane used, the permeant material and its concentration, duration of the pump to waste period (described in section 6.5.2), the duration of the 'baseline' data collection period, data sampling rates (different rates could be used in different sections of the same experimental run), textual descriptions of the experiment being undertaken for clarity in file selection at the processing stage and the filename with which to record the experimental and other data.

The user was then shown the current collecting volume solution temperature and asked whether or not to heat the cell contents. If answered yes, the desired temperature was input and the cell heater was switched on automatically. When the desired cell temperature had been reached, only then was the low concentration solution (usually distilled water) allowed to flow across the membrane surface, this was the beginning of the 'baseline' collection period.

For each of the input values set by the user, a valid range was pre-set as an added precaution against erroneous entry and should any value input be outwith the set range a warning was generated and the user prompted to re-enter the data correctly. In conjunction with this safeguard there were also

default values that could be used by merely pressing the 'return' key to speed up data entry.

The concentration step to be applied would only occur when one of two possible conditions were met, these were when; (a) the baseline period pre-set by the user had elapsed or (b) the user had overridden the baseline collection period (by a keypress). The data collection routine would now be sampling with the pre-set frequency and would only stop when either of two possible conditions were met; (a) the operator terminated the data collection via 'E' keystroke or (b) the maximum number of datasets had been collected (the normal maximum was 5000).

3.2.2 Oscillator Experiment

The input parameters required for an oscillator experiment were essentially the same as for the timelag system described above. There were however, two very important differences with the oscillator.

(a) the first value sought after the method of detection used was the number of oscillating frequencies to be used in the experiment. If this value was greater than one, then the square wave period, the number of these periods and the associated filename was required for EACH of the frequencies used in this now multi-frequency experiment.

(b) the method of the baseline (or warm-up) to be used had to

be selected. A choice of methods had been devised, these were (1) Cycles of a fixed frequency between the high & low concentration solutions; (2) Initially fast cycles but with a decreasing frequency or (3) low concentration only (as in the timelag experiment).

If either of options (1) or (2) were chosen an additional input section was activated i.e. the number of warm-up cycles to use before starting the data collection.

The use of multiple frequency runs was extremely useful but this presented a potential problem when switching from one frequency to another while maintaining one continuous experiment. This synchronisation problem was overcome by assuming that there was no (or at least an insignificant) phase shift between the input (square) wave and the emergent output wave. From this, half way through the period the wave concentration was assumed to be exactly halfway between the upper and lower concentration limits (set by the solutions being used). Using this assumption the second quarter switch time (this was a calculated value for the next switch) was changed from its previous calculated value to the value required by the new frequency. Using this method allowed the increase or decrease of the period without having to restart the experiment and therefore maintained identical experimental conditions without any disruption to the system. Once this

synchronisation was completed the calculated switch times (for the next switch) were reset to values determined by this new period in use. The maximum number of such frequency changes was limited to 10, this gave plenty of scope to the user and did not place too high a demand of computer system resource, mainly memory.

There was also the possibility of performing two different types of oscillator experiment. These were distinguished from each other by the filename extension used, either *.OSF or *.OSH when the collected data was saved to file. These two file extensions represent a full oscillation (*.OSF) about a mean collecting volume concentration or a 'half' oscillation (*.OSH) in which oscillation took place against an initial low (or zero) concentration value.

3.3 Display Outputs to System Operator

The graphical routines themselves represented a substantial effort in terms of programming. They are not described in any way here other than to show, by means of examples the text and graphical outputs shown to the system user. The display of information in real time back to the system operator was extremely important as this allowed for the user to determine (using their judgement) if the experiment was proceeding well or if there were any problems developing. The ability to make such decisions was extremely useful to prevent wasting time with experiments that were obviously at fault. To simplify this,

almost all of the system information was passed to the operator in a graphical format. This allowed for the operator to very quickly interpret trends in the data being collected, collecting volume temperature for example. All experimental data was recorded to data file at the end of every experiment for further processing.

3.3.1 Timelag Experiment Output

After the operator had input all of the experimental details if required, the cell heater would heat the collecting volume to the pre-set temperature (described in section 3.2.1) an example is shown in Figure 3.2. At this point the computer monitor displayed two data 'windows' of information simultaneously, the collecting volume temperature and the detected value (absorbance/ conductivity) in real time, these are shown in Figure 3.3. This allowed the operator to establish that the system was in a condition of equilibrium before the imposition of the concentration step. Immediately after the concentration step was imposed the monitor display changed from the two 'window' display to a single data area. This now displayed only the detected values from the cell (at the pre-set interval) but the cell temperature was displayed in text at all times and any variations could be monitored by pressing the F1 key. This toggled the display between the detected absorbance/conductivity and the cell temperature values since the imposed step. An example is shown in Figure 3.4

```
Conductivity has been selected as the Detector type.
You must now select the permeant CHLORIDE salt used :
a) H
b) K
c) Na
d) Li
e) Ba +2
f) Ca +2
g) La +3

Select Cation ?KCl
Membrane Type? Visking_V1
Permeant material? KCl
Duration for 'Pump to Waste' Period (0-20 secs.) 5
Max. Duration for BASELINE period (seconds 20-3600)1000
Time delay during Breakthrough Data Collection (seconds 0-60)2
Save collected data as filename ? prime
File Exists ! OVERWRITE (Yes/No)?Yes
MOLAR Conc. of permeant used for the conc. Step? .1078
Please enter a two line description of run
1st Line? Test run with Visking dialysis membrane with 0.1M KCl
2nd Line? Timelag determination 23/12/96_
```

Figure 3.2(a) Screen Capture of the Timelag Program
Parameter Input Section.

```
Interface initialised
Air Temp. 23.3°C
Collecting Volume 20.4°C
Warm reservoir (Yes/No)?Yes
Thermostat temp? 25.4
<Esc> to quit
```

```
Collecting Volume is now 20.2
```

Figure 3.2(b) Screen Capture of the Timelag Program
Cell Heating Period Showing the Current
Cell Temperature.

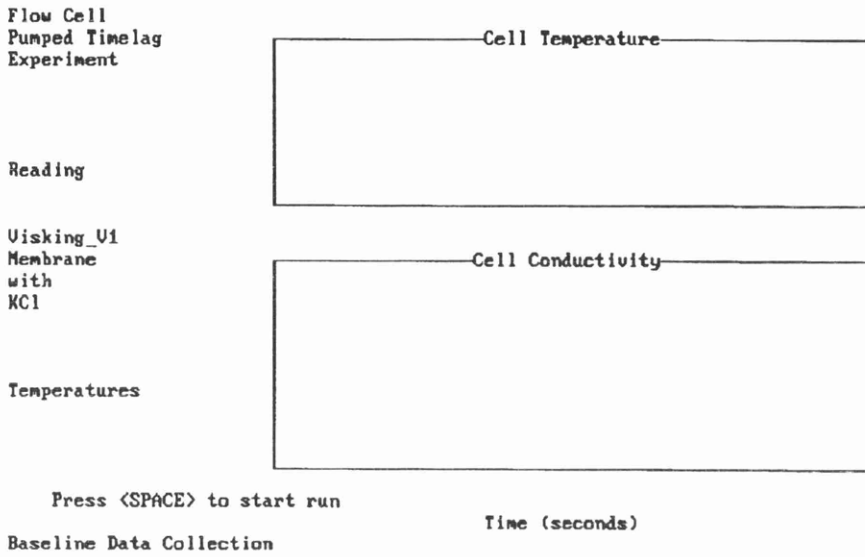


Figure 3.3(a) Screen Capture of the Timelag Program at the Run Initiation.

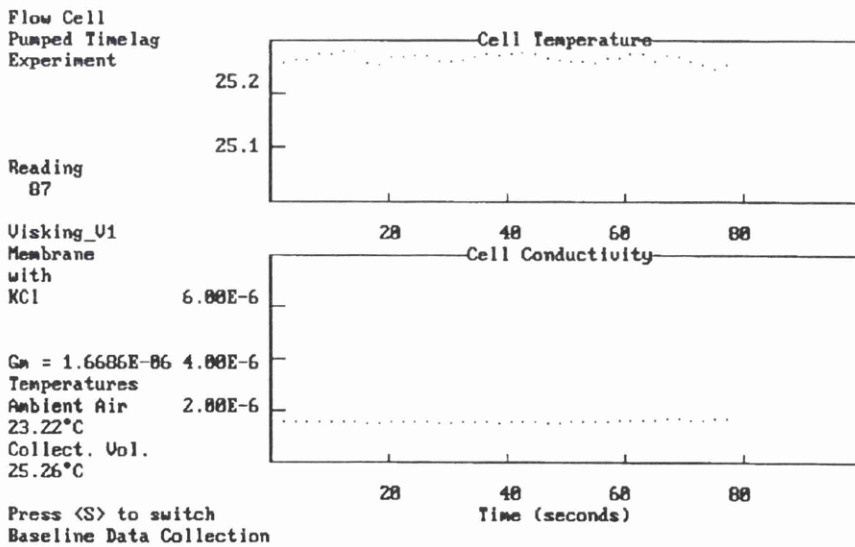


Figure 3.3(b) Screen Capture of the Timelag Program a Short Time into the Baseline Data Collection Period.

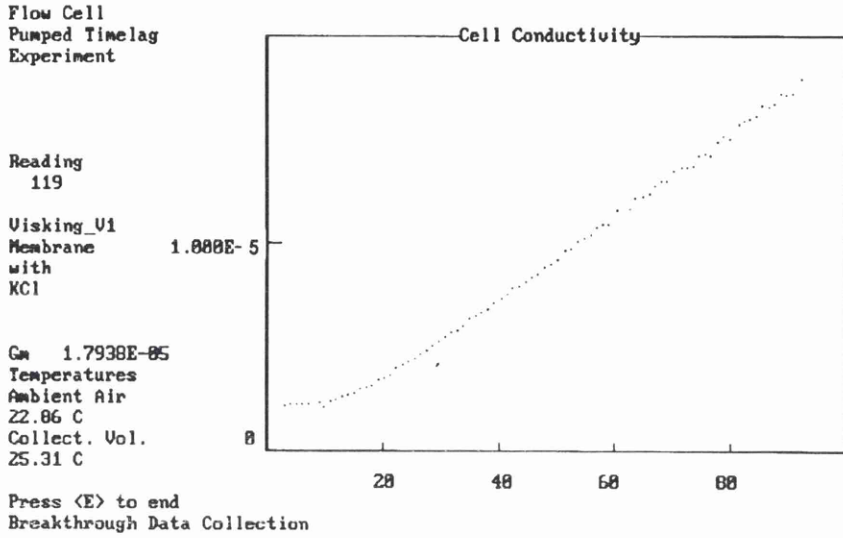


Figure 3.4(a) Screen Capture of the Timelag Program Shortly after the Concentration Step had been Imposed.

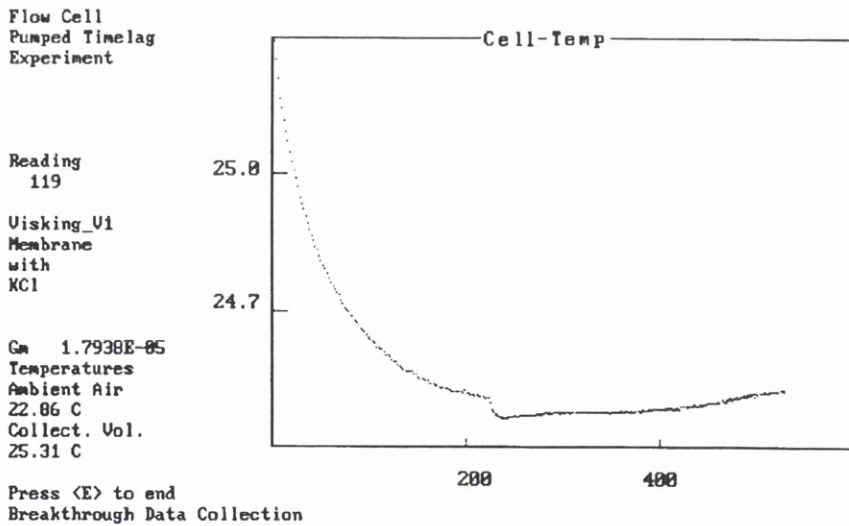


Figure 3.4(b) Screen Capture of the Timelag Program the Screen has been Toggled to Display the Cell Temperature.

3.4 Data Manipulation and Processing

The datafiles containing the raw experimental data were also processed and displayed using programs written specifically for the purpose. All of the calculations and data manipulations that required to be performed could be achieved by the operator using simple keystroke commands. This processing stage afforded the user a number of possible options.

Probably the single most important stage was the conversion of the collected detector data into concentration. The relationship between the concentration of the permeant material with elapsed time was critical and therefore great certainty of our methods was needed. In the experimental system here, two methods were routinely used for detection, electrolytic conductivity and optical density (absorbance), these will be described fully in sections 3.4.1 & 3.4.2. Permeant concentration was defined as the quantity of permeant divided by the collecting volume. From this basic definition it was clear that any error in either of these two terms would result in an incorrect value for the apparent cell concentration. The determination of the cell volumes will be described in Sections 4.2.2 (for gas) and 6.2.6 (for liquid).

3.4.1 Calculation of Cell Concentration from Absorbance Values

When a beam of light of intensity I_0 passes through a layer of solution the beam intensity can be attenuated due to interaction of the photons with an absorbing material in solution. The ratio of the attenuation with the incident beam is

more commonly known as Transmittance (T) and is denoted by Equation 3.1

$$T = \frac{I}{I_0} \quad 3.1$$

more commonly, the term absorbance (Abs) is used and this is represented by Equation 3.2

$$Abs = \log \frac{I_0}{I} \quad 3.2$$

the functional relationship between the quantity measured (in this absorbance method) and the analyte concentration is known as Beer's law and this can be written as

$$Abs = \log \frac{I_0}{I} = alc \quad 3.3$$

where a is the absorptivity, l is the cell pathlength and c the concentration.

If the concentration was expressed in mols per litre and the cell pathlength in centimetres then this proportionality constant, a is called the molar absorptivity and is given the symbol ϵ and therefore;

$$Abs = \epsilon lc \quad 3.4$$

(ϵ has units of $l \text{ cm}^{-1} \text{ mol}^{-1}$)

A rigorous proof of this law is outwith the scope of this work, this has been done previously elsewhere [1]

This linear relationship therefore permitted a simple method with which to experimentally determine the solution concentration. Deviations from this direct proportionality (at a constant pathlength) are however quite common. Beer's law is

successful in describing dilute solutions only and is therefore really only a limiting law. At concentrations below 0.01M there are very few deviations, so provided we can work within this constraint there should be very few problems. In the main, deviations from Beer's law are due to changes in the ϵ value as the refractive index of the solution changes with increasing concentration.

One aspect that was of particular interest was the relationship between different absorbing species in the same solution. Provided that there were no interactions among the various species the total absorbance for a multicomponent system could be obtained from Equation 3.5

$$Abs_{(total)} = Abs_1 + Abs_2 + \dots Abs_n = \epsilon l c_1 + \epsilon l c_2 + \dots \epsilon l c_n \quad 3.5$$

This represented a potentially very simple method for the study of coupled transport in membrane systems (provided of course that all of the components present absorb in the UV/Visible region of the spectrum.) Commonly the pathlength used for such systems is 1cm but in the cell used for this work (described in 6.2.2) the path length was 2.4cm. This made the system more sensitive at lower concentrations, which was greatly beneficial in this case but suffered from the problem of detector saturation at an earlier stage than would otherwise be 'normal'.

The construction of a calibration plot for each component

analysed was necessary if the absorbance values were to be accurately converted to concentration. This was done by careful preparation of a series of solutions at various concentrations of the solute material , the absorbance values of each being recorded. These were plotted with Absorbance as the X-axis and concentration the Y-axis and the resultant straight line was subjected to a least-squares method of analysis [2] to obtain the polynomial coefficients. Using these calculated values for the particular solute (at its lambda max.) the collected absorbance values were converted directly to collecting volume concentration (in suitable units). An example of this is shown in Figure 3.5

Molar Concentration

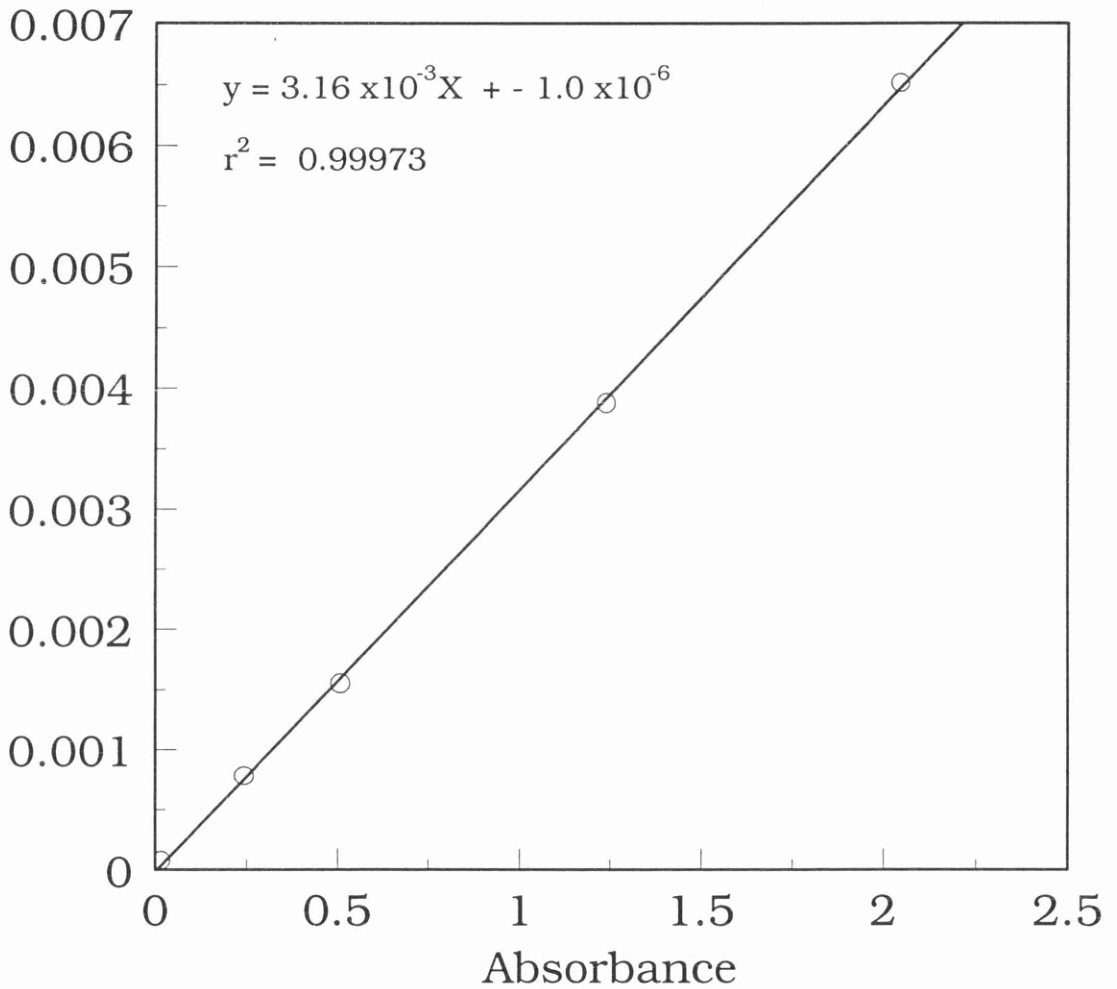


Figure 3.5 Beer's Law Plot of Absorbance versus Concentration for the Calibration of DL-Phenylalanine. Analysis Wavelength was 256.9nm

3.4.2 Calculation of Cell Concentration from Conductivity Values

For the great majority of the testing stages potassium chloride solutions were used, this has been generally accepted as the 'standard' whenever solution conductivity work was being carried out[3]. This was an extremely sensitive method but it did present some considerable problems when converting the conductivity values to a solution concentration. The molar (equivalent) conductivity of a salt solution could be calculated if the concentration of the salt was known. This is known as the Onsager limiting law [4] and can be represented in the form shown in Equation 3.6.

$$\Lambda = \Lambda_o - A\sqrt{C} \quad 3.6$$

where Λ_o is the molar conductivity at infinite dilution and C is the molar concentration of the salt and the term A takes account of the electrolyte relaxation and electrophoretic coefficients. This relationship was however only valid in very dilute solutions (<0.001M). The work of Shedlovsky [5] had extended the range of validity to close to 0.1M. This method is more useful however for extrapolation purposes to determine Λ_o . A more workable/practical method was the extended form of the Onsager limiting law shown in Equation 3.7.

$$\Lambda = \Lambda_o - (0.227\Lambda_o + 59.86)\sqrt{C} + 50C \quad 3.7$$

The specific conductivity, κ was calculated from the measured solution conductivity, G and the measurement cell constant.

The cell constant was a device dependant parameter which was associated with the cell geometry, electrode shape, area and the separation between the electrodes. The specific conductivity can be obtained from equation 3.8

$$\kappa = \frac{C\Lambda}{1000} \quad 3.8$$

and the cell constant from equation 3.9

$$\text{Cell Const.} = \frac{\kappa}{G} \quad 3.9$$

note $G = (G - G_0)$ where G_0 is the solvent conductivity.

The conductivity data were converted to solution concentration using an iterative method with equation 3.7.

An initial estimate was made using $C = (1000 \kappa / \Lambda_0)$ to start the calculation. A test of the accuracy of this method was made by feeding a κ value for a solution of 0.01M potassium chloride and the resultant calculated concentration was found to be 0.0099957M i.e. less than 0.05% in error. When this same test was applied to a 0.1M solution of potassium chloride the resultant concentration was 0.1032M, an error of 3%. It was clear to see that for high accuracy the concentration in the collecting volume must be kept low if this method was to be even considered, an upper threshold being imposed of 0.01M.

By using such a method it was possible to estimate quickly and relatively simply the concentration for a variety of

electrolytes due to the availability of excellent data for various thermodynamic transport coefficients[6]. It must be emphasised that this remains an approximation, however good and is not an absolute method.

A much more rigorous method was to produce a series of solutions of various concentrations of the electrolyte under investigation. The greatest possible accuracy was needed when using this method and this was very time consuming. Recrystallised (Analar) potassium chloride was dissolved in a known weight of distilled water (1Kg) to prepare a series of demal solutions covering a range 10^{-4} to 10^{-1} demal.

Each of these solutions were placed in the collecting volume cell and the temperature equilibrated at 25°Celsius at which time the conductivity was noted. These experimental conductivities (minus the conductivity of the distilled water used) were plotted against the solution concentration and a polynomial fit of the line was performed. Using the polynomial coefficients obtained, the experimental conductivity ($G - G_0$) was converted to a concentration. This conversion step was checked regularly by using a solution of known concentration. This procedure had to be repeated for each electrolyte used and was therefore not a simple or trivial task. The data obtained for potassium chloride are shown in Figure 3.6.

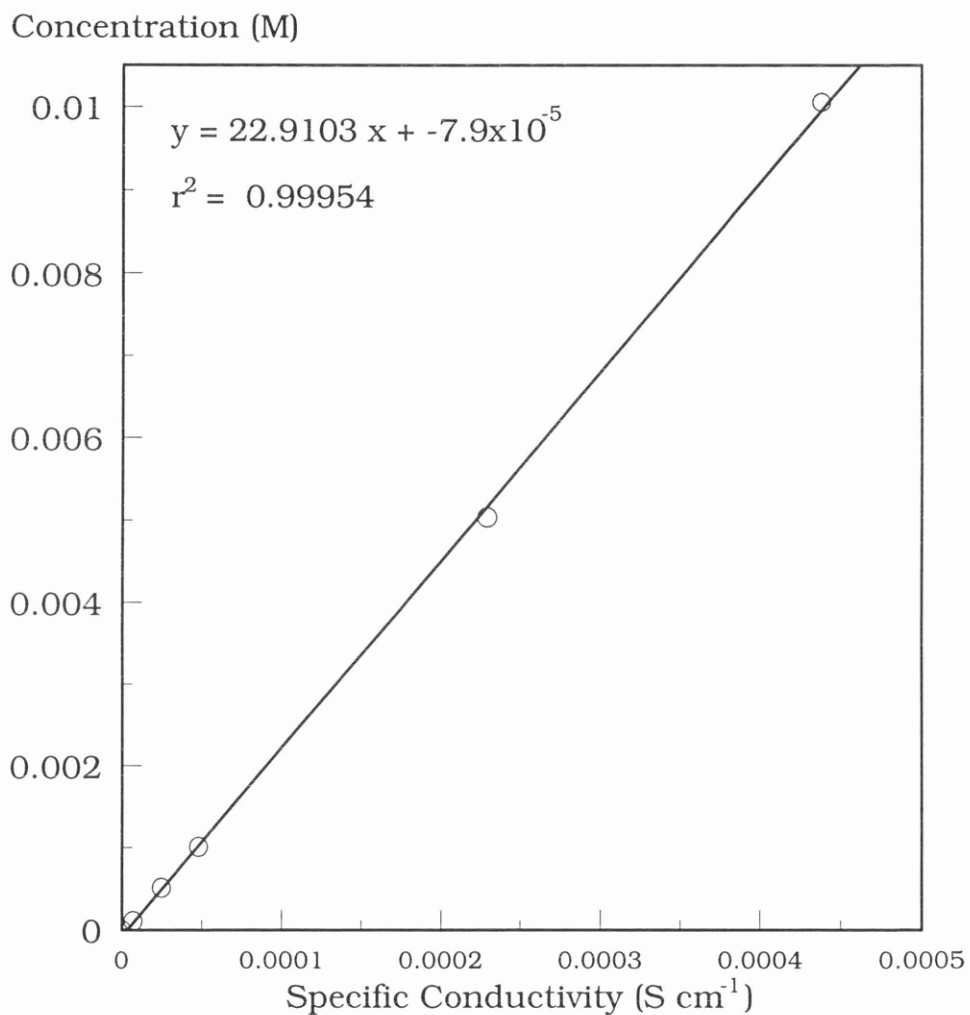


Figure 3.6 Specific Conductivity for Potassium Chloride solutions of known Concentrations at 298 K.

3.4.3 Display of Concentration Versus Time

The user had at their disposal the possibility for automated processing of any datafile, be it a timelag or oscillator experiment, an example of this is shown in Figures 3.7 and 3.8.

(A) Timelag Experiment

The timelag system was simple to process as there was only one applied concentration step and therefore only one timelag and one steady-state slope to be determined. The user was provided with a cursor to select a suitable 'baseline' area followed by a choice of a suitable portion of the rising steady-state profile. The two selected data regions were curve fitted and the resultant linear regression values were then used to determine their point of intersection (using simultaneous equations) on the time (X) axis, an example of this is shown in Figure 3.9. The exact time of the applied concentration step during the experimental run was known. The difference between the switch time and the point of the calculated intersection would result in the calculated timelag value, τ . The slope of the rising steady-state profile was also displayed to the user. It would now be a simple matter for the operator to obtain values for the diffusion coefficient and the distribution (solubility) coefficient respectively from this one experiment.

(B) Oscillator Experiment

This was made slightly more difficult due to the consecutive series of applied concentration steps. As in the timelag system the collecting volume concentration versus time is the default display. The process described for the timelag value previously, was essentially repeated as the times for all of the applied concentration steps were recorded in the datafile. For each step a timelag and a slope (and therefore a permeability value) could be obtained. This gave multiple estimates of these parameters in one experimental run, under identical conditions and this allowed the user the luxury of statistical analysis of the data.

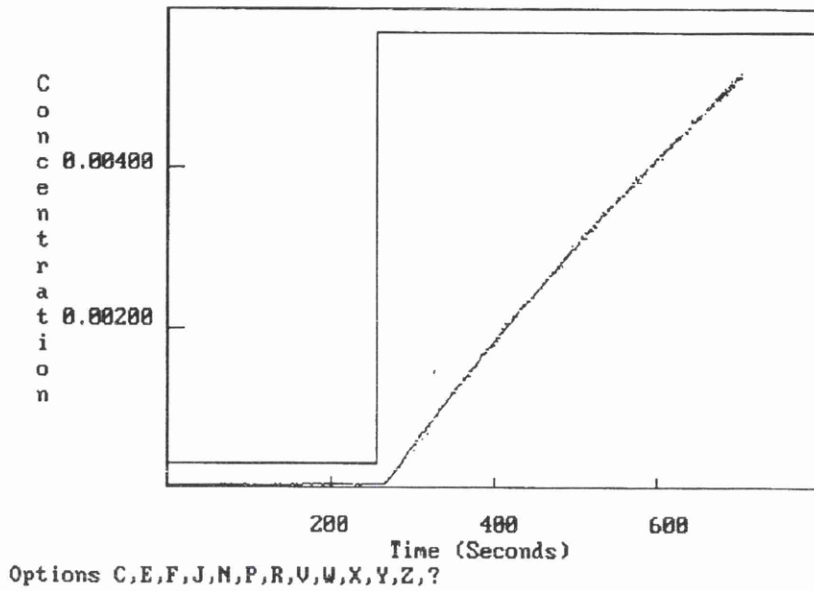


Figure 3.7(a) Screen Capture of Raw Data Display from Timelag Processing Program.

```

Command summary

C - Curve fit selected region (Orders 1-3 valid)
E - Exit this program
F - Fully expand graph - autoscale, no zoom
J - Connect or disconnect points
L - Change graph title
M - Mark or unmark points
N - New File load
P - Process to get breakthrough time
R - Manual rescaling of graph
W - Draw switching
X - Export screen data to A:\
Y - Set Y axis display
Z - Zoom in on points in selected region

? - Display this page again

Press <SPACE> to return to main display

```

Figure 3.7(b) Screen Capture of Plotting Options from Timelag Processing Program.

```
Y axis selection
A ..... Cell Concentration
C ..... Cell Conductivity (uncorrected)
D ..... Cell Conductivity (Temperature corrected)
T ..... Cell Temperature
-
```

Figure 3.8(a) Screen Capture of Y-Axis Display Options from Timelag Processing Program.

```
Electrolyte Conductivity Detection Used

Datafile reports permeant salt was NaCl
Infinite Dilution (LC) value 126.45
Conductivity of Distilled Water? 5e-7
MOLAR Conc. of Permeant Salt solution ?.1078
Conductivity of this Salt Soln. (in S/cm) ?2.392e-3
L0= 126.45 L calc = 122.4156
Cell const is 5.518043

Data ARE NOT temperature corrected
You are Strongly advised to correct Data before proceeding

Correct Data for Temperature (Yes/No)?Yes
Enter temperature ?25
Correction Factor (%)1.6_
```

Figure 3.8(b) Screen Capture of Input Section of Conversion to Concentration Routine from the Timelag Processing Program.

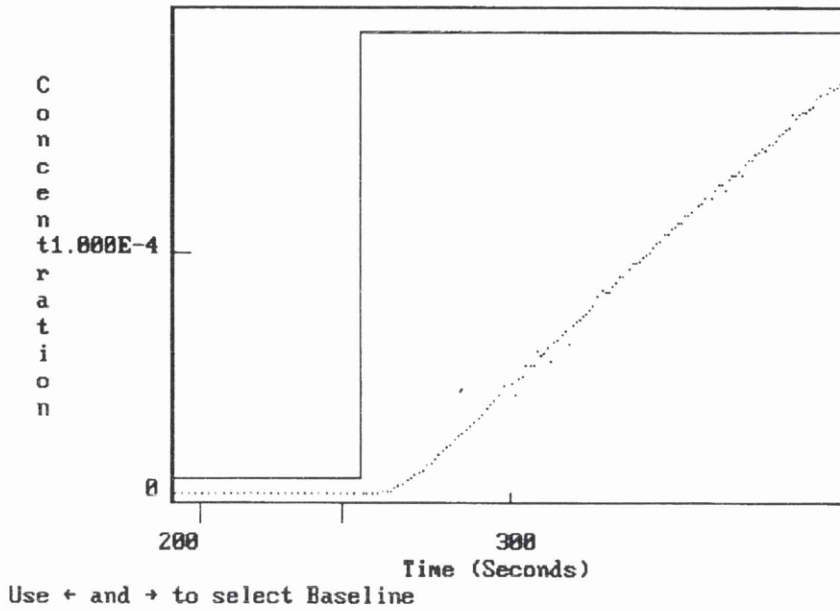


Figure 3.9(a) Screen Capture of the Baseline Selection During the Process Option (P).

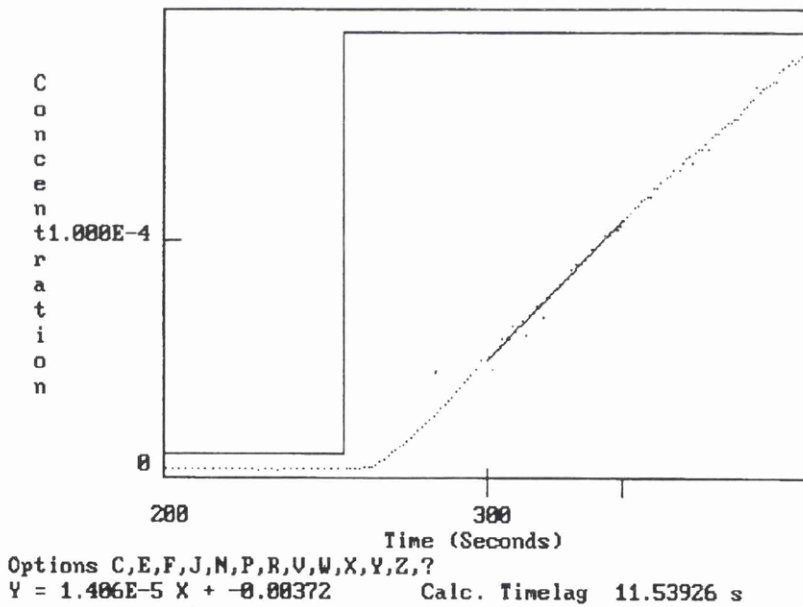


Figure 3.9(b) Screen Capture after the Slope Selection (Option P) and the Display of the Calculated Timelag, Least-Squares Equation and the Line it Describes.

3.4.4 Data Export

Any displayed information could be exported from the collecting system's data format to Lotus1-2-3™/Excel™ format for further analysis or presentation using commercial spreadsheets or presentation software. All of the experimental results to be shown in this study have been presented in such a manner. It was also possible to export data in an ASCII(text) format for direct plotting or printing etc.

As they stand the software modules that have evolved here are in a condition that could be used by any semi-skilled technician/operator within the membrane field. With very little extra work the programs could be upgraded to provide systems to rival any currently available commercial technical software. With minimal effort the programs could be transferred to a visual (Basic) language to allow the systems to be driven under the graphical Windows™ system, this is effectively an industry standard requirement today.

3.5 References

1. Swinehart, D.F., The Beer-Lambert Law, *J. Chem. Educ.*, 1962, 39, 333
2. Hood, W. G., Polynomial Curve Fitter, *Byte*, June 1987, 155-160
3. Jones, G and Bradshaw, B. C., The measurement of the conductance of electrolytes. V. A redetermination of the conductance of standard potassium chloride solutions in absolute units. *J. Amer. Chem. Soc.*, 55 (1933) 1780.
4. Onsager, L., *Physical Review*, 37, (1931), 405
5. Shedlovsky, T., An equation for electrolytic conductance. *J. Amer. Chem. Soc.*, 54 (1932), 1405.
6. Miller, D.G., Application of irreversible thermodynamics to electrolyte solutions. I. Determination of ionic transport coefficients l_j for isothermal vector transport processes in binary electrolyte systems. *J. Physical Chemistry*, 70, 8, 1966, 2639.

Chapter 4

Experimental Measurement of Gaseous Systems

Introduction

4.1 General Description.

4.2 Cell Design and Tests.

4.3 Cell Components.

4.4 Generation of a Gas Pressure Step.

4.5 References.

4 Experimental Measurement of Gaseous Systems

Introduction

In this chapter the testing apparatus related to the measurement of gaseous systems and other associated techniques developed in the course of this research will be described in detail. The designs and construction of the measurement cells will be given together with the methods used for the calibration and testing of the cells, the individual measuring devices and the overall measurement system.

Central to the entire system was computer control of the individual pieces of apparatus and also for automated data acquisition. Consequently there was a need for the development of customised software to enable both for the collection of the information and for the effective display and manipulation of the collected data. This is mentioned merely in passing in this chapter but was covered more fully in Chapter 3.

4.1 General Description

The gas permeation test system consisted of a measurement cell to which gas pressure sensors were fitted. These were in turn connected to a totally automated data collection system which recorded data at pre-set time intervals. The idea behind the system was to design a cell which would allow measurement of membranes with greatly differing permeability rates. This was accomplished by using a modular design in which the measurement cell consisted of three discrete parts. These were an input volume half-cell, an output (collecting volume) half-cell

and a membrane holder which was bolted in place between the inner faces of the two half-cells.

In all cases here, the permeabilities were derived from a 'time-lag' method which examined the response of a membrane to the imposition of a pressure step to one external face of the test membrane.

4.2 Cell Design and Tests

The gas permeation test cell was constructed from Polypenko™ (an ACETAL copolymer) which had excellent machining properties . It consisted of two half cells of identical geometry and a membrane holder which was screw clamped between the two half cells. Using this type of design allowed for the maximum flexibility in the use of the cell as membranes of different permeation rates could easily be accommodated by altering the exposed membrane area in the central membrane holder section or by changing the collecting volume.

Each half-cell consisted of basically a square sectioned block of Polypenko™ into which a chamber was made by boring out a cylindrical hole through the entire length of the block. This was tapped and threaded at one end only to allow for gas tight connectors to be fitted. Halfway along the length of each half cell and at 90° to the main chamber a second channel'was machined to allow for the attachment of the pressure transducers. These pressure transducers were fitted directly into the half cells and were the primary method of detection, no gas chromatography or mass spectrometry was used in this work as the object of this study was to design a system to look at the

fundamentals of gas transport . To this end only single gas permeabilities were studied. A schematic diagram of the system assembly is shown in Figure 4.1

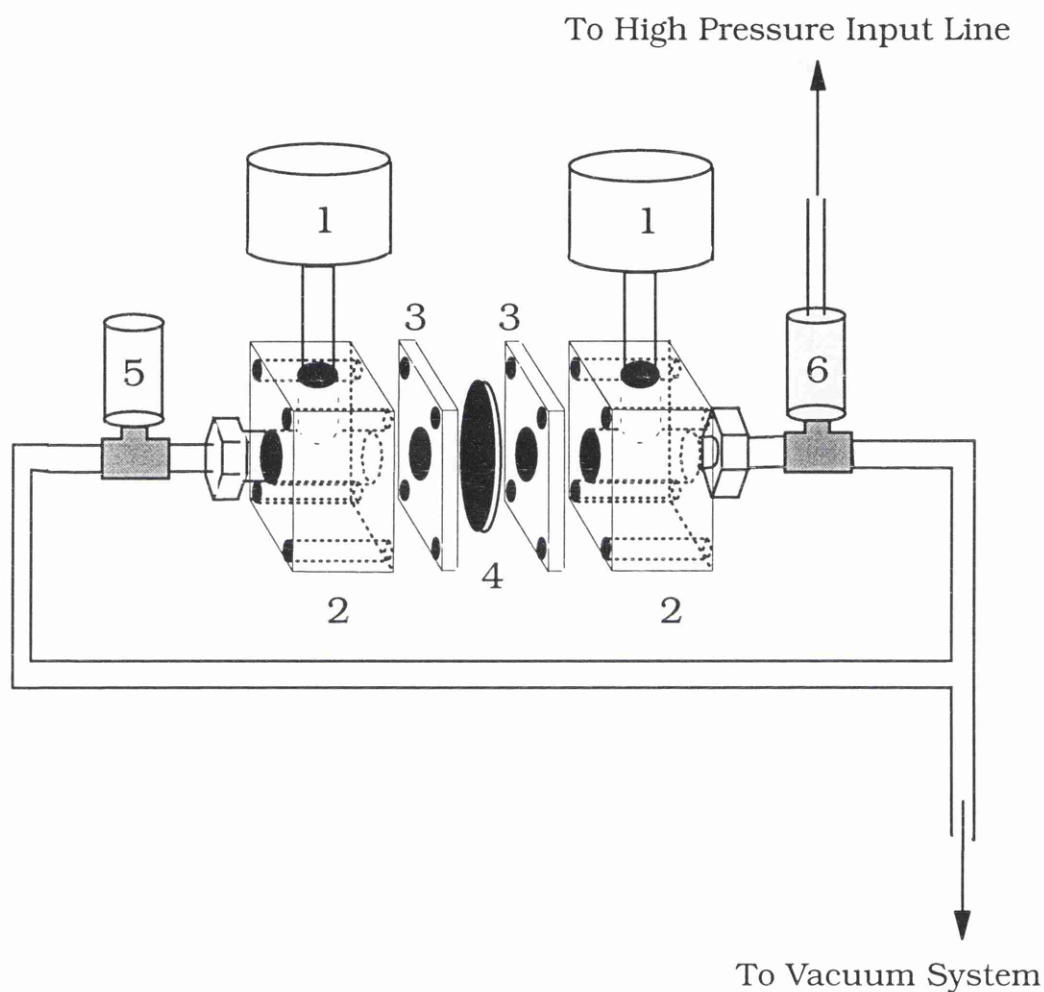
4.2.1 Gas Diffusion Cell Assembly

The two half cells and the central membrane holder were screwed together firmly to secure the system in place and also to ensure that there were no leaks from the faces or edges of the central membrane holder and the cell body. A two-way valve was attached to the collecting volume half-cell exit. This had been achieved using the smallest possible volume of copper tubing (in practice approximately 0.35cm^3). This was to ensure the smallest possible collecting volume as this in turn allowed for the maximum detection sensitivity, needed only for low permeability membranes.

At the inlet to the input half-cell a three-way valve was placed with the common output from this valve acting as the input to the cell. One of the two remaining lines was connected to the positive gas pressure inlet and the other to the vacuum system. By using only these two valves it was possible to generate a gas pressure step.

4.2.2 Determination of the Collecting Volume

The accurate determination of the collecting volume was essential. The gas cell was dried thoroughly and assembled (except the pressure transducers) and an impermeable Teflon



1. Pressure Transducer
2. Cell Body
3. Membrane Holder
4. Test Membrane
5. Collecting Volume Isolating Solenoid Valve
6. Three Way Solenoid Valve for Step Imposition.

Figure 4.1 A Schematic Diagram of the Gas Testing System

sheet placed in the membrane holder to blank off the collecting volume. The cell assembly was then weighed on an analytical balance (Mettler PJ400). The cell was then filled with degassed distilled water and allowed to reach a steady temperature of 20°C, it was then reweighed. From this weight difference and the known density of water at 20°C [1] the volume for the half-cell was obtained. This procedure was repeated twice and each time the same volume was obtained (7.873cm³).

As noted above, the pressure transducers were not included in the cell volume determination. There were two reasons for this. Firstly, the mass of the transducers were such that the range of the analytical balance was unable to cope with them. Secondly and more importantly, the pressure transducers were fitted with a protective porous frit at the entry to the sensing compartment. For this reason, it was not possible with a high degree of certainty, to ensure that the head volume was completely full and free from air bubbles. The technical literature supplied stated that the head volumes were 8.3cm³ but there was no simple way in which this could be checked.

As the total approximate volume of the collecting volume was 16.667cm³ (this included the Ultra-Torr™ fitting to attach the pressure transducer) even an error of 0.2cm³ in the head volume would result in an error greater than a 1% .

In an attempt to remedy this problem an additional larger

secondary volume was constructed. This consisted of an Ultra-Torr™ tee-piece some 6mm copper tubing and a small gas lecture bottle. The volume of this was determined in the same manner as described above (161.78cm^3) and this was placed between the collecting volume exit and the isolating solenoid valve. This now gave the system an approximate volume of 170.57cm^3 . Using this new value for the cell volume the same 0.2cm^3 error in the pressure transducer head volume would result in a volume error lower than the precision of the pressure transducer (0.15%).

4.2.3 Testing for Collecting Volume Error

With a polycarbonate $0.015\ \mu\text{m}$ track etched type membrane fitted in the cell, nitrogen test diffusion experiments were made on the gas flow through this membrane. On treatment of these test data, if the two cell volume values were correct the slopes obtained when the gas flows were plotted against pressure difference should be identical to within experimental error. However, if there were any discrepancy between the two tests, the smaller volume system would be more sensitive to volume errors due to uncertainty in the transducer head space volume. Duplicate test runs were made with both volumes. For the larger volume system the gas flows measured were reproducible to 0.14% and for the smaller volume to 0.16%, this was the experimental error between identical runs.

However, the slopes of the two different volumes tested differed by 5.5% (the smaller volume having the smaller slope). This suggested that there was indeed a difference in the transducer head space from the value quoted in the accompanying literature. The two test runs are shown in Figure 4.2. By analysis of these test data a volume correction was calculated to correct for this discrepancy. (This was achieved by solving two simultaneous equations each using the measured slope values and the observed error between the two runs.) The calculated volume correction was 1.128 cm³. Using this new calculated value (17.795 cm³ for the small volume) the two test runs were reprocessed and replotted, these are shown in Figure 4.3. The new values obtained for the slopes were 6.989x10⁻⁷(larger volume) and 6.982x10⁻⁷ mols.m².s⁻¹.kPa⁻¹(for the smaller volume) a difference of 0.1%.

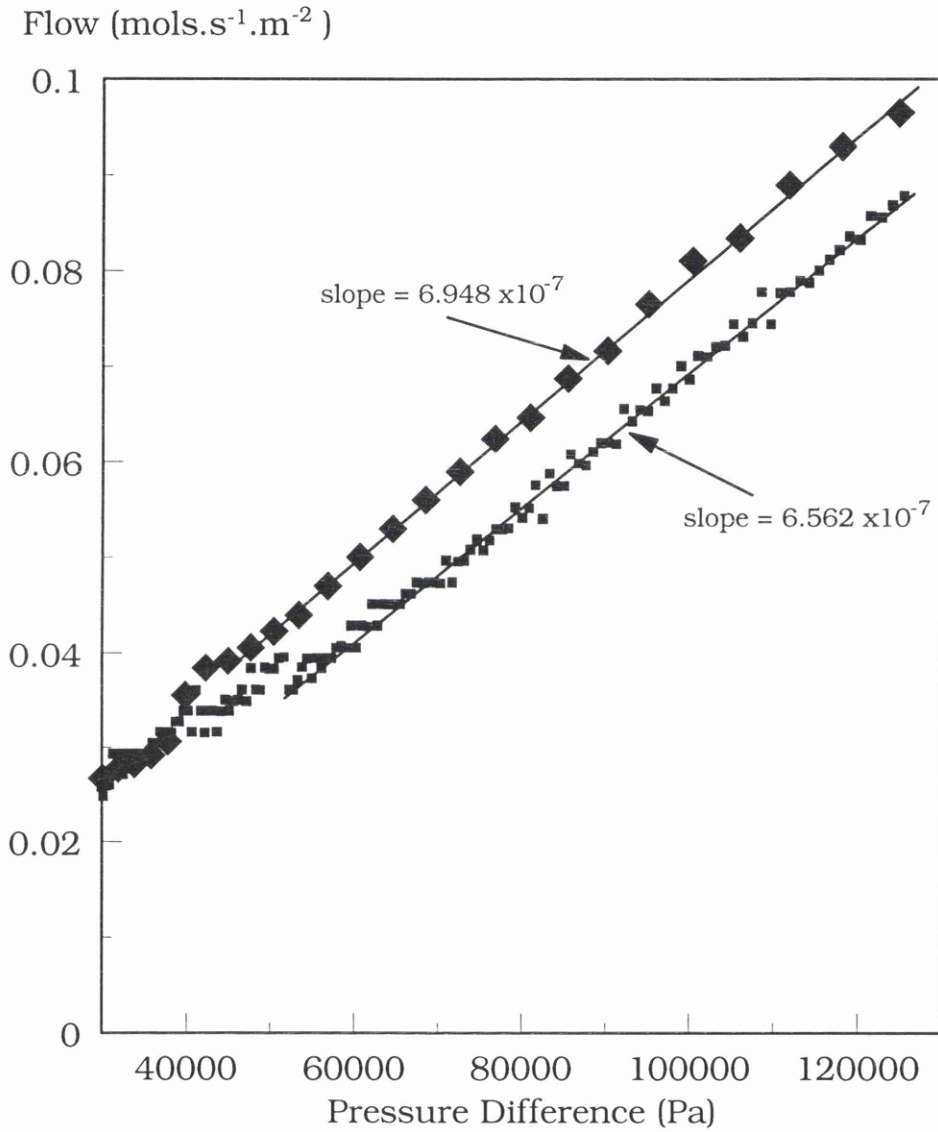


Figure 4.2 Comparison Tests For Nitrogen Flow through a Polycarbonate Track-Etched membrane(0.015 μ m) with Two Different Cell Volumes.

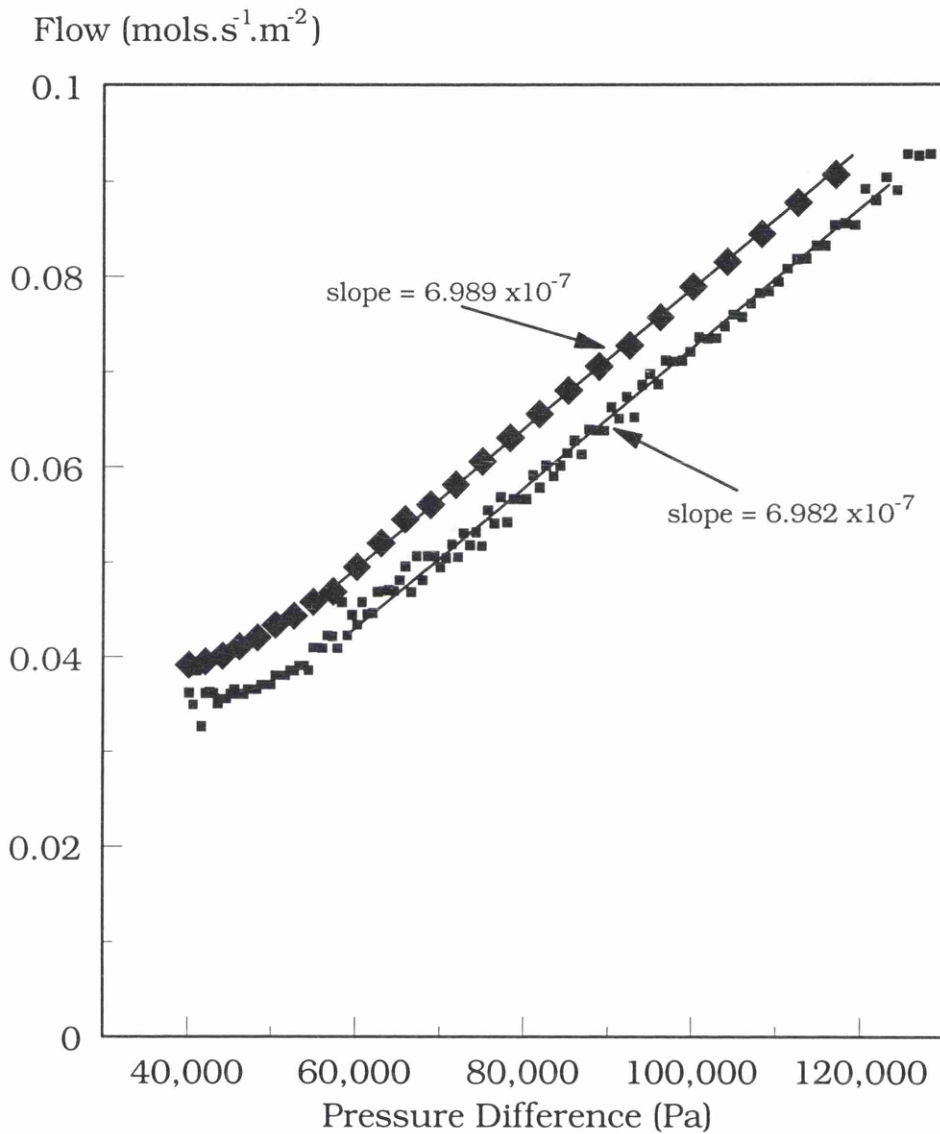


Figure 4.3 Comparison Tests for Nitrogen Flow through a Polycarbonate Track-Etched membrane (0.015 μ m) with Two Different Cell Volumes and after Applying a Volume Correction.

4.3 Cell Components

The measurement cell for gaseous systems (Figure 4.1) comprised of several component parts. The function of each is described in this section.

4.3.1 Pressure Transducers

A range of pressure transducers were used in this work in order to cover the widest range of pressures (from vacuum to moderate positive pressures) with the greatest possible accuracy. The pressure transducers used primarily in this work were of the Barocel 600 Edwards High Vacuum series. These were capacitive diaphragm type gauges and allowed for precise measurement (0.15% precision) over a wide input pressure range with excellent long term stability.

Since the pressure was sensed by electrically measuring a pressure induced displacement of a thin metal diaphragm, the calibration accuracy should be unaffected by the chemical composition/nature of the input gas. The product literature [2] even claimed that radioactive gases and liquids could also be monitored without effecting the accuracy (in these studies this was not tested.) The transducers produced a voltage (analogue) output signal which was claimed to be directly proportional to the pressure. The 15 Volt DC excitation required by these transducers was provided by a CPD100

combined transducer display and power supply module (Chell Instruments Limited, UK.)

4.3.2 Calibration of Transducers

The transducers provided a linear output voltage in the range 0 to +10 volts DC depending upon the applied pressure. The linearity of the outputs were checked on a regular basis (typically once per month) to ensure that they maintained their high precision (0.15%). Using a high vacuum system with dual rotary pumps and an oil diffusion pump, the transducer zero values were established. A range of input pressure values were then generated using a gas feed from a bottled Nitrogen cylinder to which a three stage cylinder regulator was fitted. In series with this and to allow for the fine adjustment of the feed pressure a Norgren Martainair Limited (U.K) RO7 series back pressure flow regulator was fitted. The analogue outputs from the transducers were then passed through the Programmable Gain Amplifier (PGA) module to the Analogue to Digital Converter (ADC) in the Microlink housing . This process could be repeated at pre-set time intervals, since each reading takes about 65 microseconds this sets the maximum scanning rate possible. The output voltages were plotted against applied pressure and the linearity checked. A typical example of a calibration profile is shown in Figure 4.4.

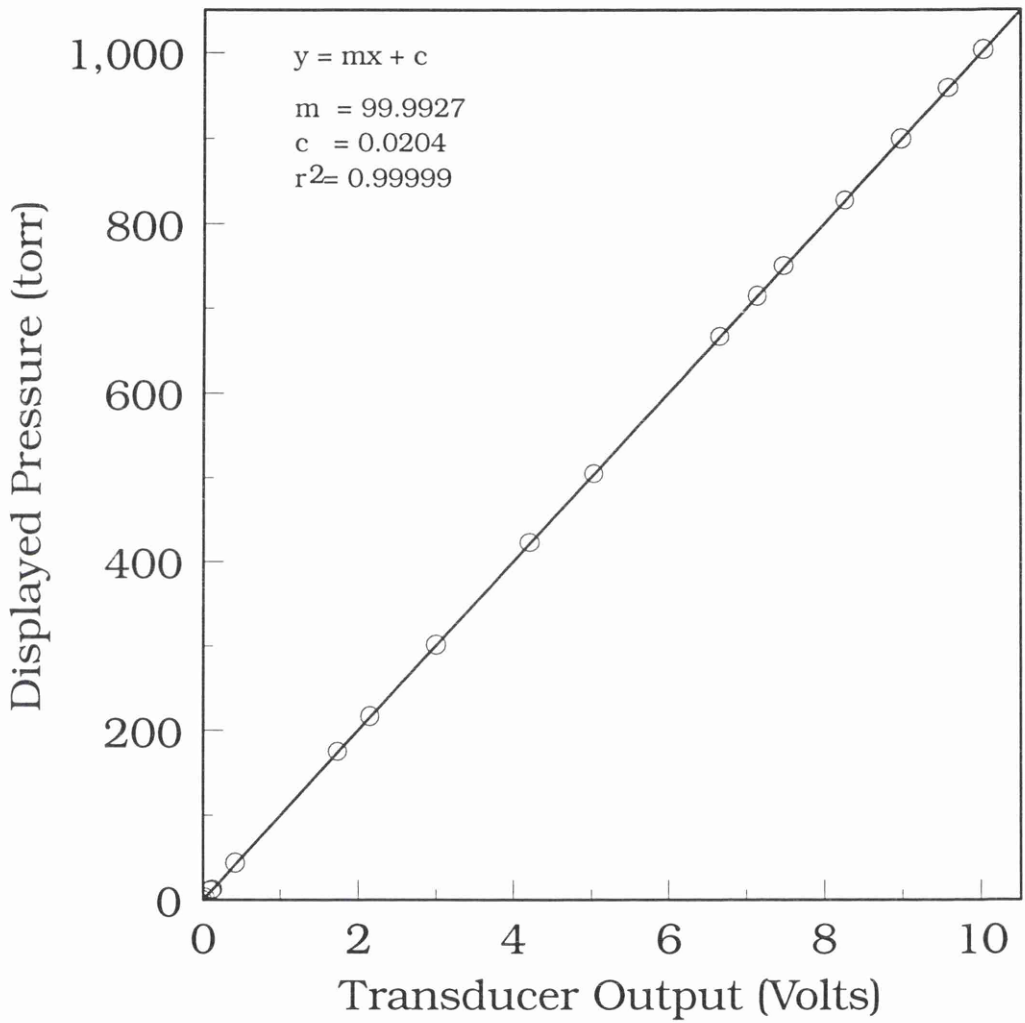


Figure 4.4: Plot of the Collecting Volume Pressure Transducer Voltage Output versus the Displayed Pressure.

4.3.3 Tubular Connections and Fittings

The gas cell was connected to a vacuum pump and the positive gas pressure inlet by way of 6 mm copper tubing. All of the cell connections and pipe adapters used in the system were Cajon™ Ultra-Torr™ fittings. These were stainless steel bodied and designed to provide vacuum tight seals with quick finger tight assembly. They were also reusable unlike the more conventional Swagelok™ fittings and could be reused time and time again on glass, metal and even some types of plastic tubing. These fittings were rated to be consistently Helium leak free and have been tested to a rate of 4.0×10^{-9} atm,cm³.s⁻¹ [3].

4.3.4 Solenoid Valves

The type of valves chosen for use in these studies were Angar Scientific Company (USA), Direct Acting Solenoid Valves (Model Numbers 340 and 341). These were straight-through (2 way) and tee-format (3 way) valves respectively. They were 12 Volt DC latching valves and required that an actuating voltage be passed for only a short time (less than 1 second). They did not require any holding current to maintain their position. Each valve also had a double coil assembly. When an electrical pulse was applied to the 'opening' coil the valve opened and maintained its position by means of a magnetic latch. When a voltage pulse was applied to the 'closing' coil of the valve, it closed and maintained this position by way of a spring load.

This had two advantages, firstly the valves did not heat up due to continuous current flow in the coils and secondly there was no possibility of electrical noise generated by the coils to interfere with the pressure measurement signals, both of these factors were major problems with earlier systems. The valves were also physically small, 4cm high and 1 cm in diameter and had a small internal volume (0.10cm³). They had a response time of 2.8 milliseconds to open and 7.8 milliseconds [4] to close. These combined attributes made them an excellent choice for this type of application.

4.4 Generation of a Gas Pressure Step

As stated in the General Introduction, the chosen method for the study of the permeation rates in this work was by the sudden imposition of a pressure or concentration step at one face of the test membrane and then to monitor the consequent emergent flows. The successful generation of a sharp (instantaneous) pressure step was central to the efficacy of the timelag systems. In this instance the pressure step was generated using a series of valves triggered remotely by the controlling computer system.

4.4.1 General Procedure for the Production of a Gas Step

Using a double stage rotary vane vacuum pump (Edwards High Vacuum 2SC20A) both half cells were evacuated. Under computer control, the valve at the collecting volume exit was closed. This isolated the collecting volume from the vacuum

pump and at this point the 'baseline' data collection commenced for the user predefined period. At the end of this period, a voltage pulse to the three-way valve caused the rapid changeover (2.8mS) of the valve and the vacuum was replaced by the desired positive gas pressure. Purely as an added precaution, to avoid overloading and damaging the pressure transducers, the gas input line was protected by a manually adjustable in line pressure regulator (Omnifit (U.K) Limited, Model 3102). This was normally adjusted (manually) to a value just below the maximum permissible transducer pressure.

4.4.2 Pressure Step Calibration Test

A special test experiment was carried out to determine the minimum time base that could be used with confidence in this system and to ascertain the 'sharpness' of the step. In this test two independent computer systems were used, one to measure the pressure transducers only and the other to control the valve switching and all other 'normal' system functions. In this way the data collection speed was increased slightly and the uncertainty in the time base therefore minimised.

The data collection system was started with the maximum data reading rate (15 readings per second) and almost simultaneously the second (controlling) computer was started for its sequence of valve switching and control. The entire process was repeated several times to establish the

reproducibility of the step. Two examples of this are shown in Figures 4.5 and 4.6 in which a pressure step of 1010 torr was applied at the 'inlet' face of an impermeable Teflon sheet placed in the membrane holder.

By analysis of the data shown in Figures 4.5 and 4.6 the maximum pressures attained were 1009 and 1008 torr respectively for the two test example runs shown. In both of these cases (and in the other tests not illustrated) a pressure value greater than 99% of the final pressure was achieved in 1.3 seconds.

Having now being satisfied with the calibration of the gaseous system components, the gas testing apparatus was ready for use.

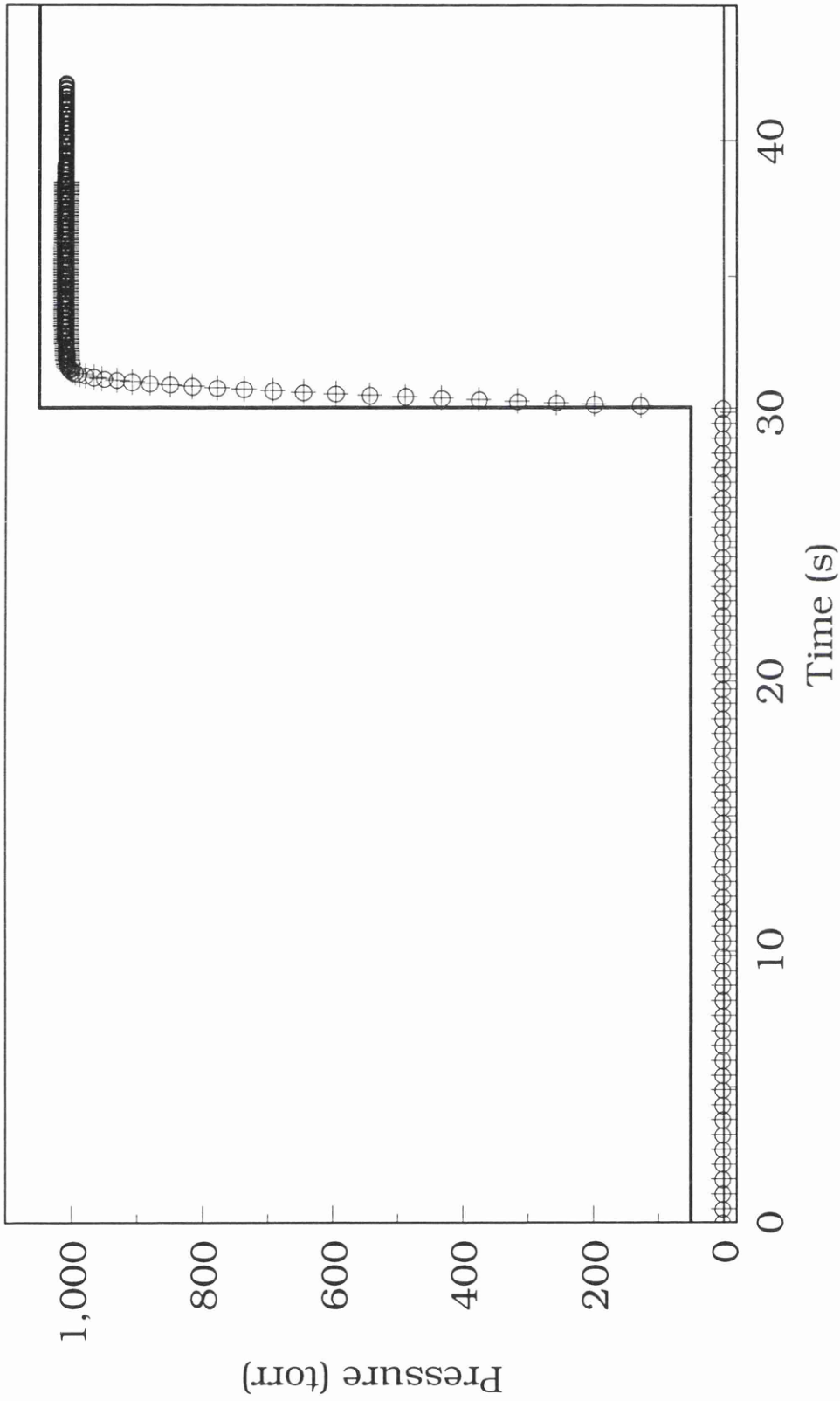


Figure 4.5: Measured Response of the Gas System to an Imposed Pressure Step of 1010 torr. Two examples are superimposed to show the system reproducibility. The switches occurred at 30.26 seconds(o) and 30.27 seconds(+).

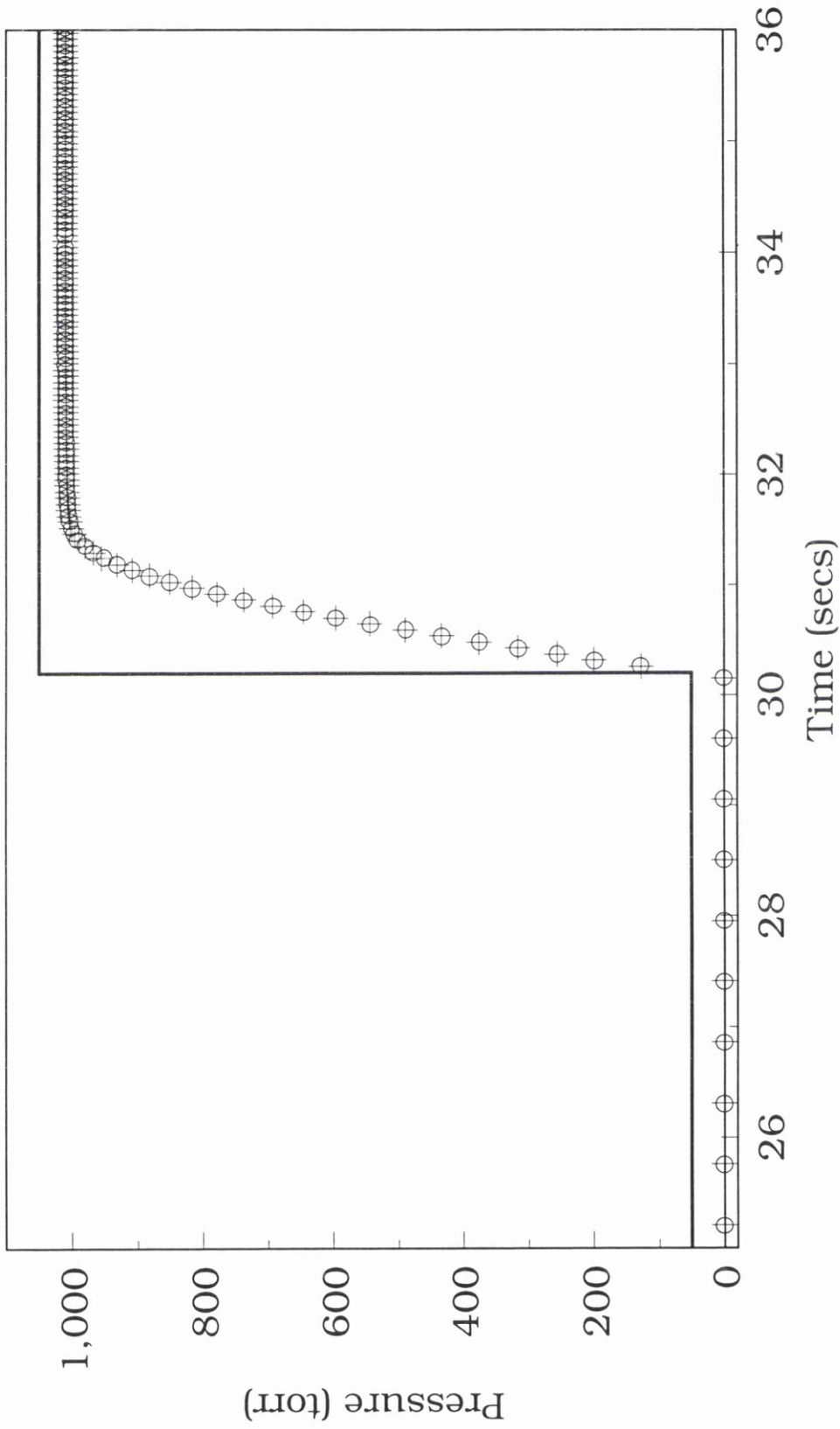


Figure 4.6: Close-up view around the time of the applied pressure step.

Two examples are superimposed to show the system reproducibility.
The switches occurred at 30.26 seconds(o) and 30.27 seconds(+).

4.5 References

- [1] Chemical Rubber Company, Handbook of Chemistry and Physics, 75th Edition , 1995, David. R. Lide (Editor-in-chief), CRC Press, ISBN 0-8493-0596-9.
- [2] Edwards High Vacuum International, (Wilmington, MA, USA.) Model 600 Barocel Capacitive Manometer Instruction Manual, W609-00-020, Issue B, July 1992.
- [3] Cajon Co, (Ohio, USA) Technical Brochure Ca-687, 6-87-125M-BL, MS-01-32.
- [4] Angar Scientific Company Inc., (Cedar Knolls,N.J.,USA) Technical Literature Form Nos. AV-001R.

Chapter 5

Membrane Characterisation Using the Gas Permeation System

Introduction

- 5.1 Background
- 5.2 Experimental Data Treatment
- 5.3 Experimental
- 5.4 Results and Discussion
- 5.5 Conclusions
- 5.6 References

5 Membrane Characterisation Using the Gas Permeation System.

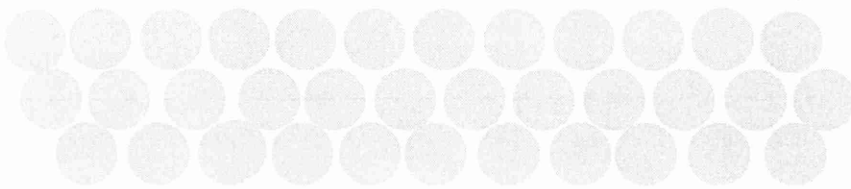
Introduction

The transport of material will be effectively determined by the structure of the membrane. These structural properties of the test system will determine the mechanism of transport and therefore its rate. In gaseous systems the conventional driving force is a concentration difference, although the preference is to describe this in terms of the partial pressures (Henry's Law). Porous membranes, these could be polymeric or inorganic/oxide membranes, will influence the gas flow depending upon two main physical properties; (a) the effective pore size and (b) the pore geometry of the membrane in question. A great variety of these two parameters can be found in commercial membranes today, examples of these are shown schematically in Figure 5.1.

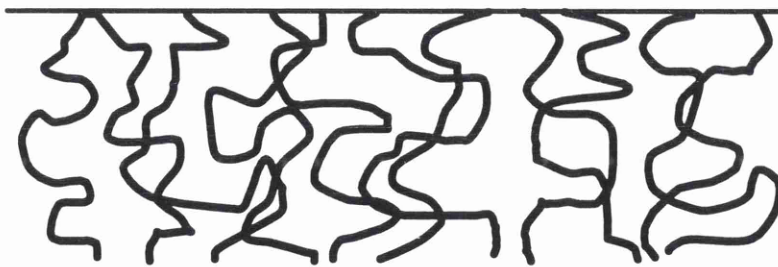
With microfiltration membranes, the structural properties tend to be uniform across the membrane thickness (symmetrical) and so the membrane resistance to flow extends across the entire thickness. With ultrafiltration and nanofiltration membranes these generally have an asymmetric structure in which an active (top) layer determines the overall membrane resistance. In non-porous membranes (although there must be pores of some description to allow gas flow) gas transport/separation will be governed by different mechanisms. These membranes require more demanding operating conditions e.g. higher operating pressures, higher engineering demands which in turn will result in higher installation and running costs. It is this type of



(a)



(b)



(c)

Figure 5.1 Schematic Representation of the Possible Pore Geometries Present in Membranes.

membrane that has historically been used in membrane gas experiments and there is a huge literature that has amassed as a result.

The emphasis of this current study was to examine the porous type of membrane with respect to gas permeation and therefore the rubbery/glassy classification of polymer membrane will be effectively ignored in this work.

Of the structural types shown in Figure 5.1 (a) the parallel pore geometry was chosen for the preliminary tests. These were anodic alumina membranes prepared using methods developed in earlier work [1]. The membranes obtained in this manner had somewhat special features that made them an ideal system to study initially. They had a uniform planer structure with regular parallel pores set in hexagonal arrays perpendicular to the surfaces. Membranes could be produced in an extremely reproducible manner with predetermined structural properties such as pore size and membrane thickness. This allowed for the testing of the gas transport mechanism and (it was hoped) the determination of the effective pore size of the membrane. Other structural types were also tested, these were ceramic membranes of different pore sizes and geometries, one being a disc in the ultrafiltration range the other a tube format of nanofiltration pore size.

5.1 Background

There is a huge literature covering the transport of gases (and liquid vapours) through porous materials. A few of the key references related

to this current are cited here [2-10]. When this involves more than one geometrical structure or layer(s) the mechanism can change (governed mainly by the pore size). For porous membranes (1-200 nm pore size) there are three significant mechanisms accounting for the gas flow, these are surface, Knudsen and Poiseuille flows.

Surface diffusion occurs when the gas molecules interact strongly with the pore wall, or are even physically/chemically absorbed. Knudsen flow occurs if the size of the pore is smaller than the mean free path of the gas molecules. Under these conditions the gas molecules collide with the pore more frequently than with each other and so the lighter gases travel through the pore more rapidly than the heavier molecules. With Poiseuille flow (sometimes called viscous flow) the gas molecules collide exclusively with each other and effectively do not even 'see' the pore. It is clear that there can be no separation in this regime. The three mechanisms are represented schematically in Figure 5.2. In general the gas flux density across a membrane , per unit area per unit time is defined by

$$J = P \Delta p \quad \text{Equation 5.1}$$

where J is the gas flux density ($\text{mol.s}^{-1}.\text{m}^{-2}$), P is the permeability ($\text{mol.s}^{-1}.\text{m}^{-2}.\text{Pa}^{-1}$) and Δp is the pressure difference (Pa)

5.1.1 Poiseuille (Viscous) Flow

For the Poiseuille mechanism, assuming that we have a structure as shown in Figure 5.1 (a) then it can be shown that

$$J_p = \frac{\epsilon r^2 \mu_p}{8\eta RT} \cdot \frac{\Delta p}{l} \quad \text{Equation 5.2}$$

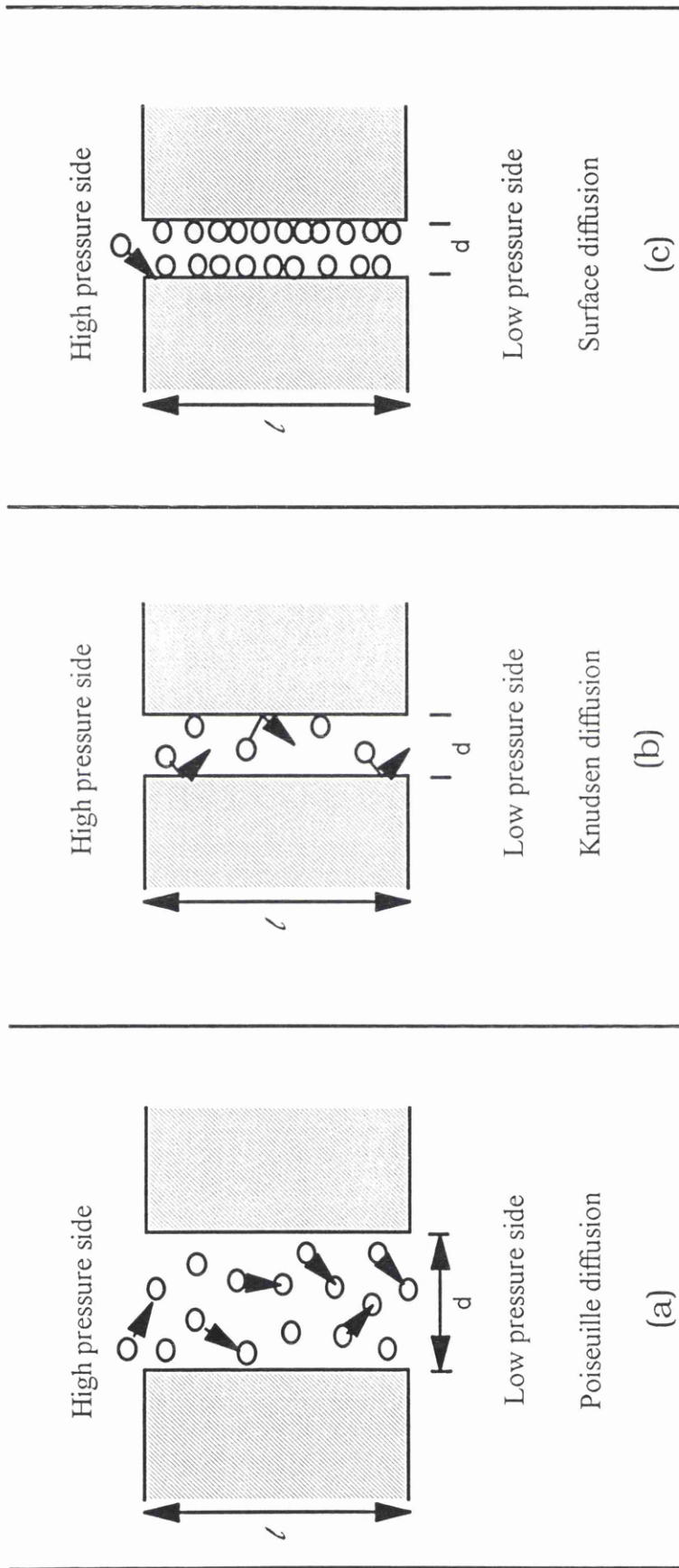


Figure 5.2 Schematic drawing showing possible membrane gas transport mechanisms: (a) Poiseuille, (b) Knudsen and (c) Surface diffusion.

where ϵ is the membrane porosity, η the gas viscosity (Pa.s), μ_p the pore tortuosity (unity in this case), Δp is the pressure difference (Pa), l is the membrane thickness (m), R is the gas constant ($8.314 \text{ J.mol}^{-1}.\text{K}^{-1}$) and T the temperature (K).

This indicates that the flux will be proportional to the applied driving force (pressure) across the membrane, the pore radius (r^4) and inversely proportional to the viscosity of the gas.

5.1.2 Knudsen Flow

The mean free path of a gas (λ) can be defined as the mean distance travelled by a molecule between collisions. In liquids the molecules are very close together and the mean free path is extremely small (a few nm) and so Knudsen diffusion can be totally ignored in liquid systems. The mean free path of a gas however, depends upon the pressure and temperature and so can be defined by

$$\lambda = kT / (\pi d^2 p \sqrt{2}) \quad \text{Equation 5.3}$$

where d is the gas molecule diameter (m) and T the absolute temperature.

It can be seen that as the pressure decreases the mean free path would increase and this would be proportional to temperature at constant pressure. For the membranes used in this study the pore sizes varied in the range 5 to 200 nm and therefore it was expected that Knudsen diffusion would have a significant effect [11, 12, 13]. The contribution to the flux by a Knudsen regime can be shown to be

$$J_K = \frac{2\varepsilon\mu_K v r}{3RTl} \Delta P \quad \text{Equation 5.4}$$

where ε is the membrane porosity, μ_k is the tortuosity factor, r is the mean pore radius (m) and v the gas velocity (m.s⁻¹). Remembering that the gas velocity can be described by

$$v = \sqrt{\frac{8RT}{\pi M}} \quad \text{Equation 5.5}$$

where M is the molecular weight of the molecule (kg.mol⁻¹)

From this relationship (Equation 5.5) it is obvious that the gas flux is dependant upon the square root of the molecular weight and from this, that separation between gases will be proportional to the inverse of the square root of the molecular weight. This is in some respects as was predicted initially in Graham's law of Effusion in 1846 [14] but this omitted the geometrical contribution of the pore in the separation process, described by Knudsen[15]. This means that there is a limiting separation factor (α) described by

$$\alpha = \sqrt{\frac{M_b}{M_a}} \quad \text{Equation 5.6}$$

where M_a and M_b are the masses of molecules a and b respectively.

5.1.3 Surface Diffusion

Surface diffusion/transport occurs due to strong interaction of the gas and the pore wall surface. This process can be described in a number of different ways the most commonly

accepted being the random walk model. This is based on a two dimensional form of Fick's law

$$|J_s| = A \rho_{app} D_s \mu_s \frac{dq}{dl} \quad \text{Equation 5.7}$$

where J_s is the surface transport (kg.m^{-3}), A is the outer surface (m^2), ρ_{app} the apparent density (kg.m^{-3}), D_s is the surface diffusion coefficient ($\text{m}^2.\text{s}^{-1}$) and dq/dl the gradient in surface occupation.

On rewriting the surface diffusion transport [16] it can be shown that

$$|J_{os}| = \frac{|J_s|}{\Delta p} = \frac{2\varepsilon\mu_s D_s}{\bar{r} A_o N_A} \frac{dx_s}{dp} \quad \text{Equation 5.8}$$

where μ_s is the surface diffusion shape factor, A_o is the surface occupied by one molecule (m^2), N_A is Avogadro's constant and χ_s the fraction of surface covered (in relation to the monolayer value).

From this relationship, the surface flux will increase as the pore size (r) decreases. However, the actual surface diffusion is dependant upon the product of the $(D.\text{d}\chi_s/\text{d}p)$. On a given surface the quantity of material absorbed will be larger at higher absorption energies. The energy of diffusion (which is coupled to the absorption energy) also increases and this acts to lower the surface mobility. In general, the occurrence of surface diffusion only acts to decrease the possibility of separation when a Knudsen mechanism is in operation, the

exception being for hydrogen on metal surfaces.

For the anodic alumina membranes used here, the pore sizes were in the range approximately 20 -70 nm. With these three mechanisms taken into account the permeability, P as represented in Equation 5.1 may have some contribution from each and so could be broken down into these three components as shown in Equation 5.9

$$J = P_{tot} \Delta p = (P_{Poiseuille} + P_{Knudsen} + P_{Surface}) \Delta p \quad \text{Equation 5.9}$$

5.1.4 Determination of a Suitable Transport Mechanism

For membranes with pore sizes smaller than about 100 nm and at low gas pressures, the contribution to the gas flux by the poiseuille and surface diffusion can be neglected and the gas transport would be determined due only to the Knudsen diffusion term

$$P = P_k = \frac{2\varepsilon\mu_K v r}{3RTl} \Delta P \quad \text{Equation 5.10}$$

By substituting the mean gas velocity and porosity terms into Equation(5.10) we can obtain

$$P = P_K = \frac{8\eta\mu_K r^3}{3l} \left(\frac{2\pi}{RTM} \right)^{\frac{1}{2}} \quad \text{Equation 5.10(a)}$$

and as the value of $\frac{8\eta\mu_K}{3} \left(\frac{2\pi}{RT} \right)^{\frac{1}{2}}$ will be a constant (B) we can rewrite Equation (5.10a) as

$$P = \frac{B r^3}{l \sqrt{M}} \quad \text{Equation 5.11}$$

5.1.5 Membrane Structural Considerations

In order that a membrane have good separation qualities and a high flux rate it requires very small pore sizes and extremely thin active layers, something of a dichotomy in practical terms. In practice it is not feasible to have extremely thin unsupported porous layers (yet) and so some sort of support structure is needed to add mechanical strength and resilience. This leads to the formation of asymmetric membranes, this is true for polymeric and inorganic membranes.

For a multi-layer membrane of n layers (normally not more than three in practice) if each individual layer obeys the Knudsen criteria independently, the total permeability, P can be related to the individual layers, as in Equation (5.11) and show a root M relationship

$$\frac{1}{P_m} = \frac{1}{P_1} + \frac{1}{P_2} + \dots + \frac{1}{P_n} = \sqrt{M} \left(\frac{l_1}{Br_1^3} + \frac{l_2}{Br_2^3} + \dots + \frac{l_n}{Br_n^3} \right) \text{ Equation 5.12}$$

where P_m is the composite permeability, P_n the individual layer permeabilities, B constant from Equation (5.11) which is membrane dependant, M is the molecular weight of the gas, l_n is the thickness of each layer and r_n the mean pore radius of each individual layer.

Provided that we can produce membranes with suitable layer structures of known thickness and pore size and the layers

follow a Knudsen regime, it should be possible to obtain data that accurately reflects the area of interest, the active layer.

5.2 Experimental Data Treatment

In all of the experiments performed in this present study, an instantaneous pressure step was generated at one face of a membrane to produce a transmembrane pressure difference. The measurement cells and the associated methods were described fully in Chapter 4. Due to the pressure difference generated across the membrane, gas permeates through the membrane from the high to the low pressure side of the cell. In these experiments the input half cell was maintained at a constant pressure, p' and as the experiment proceeded the pressure in the collecting volume half cell, p'' , increased. These pressures were monitored by pressure transducers. The low pressure side (collecting volume) had a known volume, V , and the rate at which the gas permeated, dn/dt , could be evaluated from the gas pressure increase, dp''/dt from

$$p'' V = nRT \quad \text{Equation 5.13}$$

from this, the rate of the gas permeation becomes,

$$\frac{dn}{dt} = \frac{V}{RT} \cdot \frac{dp''}{dt} \quad \text{Equation 5.14}$$

If this is defined as a gradient per unit area of membrane, A

$$J = \frac{1}{A} \cdot \frac{dn}{dt} = \frac{V}{ART} \cdot \frac{dp''}{dt} \quad \text{Equation 5.15}$$

In general, $\frac{d\Delta p}{dt} = \frac{dp'}{dt} - \frac{dp''}{dt}$ but in this case $\frac{dp'}{dt} = 0$ because p' is maintained at a constant level, and so $\frac{d\Delta p}{dt} = -\frac{dp''}{dt}$ substituting for $\frac{dp''}{dt}$ in Equation (5.15) this becomes

$$J = \frac{V}{ART} \cdot -\frac{d\Delta p''}{dt} \quad \text{Equation 5.16}$$

When the system is in the steady state, $\frac{d\Delta p}{dt}$ is constant and Equation (5.16) can be approximated to

$$J = -\frac{V}{ART} \cdot \frac{d\Delta p}{dt} \approx -\frac{V}{ART} \cdot \frac{\Delta p}{\Delta t} \quad \text{Equation 5.17}$$

where V is the collecting volume (m^3), A the exposed membrane area (m^2), T is the absolute temperature (K), Δp is the transmembrane pressure difference (Pa).

Using Equation (5.17) the experimental flux density could be determined from the values recorded during the experiment, the pressures in the input and output half cells and the elapsed time since the run commenced. From the slopes of the plots of gas flux versus transmembrane pressure, the permeability could be obtained directly from the slopes ($\text{mol}\cdot\text{s}^{-1}\cdot\text{m}^2\cdot\text{Pa}^{-1}$).

5.3 Experimental

The experimental systems used have been described in detail in Chapter 4. It only remains to reiterate that in this current research only single (pure) gas experiments were performed. All of the gases used were supplied (in Labcan™ format) by Messer Griesham Gases, Germany, with the exception of Nitrogen (Oxygen free) which was supplied by BOC Ltd, UK. All gases were of 99.99% (or better) purity, a

summary of their physical properties are shown in Table 5.1.

The membranes were secured in a holder of well defined area and each experiment was performed in triplicate at 293K. The experimental data was collected and processed using software written specifically for this task. The raw data was treated as described in section 5.2 above, and the gas flux (J) determined when the system was in the steady-state condition.

Gas	H ₂	He	CH ₄	N ₂	O ₂	Ar	CO ₂	i-C ₄ H ₁₀
M _w (g/mol)	2	4	16.04	28.02	32	39.94	44	58.12
λ(nm)(a)	111	174	-	59	63	63	55.0(b)	-
σ(Å)(c)	2.89	2.6	-	3.64	3.46	3.4	3.3	-
v(m/s)(d)	1760.7	1245	621.8	470.6	440.2	393.7	375.4	326.7
η(Pa.s)x10 ⁶	9	20	11.2	17.9	20.8	22.9	15	-

Table 5.1 Summary of Physical Properties of Gases Used for Permeation Studies.

(a) Mean free path (λ) of gases at pressure of 1 atm and 273 K [32]

(b) Mean free path (λ) of the gas CO₂ at 1 atm and 298 K [33].

(c) Minimum kinetic (sieving) diameters (σ) from the zeolite literature [34].

(d) Velocity of gases (v) calculated using the Equation $(8RT/\pi M)^{1/2}$ at 293 K.

(e) Viscosity data taken from CRC Handbook of Physics and Chemistry at 300K.

5.4 Results and Discussion of the Gas Permeability System

In this section the results of the gas permeation studies will be discussed. For each of the membrane systems to be investigated in this research, the actual membrane, that is the composite membrane, and the associated support material alone were available. As a great number of commercial membranes are in fact multi-layer membranes, it was important that the contribution of the support structure was known, if any significant attempt was to be made at characterising the active layer alone as the active layers tend to be extremely thin in relation to the support media. It was shown earlier, Equation (5.12), that the total permeability of a system is the sum of the component parts. From this, it was clear that if we could obtain accurate information for the support alone and the composite (asymmetric) membrane, then it would be possible to resolve the effect and contribution of the active layer in isolation as shown in Equation 5.18.

$$\frac{1}{P_{layer}} = \frac{1}{P_{Composite}} - \frac{1}{P_{Support}} \quad \text{Equation 5.18}$$

We must keep in mind that in sections 5.1.4 and 5.1.5 it was stated that gas permeation was due exclusively to a Knudsen mechanism, even in the composite. If any additional layer did not satisfy this constraint the data handling method chosen here would clearly not be valid. For this reason, each contributing layer in each membrane was checked to ensure the Knudsen mechanism was in operation. If this were not the case, some alternative method of interpretation would become necessary. Experimental precision was typically $\pm 5\%$.

5.4.1 Anodic Alumina Membranes

In this type of membrane we have an idealised structure with regard to pore size, geometry, tortuosity and thickness. Membranes were prepared by an electrolytic method [17] that allowed for the control of most of these parameters. This type of membrane has itself been the centre of a great deal of research[18, 19] but in this current study we make use of them purely as 'test' systems. SEM pictures of these membranes are shown in Plates 5.1 and 5.2.

Two basic tests were performed here (i) the effect of thickness to the gas flow in a single homogeneous layer and (ii) the effect of producing a multi-layer (2 layer) system in which the active layer thickness was varied.

In the first instance, three membranes were prepared. All were homogeneous of nominal pore size, 70 nm but of increasing thickness, 48, 80 and 128 μm , these were labelled SAA1, SAA2 and SAA3 respectively.

Secondly, the 48 μm 'support' was chosen as a base material and on the leading face of this an active layer was grown with a nominal pore size of 20 nm. The thickness of the active layers were 9 and 22 μm and these were labelled LAA1 and LAA2 respectively.



Plate 5.1 SEM photograph of an Anodic Alumina Membrane.
Cross sectional view showing the regular and parallel
pore structure.

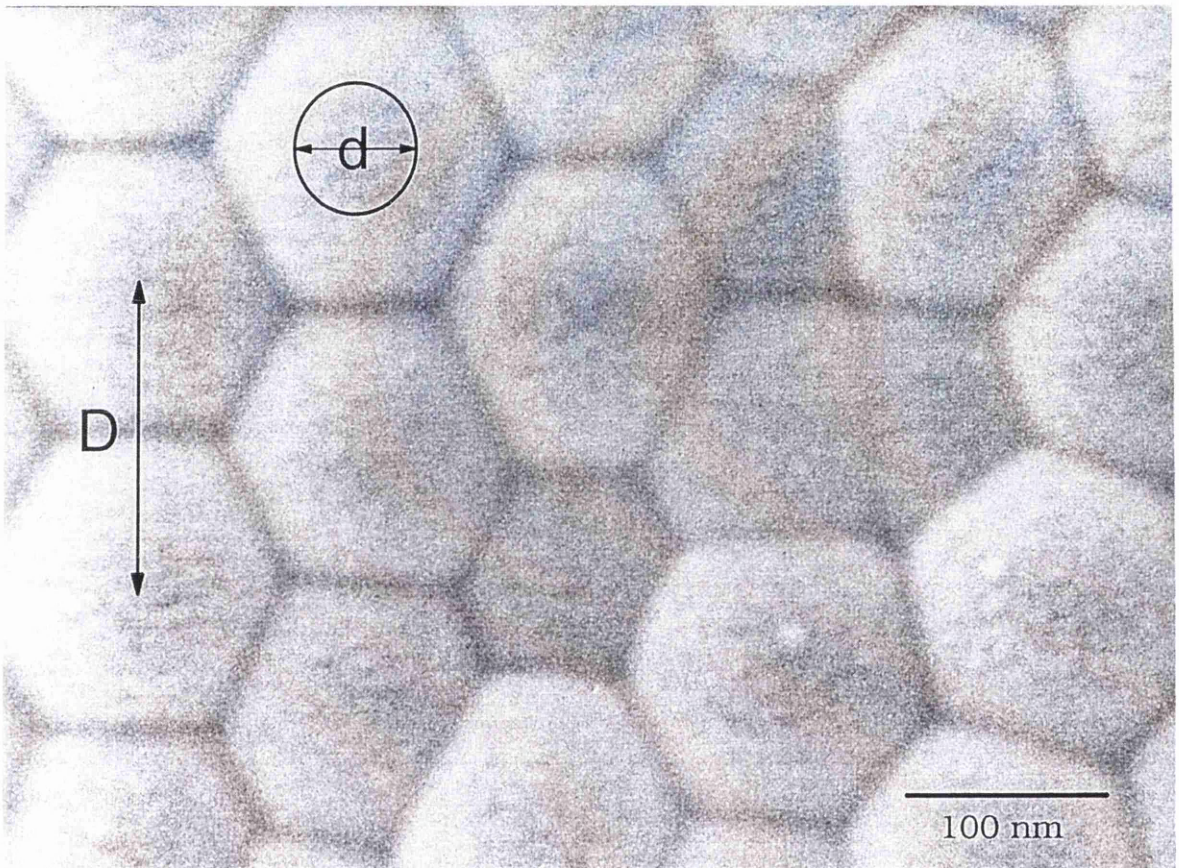


Plate 5.2 SEM photograph of an Anodic Alumina Membrane. Planer view showing the regular hexagonal array of the cell structure. D denotes the centre to centre distance and d the pore diameter

For each membrane, the three supports and two bilayer samples, the transmembrane pressure dependence of the flux (for several gases) at constant temperature are shown in Figures 5.3 to 5.12. The observed gas fluxes were linear with upstream gas pressure indicating that the permeabilities were constant over the period of the experiment.

As stated earlier (in section 5.2) the permeabilities were calculated directly from the slope of these experimental lines. The obtained experimental permeabilities for each membrane are summarised in Table 5.2. By choosing to prepare bilayer membranes using the 48 μm 'support' (SAA1) with a further applied layer, the permeabilities of the layer alone can be determined using Equation (5.18). The 'support' having a permeability, P_b , and the composite membrane (LAA1 or LAA2) having a permeability, P_{ab} .

To assist with clarity, due to the variation in thickness of the samples, it was clearer to normalise the data as the product of the permeability and the thickness, ($P.l$), these data are shown in Table 5.3, for the symmetric 'support' membrane and Table 5.4 for the asymmetric samples.

From the data it was clear to see that there was a general decrease in the permeability values as the molecular weight of the gas increased. It was also clear that the addition of the active layer dramatically reduced the total gas permeability

(P_{ab}) shown in Table 5.2. This was not unexpected, as there was a pore size reduction (from 70 to 20 nm) at the interface between the support and the top layer structure but the magnitude of the effect was surprising. With the presence of a 9 μm active layer (LAA1) the permeability of the composite membrane was reduced by an average of 58.9% and for the 22 μm layer (LAA2) the reduction was 74.3% in relation to the total permeability of the samples (data taken from Table 5.5). Furthermore the difference in thickness by the addition of the active layers were only 15% and 31% for LAA1 and LAA2 respectively.

At the preparation stage the alumina films do not actually show pores through their entire thickness. At the initial interface with the aluminium substrate and the electrolyte a continuous 'barrier' layer is formed. It is only when this is removed (conventionally by chemical dissolution) that the pore structure is revealed. Gas permeation studies with a 'barrier' layer film, shown in Plate 5.3, proved that no gas transport occurred across the barrier layer.

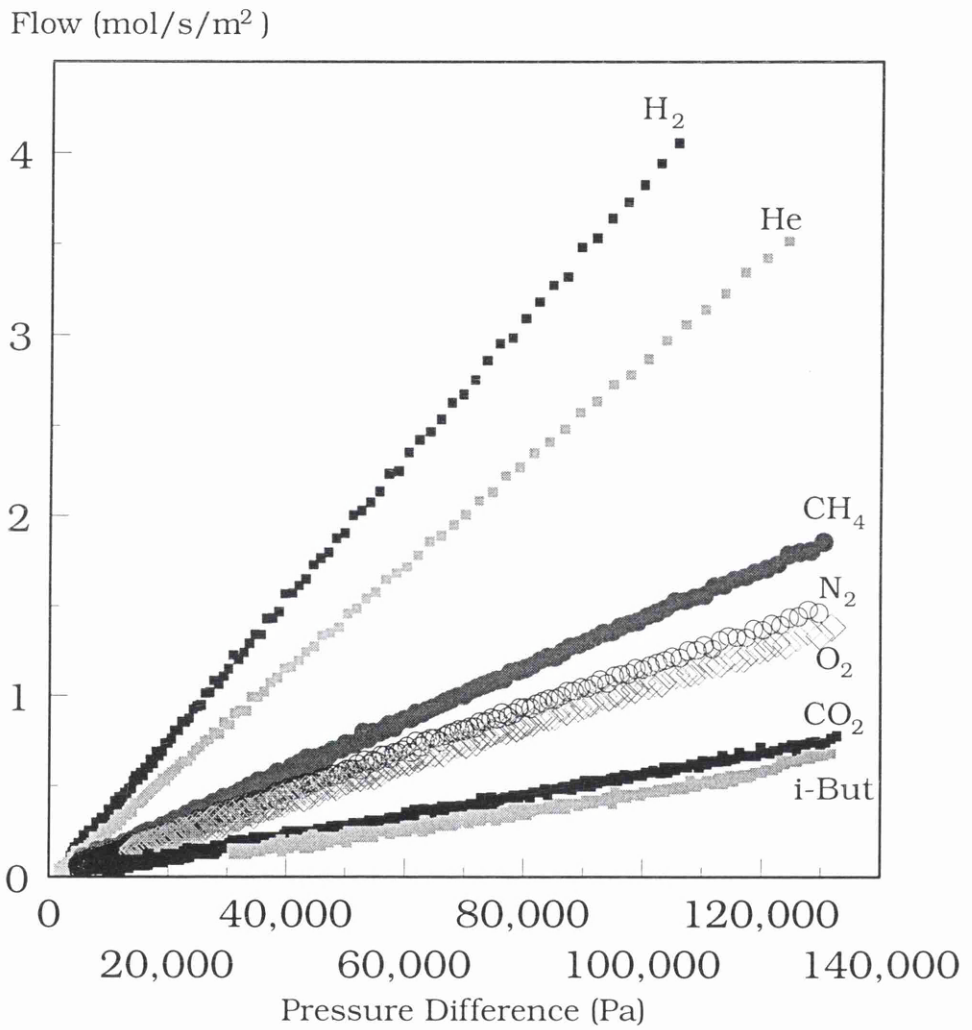


Figure 5.3 Gas Permeation Tests of a Homogeneous Anodic Alumina Membrane (SAA1) with different gases. The Membrane Thickness was 48μm.

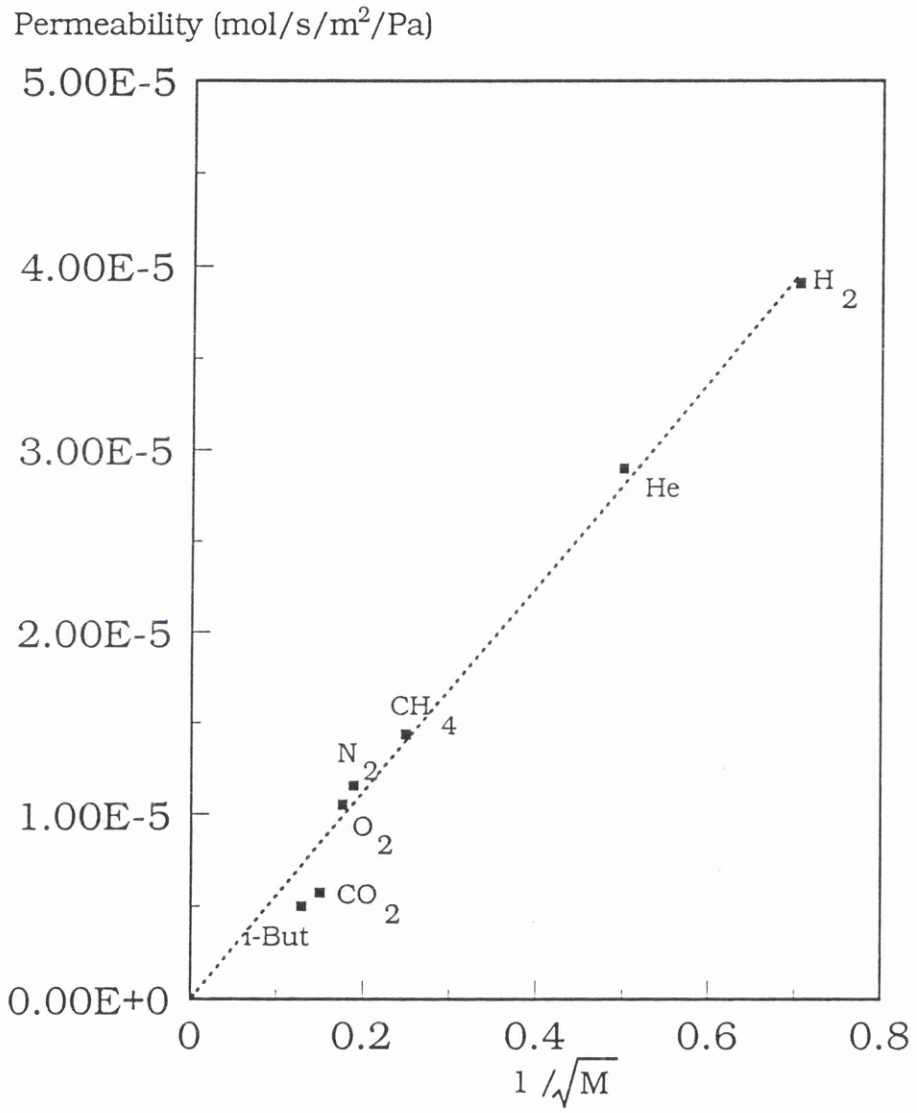


Figure 5.4 Knudsen plot for the membrane (SAA1)

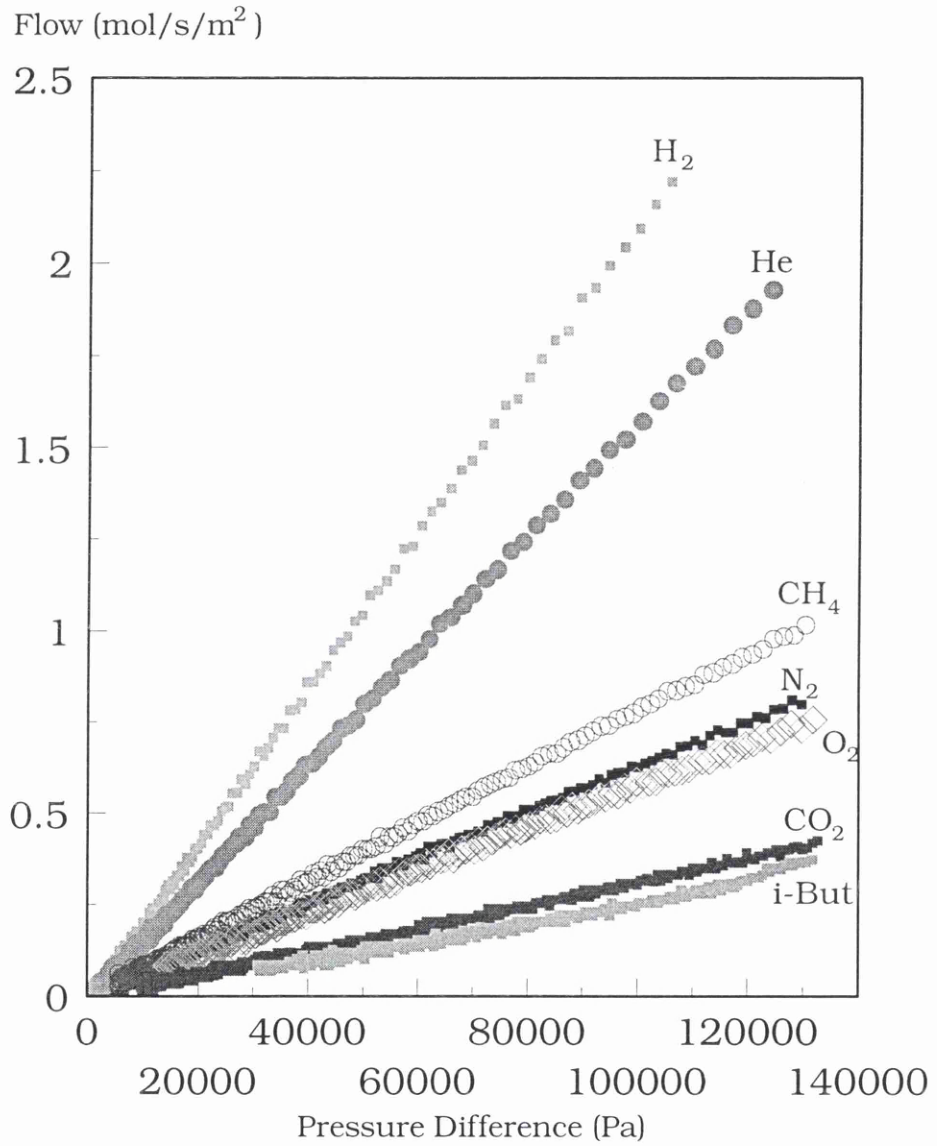


Figure 5.5 Gas Permeation Tests of a Homogeneous Anodic Alumina Membrane (SAA2) with different gases. The Membrane Thickness was 80 μm.

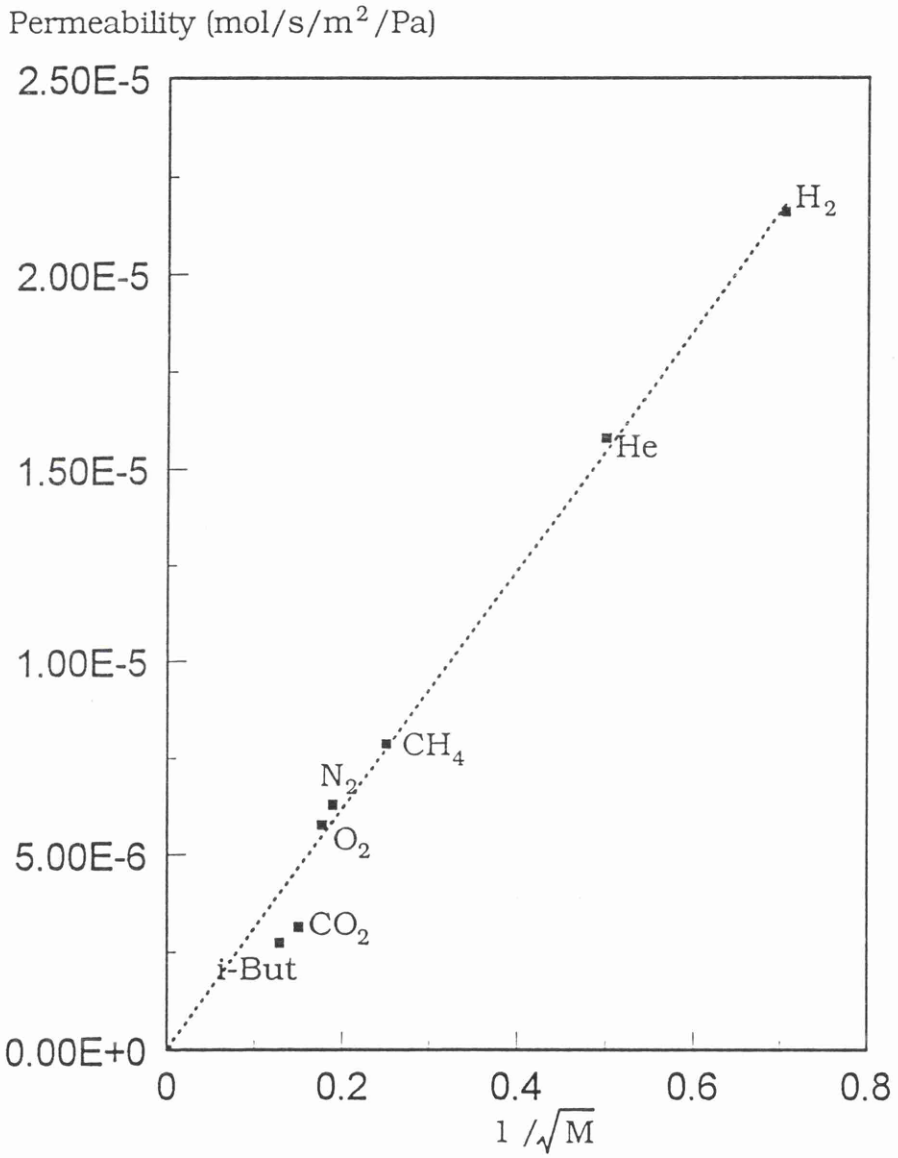


Figure 5.6 Knudsen plot for the membrane (SAA2)

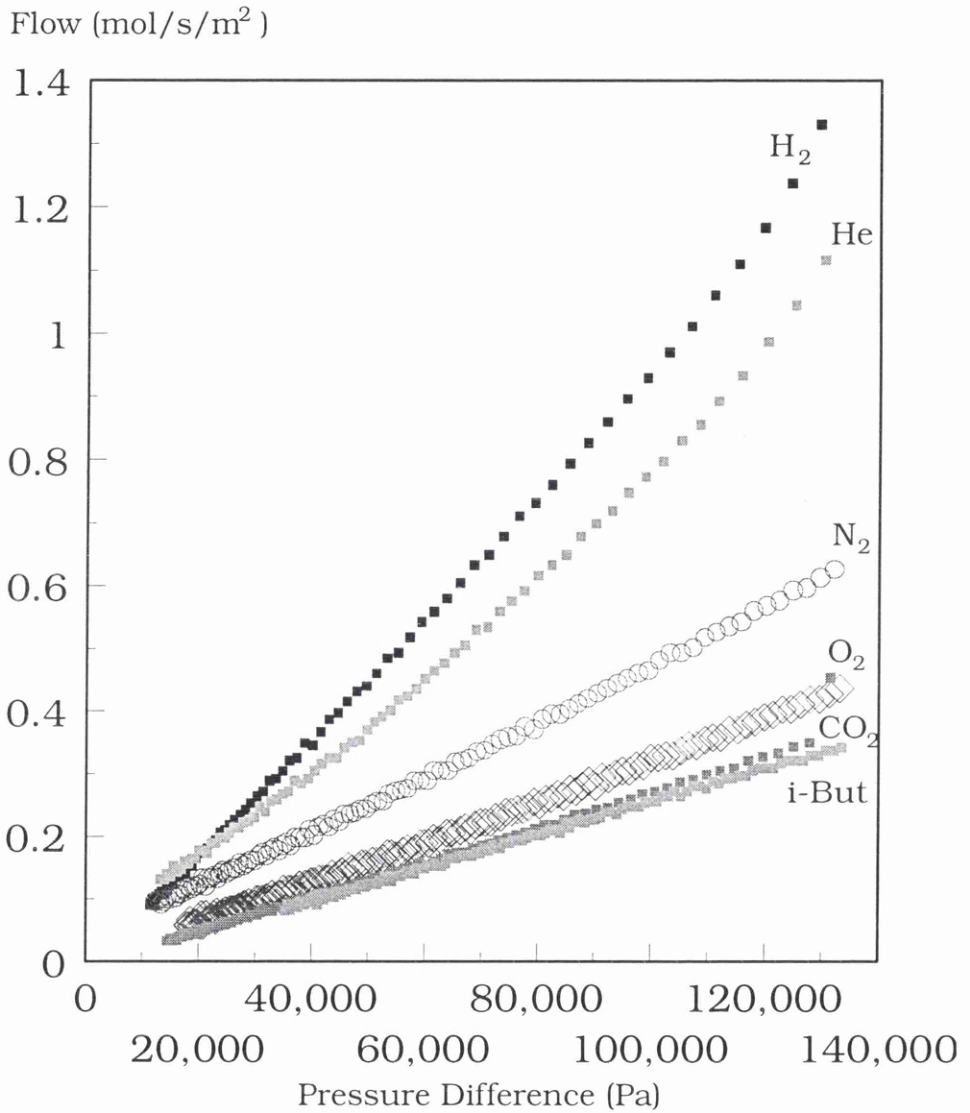


Figure 5.7 Gas Permeation Tests of a Homogeneous Anodic Alumina Membrane (SAA3) with different gases. The Membrane Thickness was 129 μ m.

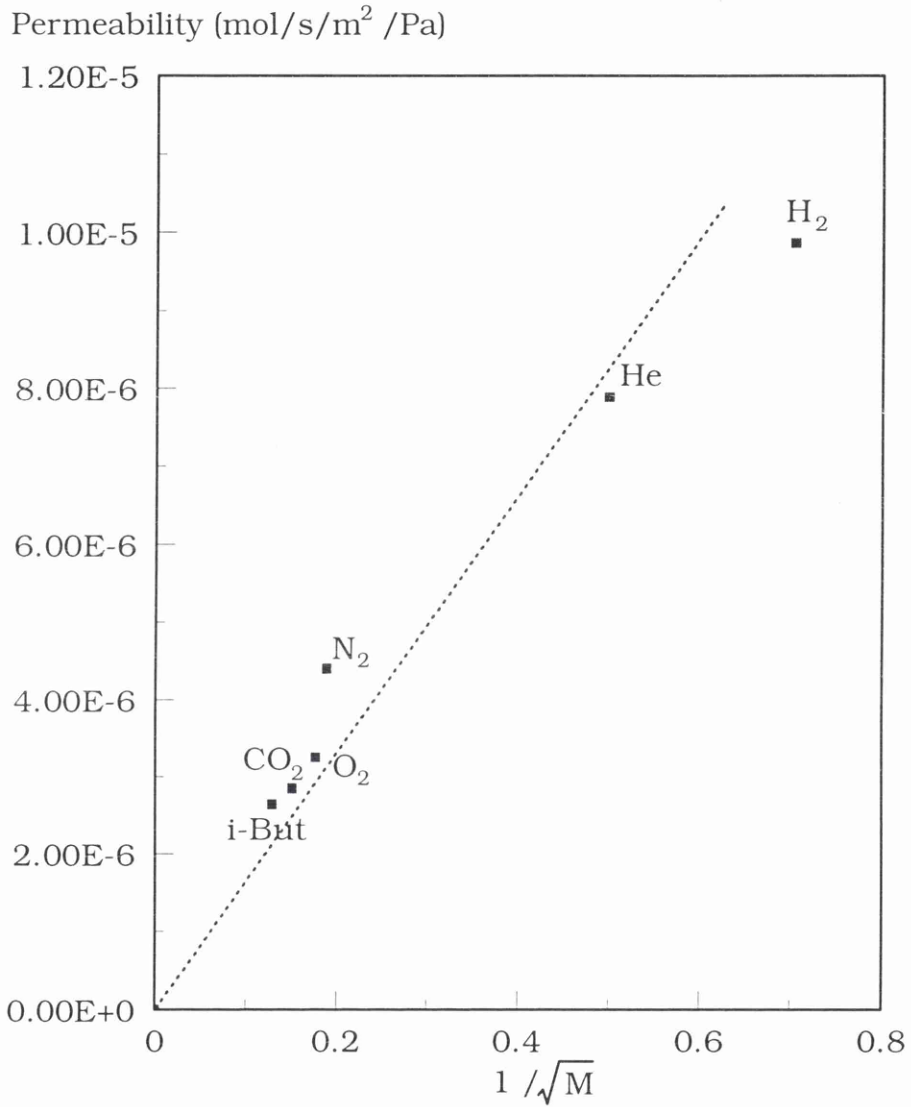


Figure 5.8 Knudsen plot for the membrane (SAA3)

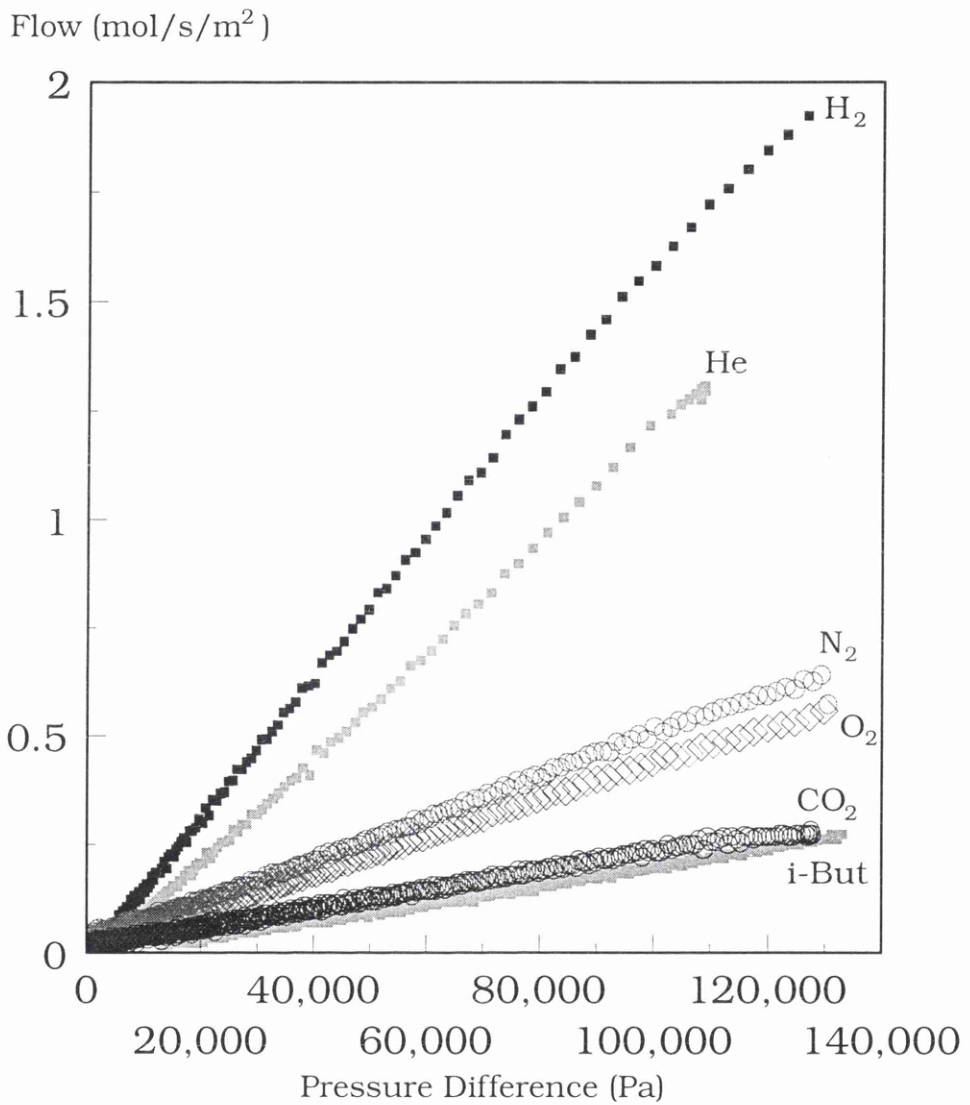


Figure 5.9 Gas Permeation Tests of an Asymmetric Anodic Alumina Membrane (LAA1) with different gases. The Membrane Support was 48 μ m thick and the Active Layer 9 μ m.

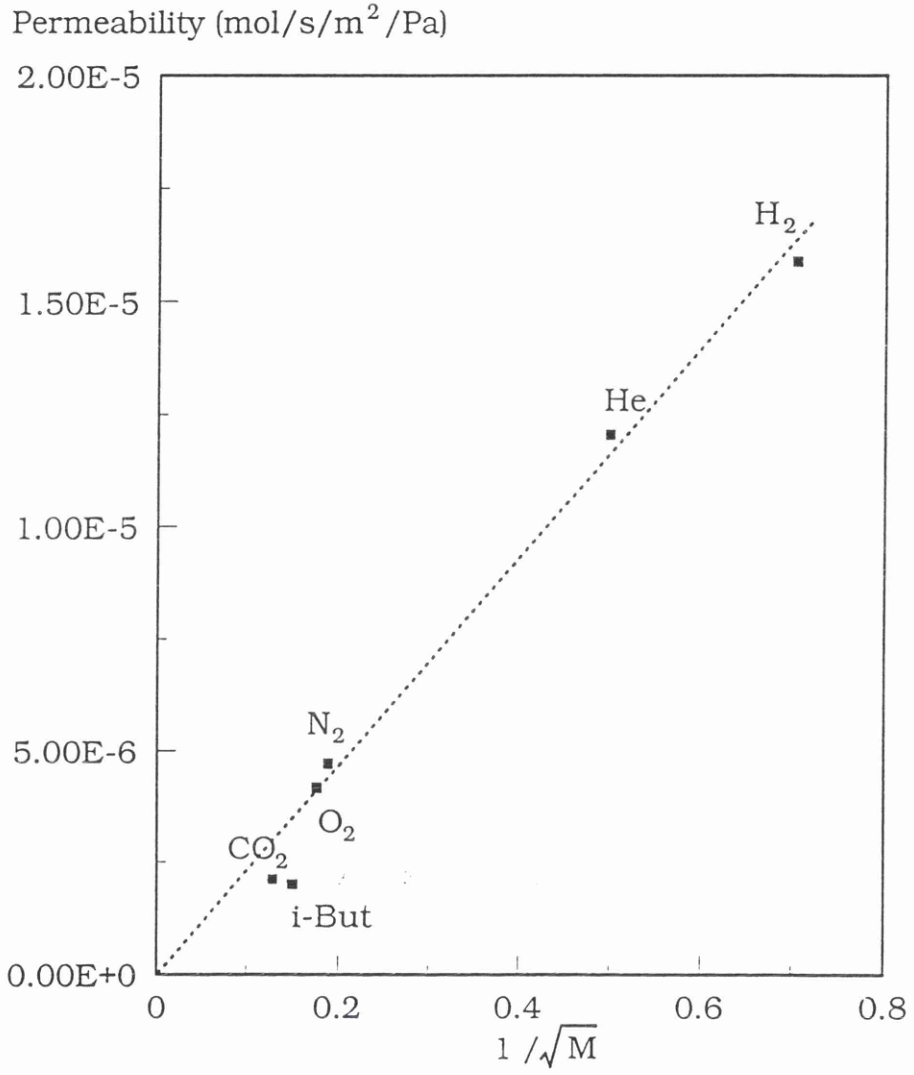


Figure 5.10 Knudsen plot for Bilayer membrane (LAA1)

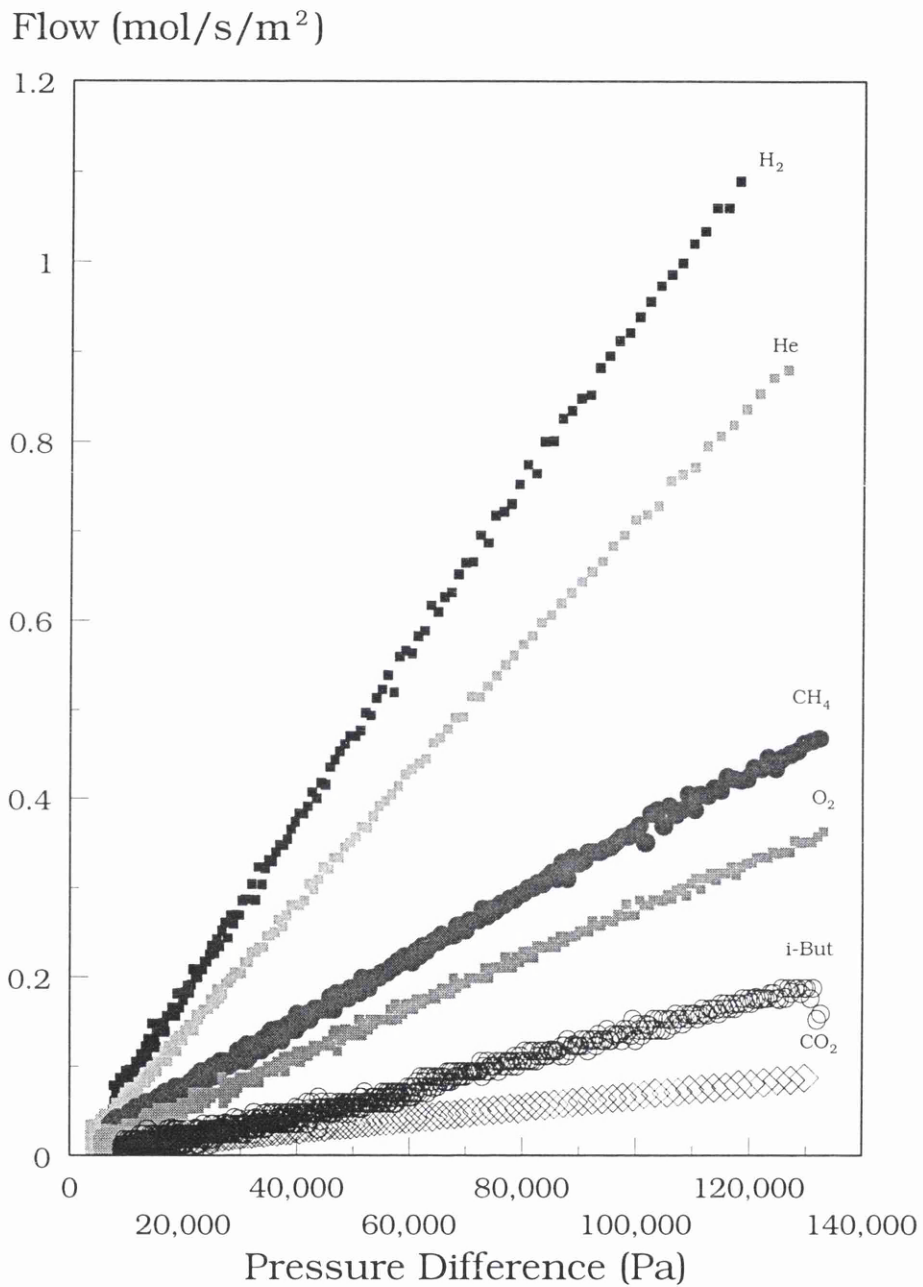


Figure 5.11 Gas Permeation Tests of an Asymmetric Anodic Alumina Membrane (LAA2) with different gases. The Membrane support was 48 μ m and the Active Layer 22 μ m.

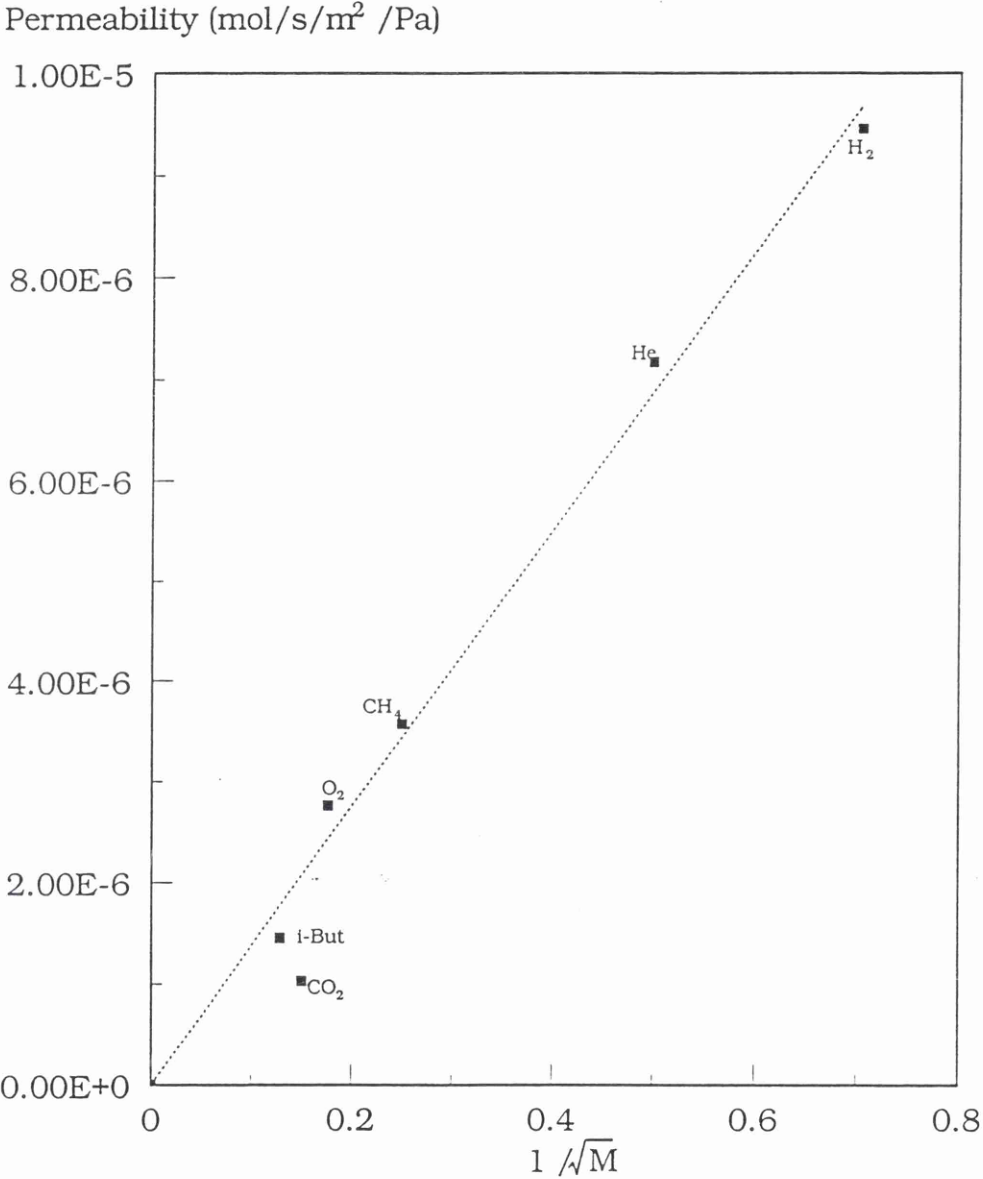


Figure 5.12 Knudsen plot for Bilayer membrane (LAA2)

Permeability ($\text{mol}\cdot\text{s}^{-1}\cdot\text{m}^{-2}\cdot\text{Pa}^{-1}$) $\times 10^5$						
Membrane Sample Code						
Gas	SAA1	SAA2	SAA3	LAA1	LAA2	
H ₂	3.906	2.16	0.986	1.588	0.946	
He	2.896	1.581	0.788	1.205	0.717	
CH ₄	1.436	0.786	-	-	0.357	
N ₂	1.157	0.629	0.434	0.471	0.348	
O ₂	1.054	0.577	0.325	0.416	0.276	
CO ₂	0.573	0.314	0.284	0.201	0.145	
i-C ₄ H ₁₀	0.501	0.274	0.264	0.212	0.103	

Table 5.2 Experimental Gas Permeabilities of Anodic Alumina Membranes:

Supports(SAA) and Bilayers (LAA). Total Sample Thicknesses were

48, 80 & 128 μm for 'Supports' and 57 & 70 μm for Bilayers.

Permeability x Thickness ($\text{mol}\cdot\text{s}^{-1}\cdot\text{m}^{-1}\cdot\text{Pa}^{-1}$) $\times 10^{10}$			
Membrane Sample Code			
Gas	SAA1	SAA2	SAA3
H ₂	18.75	17.28	12.63
He	13.9	12.65	10.08
CH ₄	6.89	6.29	-
N ₂	5.55	5.03	5.62
O ₂	5.06	4.62	4.16
CO ₂	2.75	2.51	3.63
i-C ₄ H ₁₀	2.4	2.19	3.38

Table 5.3 Experimental Permeabilities Multiplied by Membrane Thickness for Homogeneous Anodic Alumina Membranes (Supports).

Gas	Permeability $\times 10^5$ ($\text{mol}\cdot\text{s}^{-1}\cdot\text{m}^{-2}\cdot\text{Pa}^{-1}$)		Permeability \times Thickness $\times 10^{10}$ ($\text{mol}\cdot\text{s}^{-1}\cdot\text{m}^{-1}\cdot\text{Pa}^{-1}$)	
	LAA1	LAA2	LAA1	LAA2
H_2	2.675	1.248	2.408	2.746
He	2.067	0.953	1.857	2.096
CH_4	-	0.475	-	1.046
N_2	0.794	0.437	0.714	0.962
O_2	0.687	0.374	0.618	0.823
CO_2	0.309	0.125	0.278	0.276
i-C ₄ H ₁₀	0.367	0.204	0.306	0.449

Table 5.4 Calculated Gas Data for Active Layers of Anodic Alumina Bilayer Membranes. Layer Thicknesses were 9 μm and 22 μm for LAA1 and LAA2 Respectively.

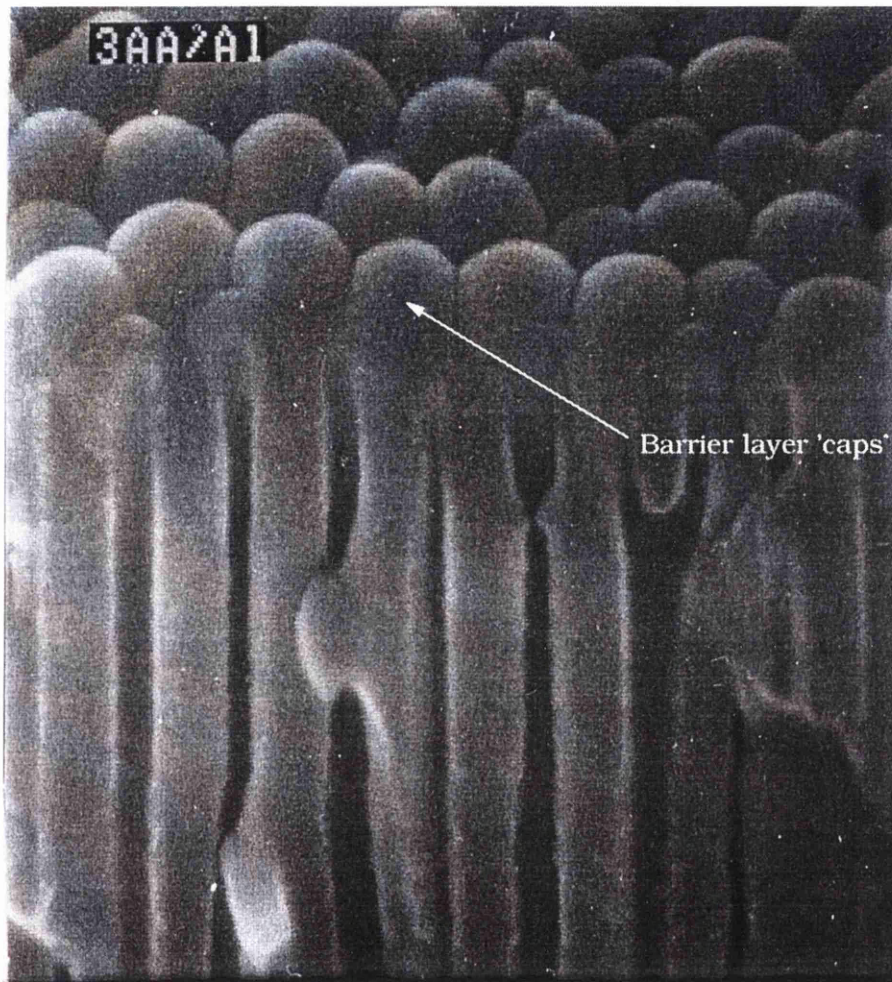


Plate 5.3 SEM photograph of an Anodic Alumina Membrane. Cross sectional view showing the original Capped Pore Structure.

Before moving on to other membrane types, some investigation of an anodic alumina support disc, 50 μm thick with a pore size of 0.2 μm which had been coated on one face with a layer of aluminium nitride was carried out. This material has potential uses in the electronic industry and for possible separations in extreme conditions due to its high chemical stability and strength. This layer was deposited using a Plasma Enhanced Chemical Vapour Deposition (PECVD) technique and had a thickness of 0.5 μm . An example is shown in Plate 5.4. Gas permeation tests with nitrogen showed no detectable gas flow over the period of one hour. A similar test using hydrogen, proved to be more interesting.

If an open pore system is blocked at one end by a thin dense layer, the porous support would of course retain a Knudsen mechanism for gas transport down the pore but the transport rate through the dense layer would be the rate determining step and this would no longer be by a Knudsen mechanism. Upon determination of the hydrogen permeation rate through this thin dense layer we could establish two main points:

(i) gas permeation was **much** slower than for the uncoated support but considering that this was such a thin layer it was also significantly slower than the bilayer alumina samples prepared previously. Based on pressure values, the rate was close to 5000 times slower for the AlN coated layer when

compared to the bilayer samples described earlier

(ii) Due to the slow permeation rate, it was possible to obtain by experiment, a time-lag value (τ). The time-lag value obtained was sufficiently large, so as to reduce any error in the switching to a negligible level and attaining the highest possible accuracy. This value of the time-lag, in turn allowed for a calculation of the diffusion coefficient from

$$D = \frac{l^2}{6\tau}$$

The experimental data are shown in Figures 5.13 to 5.15. In the first of these (Figure 5.13) the response of the 'support' to a hydrogen pressure step is shown. In this instance the system reached >90% of the equilibrium value in only 50-60 seconds. In Figure 5.14 the support data was superposed to the AlN coated sample for comparison between the two systems. Finally, in Figure 5.15 the AlN coated data are shown. In this experiment over a period of approximately 20,000 seconds (5.5 hours) the pressure value increased by an amount equivalent to only 3% of the equilibrium value.

The time-lag value obtained was 1125 seconds and this corresponded to a value for the diffusion coefficient of $3.7 \times 10^{-13} \text{ m}^2\text{s}^{-1}$, using the $l^2/6\tau$ relationship.

On a purely qualitative basis, this experiment clearly showed that the AlN layer had been successfully deposited defect free.

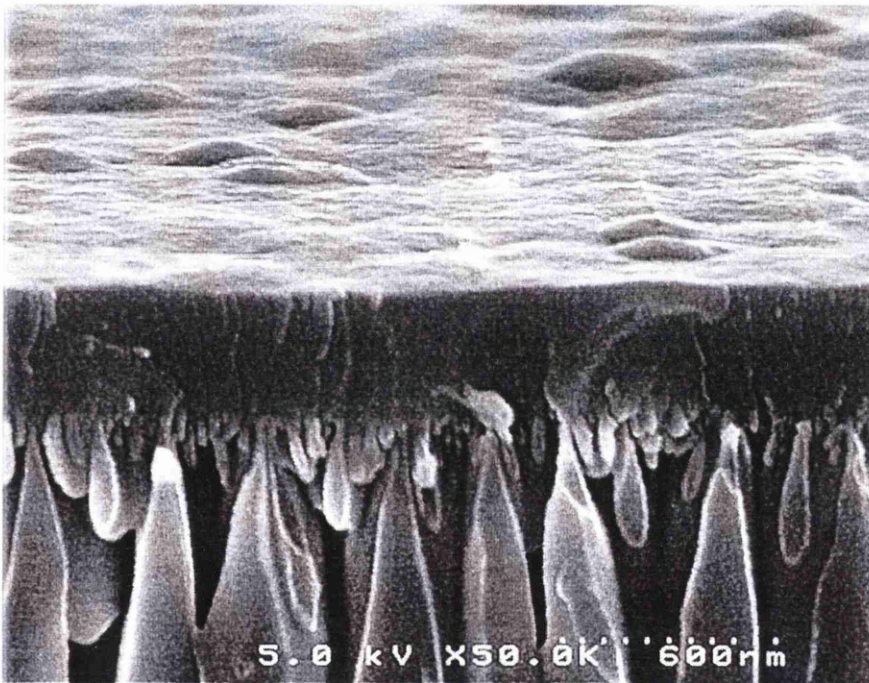


Plate 5.4 SEM photograph of an AlN coated Anodic Alumina Membrane. Cross sectional view showing the defect free layer.

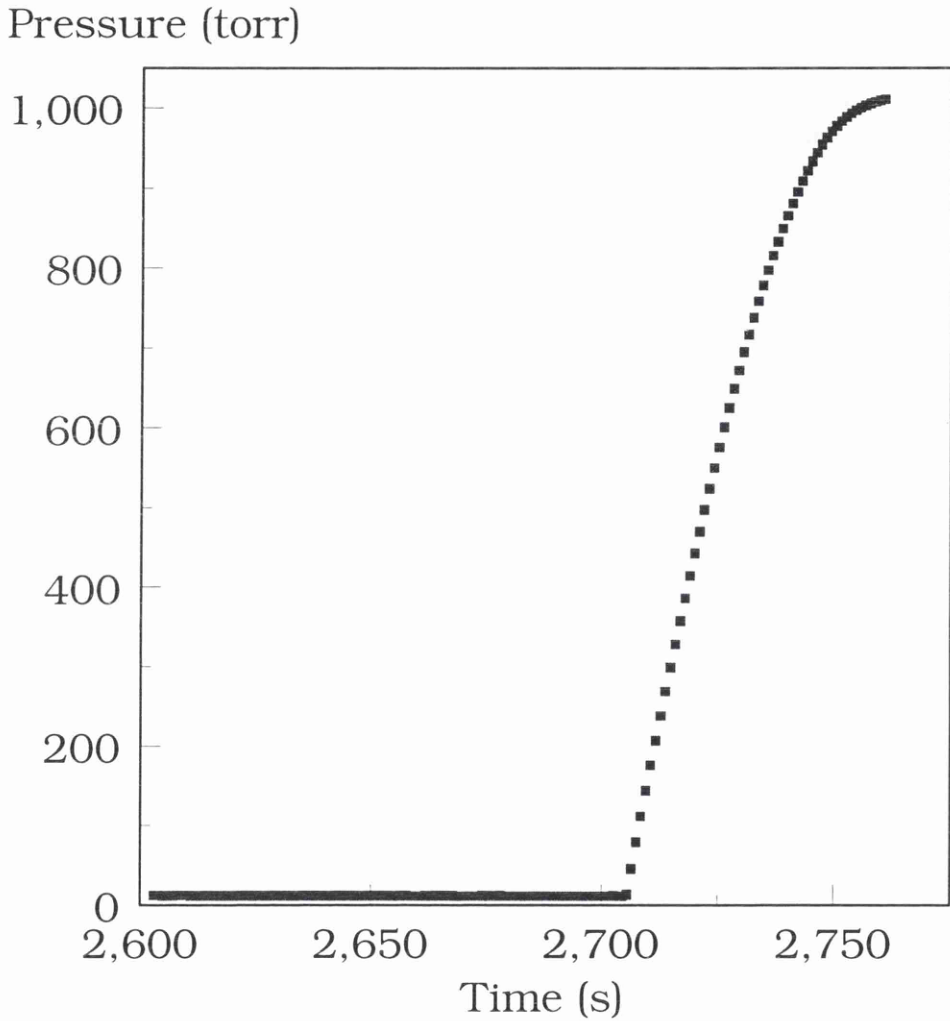


Figure 5.13 Hydrogen gas permeation through an Anodic Alumina membrane, 60 μm thick and with a nominal pore size of 0.2 μm . The gas pressure step imposed was 1000 torr.

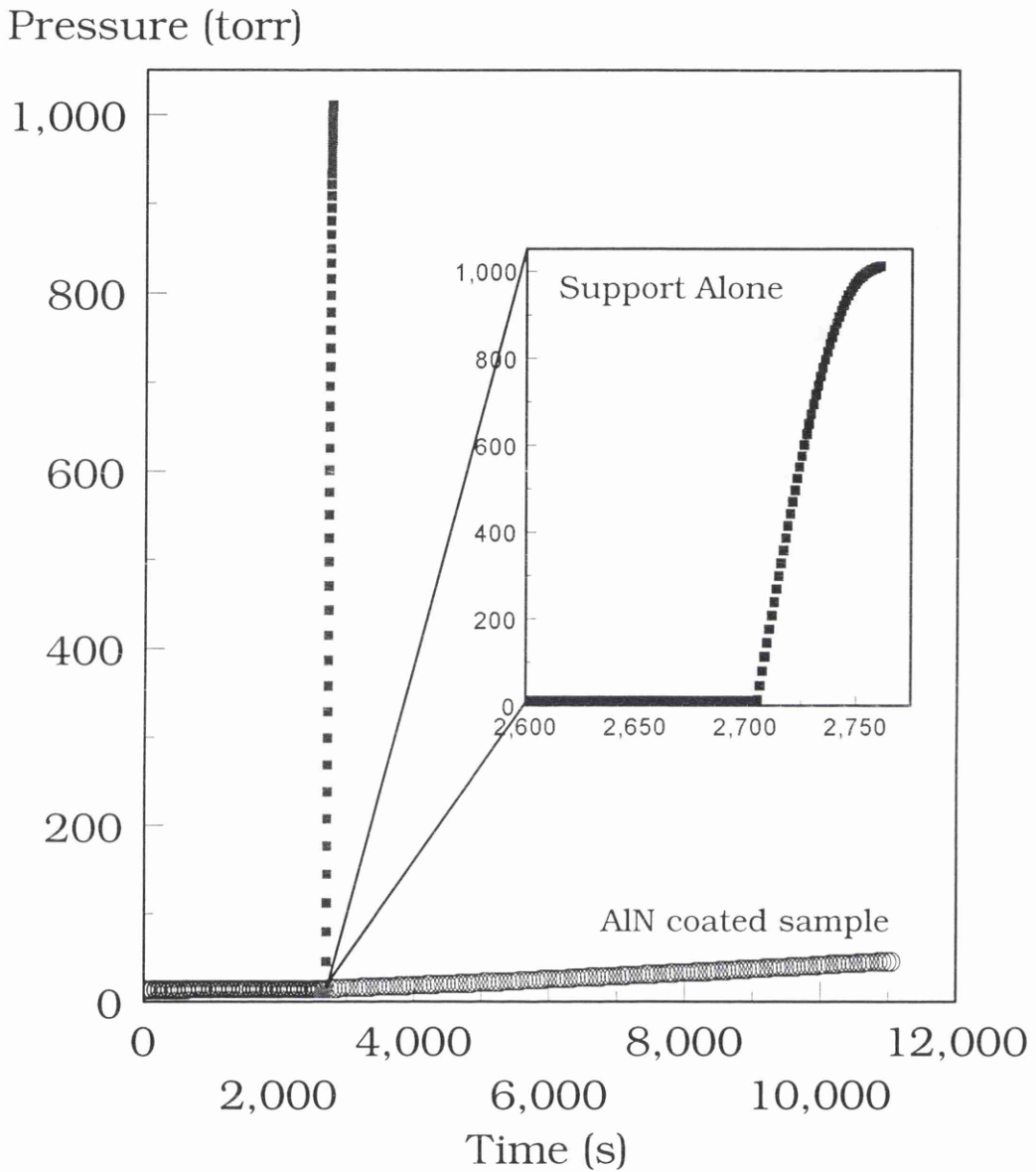


Figure 5.14 Comparison in relative hydrogen flow between an Anodic Alumina membrane, 60 μ m thick and with a coated layer of AlN (0.5 μ m). The gas pressure step imposed was 1000 torr.

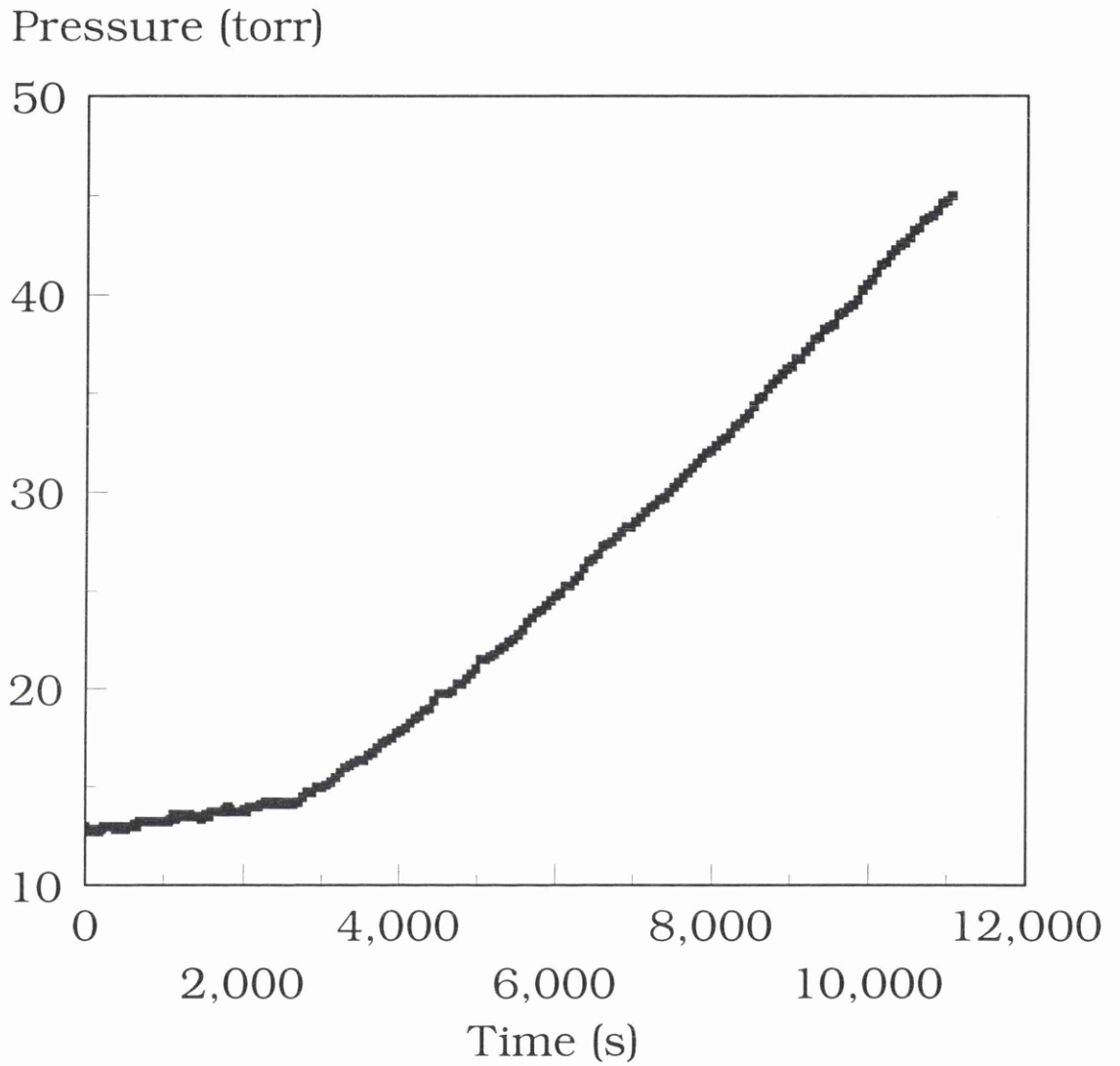


Figure 5.15 Hydrogen permeation through AlN coated Anodic Alumina membrane. The estimated τ value was 1125 s.

Other samples coated to a layer thickness of 0.1 μm did not show the same low order flows, these reached pressures close to 50% of the equilibrium values in a matter of only twenty minutes. This showed beyond doubt that the deposited AlN layers were in this case either incomplete or not defect free.

5.4.2 Ceramic Disc Membranes

Unlike the anodic alumina membranes described above, the ceramic membranes here did not have the same type of regular geometric pore structure. These ceramic membranes were prepared by sol-gel methods and sintering to produce the final membrane [20]. There was still some degree of control in the layer thickness and the pore size of the membrane and the active layers could be produced defect free and additionally without significant percolation into the support substrate to leave a 'sharp' interface between the membrane component parts.

The support structure in this case was prepared from α -alumina with the thin active layer being of zirconia. The discs were 25 mm in diameter with a support thickness of 600 μm and an active layer thickness of 2.5 μm . As previously, the permeabilities of the support alone and those of the composite membrane were determined experimentally with the permeabilities of the active layer being determined using

Equation (5.18). Checks were also made to ensure that the Knudsen diffusion regime was still valid in both of these samples. The plots of the gas flux density versus trans-membrane pressure for the support (Figure 5.16) and for the composite membrane (Figure 5.17) were linear. This again confirmed that the permeabilities were constant over the period of the experiment. The plots that confirmed Knudsen flow are shown in Figure 5.18 (for the support) and Figure 5.19 (for the bilayer membrane). All of the experiments were conducted using an imposed pressure step of 100 kPa.

A summary of the permeation results for the support (ZrSup) and the composite membrane (ZrAL1) are shown in Table 5.5. From the data obtained it was clear that there was again a general decrease in permeability as the gas molecular weight increased. It was also clear that the addition of the active layer made a significant difference in the permeation rates as compared to the support. In this case the layer thickness (2.5 μm) changed the total thickness by only 0.4% but on average reduced the permeability by slightly over 10%. This figure is not as marked as for the anodic alumina system but the ZrO_2 active layer in this case had a nominal pore size more than twice as large (43nm). The data calculated for the active layer is shown in Table 5.6.

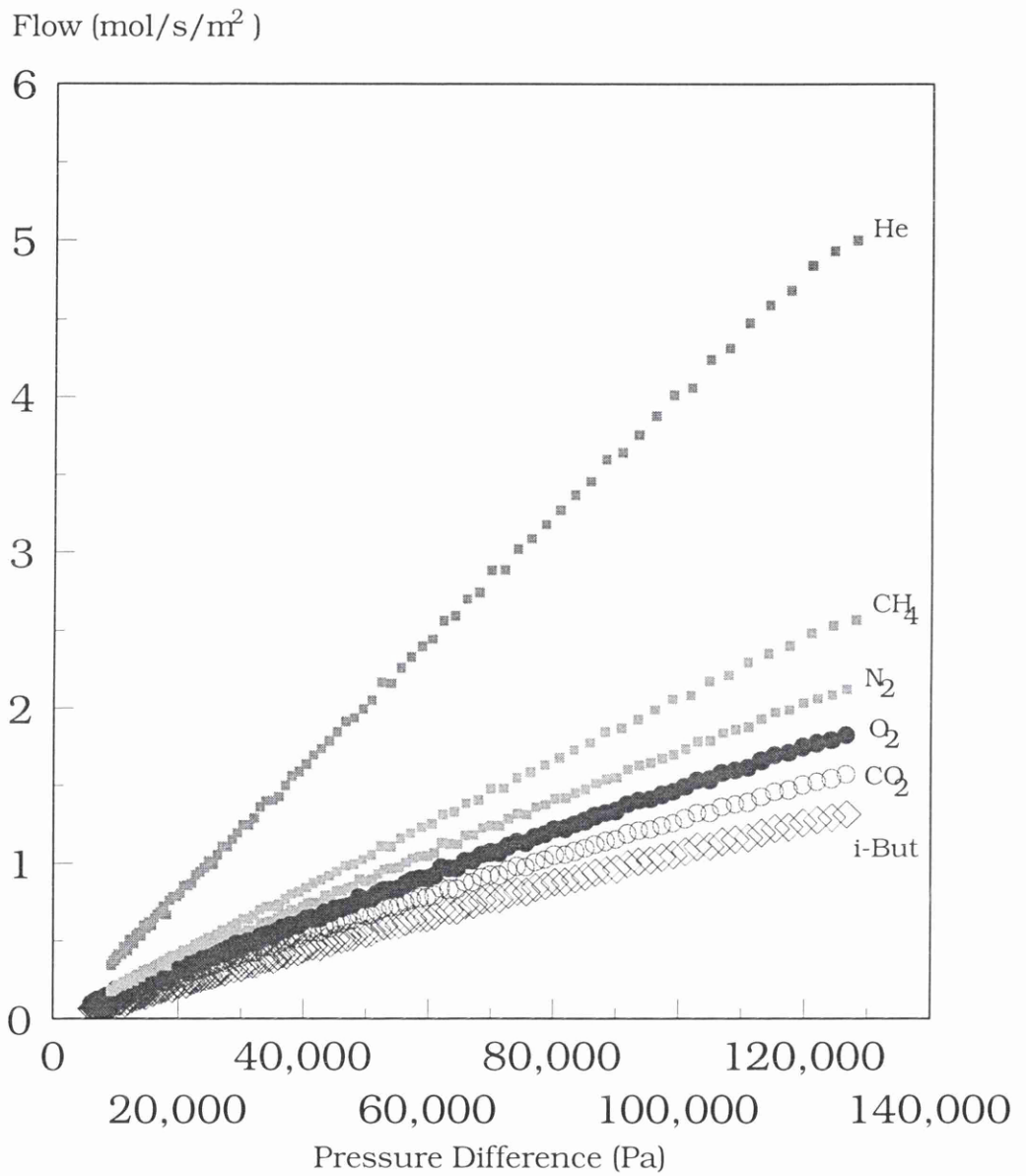


Figure 5.16 Gas Permeation Tests of a Homogeneous ceramic 'support' disc (ZrSup) with different gases, the thickness was 61 μm .

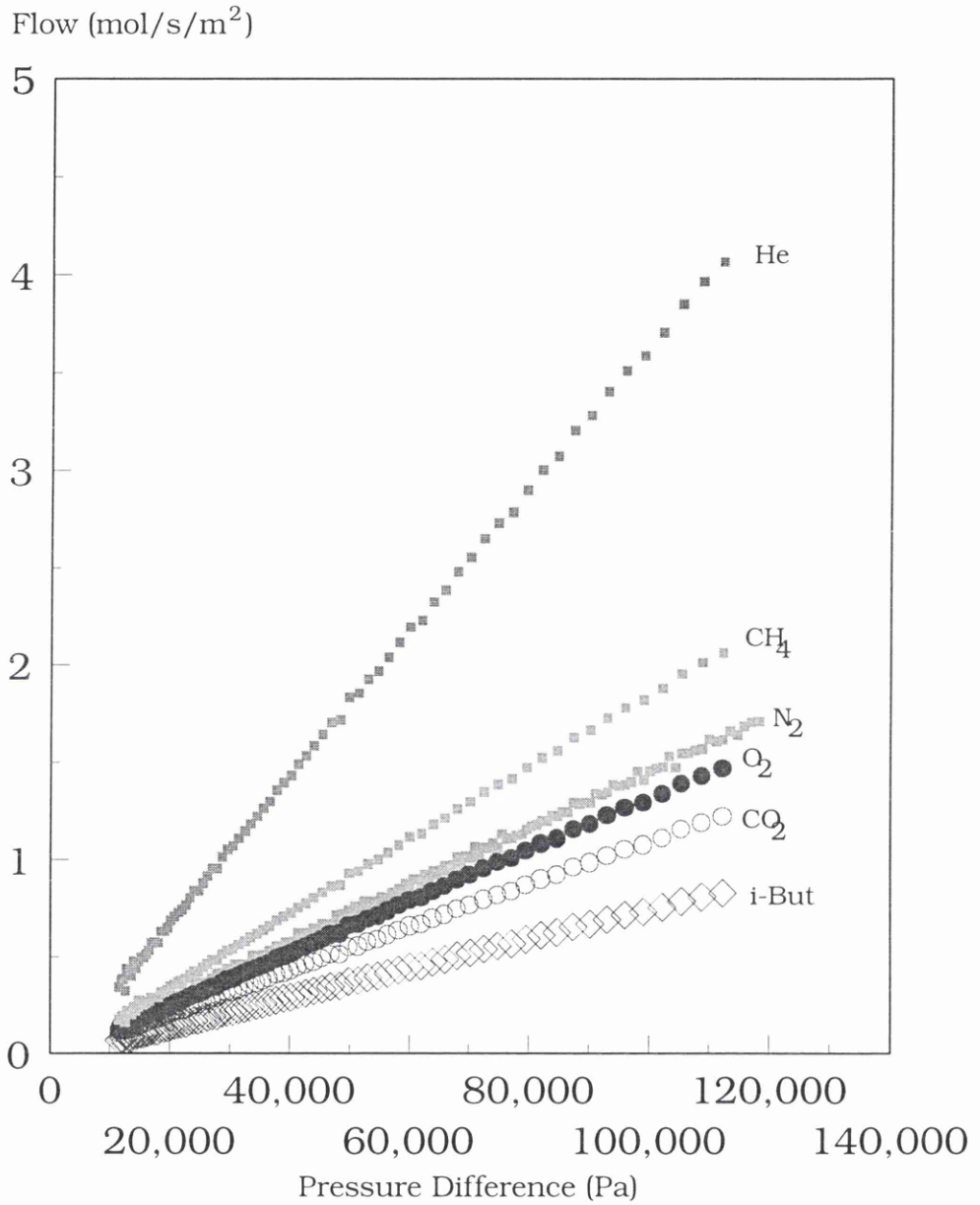


Figure 5.17 Gas permeation tests of an asymmetric ceramic membrane (ZrAl1) with different gases. The total thickness was 619 μm , the active layer was 2.5 μm thick.

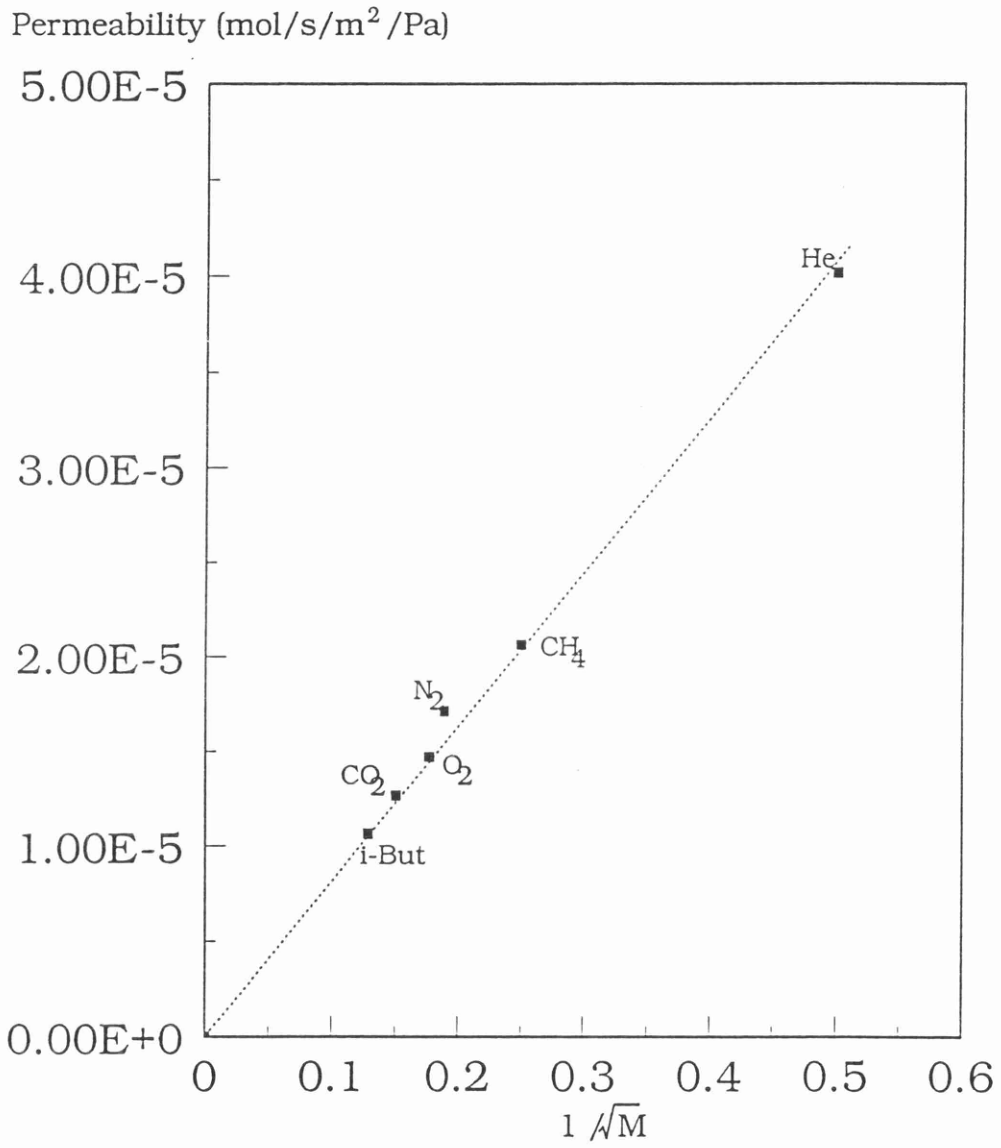


Figure 5.18 Knudsen plot for support disc (ZrSup)

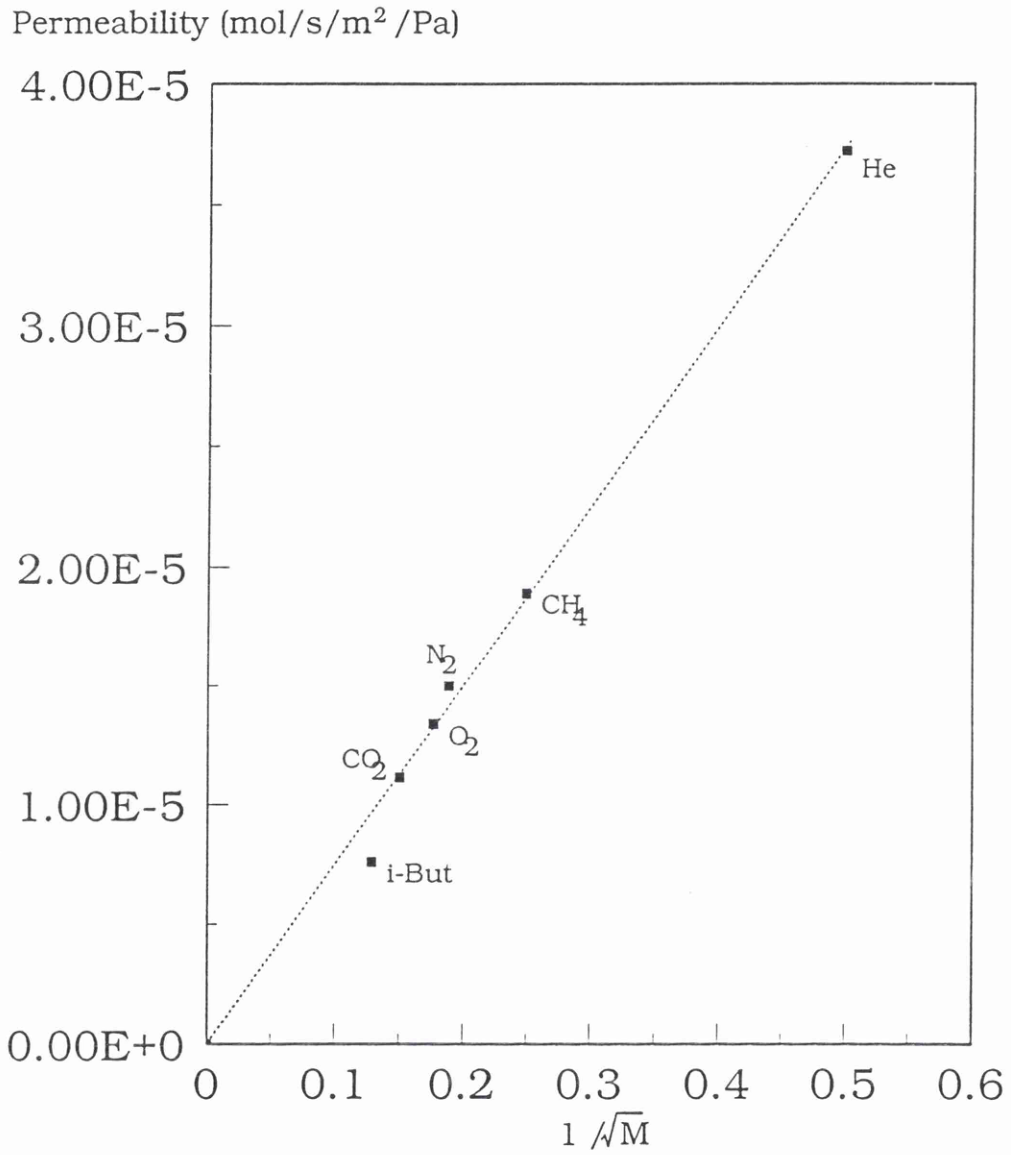


Figure 5.19 Knudsen plot for ceramic membrane (ZrAl1)

Gas	Permeability $\times 10^5$ ($\text{mol}\cdot\text{s}^{-1}\cdot\text{m}^{-2}\cdot\text{Pa}^{-1}$)		Permeability \times Thickness $\times 10^8$ ($\text{mol}\cdot\text{s}^{-1}\cdot\text{m}^{-1}\cdot\text{Pa}^{-1}$)	
	ZrSup	ZrAL1	ZrSup	ZrAL1
He	4.016	3.723	2.454	2.304
CH ₄	2.06	1.888	1.258	1.168
N ₂	1.712	1.498	1.046	0.927
O ₂	1.469	1.339	0.897	0.829
CO ₂	1.265	1.113	0.773	0.688
i-C ₄ H ₁₀	1.061	0.758	0.648	0.469

Table 5.5 Experimental Gas Permeabilities of an Ultrafiltration Ceramic (Sol-Gel) Membrane.

Total Thickness of ZrAL1 was 619 μm , the Active Layer Thickness was 2.5 μm .

Gas	Permeability $\times 10^4$ ($\text{mol}\cdot\text{s}^{-1}\cdot\text{m}^{-2}\cdot\text{Pa}^{-1}$)	Permeability \times Thickness $\times 10^{10}$ ($\text{mol}\cdot\text{s}^{-1}\cdot\text{m}^{-1}\cdot\text{Pa}^{-1}$)
He	5.103	12.76
CH ₄	2.261	5.653
N ₂	1.198	2.996
O ₂	1.513	3.783
CO ₂	0.927	2.315
i-C ₄ H ₁₀	0.266	0.665

Table 5.6 Calculated Gas Data for the ZrO₂ Active Layer of Ceramic Ultrafiltration (Sol-Gel) Membrane (ZrLA1). The Active Layer Thickness was 2.5 μm .

5.4.3 Ceramic Tube Membranes

This type of membrane was perhaps the most important as it will be in this format that these systems will be used in commercial, industrial and process applications. It consisted of a porous ceramic tube (up to 5 metres in length) which was then processed to produce a continuous defect free active layer over its length. Currently, using sol-gel methods it is claimed to attain pore sizes as small as 1nm [21].

The experimental data obtained in this instance was for a single tube format (multi-channel versions are available) with a 1 cm outer diameter and a wall thickness (support layer) of 1.75 mm with the active layer of 2 μ m thickness with a 5 nm nominal pore size, truly approaching nanofiltration dimensions.

Gas permeation studies were performed in a similar manner to those previously described. In order to accommodate the tubular geometry, some alteration to the gas permeation cell was necessary. This did not in anyway effect the efficiency of the gas pressure step generated nor the data collection. Experimental runs were performed over a range of driving pressures (up to 30 kPa) and the resulting data are shown in Figures 5.20 to Figure 5.24.

A comparison is shown in Figure 5.20 for the raw pressure data for two tubular systems with nitrogen. In the first only

the support tube is exposed to the pressure step (10 kPa). It is clear to see from this data that the support reached the equilibrium value in approximately 2 seconds. In the second trace, the only difference was the presence of the active layer (2 μ m thick, 5 nm pore) and the time taken to reach equilibrium approached one hour. In Figures 5.21 to 5.23 the transmembrane pressure versus gas flux density are plotted for applied pressure steps of 100k, 200k and 300k Pa respectively. The Knudsen plot for the membrane is shown in Figure 5.24. The permeabilities obtained from these experiments are shown in Table 5.7 with the calculated permeabilities for the active layer alone, shown in Table 5.8.

With this membrane, due to the very small nominal pore size in the active layer (5nm) the effect of the active layer was startlingly clear. Simply by the presence of a 2 μ m layer the gas flows were reduced by a factor greater than 500 times (for a 300kPa applied step). It was also clear from this data that there was a significant difference in the permeability of CO₂ compared to the other gases tested. When compared to the data for nitrogen the ideal separation factors (α) were found to be 1.85, 6.75 and 7.48 at applied pressure steps of 100, 200 and 300kPa respectively. These last two values were significantly larger than the Knudsen ideal value of 1.25 (Equation 5.6). This showed conclusively that there must be

an alternative transport mechanism which was aiding separation. Finally, several samples of membrane were made available that claimed to have a nominal pore size of 1nm. All of the samples tested showed that the active layer was not free of defects as the gas permeation rates were all substantially higher than for the 5nm pore membrane samples.

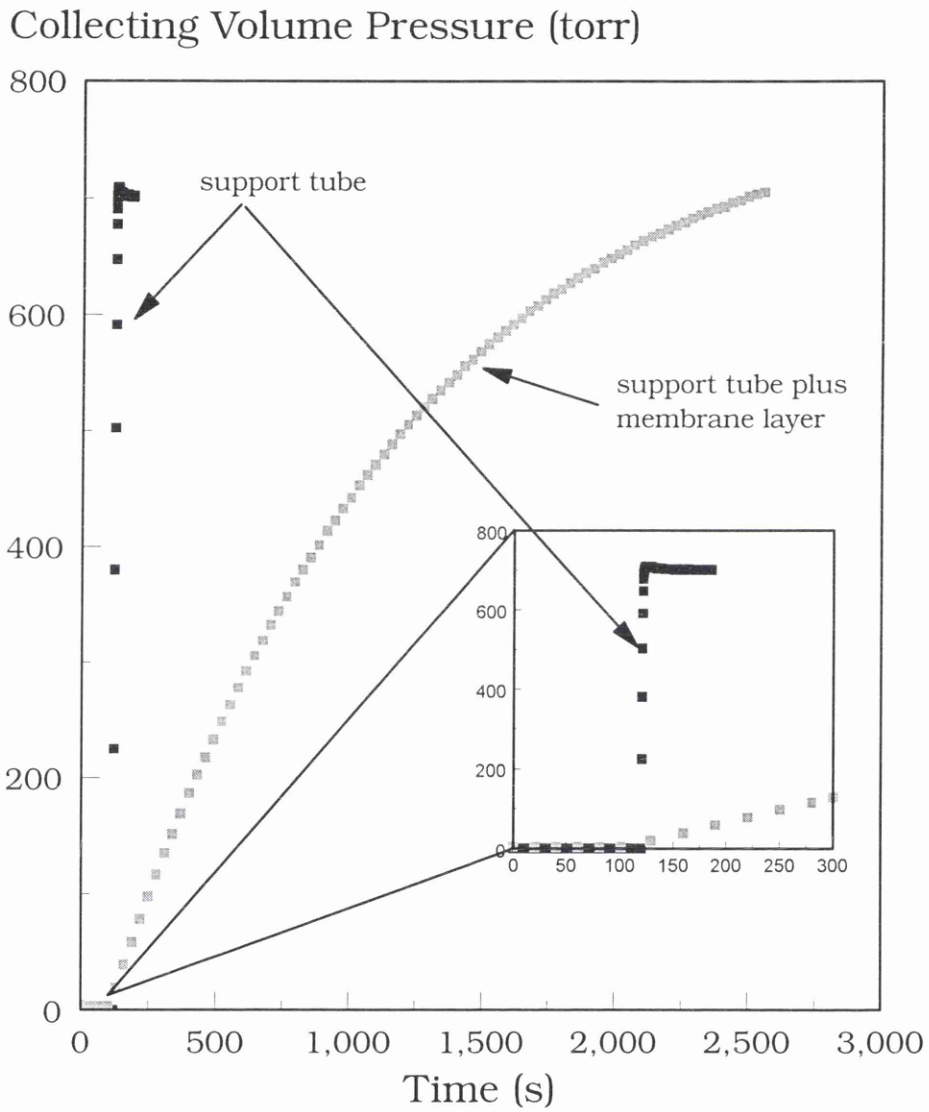


Figure 5.20 Comparison between the support tube and the 5nm membrane response to a +1bar nitrogen pressure step.

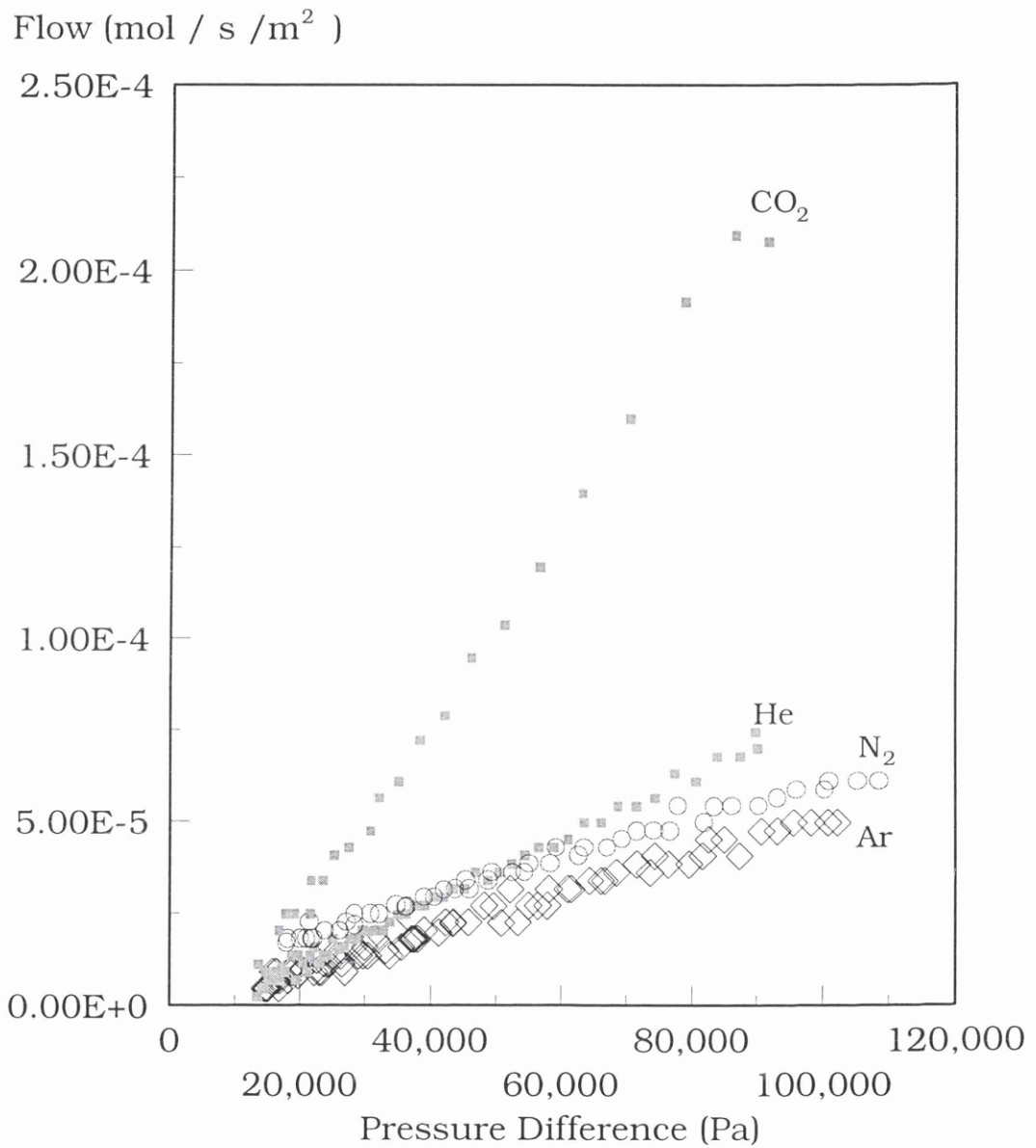


Figure 5.21 Gas Permeation Tests of a tubular ceramic membrane (TLa1) with different gases. Imposed step was +1 bar and the membrane thickness was 2 μ m.

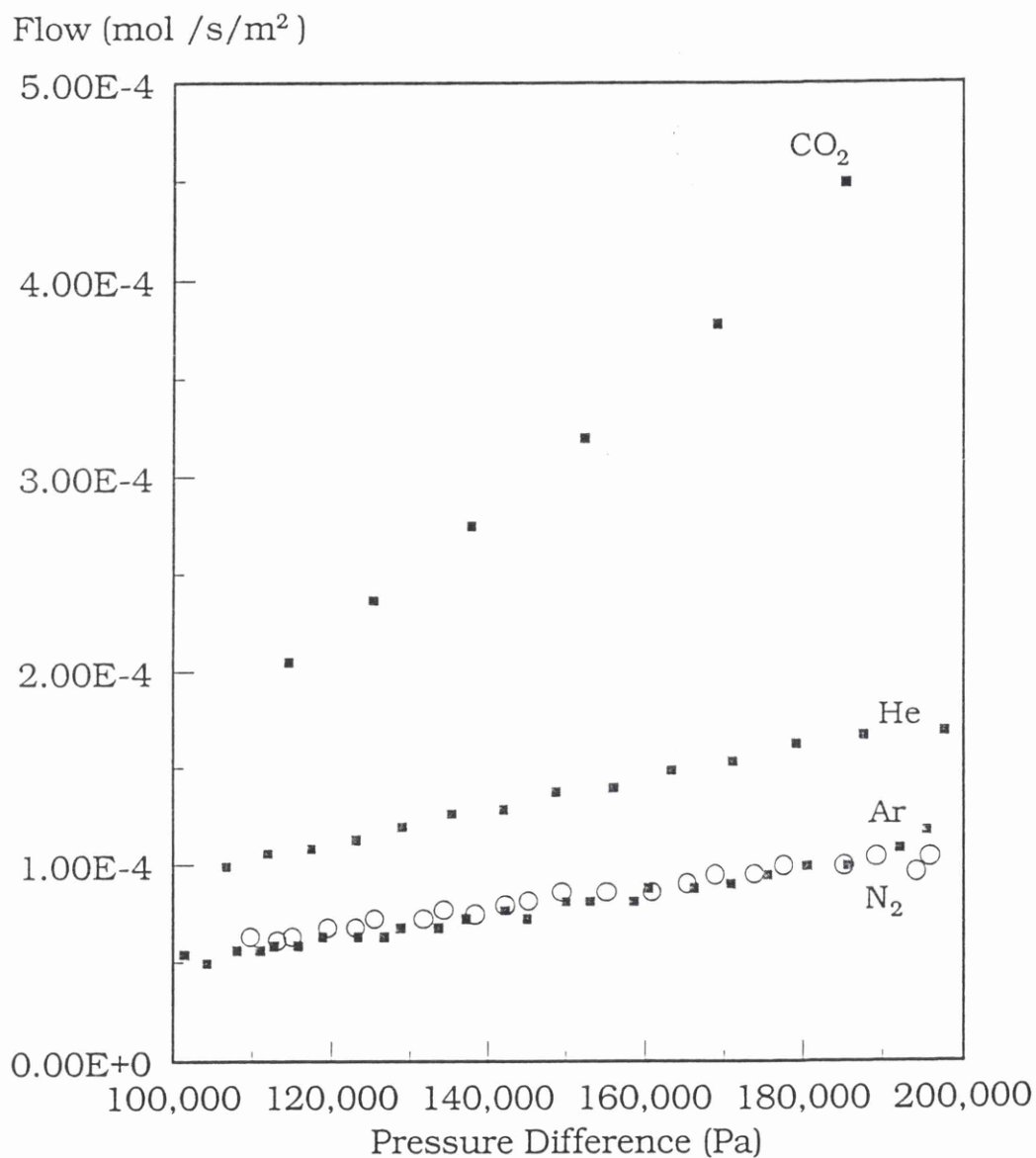


Figure 5.22 Gas Permeation Tests of a tubular ceramic membrane (TLa1) with different gases. Imposed step was +2 bar and the membrane thickness was 2 μ m.

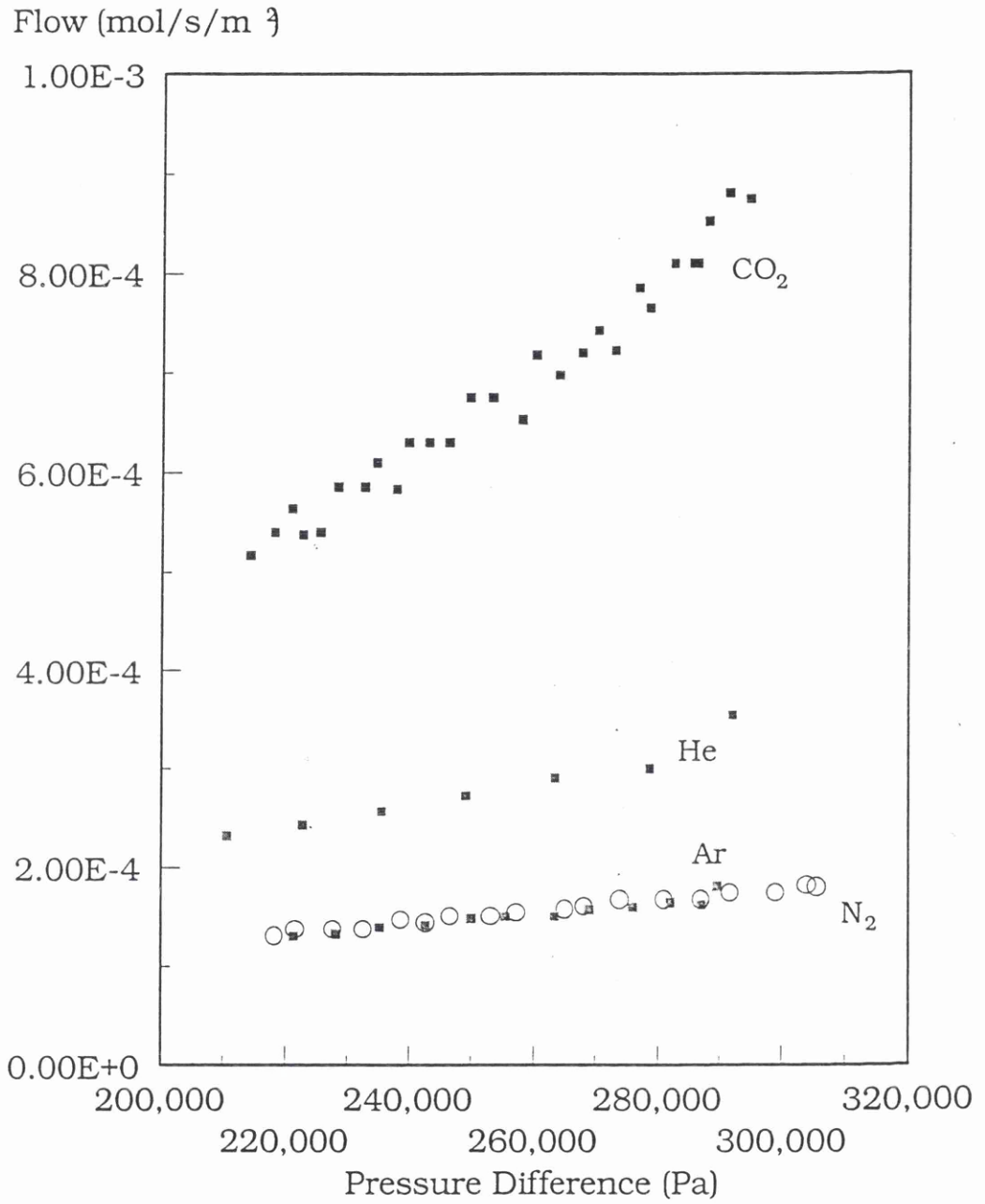


Figure 5.23 Gas Permeation Tests of a tubular ceramic membrane (TLa1) with different gases. Imposed step was +3 bar and the membrane thickness was 2 μ m.

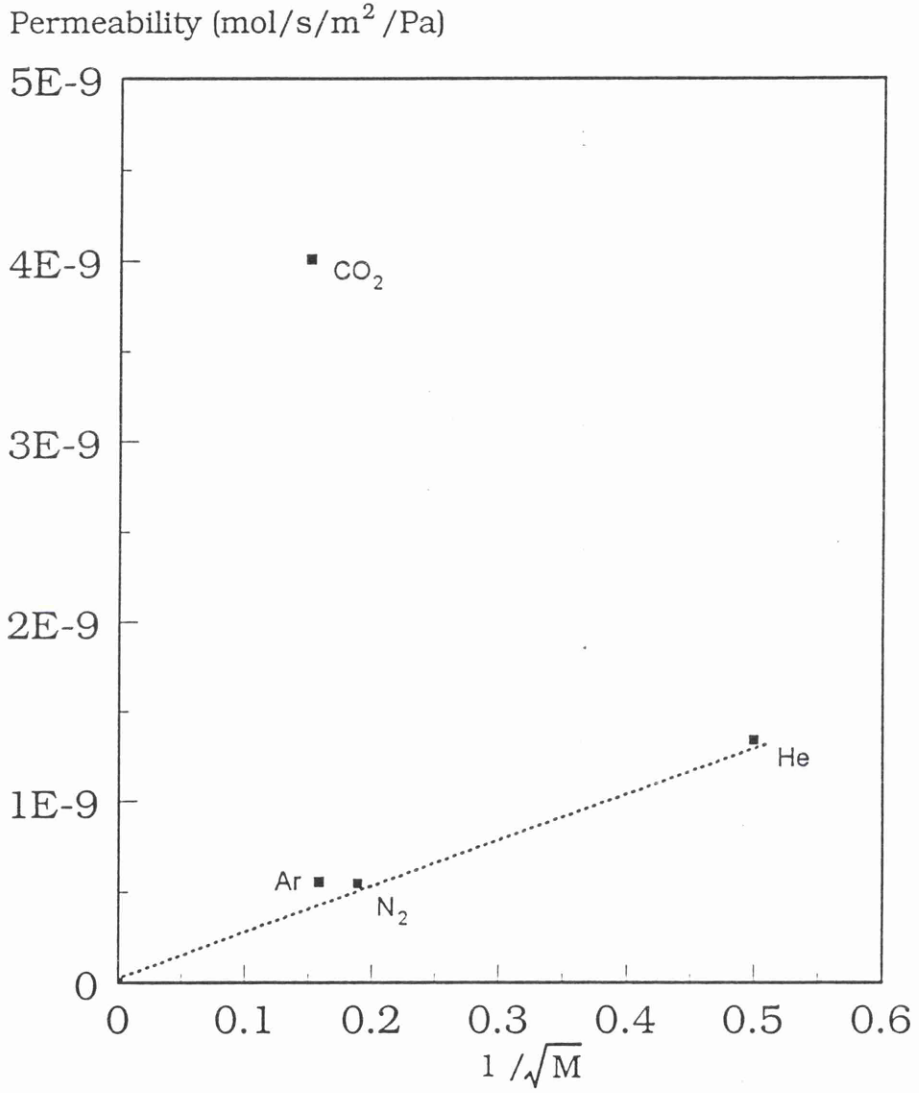


Figure 5.24 Knudsen plot for a 5nm tube membrane (TLa1) with +3 bar pressure step.

	Permeability $\times 10^9$ ($\text{mol}\cdot\text{s}^{-1}\cdot\text{m}^{-2}\cdot\text{Pa}^{-1}$)	Permeability \times Thickness $\times 10^{12}$ ($\text{mol}\cdot\text{s}^{-1}\cdot\text{m}^{-1}\cdot\text{Pa}^{-1}$)
Membrane Sample Code		
Gas	TS1	TLa1
He	691.1	1.339
N ₂	294.5	0.545
Ar	221.6	0.555
CO ₂	217.6	4.011
i-C ₄ H ₁₀	182.5	-
	TS1	TLa1
	1201	2.329
	511.7	0.949
	385.1	0.964
	378.1	6.979
	317.1	-

Table 5.7 Experimental Gas Permeabilities of a Ceramic (Tube) Support (TS1) and Nanofiltration Membrane(TLa1) for an Applied Pressure Step of 30 kPa.

Gas	Permeability $\times 10^9$ ($\text{mol}\cdot\text{s}^{-1}\cdot\text{m}^{-2}\cdot\text{Pa}^{-1}$)	Permeability \times Thickness $\times 10^{15}$ ($\text{mol}\cdot\text{s}^{-1}\cdot\text{m}^{-1}\cdot\text{Pa}^{-1}$)
Active Layer Values TLal		Active Layer Values TLal
He	1.342	3.086
N ₂	0.546	1.256
Ar	0.556	1.277
CO ₂	4.086	9.398

Table 5.8 Calculated Gas Data for Active Layer(2 μm thickness) in Ceramic (Tube) Nanofiltration Membrane (TLal) for an Applied Pressure Step of 300 kPa.

5.4.4 'Dense' Polymer Film

Although the emphasis of this current research was to attempt to examine inorganic(porous) systems, it seemed only sensible to show that the system designed and constructed for this study was also suitable for the more conventional gas permeation studies with polymeric membranes.

There is a huge literature in this area of research and it was clear from reading that much higher gas pressures were used than in this current work [22, 23]. Due to the design of the gas cell (for flat sheets and discs) being machined from Perspex™ it was deemed unwise to proceed with gas pressures larger than 50 kPa.

In the test experiment a polycarbonate film (Bayer MACROFOL KG) of 10 µm thickness was used to investigate the separation of carbon dioxide and methane. The resulting data are shown in Figure 5.25.

By examination of the relative slopes for the CO₂/CH₄ permeation runs, a separation factor of 19.53 was obtained. This compares favourably with data published by Koros & Fleming [23] in which a separation factor of 19.0 was cited. With no redesign of the current cell , simply a reconstruction in tougher materials e.g stainless steel, there are no reasons why this system could not be used at higher temperatures and pressures if so required.

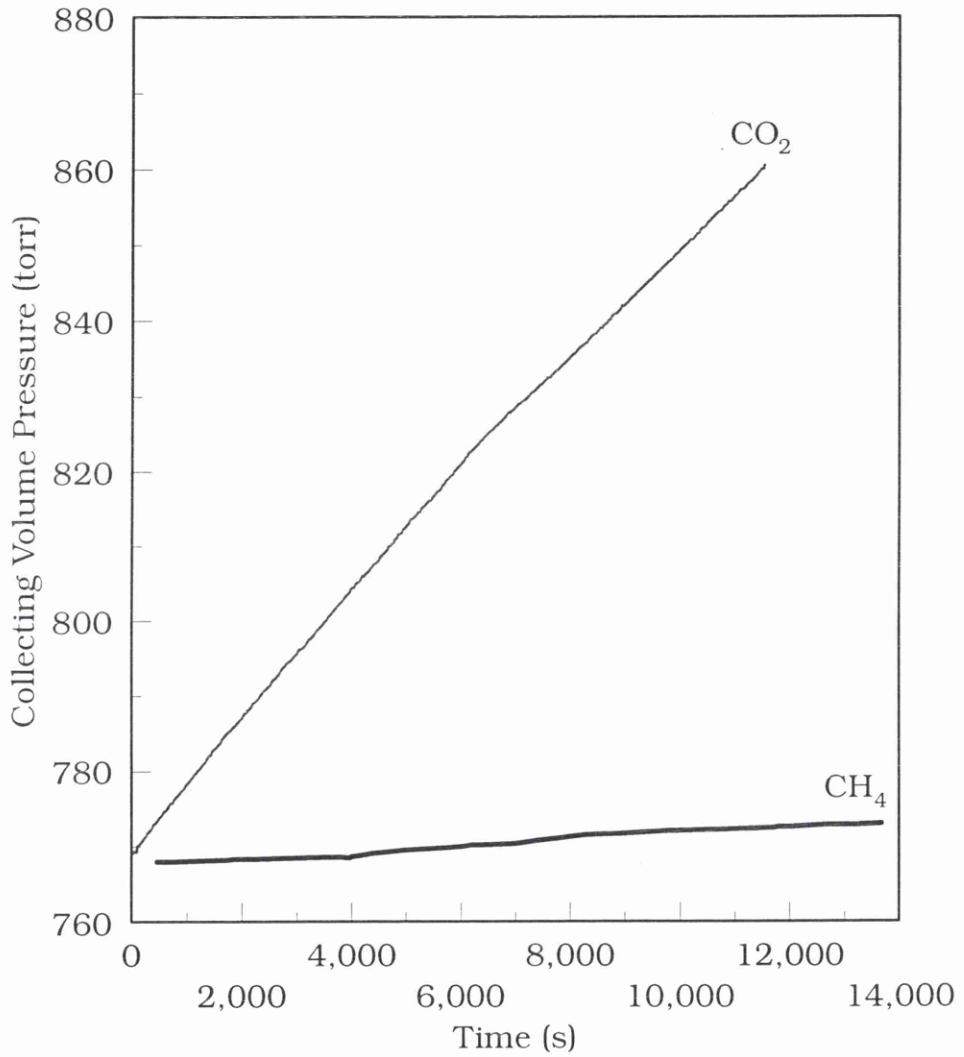


Figure 5.25 Relative gas flows for a Bayer Macrofoil KG Polycarbonate film (10µm thick) with +5 bar applied pressure steps.

5.5 Pore Size Estimation

The measurement of membrane pore sizes is not a trivial matter, particularly as the pore size decreases. There have been methods of measurement available for some time but these almost always involve some physical change in the pore being examined, e.g. microscopy requires conductive coatings that may change the pore size, mercury porosimetry which may cause an enlargement of the pore.

One method attempted by several workers [24, 25, 26, 27] was to use a gas permeation technique. One method in particular, by Yasuda & Tsai used a pressure decay method to determine pore sizes for microporous polymer membranes [28]. Using this as a basis for data treatment of the gas permeation experiments performed in this current study, an attempt was made to ascertain the simplicity and validity of the method. Yashuda and Tsai report that the permeability coefficient K , of a porous medium could be expressed by

$$K = K_0 + \left(\frac{B_0}{\eta}\right) \Delta \bar{p} \quad \text{Equation 5.19}$$

where K_0 is the Knudsen permeability coefficient, ($\text{cm}^2 \cdot \text{s}^{-1}$) η the gas viscosity (Pa.s), B_0 is a geometric factor (m^2) and $\Delta \bar{p}$ is the mean pressure i.e. $[(p_1 + p_2) / 2]$ and not the pressure difference ($p_1 - p_2$).

Further detailed descriptions of K_0 and B_0 are given and by substitution into Equation (5.19) yields

$$d = \left(\frac{B_0}{K_0}\right) \left(\frac{16}{3}\right) \left(\frac{2RT}{\pi}\right)^{\frac{1}{2}} M^{-\frac{1}{2}} \quad \text{Equation 5.20}$$

This indicates that the mean pore size, $d(\text{m})$ can be calculated directly

from the pressure dependence of the gas permeability without any further estimation of porosity, ϵ , or the tortuosity factor, μ_K . The value for K_0 can be obtained by extrapolation of the permeability data back to zero pressure and the value of B_0 from the slope of the linear plot (multiplied by the gas viscosity).

A repeat of a test performed by Yashuda and Tsai, using a $0.025\mu\text{m}$ Millipore VSWP (a mixed cellulose acetate & nitrate) membrane was performed. This yielded very discouraging results as the nominal pore size quoted was $0.031\mu\text{m}$ but the value obtained in this study was $0.011\mu\text{m}$ (repeatedly). The experimental data for this experiment are shown in Figure 5.26. As there were no additional experiments required merely an alternative data processing method for the experimental data already obtained, estimates for the membranes used in this study were performed, these are shown in Table 5.9. Unlike the test experiment, the pore sizes obtained were in general agreement with other methods.

Estimation of the pore size could also be produced from the Knudsen relationship to the gas flux, Equation (5.4) as the flux is proportional to the pore size, r^3 . This method has been used in the past but it suffers greatly from sensitivity to deviations in the actual pore size in the membrane. With the anodic alumina systems this is not true due to the highly ordered pore geometry. Use of this method with this type of membrane has been shown to produce excellent agreement with other methods of pore size estimation [29]. Finally, again due to the

unique structure of the anodic alumina system a very interesting effect has been shown with regard to estimating the pore size. The pore size can be estimated (and controlled) in the preparation stage as the electrolysis voltage used effectively controls the pore size produced. The membranes grow in hexagonal cells and the ratio of the cell width, D , to the pore diameter, d , is fixed if all other electrolysis conditions are constant [29] as shown in Plate 5.2. For the membranes produced in this study the relationship was found to be

$$\frac{D}{d} = 2.55 \quad \& \quad D = 2.8V \quad \text{Equation 5.21}$$

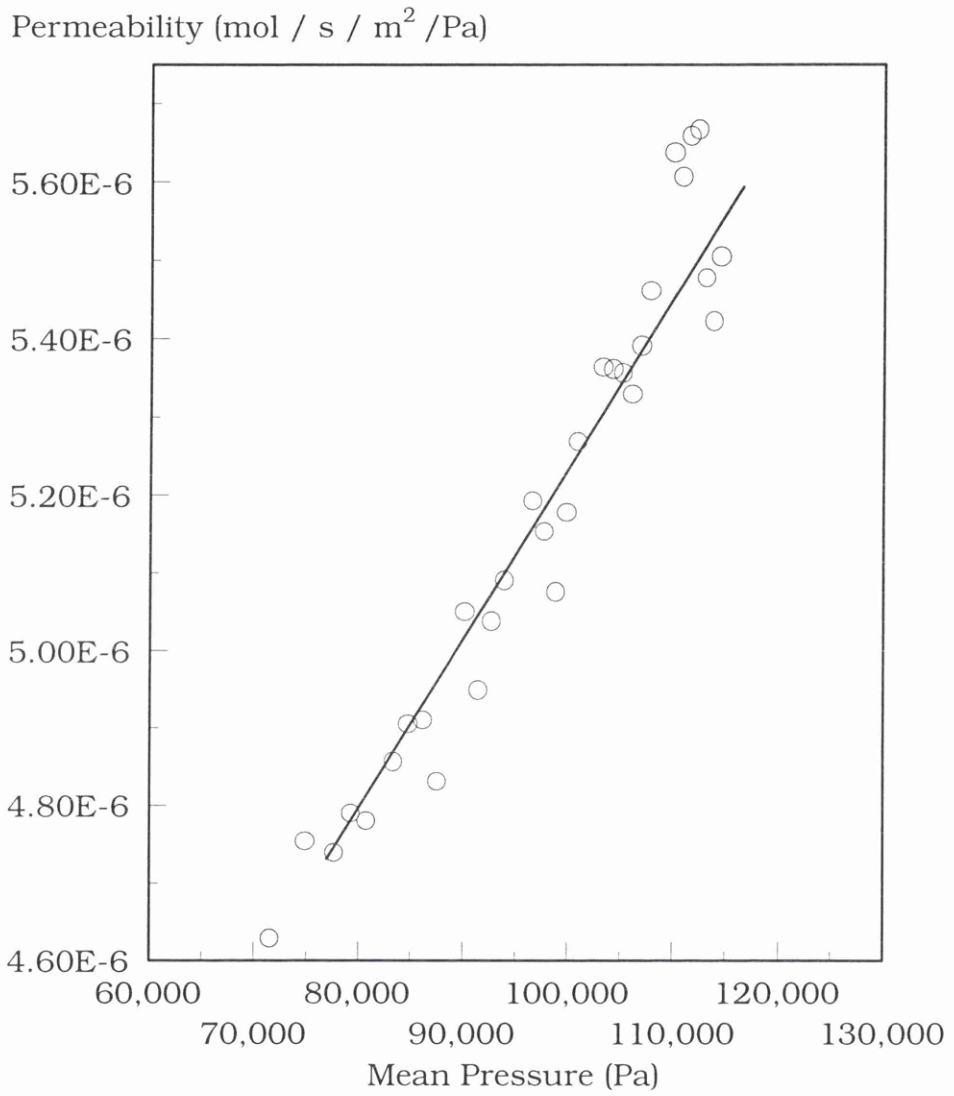


Figure 5.26 Pore size estimation test plot using a Millipore VSWP 0.025 μ m membrane filter.

Pore estimation method					
Membrane Type	Code	S.E.M	Gas Permeation	Anodisation Voltage	
Anodic Support	SAA1	62 nm	69-75 nm	79.1 nm	
Anodic Layer	LAA1	-	21-25 nm	18.6 nm	
Ceramic Support	ZrSup1	0.2 μ m	-	-	
Zirconia Active Layer	ZrAL1	-	40-44 nm	-	
Ceramic Tube Support	TS1	0.2 μ m	-	-	
Tube Active Layer	TLa1	-	7-12 nm	-	

Table 5.9 Pore Size Estimation by Various Methods for the Membranes Tested in this Study.

5.6 Conclusions

The equipment designed and used in this study was predominantly for the investigation of gas transport in porous (inorganic) membranes. This was due to an increased use of these membranes at a commercial / industrial level. It was felt that a greater understanding of the active layers of these membranes was needed and therefore a method of determination. We are fortunate in that these membranes are fabricated in layers (similar to a modern roadway), and that samples were made available at each step of the preparation process. This was certainly not true of the conventional polymeric membranes, in any format.

It was hoped at the outset, that both qualitative and quantitative data would be made available by this system. Initially, qualitative tests could rapidly show if defect free layers were present. In the case of gaseous transport this was particularly sensitive as the slightest surface defect was clearly shown.

On a quantitative basis, the effect of the active layer in terms of reducing the gas flow rate and aiding separation has been shown for simple 'unmodified' membranes. In other work using this equipment (within the same research group) it has been possible to show the scale and effect due to the chemical grafting of molecules onto the surfaces of these ceramic membranes [29, 30, 31].

The vast majority of the results shown here were based upon permeability data. It was hoped that use of the time-lag value (τ) could

also be used to determine values for the diffusion coefficients. This proved to be impractical as the observed time-lag values were of the order of a few seconds in these porous materials. This meant that the uncertainty of the time-lag value, in relation to the time taken for the imposition of the pressure step, was too high and therefore it was unsound to attempt this calculation. This was not the case for when dense layers were present and the system showed that it was capable of dealing with this more 'conventional' membrane system.

5.7 References

- [1] Final Report to EPSRC Research Grant (GR/J18729) 1994.
- [2] Uchytil, P., Nguyen, X.Q. and Broz, Z., Characterization of membrane skin defects by a gas permeation method, *J. Mem. Sci.* 73 (1992) 47.
- [3] Keizer, K., Uhlhorn, R.J.R., Van Vuren, R.J. and Burggraaf, A.J, Gas separation mechanisms in microporous modified $\gamma\text{-Al}_2\text{O}_3$ membranes, *J. Mem. Sci.*, 39 (1988) 285.
- [4] Uhlhorn, R.J.R., Keizer, K. and Burggraaf, A.J, Gas transport and separation with ceramic membranes. Part I. Multilayer diffusion and capillary condensation, *J. Mem. Sci.*, 66 (1992) 259.
- [5] Levitz, P., Knudsen diffusion and excitation transfer in random porous media, *J. Phys. Chem.*, 97 (1993) 3813.
- [6] Rowell, R.L., Carrano, S.A., Bethune, A.J. and Malinauskas, A.P., Gas and vapour permeability: surface flow through porous media, *J. Colloid Interface Sci.*, 37 (1971) 242.
- [7] Schofield, R.W, Fane, A.G and Fell, C.J.D., Gas and vapour transport through microporous membranes.I. Knudsen-Poiseuille transition, *J. Mem. Sci.*, 53 (1990) 159.
- [8] Datta, R., Dechapanichkul, S. J., Kim, S., Fang, L.Y. and Uehara, A generalized model for the transport of gases in porous, non-porous, and leaky membranes.I.Application to single gases, *J. Mem. Sci.*, 75 (1992) 245.

- [9] Uhlhorn, R.J.R, Keizer, K. and Burggraaf, A.J., Gas and surface diffusion in modified γ -alumina systems, *J.Mem. Sci.*, 46 (1989) 225.
- [10] Bhandarkar, M., Shelekhin, A.B., Dixon, A.G., and Ma, Y.H, Adsorption, permeation, and diffusion of gases in microporous membranes. I.Adsorption of gases on microporous glass membranes, *J.Mem. Sci.*, 75 (1992) 221.
- [11] Yuxun Y. and Diyong, W., Pore size of composite inorganic membranes, *Proceedings of the Third International Conference on Inorganic Membranes*, Worcester, July, 1994, 525.
- [12] Keizer, K., Uhlhorn, R.J.R., Zaspalis, V.T. and Burggraaf, A.J., Transport and related (gas and vapour) separation in ceramic membranes, *Key Eng. Mater.*, 61 & 62 (1991) 143.
- [13] Mulder, M., Chapter V, Transport in membranes, *Basic Principles of Membrane Technology (2nd Edition)*, Kluwer Academic Publishers, ISBN 0-7923-4248-8, 1996.
- [14] Graham, T., The law of effusion, *Phil. Trans. Royal Soc. (London)*, 4 (1846), 573.
- [15] Knudsen, M., The laws of molecular flow and of inner friction flow of gases through tubes, *Annalen der Physik*, 28 (1909) 75-130.
- [16] Tamon H., Okazaki, M. and Toei, R., Prediction of Surface Flow Coefficient of Adsorbed Gases, *AIChE Journal* 1985, 31, 1226.
- [17] Mardilovich, P.P., Govyadinov, A.N., Randon, J., McFadzean, S.

- and Paterson, R., New high temperature chemically resistant anodic alumina membranes: preparation, modification, properties, Proc. 3rd International Conference on Inorganic Membranes, Worcester, Massachusetts, USA, 1994, 457.
- [18] Furneaux, R.C and Thornton, M. C., Porous "ceramic" membranes from anodizing aluminium, Adv. Ceram. Chem. Process Eng., 43 (1988) 93.
- [19] Randon, J., Mardilovich, P. P., Govyadinov, A. N. and Paterson, R., Modelling the pore structure of anodic alumina membranes, Proc. 3rd International Conference on Inorganic Membranes, Worcester, Massachusetts, USA, 1994, 613
- [20] Larbot, A., Alary, J.A., Guizard, C., Cot, L. and Gillot, J., New inorganic ultrafiltration membranes: preparation and characterisation, High Tech. Ceram.,3 (1987) 143.
- [21] Larbot, A., Alami-Younssi, S., Persin, M., Sarrazin, J. and Cot, L., Preparation of a γ -alumina nanofiltration membrane, J. Mem. Sci., 97 (1994) 167-173.
- [22] Mazid, M.A., Matsuura, T., Membrane gas separation: A critical overview, Separation Science and Technology, 28, (15 & 16), 1993, 2287-2296.
- [23] Koros, W.J. and Fleming, G.K., Membrane based gas separation, J. Mem. Sci., 83 (1993), 1-80.
- [24] Uchytel, P., Gas Permeation in ceramic membranes. Part I. Theory and testing of ceramic membranes, J. Mem. Sci., 97 (1994) 139

- [25] Uchytil, P. and Broz, Z., Gas permeation in ceramic membranes. Part II. Modelling of gas permeation through ceramic membrane with one supported layer, *J. Mem. Sci.*, 97 (1994) 145.
- [26] Uchytil, P., Wagner, Z., Rocek, J. and Broz, Z., Possibility of pore size determination in separation layer of a ceramic membrane using permeation method, *J. Mem. Sci.*, 103 (1995) 151.
- [27] Altena, F. W., Knoef, H. A. M., Heskamp, H., Bargeman, D. and Smolders, C.A., Some comments on the applicability of gas permeation methods to characterize porous membranes based on improved experimental accuracy and data handling, *J. Mem. Sci.*, 12 (1983) 313.
- [28] Yasuda, H. and Tsai, J.T., Pore size of microporous polymer membranes, *Journal of Applied Polymer Science*, Vol. 18, 1974, 805-819.
- [29] Lira, H. deL., PhD. Thesis, University of Glasgow, 1997.
- [30] Leger, C., Lira, H. deL and Paterson, R., Preparation and properties of surface modified ceramic membranes. Part II. Gas and liquid permeabilities of 5nm alumina membranes modified by a monolayer of bound polydimethylsiloxane(PDM) silicone oil, *J. Mem. Sci.* 120 (1996) 135-146.
- [31] Leger, C., Lira, H. deL and Paterson, R., Preparation and properties of surface modified ceramic membranes. Part III. Gas permeation of 5nm alumina membranes modified by trichloro-octadecylsilane, *J. Mem. Sci.* 120 (1996) 187-195.

- [32] Handbook of Chemistry and Physics, CRC Press Inc., USA, 75th Edition, 1994.
- [33] Atkins, P.W., Physical Chemistry, 3rd Edition, Oxford University Press, Oxford, p652, 1987.
- [34] Breck, D.W., Zeolite Molecular Sieves, John Wiley and Sons, New York, 1974.

Chapter 6

Experimental Measurement of Liquid Based Systems

Introduction

6.1 General Description

6.2 Measurement Cell Design

6.3 Measurement Equipment

6.4 Measurement System and Instrument Calibration

6.5 The Generation of a Concentration Step

6.6 'Null' Cell Tests

6.7 References

6 Experimental Measurement of Liquid Based Systems

Introduction

In this chapter the membrane testing apparatus and other associated techniques developed in the course of this research relating to liquid based systems will be described in detail . The designs and construction of the measurement cells will be given together with the methods used for the calibration and testing of the cells, the individual measuring devices and the overall measurement systems.

Due to the complexity of the tasks required, in a suitable timescale, the use of modern computer based data acquisition and control was essential. This resulted in a need for the development of customised software to enable both for the collection of the information and for the effective display and manipulation of the collected data. This is again mentioned merely in passing in this chapter but has been covered more fully in Chapter 3.

6.1 General Description

The construction of a membrane testing system capable of measuring transport through membranes in liquid based systems is much more difficult than for gaseous transport. Several systems have been described in the literature [1,2,3] but each of these have some major problem or difficulty in operation. In practice there are several difficulties (when compared to a gas system) that need to be overcome, these will be described in the following section.

In this present research, the mechanism chosen was for a solution of

one concentration to be changed in principle, instantaneously to another concentration level at one face of the test membrane. The liquid (solution) based test system designed and constructed in this study used pumped liquid flows across one exposed face of a test membrane. The solution flow was generated by a peristaltic pump (Watson-Marlow MHRE 200 Mk 3, UK). This in fact, was quite a crude pump of this type as it employed only three pump rollers compared to the more modern type (up to 20 rollers) of pump. This was however, considered to be an advantage as the pulsatile nature of the induced flow would help to reduce unstirred layers at the membrane surface.

The solutions were circulated around their respective loops through P.T.F.E tubing (0.8mm ID) with the exception of two small lengths of Marprene (food quality) silicone tubing fitted at the pump head required to induce the flow. The solutions were maintained at a constant temperature by storing them in borosilicate, liquid chromatography reservoirs (500cm³) (Omnifit Ltd., UK, Part number 3201) which were located in a circulated water bath thermostatted to 25°C ± 0.05 °C, Hakke (Germany) Thermostirrer Model 100. The collecting volume was stirred by a P.T.F.E coated magnetic stirring bar driven by a small external electromagnetic stirrer (Variomag 100, Camlab, UK) which had no moving parts and was capable of being totally submerged as it used only low voltage electromagnets to induce stirring. A schematic of the system layout is shown in Figure 6.1

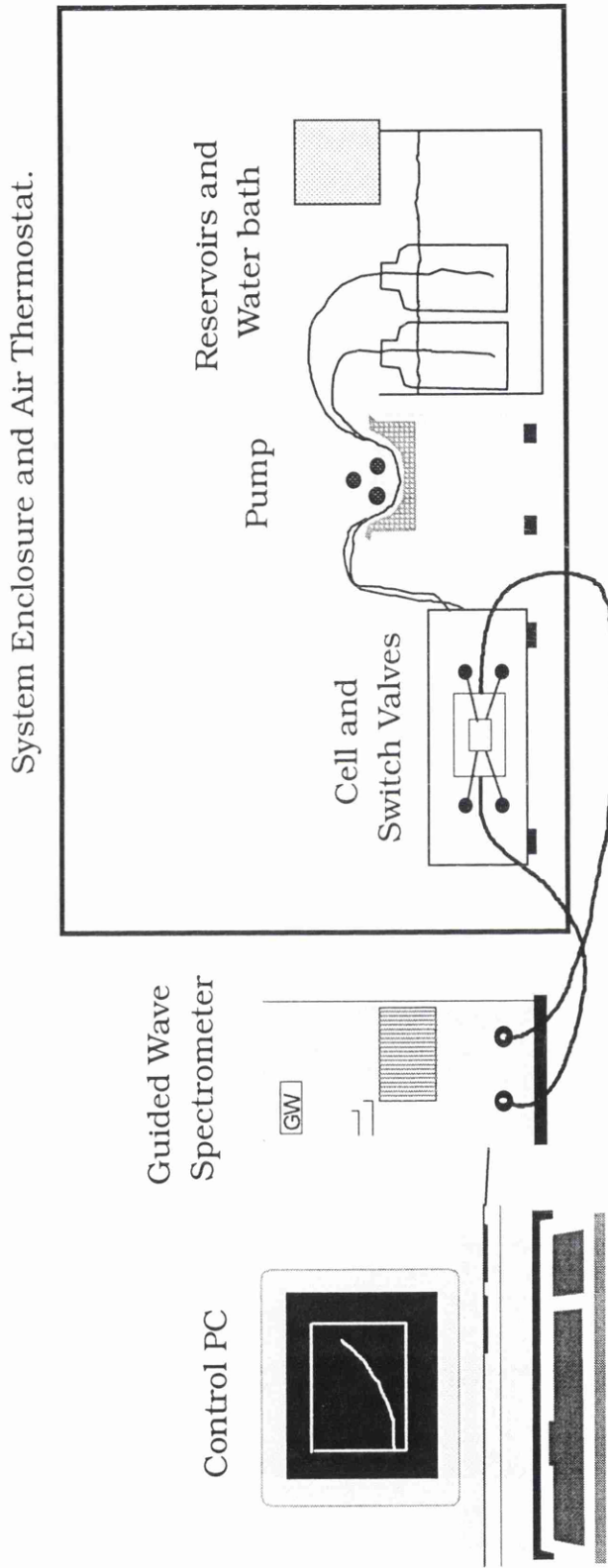


Figure 6.1 A Schematic of the Pumped Liquid Flow System Showing the Major System Components.

6.2 Measurement Cell Design

The liquid permeation test cell described here has evolved through several different stages. This was discussed in the General Introduction (Chapter 1). The cell comprised of two main sections. The cell body and a top piece (solution delivery head) were both constructed from Perspex™ (Polymethylmethacrylate). This material was chosen for its excellent machining properties and that it can be highly polished to leave a clear, transparent finish. This allowed for easy visual inspection to ensure no trapped air bubbles resided in the collecting volume and to ensure the membrane was mounted properly in the cell. By choosing this material we were limiting our use of the system to effectively aqueous based systems but this was not considered a disadvantage or restriction at this stage of development. The cell body was itself sectional in its design. This was to allow for the possibility of interchanging sections of the cell. By using such a modular design the collecting volume could easily be modified to accommodate a variety of different cell parameters. These included increasing or decreasing the cell volume, quickly replacing damaged sensors, placement of additional sensors or any combination of these as the test system required. Each of the component parts of the cell will be described below.

6.2.1 The Support Frame

This was an L-shaped block of Perspex™ onto which the two other cell sections were located and secured in place. On one

face of this 'L' section a circular opening (12mm diameter) was located. This opening was tapped and threaded and was fitted with a threaded screw cap. This cap served two purposes, firstly it sealed the contents of the collecting volume and secondly, it had located within it a temperature measuring device. Full engineering drawings are shown in Figure 6.2.

The opening for this screw cap was positioned in such a way that the temperature probe (a thermistor) was located centrally in the collecting volume (position A, Figure 6.2). The four holes drilled through the main face were for the screws that fastened to the stirrer block and which sealed the collecting volume together. The faces of all three sections of the cell were milled flat and polished to ensure that when the cell body was assembled together that the cell was leak free. The two holes on the top of the L-Piece (position B, Figure 6.2) were tapped and threaded and these (plus two others on the stirrer block) located the cell top piece and flow head.

6.2.2 The Detector Block

This was a rectangular sectioned block of Perspex™. This section served three basic purposes: (a) it acted as the main constituent part of the collecting volume itself (b) it contained and located the cell detection probes and (c) it defined the exposed test membrane area. Full engineering drawings are shown in Figure 6.3.

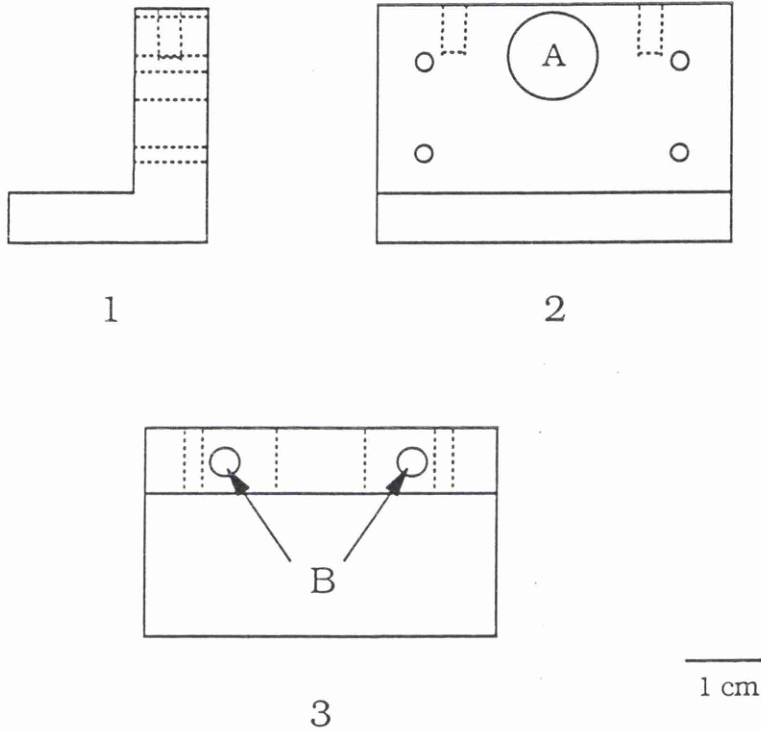


Figure 6.2 Engineering Drawing for the Support Frame Section of the Liquid System Test Cell Depicted from (1) End Elevation (2) Front Elevation and (3) Plan Viewpoints.

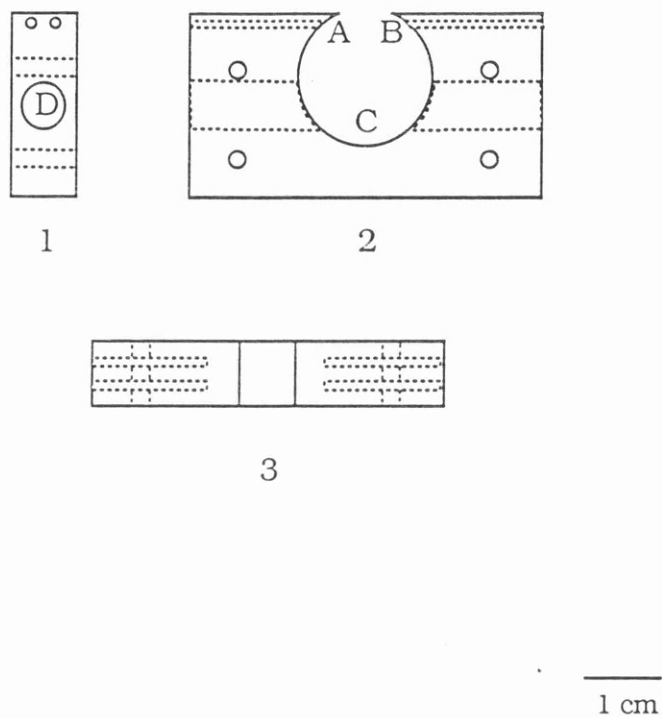


Figure 6.3 Engineering Drawing for the Detector Block Section of the Liquid System Test Cell Depicted from (1) End Elevation (2) Front Elevation and (3) Plan Viewpoints.

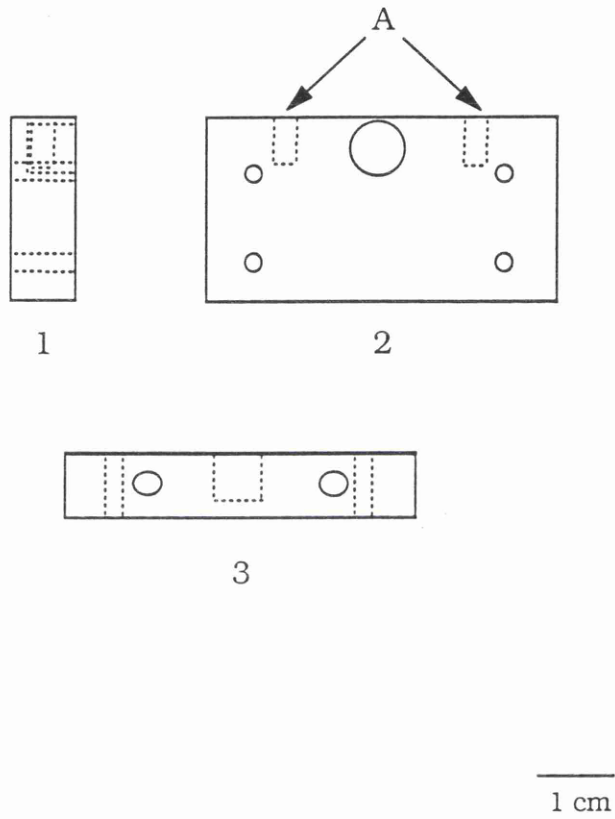


Figure 6.4 Engineering Drawing for the Stirrer Housing Section of the Liquid System Test Cell Depicted from (1) End Elevation (2) Front Elevation and (3) Plan Viewpoints.

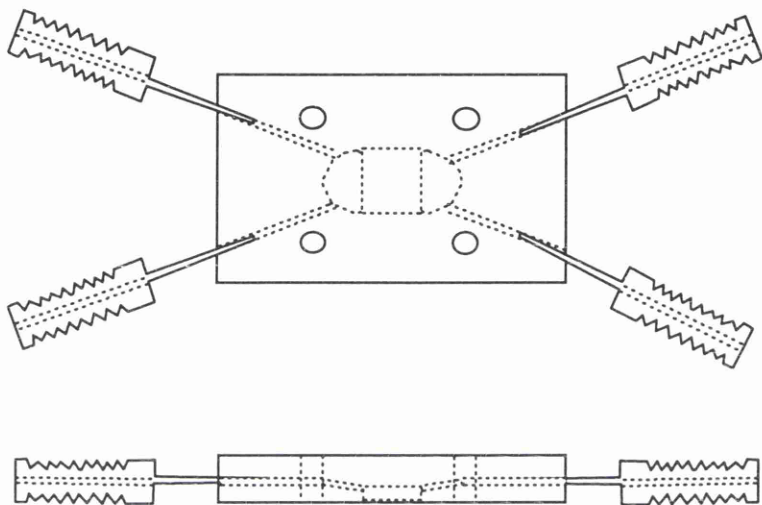


Figure 6.5 Engineering Drawing for the Liquid System Test Cell Solution Delivery Head Depicted from (1) Front Elevation and (2) Plan Viewpoints.

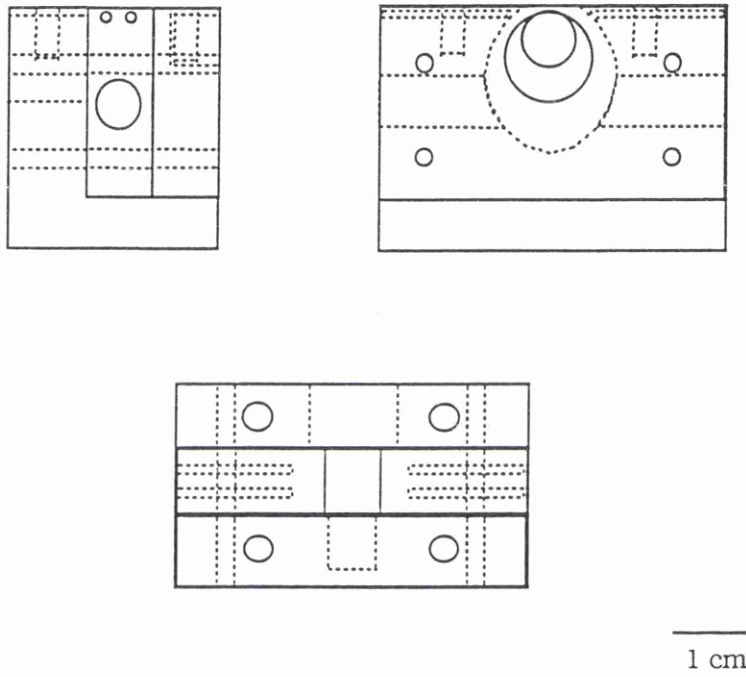


Figure 6.6 Drawings of the Assembled Liquid System Test Cell Depicted from (1) End Elevation (2) Front Elevation and (3) Plan Viewpoints.

The circular design of the main collecting volume was chosen to enhance the mixing within the detection cell. There were no projections or obstructions around this inner circumference to again minimise the possibility of unstirred layers or areas within the collecting volume.

The detector section illustrated in Figure 6.3 contained two different types of in-built probes. These were electrical conductivity electrodes and optical (fibre optic) sensors.

6.2.2.1 Conductivity Measurements

Initially, a pair of conductivity probes were placed as close as possible to the back face of the test membrane. At the development stages tests were carried out to determine the optimum position and configuration of the conductivity electrodes.

The first tests had pairs of electrodes at positions A,B & C (shown in Figure 6.3) with each pair being tested individually to measure the conductivity of a known concentration solution. As these electrodes consisted of extremely short lengths of platinum wire the noise in the measured conductivity was considerable. The next step was to 'mix' the pairs and measure between two electrodes in position A-B, A-C (in Figure 6.3) . This resulted in a similar 'noisy' signal , which was considered to be unacceptable. The next step was to increase the electrode area. This was

achieved by using a 'loop' electrode at positions A and B (Figure 6.3) and measuring the conductivity across this section of the cell. This resulted in significantly improved stability of the conductivity readings and was the configuration adopted for practical use.

6.2.2.2 Electrode Preparation

The conductivity probes were constructed from 0.5mm grade 1 platinum wire. This was fed through one of the two holes (A&B Figure 6.3) and then looped back down the other hole on the same side of the cell. The holes were then very carefully sealed using a two part encapsulating resin (CY1301 & HY 1300 ,Ciba-Geigy Plastics, UK) on the inside face of the collecting volume cell. Great care was taken to ensure that none of this resin touched the platinum wire loops that now extended into the collecting volume. When this had cured fully (3 days) the platinum electrodes were platinised (to add a layer of platinum black to the wire surface). This was performed by electrolysing the two platinum wires (as the cathode) in a solution of chloroplatinic acid (2% w/v in 2M hydrochloric acid) to which 0.02% lead acetate was added [4]. The anode in the circuit was a small platinum foil and the electrolysis was allowed to continue for three minutes with a current of 0.4 mA using a Solartron AS1413 laboratory power supply

unit. On the outside edges the remaining platinum wire was twisted together carefully to create a small stub of wire. This was then soldered into a gold plated pin socket taken from a Cannon D-type connector (used in computer systems). This entire assembly was then covered with Araldite™ adhesive (Ciba-Geigy) and fixed to the outside edges of the detector section to give increased mechanical strength to the connection.

6.2.2.3 Optical Pathway

In an alternative configuration, solution optical densities were used to detect concentration changes. A hole (6.5 mm diameter) was drilled through the detector section parallel to the top face (Position D, Figure 6.3). This was tapped and threaded and a stainless steel fibre optic terminator, a 905/906 SMA bulkhead (Fibre Optics Centre Ltd, UK, Part number 635) was then sealed in position. These terminators had previously been fitted with optical windows of Far UV grade silica (Thermal Syndicate Ltd, UK) at their inner ends. With these in place the optical fibres from the spectrophotometer could be securely located and held in perfect alignment.

6.2.3 Stirrer Housing Block

This was a rectangular sectioned piece of Perspex™. It contained a recessed hole (8 mm diameter) into which a

P.T.F.E coated magnetic stirring bar was located (Radleys Laboratory Supplies Ltd, UK, Cat. Number F3725-0014). This section also acted as the locking piece which held the cell body together, full engineering drawings are shown in Figure 6.4.

The positioning of this stirrer was extremely important. This was the only means of ensuring that there was concentration homogeneity throughout the collecting volume. For this reason the stirrer was placed off centre and as close as possible to the back face of the test membrane. The recessed hole in which the stirrer was located was only marginally wider than the stirrer itself. This was to reduce any possible 'dead volume' around and below the stirrer and also to ensure that the stirrer could not move around in the cell or indeed touch against the membrane surface. The depth of this locating hole was also critical. If this was not deep enough the top of the rotating stirrer would encroach into the optical path (this would be totally unacceptable). Finally, the two threaded holes (Position A, Figure 6.4) were for the screws that retained the flow head (in conjunction with those in the support frame, Figure 6.2)

6.2.4 Screw Cap Seal

This was a threaded screw cap machined from Perspex™. This sealed the contents of the cell and also housed a temperature probe, a 'micro' heater and a bleed vent. Measurement of the

cell temperature was extremely important as electrolyte conductivity varies with temperature. For potassium chloride the conductivity changes by approximately 2% per degree Centigrade [5]. Thermocouples were used originally but they proved to have too slow a time response. The temperature probe used in this design was a negative temperature coefficient (n.t.c) thermistor (R.S Components Ltd,UK, Cat Nos. 151-013). This was a resistance variable device (0 to 1 Mohm) dependant on temperature. They were physically very small and could be easily encapsulated into such a device. The connections were made using the gold plated Cannon D-type plugs and sockets referred to earlier (in section 6.2.2.2). The 'micro' heater was also a n.t.c thermistor (R.S , Cat Nos. 151-029) of a similar type but with a different resistance range value (0 to 2k ohms). This was connected to a laboratory power supply (Solartron Instruments Ltd, UK Model AS1413) and could be switched in and out of circuit on demand using a contact closure controlled from the computer. Both of these devices were securely located with Araldite™ adhesive to protect the delicate connections.

6.2.5 Solution Delivery Head

The solution delivery head was also constructed from Perspex™ and is shown in Figure 6.5. Like the other component parts of the measurement cell the mechanical

engineering needed in this design was of the highest quality. A single piece of rectangular Perspex™ 46x25x5mm had a small rectangular channel 6x9x2 mm milled out from the centre of the block, this was to form the chamber into which the solution would flow. Immediately adjacent to this (on the longer sides) another channel was milled out. This time the channels were offset at approximately 40° from the horizontal plane to create a double wedge shape. On the slopes of these wedges two small semi-circular channels were made to direct the solution flow on to the chamber immediately above the test membrane. Close to the four corners but on the edges of the block, four holes were drilled diagonally towards the central chamber. Into these holes the solution delivery tubes were fixed in place. These were stainless steel tubing adapters (Omnifit Ltd., UK, Cat Nos. 2505) that allowed for connection to the larger P.T.F.E tubing used in the two pumped solution loops. The flows were arranged in such a way that both solutions (low & high concentration) would flow diagonally across and upwards over the test membrane surface. The inlet and outlet ports were also offset slightly to ensure that the flow pattern in the chamber was as turbulent as possible during the short residence time of the solution 'slab' in the chamber. Full engineering drawings for the cell solution delivery head are shown in Figure 6.5.

6.2.6 Measurement of the Cell Volume

The cell was taken apart, washed and then thoroughly dried and reassembled. A diagrammatic view of the assembled cell is shown in Figure 6.6. The cell flow head was screwed into position with a microscope cover slip placed over the cell opening, this was to seal the collecting volume off. The cell was weighed on an electronic top pan balance (Metler AE163) and the weight and temperature noted. The cell was then filled with degassed distilled water and placed back on the balance. It was allowed to attain the same temperature as the previous weight reading (20°C) and the weight recorded. This procedure was repeated three times and the weights differed by no more than 5mg. The volume was then obtained by using water density values at 20 °C and converting the weight to a volume. The total cell volume was found to be 1.752cm³

6.3 Measurement Equipment

The individual measurement devices used in the system are described briefly in this section.

6.3.1 Temperature

The ohmic resistance of the n.t.c thermistor bead sealed into the screw cap was measured using an electronic digital multimeter (Solartron Instruments Ltd, UK, Model 7151). This particular instrument had a measurement precision of 0.003% (over 24 hours) for the measurement range used (200

Kohms) and used a measurement current of 1 μA . This was a totally programmable instrument as it had in built IEEE-488 and RS-232 interfaces. For speed and ease of use with the other electronic components in the system the IEEE-488 interface was used for the data collection

6.3.2 Solution (Electrolytic) Conductivity

Electrolytic conductivity in this study was measured using a Wayne Kerr Instruments, UK, B905a bridge. This bridge measured the conductivity of the test solution using a high frequency (minimum 1 KHz) sinusoidal alternating potential from an internal oscillator to prevent electrolysis of the test solution occurring. Further general information regarding the design of such instruments can be found elsewhere [10]. The measurement range of the 905a was from 0 to 1 Seimens \pm 0.05% (or \pm 1nS). The instrument was also fitted with an optional IEEE-488 interface which permitted fully automated data collection and control of the instrument.

Connection from the bridge to the measurement cell was made through Kelvin leads. These were fully screened four terminal leads that allowed connection to one pair of measurement points. Additionally the bridge was capable of 'trimming' out the resistive and capacitive elements of the measurement leads, thus ensuring that any measured effect was not being

generated by polarisation of the leads but by the test system under investigation.

6.3.3 Optical Density (Absorbance) Measurement

Solution absorbance in the ultra-violet to visible region of the electromagnetic spectrum was measured using a UV-Visible spectrophotometer. The instrument used in this study was a Guided Wave Model 260,(UOP Inc., USA) this was a high resolution, single beam scanning spectrophotometer. It was modular in design and a variety of gratings, filters, detectors and slits were readily available.

Unlike conventional spectrophotometers this instrument did not have a sample compartment. Instead, optical fibres carried the light to the sample and returned the sample-modified light to the instrument for analysis. This allowed *in situ* measurement of chemical composition and this was extremely powerful in its implications for real time measurement of membrane transport phenomena as many of the permeant materials of interest absorb radiation in the range of frequencies covered by this type of instrument.

The instrument was totally automated and all of its functions were available via computer control. Data and instructions could be passed either by RS-232 data link (slow option) or by way of a dedicated interface board. The latter allowed much faster data collection rates and also had some additional

features such as in built diagnostic tests and was therefore the interface of choice.

6.4 Measurement System and Instrument Calibration

If great confidence was to be taken from the readings obtained from the various component parts of the measurement system, tests to prove the range and accuracy of the measurements had to be obtained. In this section the methods used for this purpose are described.

6.4.1 Calibration of Thermistors

The bead type thermistors used in this work were of the glass sheathed variety. Their resistance value changed with temperature, accordingly a measurement check of the range of temperature was performed. The thermistor, encapsulated in the screw cap assembly was carefully positioned in a water bath, ensuring that the electrical contacts were not themselves below the surface at any time. The bath temperature was varied and controlled using a Hakke Thermostirrer 100 (Germany) heater/ circulator between 20 and 40 °C with the resistance values being recorded when the readings stabilised. The bath temperature readings were recorded using a recently calibrated platinum resistance thermometer. This resulted (not unexpectedly) in a non-linear response over this temperature range. The procedure was repeated but over a narrower temperature range (22 to 27°C) and on this occasion the bath

temperatures were measured using a narrow range dip-type mercury thermometer (15 cm immersion, G.H Zeal, London, UK, serial nos. HEG/776). This thermometer had National Physics Laboratory (NPL) certification (Reference 121478) and was traceable back to British Standards [6]. The resistance versus temperature relationship was recorded and is shown in Figure 6.7. A least squares analysis of this data yields an equation that very accurately describes the line. Using the line fit values obtained, the experimental recording of resistance was converted directly to the temperature of the collecting volume.

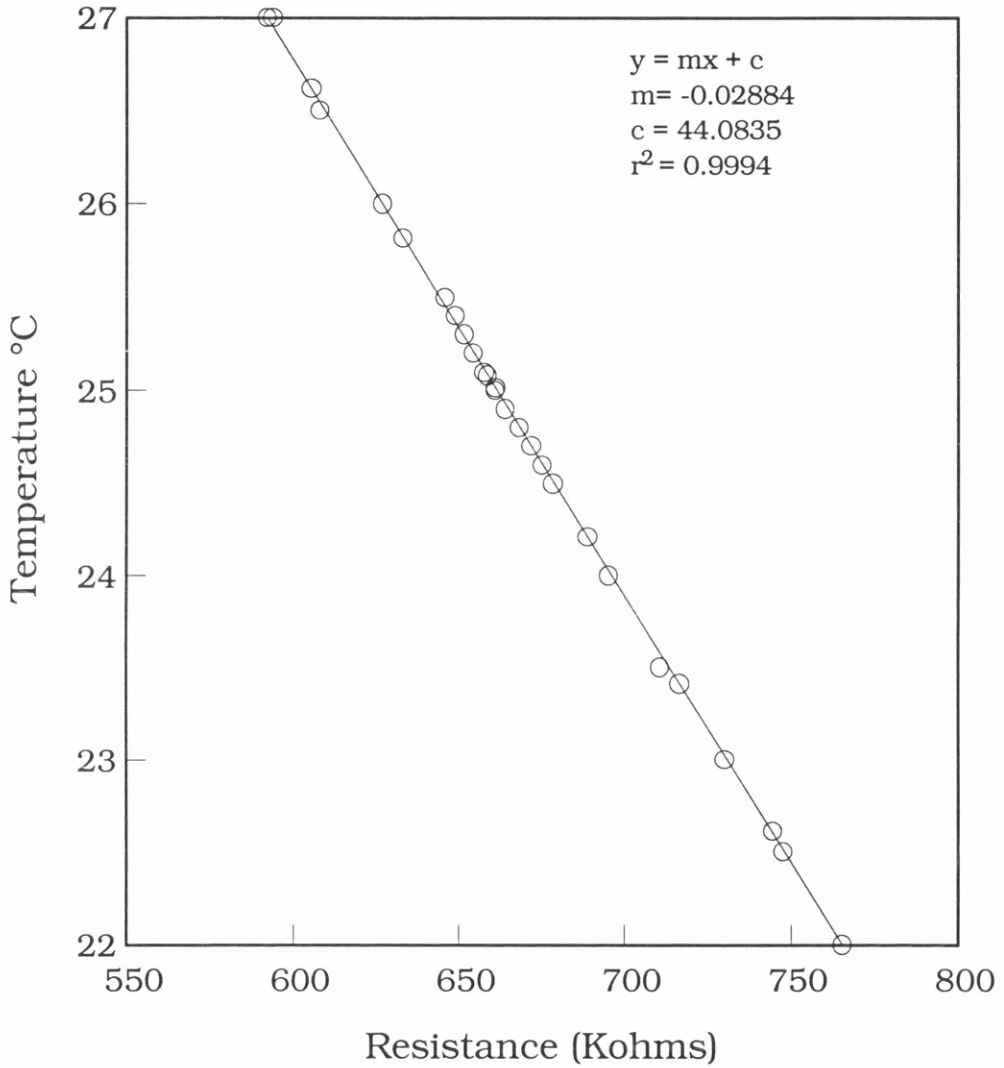


Figure 6.7 Calibration Profile for the n.t.c Thermistor Bead Encapsulated in the Screw Cap Assembly of the Membrane Test Cell.

6.4.2 Ultra-Violet/Visible Spectrophotometer

The Guided Wave 260 was a single beam instrument and as such required certain conditions if the highest accuracy was to be achieved. In the instrument used in this study the detection system used was a Photomultiplier device and had a working range between 190-700nm. Obviously, wavelength selection was very important and to check that the diffraction grating could accurately resolve to a specified wavelength two independent tests were used for calibration. Before every series of analysis at least one of the two tests described below were performed.

(A) Didymium Filter

This was a glass slide with a coated film of Didymium oxide and this has been used extensively for wavelength calibration in the visible spectral region. This has two sharp and well resolved peaks at 573 ± 3 nm and 586 ± 3 nm, the latter having a slightly stronger absorbance. The Guided Wave reported the peak maxima to be at 572.5 nm and 584.6 nm with the absorbance values being 1.018 and 1.274 Abs respectively. These values were well within the allowed range of acceptability and are shown in Figure 6.8

(B) Narrow Band Interference Filter

These optical filters were specified to be 1.5 nm wide ± 0.2 nm with approximately 30% peak transmission (note, the peak

height will vary depending upon the bandwidth of the analyser used). The most commonly used of these narrow band filters is the primary He-Ne laser line at 632.8nm. Using such a filter (Speirs Robertson Ltd, UK, Part Number 29-6100) a wavelength scan either side of this value was performed, the maximum transmission value was found at 632.8nm . The results are shown in Figure 6.9.

Absorbance

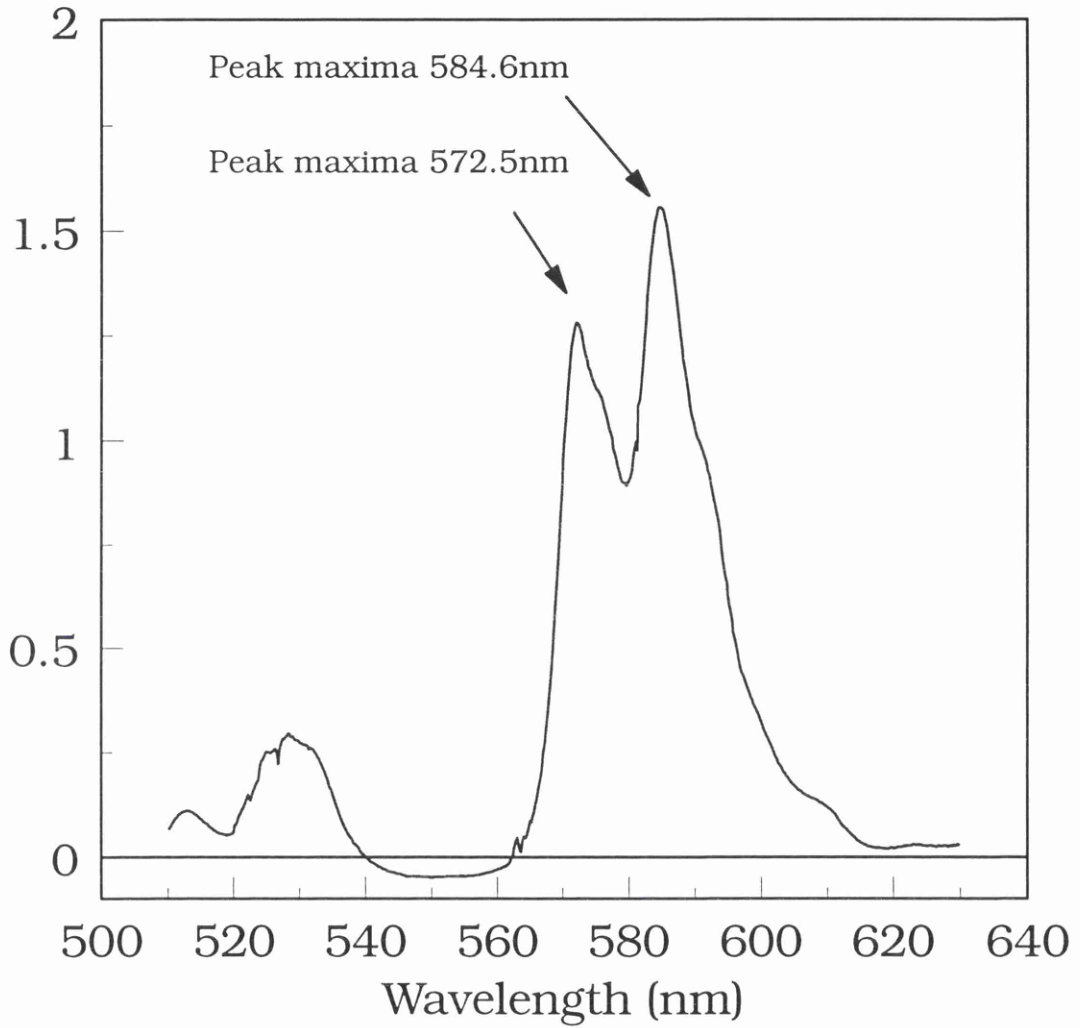


Figure 6.8 Wavelength Accuracy Calibration Test Using a Didymium Coated Optical Glass Slide.

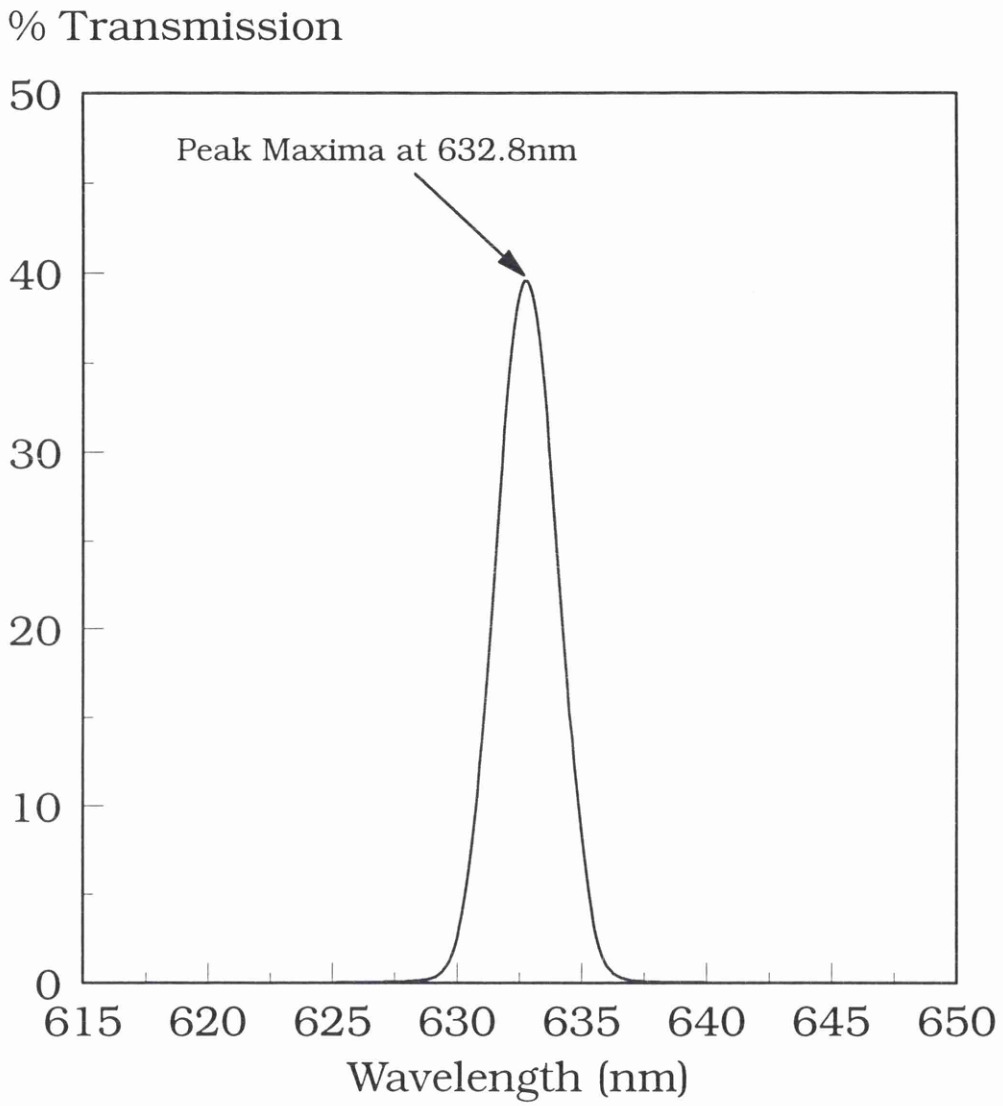


Figure 6.9 Diffraction Grating Calibration Test Using a Narrow Band Filter at the Primary He-Ne Laser Wavelength(632.8nm)

6.4.3 Conductivity Bridge Measurements

The measurement of the solution conductivity was a relatively simple matter. The bridge was 'trimmed' before every analysis to remove any influence of the measurement leads. A sample of thermostatted distilled water was placed in the measurement cell and the conductivity noted. This water reference value was then subtracted from all subsequent readings to give the conductivity due to the solution alone. The importance of temperature must not be overlooked when accurate conductivity measurements are required as we are in effect measuring a resistance, this temperature effect was noted earlier (section 6.2.4). In some cases this could be significant due to the extremely low salt concentration of the collection volume solution.

6.5 The Generation of a Concentration Step

The ability to generate a sudden and reliable concentration step at the external face of a test membrane was imperative to the success of the system. This was achieved in a manner similar to that described previously in Chapter 4 (Gaseous System). Unlike the gaseous system, the generation of a sharp concentration change in the solution phase is not so simple a matter. At the point of the switch there will be significant mixing of the two solutions and this represents a substantial problem. The low concentration solution (normally distilled water) will be very easily contaminated and the higher concentration

also diluted by a similar amount. To overcome this, for a period of time after the switch was imposed the solution flow exiting the flow head was pumped out of the looped flow system to waste. The same type of electrical solenoid valves were used, Angar Scientific Co., USA, Direct Acting Solenoids Models 340 & 341, for all of the reasons described previously in Section 4.3.4.

6.5.1 System Assembly and Layout

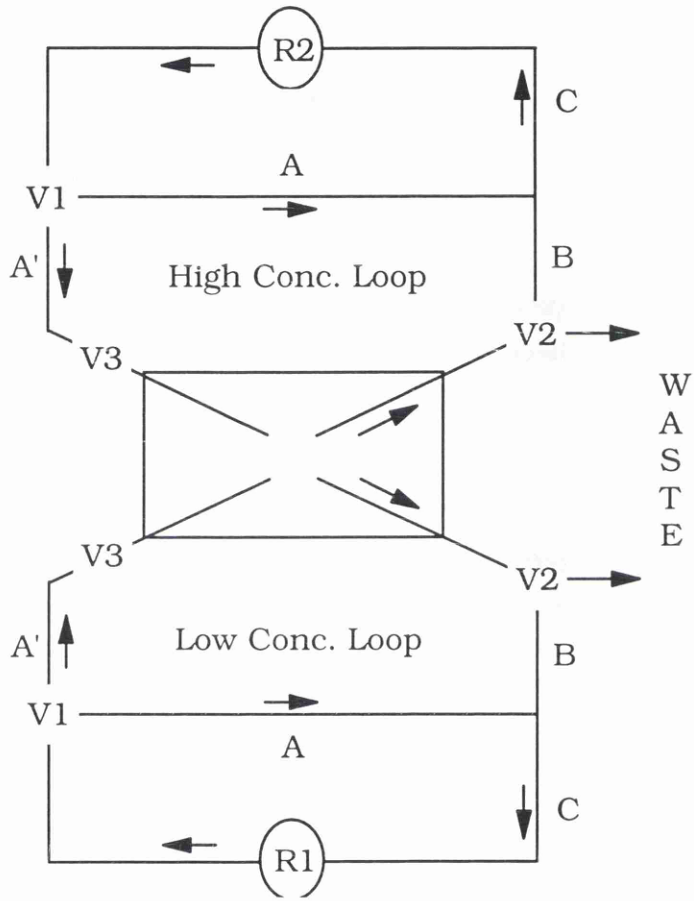
The two flow solutions were completely isolated from each other in two discrete loops with the exception of the small portion of solution that actually flowed through the flow head and across the exposed membrane surface. Both of these loops were as identical as possible with regard to their overall volumes, lengths and types of tubing used and the physical locations of the switching solenoid valves. Three solenoid valves were used in each of the two solution loops, two three way and one two way valves. Both of the two 'mirrored' loops were effectively divided into two sub-loops within the one major loop. This configuration is shown diagrammatically in Figure 6.10. The reasons for this layout were; (a) to ensure that there was no possibility of a pressure build-up in the pumped loops and (b) to ensure that there was no solution cross contamination as this would reduce the system efficacy. Each valve in the system had a specific purpose in the loop and this will now be explained.

The solution was pumped from the reservoir and directed through valve V1 to follow route A, towards the T-piece junction. As valve V2 is positioned such that solution could flow towards the flow head, using route B, the valve V3 is closed. As valve V3 is closed this prevents, by means of an air block or by stationary solution, a flow into the flow head assembly (via route B) and the solution takes the path of least resistance, route C, back into the solution reservoir.

The test cell was fitted with the test membrane and the flow head screwed into position. The four solution flow tubes were then fixed in place with the solution feeds being at the bottom entry points and the related solution exits being on the top diagonally opposite. The solutions to be used were fully temperature equilibrated and the cell stirrer started. The measurement leads were connected to their related sensors and the system was now ready for an experiment to begin.

6.5.2 Solution Flow to the Test Cell (Switch Logic)

When flow of the low concentration solution was allowed across the membrane surface by the computer meeting all of its parameter criteria (discussed earlier) a series of valve switches occurred in a very well defined sequence over a short time period. In the following description all valve values refer to those shown in Figure 6.10.



V1 & V2 : 3 way valves
 V3 : 2 way valve
 R1 & R2: Solution Reservoirs

Figure 6.10 A schematic representation of the Liquid Flow System Layout and Valve Configuration.

At the instant of the switch, valve V1 redirects solution away from route A to A', an instant later (<0.1s) valve V3 opens. This allowed solution to flow through the cell head and over the exposed surface of the test membrane. Another instant later (<0.1s) valve V2 redirects the solution exiting the flow head to a waste bottle. This flow pattern continues for the user predefined time period (normally 5-10 s). This allowed any mixed solution to be ejected from the system. At the end of this 'to waste' period, valve V2 changed state and redirected flow back into the loop and subsequently back to the solution reservoir. The solution volume left in the tubing between the T-piece and valve V1 was now stationary due to valve V1 being switched to the A' position.

When the desired concentration step was to be imposed the reverse of the sequence above took place on the low concentration side. Valve V3 closed and V1 redirected liquid flow back to the reservoir. On the high concentration side the switching sequence described above was replicated and the concentration step was applied. This solution flow logic for a full cycle (low to high and back to low concentration) is shown diagrammatically in Figure 6.11.

6.5.3 Pumped Solution Flow Rates

The two solutions pumped across the exposed membrane surface were responsible for the generation of the

concentration step. It was obvious that the liquid flow velocity used would greatly determine the effectiveness of this process. When the solutions were pumped at high speed through the tubing and valve network and across the flow head delivery channel, large quantities of air bubbles were generated. These caused two problems; (a) they caused air pockets to form at the pump head and as a result little or no solution flow was induced and (b) air bubbles formed and got trapped in the flow head chamber, this effectively reduced the exposed membrane area on the outer membrane face exposed to the flowing solutions.

When very slow pump speeds were used no air bubbles were formed but of course the solution changeover when a step was applied was extremely slow and therefore, totally inadequate. A compromise between these two extremes was necessary.

After a series of tests to determine the optimum solution flow rates, a value was accepted that gave good solution changeover and did not give excessive problems with large quantities of air bubbles being produced. In the diagram of the flow head (Figure 6.5) the solution void directly above the exposed membrane had a total volume of only 0.18cm^3 . The volumetric flow rate decided upon (and verified in both loops) was $1.15\text{ cm}^3\text{s}^{-1}$.

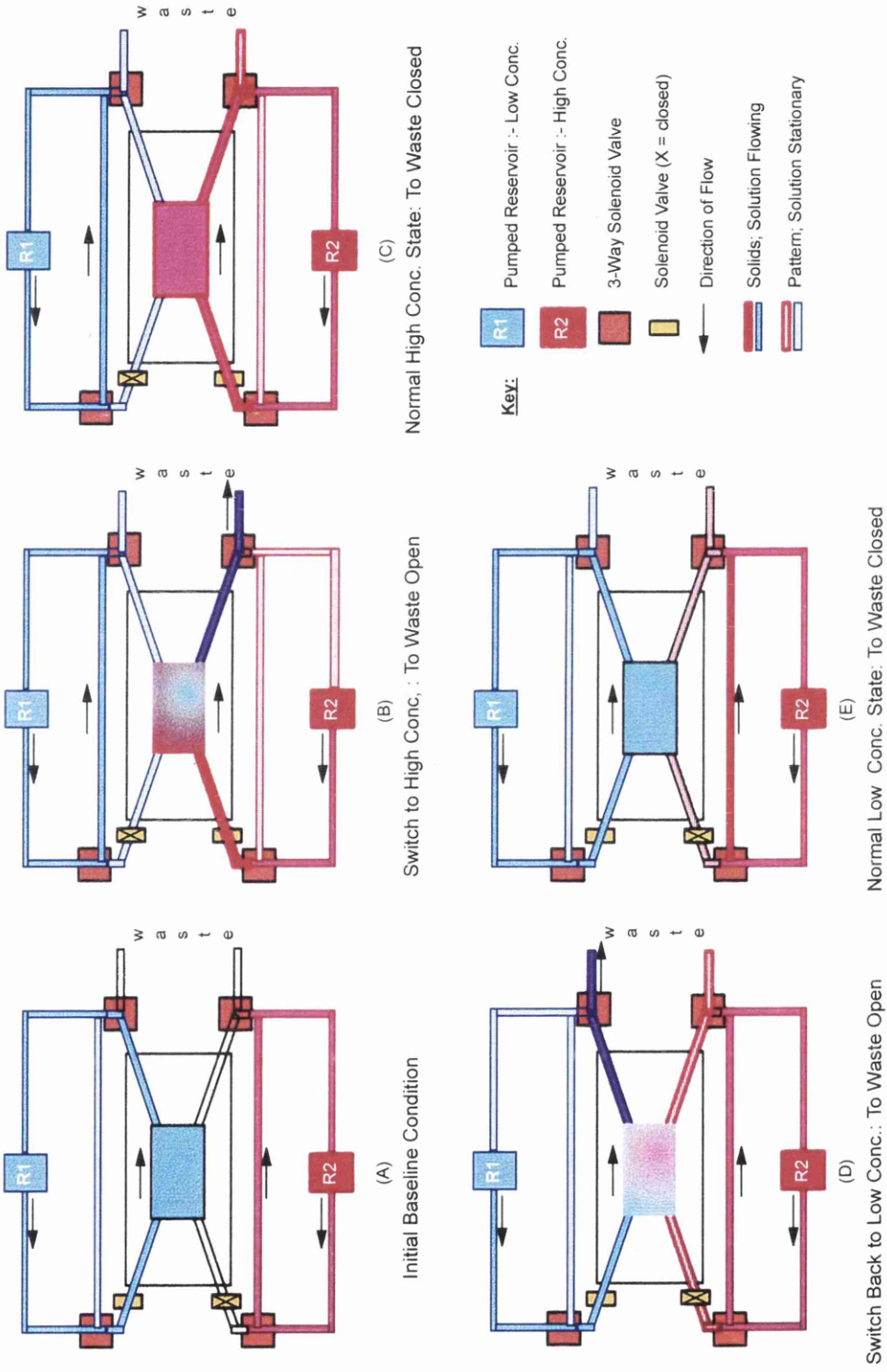


Figure 6.11 Flow Control Logic for Membrane Test Cell. Example shows a Full Oscillator Cycle.

Using such a flow rate the solution 'slab' in the flow head void was replenished more than six times per second. In conjunction with the pulsatile nature of this flow and the hydrodynamic flows in the void it was considered that such a flow rate was sufficient to ensure that unstirred layers near the membrane surface had been minimised .

6.5.4 Calibration Test for an Imposed Concentration Step

A control test was performed to determine the sharpness, regularity and the effective minimum timebase of any applied concentration step. During this test two computer systems were used, one to perform all of the 'normal' valve switching, timing and control functions and the second system to solely collect data from the detection system. In this particular test the U.V-Visible spectrophotometer system was used for collection of the test data.

The membrane cell flow head was isolated from the collecting volume by using a clear glass microscope cover slip. This was to mimic as closely as possible the 'normal' dimensions of a test membrane and also to ensure a transparent optical pathway at 90° to the membrane surface. The two optical fibres carrying the light source were arranged in a manner that the flow head 'window' was monitored, rather than the normal collecting volume position.

In order to run this test successfully a highly coloured

substance, which was easily water soluble and would not present a problem with respect to absorption onto the cell or any of the tubing was sought. Using these criteria a blue anionic dye (Erioglaucine or Brilliant Blue FCF, CAS No [3844-45-9]) was chosen[7].

The two solutions used for this step test were distilled water (low conc.) and the blue coloured food dye . A solution of the dye was prepared (1%v/v) and a scan taken in the visible region of the spectrum. From this spectra the maximum absorbance (λ_{max}) was found to be at 625nm and this was the analysis wavelength used for the test.

The two thermostatted solutions were pumped around in their 'standby' loops and the data collection system started at its maximum collection rate (10 readings per second). Almost simultaneously the switch controlling system was started and a series of successive switches between the clear and the coloured solutions begun using the switching logic described previously (Section 6.5.2). This entire procedure was repeated several times to check the regularity and reproducibility of the imposed step with particular attention being paid to the step amplitude. Any diminution of the amplitude would be a clear indication of cross contamination of the two solutions.

A selection of data from these test runs are shown in Figures 6.12 and 6.13 In the first of these, Figure 6.12 a series of

concentration steps (both up and down) are shown in their entirety. From this data it is clear that the regularity of the imposed step is excellent, 29.9 seconds between each of the wave steps, for a set wave period of 60 seconds and that there was no detectable decrease in the wave amplitude as the run progressed.

In the second figure, Figure 6.13, the timebase of the switch was more rigorously examined. In this figure three switch cycles were superposed on each other. Further analysis of this data shows that for the six switches shown the absorbance values measured changed between 0.01Abs to 0.14 Abs in an average of only 0.75 seconds. It was also clear from this Figure that the time taken to return to an acceptable 'zero' value (after a switch to the low concentration) took longer, in excess of 1.5 seconds. The reason for this remains unclear but this was not a significant problem in terms of the systems use, provided the timebase of any effect is large relative to this 'tail' on the step down to a low concentration.

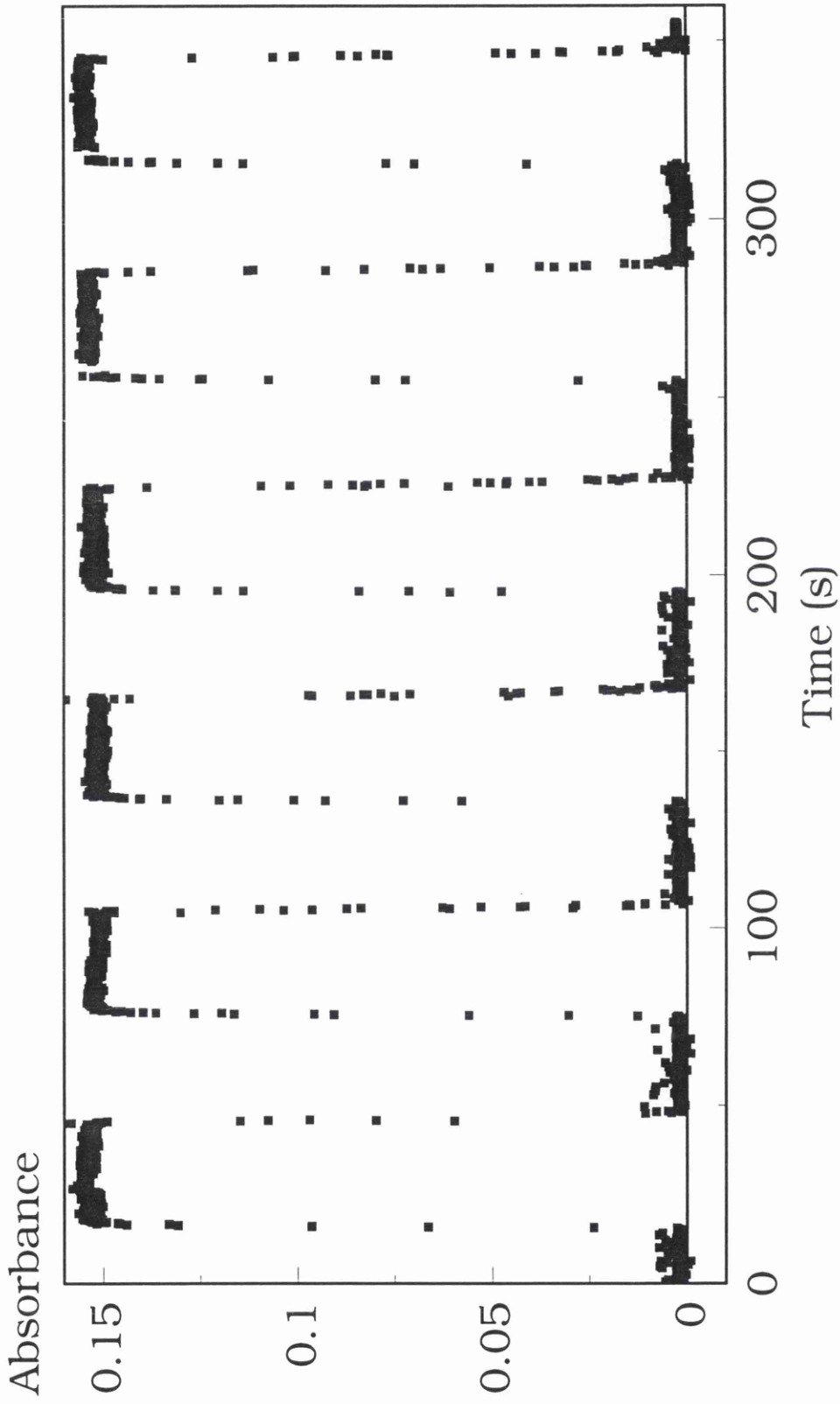


Figure 6.12 Measured Response of the Liquid System to a Series of Imposed Concentration Steps using Brilliant Blue FCF Dye with the Optical Detection System. The Square Wave Period was set at 60 seconds.

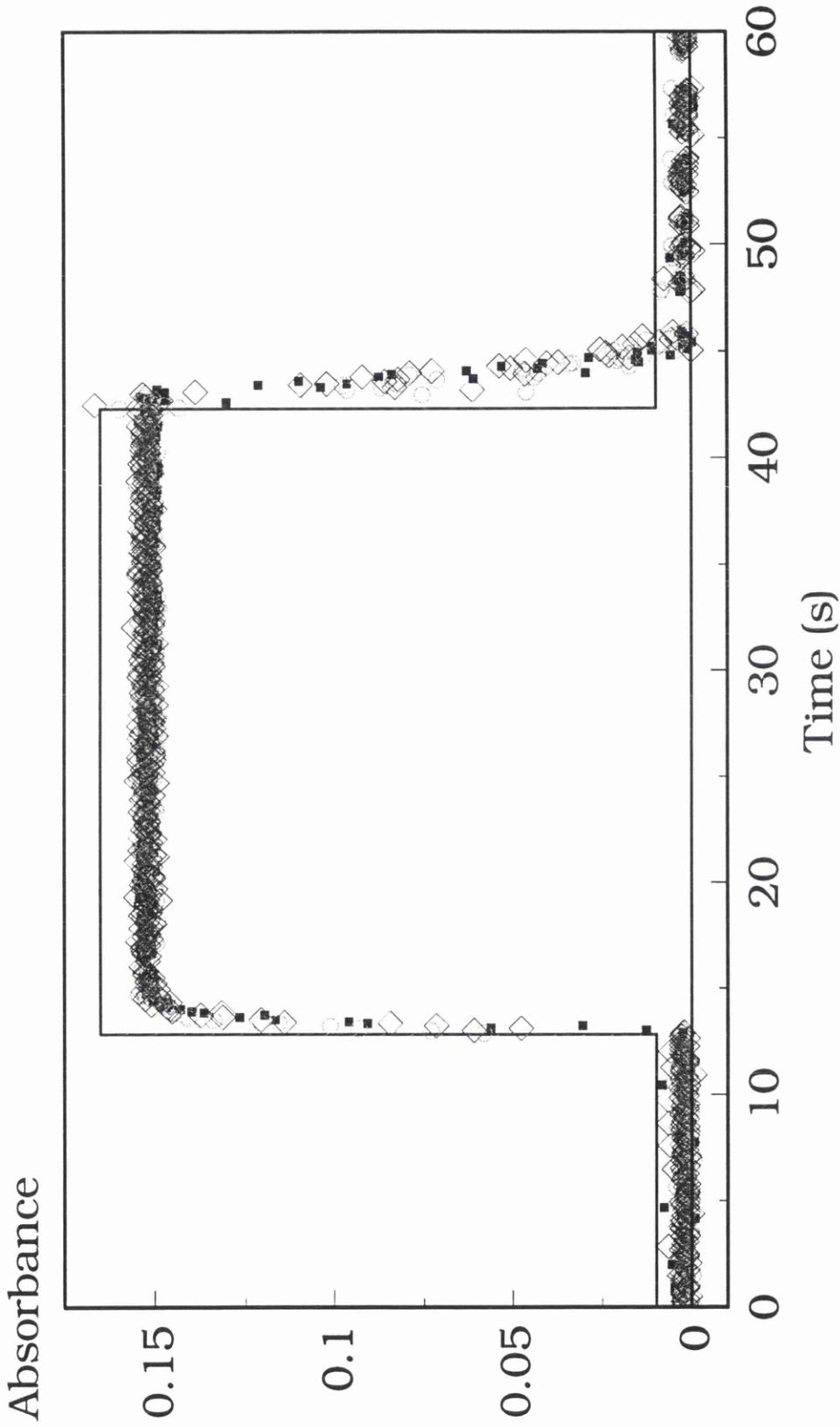


Figure 6.13 Three Concentration Step Cycles Superimposed. This Shows the Excellent Regularity of the Step Period and the Sharpness of the Upward Step but a Slight Tail on the Step Down.

6.6 'Null' Cell Tests

The final stage in the commissioning and testing of this solution based membrane transport system was to ensure that the complete system itself did not generate effects (artefacts) that may mistakenly be interpreted as membrane based phenomena. To ensure that this was not the case, tests were performed in which all valve switches etc. were carried out as normal but with no membrane present and with a constant background test solution (of very dilute potassium chloride) in the collecting volume and using this same solution in both pumped loops. No changes were observed with this test, due to valve switching or any of the other measurement procedures.

The final tests performed were with a Whatman Anpore™ Alumina membrane (0.02 μm) placed in the cell. The collecting volume was filled with a 0.0001M potassium chloride solution and a test concentration step run started. In the first test run, both the low and the high concentration solutions used were the same (0.0001M potassium chloride) and the conductivity value in the collecting volume monitored. In an ideal situation a horizontal 'null' line would be the result of such a test. The results of this test are shown in Figure 6.14 and show very good agreement with this ideal situation.

In the second (and final) test as a comparison, the high concentration solution used was changed to 0.01M potassium chloride, all other system parameters remained as before. The result of this imposed (real) concentration step is shown in Figure 6.15 and proved

conclusively that the very small variation in the null test (due to a very slight temperature variation) was totally negligible when compared to this 'normal' situation.

With the testing stage for the liquid based system now completed it was with great confidence in this system that we could now proceed to investigate some of the fundamental properties of solution based membrane transport processes.

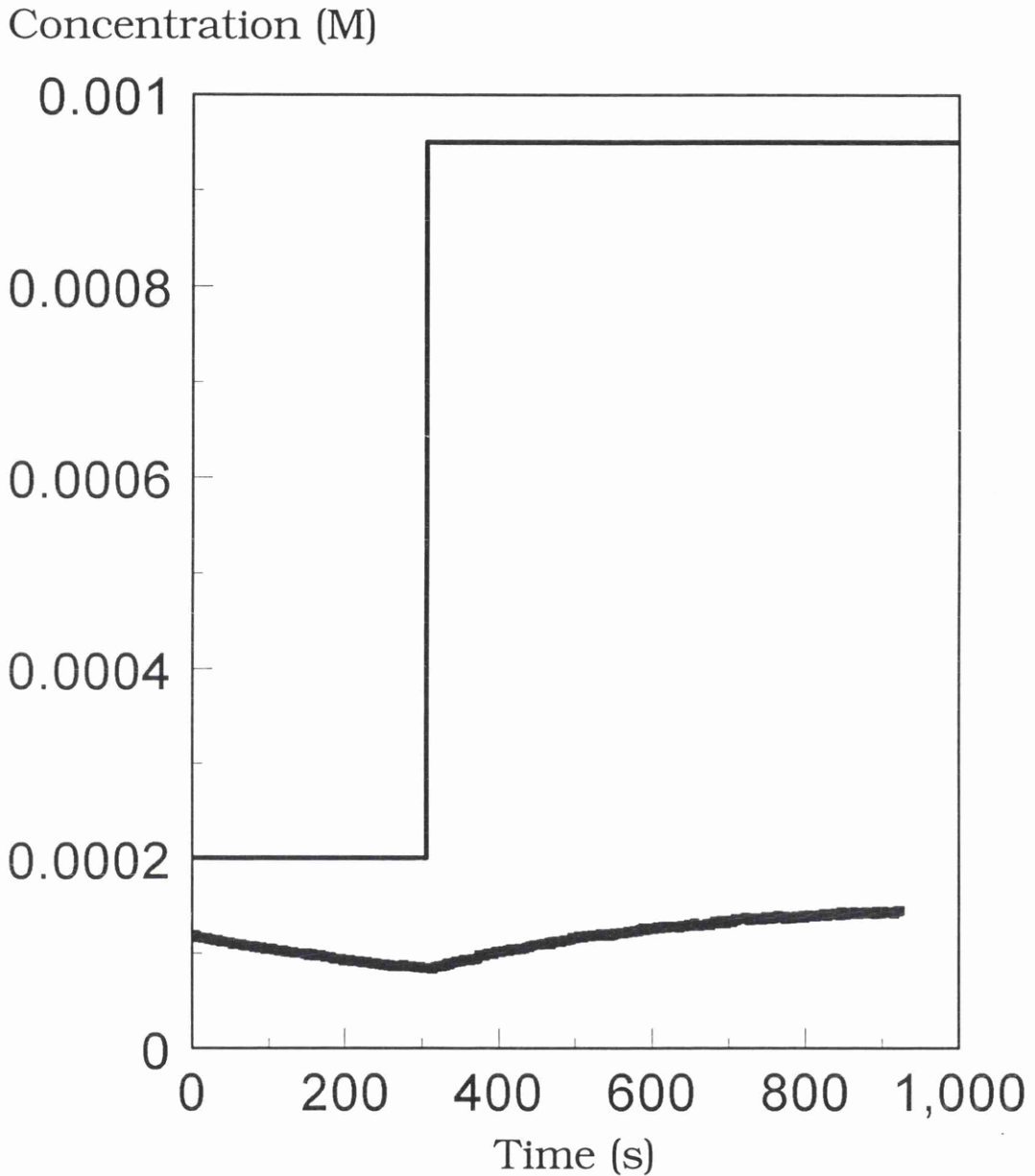


Figure 6.14 A Null Test Experiment in which 0.0001M KCl is used as both the low and the high Concentration Solution using an Anotec 0.02 μ m Asymmetric Membrane (60 μ m thick). The slight deviation from the horizontal is due to a temperature fluctuation.

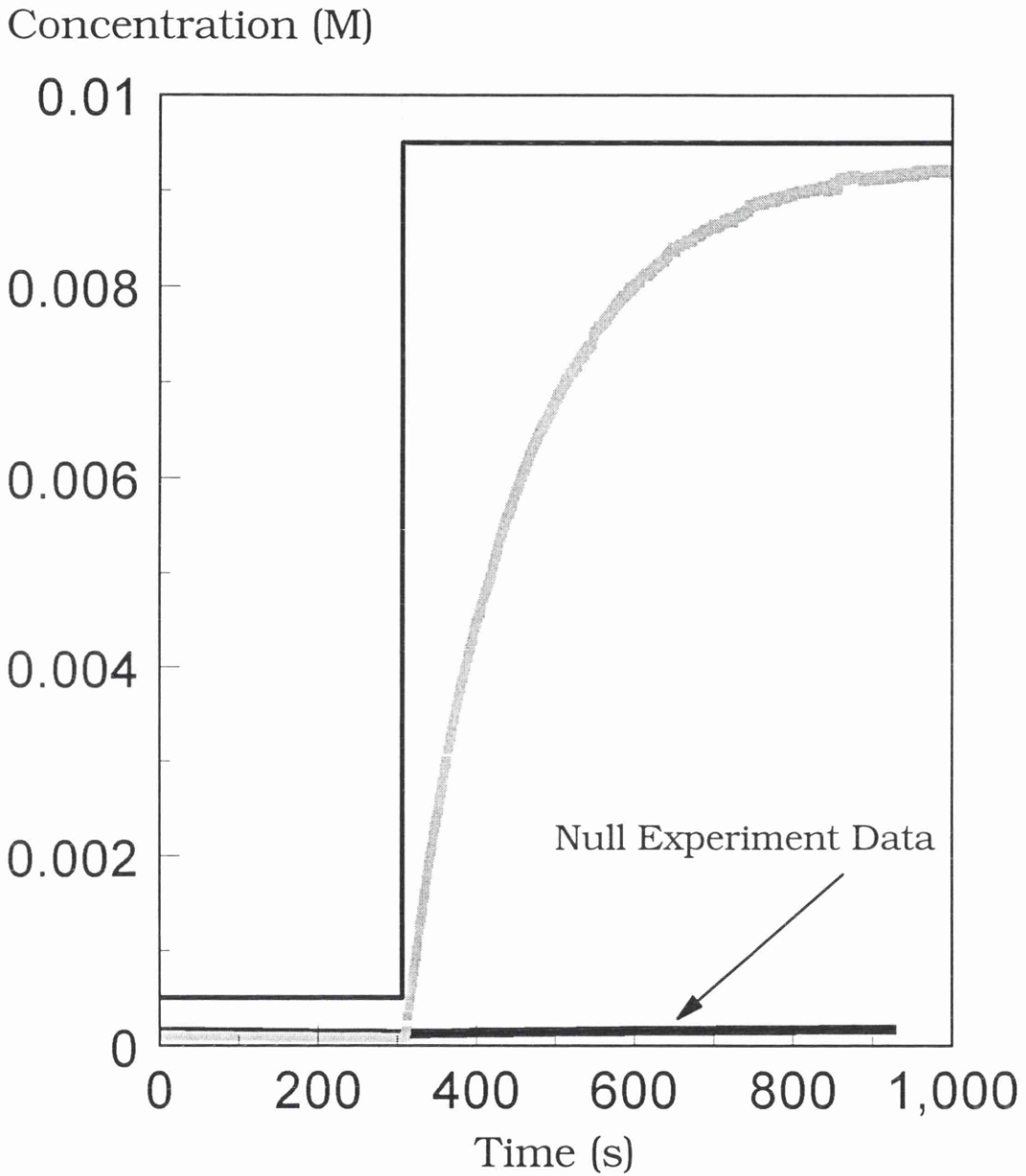


Figure 6.15 Comparison of the Null test to an Experiment in which 0.01M KCl was used as the High Concentration Solution. As in the Null test this was with an Anotec 0.02 μ m asymmetric membrane (60 μ m) thickness.

6.7 References

- [1] Dialysis apparatus for Measuring Permeation Rates through Polymer Films: Little, C. M and Osterhoudt, H. W., Ion Exchange and Membranes, 1972, Vol. 1, p75-80
- [2] Transport Phenomena in Ion Exchange Membranes, D'Alessandro, S., Ion Exchange and Membranes, 1974, Vol. 1, p187-191
- [3] Membrane Oscillations and Ion Transport; Kihara, S. and Maeda, K., Progress in Surface Science, Vol. 47, Nos. 1/2, 1994, p1-54
- [4] Reference Electrodes: Theory and Practice, Eds. Ives D. J. G. and Janz, G. J., Academic Press 1961.
- [5] Electrolyte Solutions, Chapter 5, Measurement of Conductivity and Transport Numbers, Eds. Robertson, R.A., and Stokes, R.H., Second Edition (Revised), Butterworths, 1970, ISBN 0 408 18490 6
- [6] British Standards Institution: BS 791: 1975, Specifications for Solid-Stem Calorimeter Thermometers, B.S. Index Nos. BS17; 17013-C4
- [7] Sigma-Aldrich Handbook of Stains, Dyes and Indicators, Ed. Green, Floyd, J. , ISBN 0-941633-22-5, 1992

Chapter 7

Membrane Characterisation Using the Liquid Permeation System.

Introduction

- 7.1 Background
- 7.2 System Validation
- 7.3 Results & Discussion
- 7.4 Conclusions
- 7.5 References

7 Membrane Characterisation Using the Liquid Permeation System.

Introduction

In this chapter the experimental results obtained from the liquid based measurement system (described in Chapter 6) will be shown and discussed. The entire basis upon which the method depended was the response of a membrane to an instantaneous step (up or down) in the driving force, in this instance, solution concentration. If the system was initially at equilibrium and a step was imposed to one face of the membrane, then after a sufficient period of time the quantity of the permeant material entering through the membrane into the collecting volume (of effectively infinite volume) would tend to a steady state flux.

This method was first used by Daynes in 1920 to study the diffusion of gases through various materials as part of ongoing research into airship technology at that time. Daynes showed that by extrapolation of the steady state portion of the flux in the collecting vessel back to the initial equilibrium concentration, that the so called breakthrough time (τ) was obtained. Daynes also showed that this τ value was a function of only two parameters, the diffusion coefficient of the permeant (gas) and the membrane thickness. In using this method it was therefore possible to obtain with a single experiment an estimate for the permeability, from the the steady state slope and the diffusion coefficient from the extrapolated breakthrough time. As a consequence from these two parameters it was also possible to estimate the distribution coefficient.

In the following chapter, the results shown were all determined by

either 'simple' timelag experiments or by oscillator experiments. In the oscillator experiments (an extension to the timelag) a consecutive series of timelags were performed within a single experiment. This resulted in multiple estimates for the transport properties obtained by the 'simple' timelag method. This has allowed for more accurate interpretation of the data due to the possibility of using simple statistics within a single experiment under identical conditions.

7.1 Background

7.1.1 Bond Graph Modelling of Cell Parameters

Bond graph modelling, based around Network Thermodynamics was mentioned earlier (Chapter 2) for the analysis of imposed concentration waves. Here the technique was used to examine the practical implications on the measurement system. In this example the effect of the collecting volume will be discussed.

A series of simulations were performed in which typical membrane parameters were used, these were given earlier in Table 2.1. The only variable in this parameter list was the value used for the cell collecting volume. For a series of six chosen volumes, the quantity of material (Q) and the concentration profiles of the chosen collecting volume versus time were obtained. The values chosen for the collecting volume were 1000, 100, 3.5, 1.75, 0.87 and 0.17 cm³. The resultant profiles are shown in Figures 7.1 and 7.2

respectively.

From the plots of Q versus time (Figure 7.1) there at first sight appeared to be very little difference between the volumes. Both of the largest volumes (1000 & 100 cm^3) gave identical results i.e. they represent infinite bath conditions. On moving to a value of 3.5cm^3 the deviation of the slope from the infinite bath case was 0.09%. At 1.752 cm^3 this became 0.21% and at 0.87cm^3 this increased to 0.44% and finally at 0.175cm^3 the deviation was 2.2%

Conversely, looking at the plots of concentration versus time (Figure 7.2) there was a very significant change brought about by decreasing the volume. From these two plots a compromise position was chosen, one where the Q value slopes would be well within experimental error but the detected concentration in the collecting volume would be manageable on a routine basis, the chosen value being 1.752cm^3 .

These simulations were performed prior to the construction phase (described earlier in Chapter 6) where a value of 2cm^3 was chosen as the optimum cell volume.

From previous investigations of pulsed sources, it has been shown that the shape of the input wave (square, triangular, sine or cosine) made no significant effect to the observed phase change in the collecting volume, and hence to the calculated diffusion coefficient [1]. It was also shown that the error in the

calculated diffusion coefficient by this method, due to an imperfect square wave was of the order of only 0.05%.

This indicated that the experimentally generated square wave (shown in 6.5.4) would be insignificantly different (from an ideal wave) in terms of calculated diffusion coefficients obtained from the system.

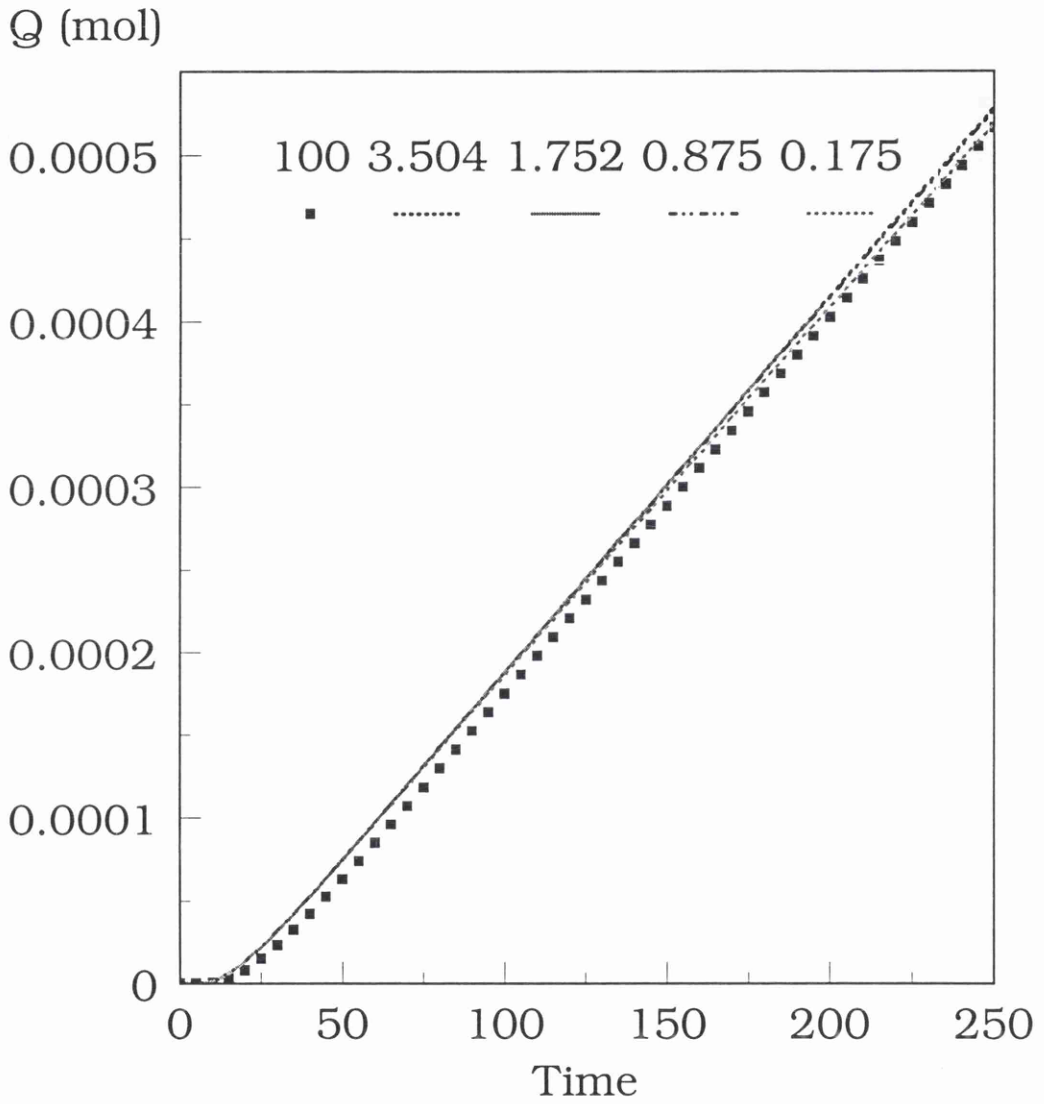


Figure 7.1 Simulated Data for Various Collecting Volume Values where $Q = (C \cdot V)$. The model parameters are those of Table 2.1

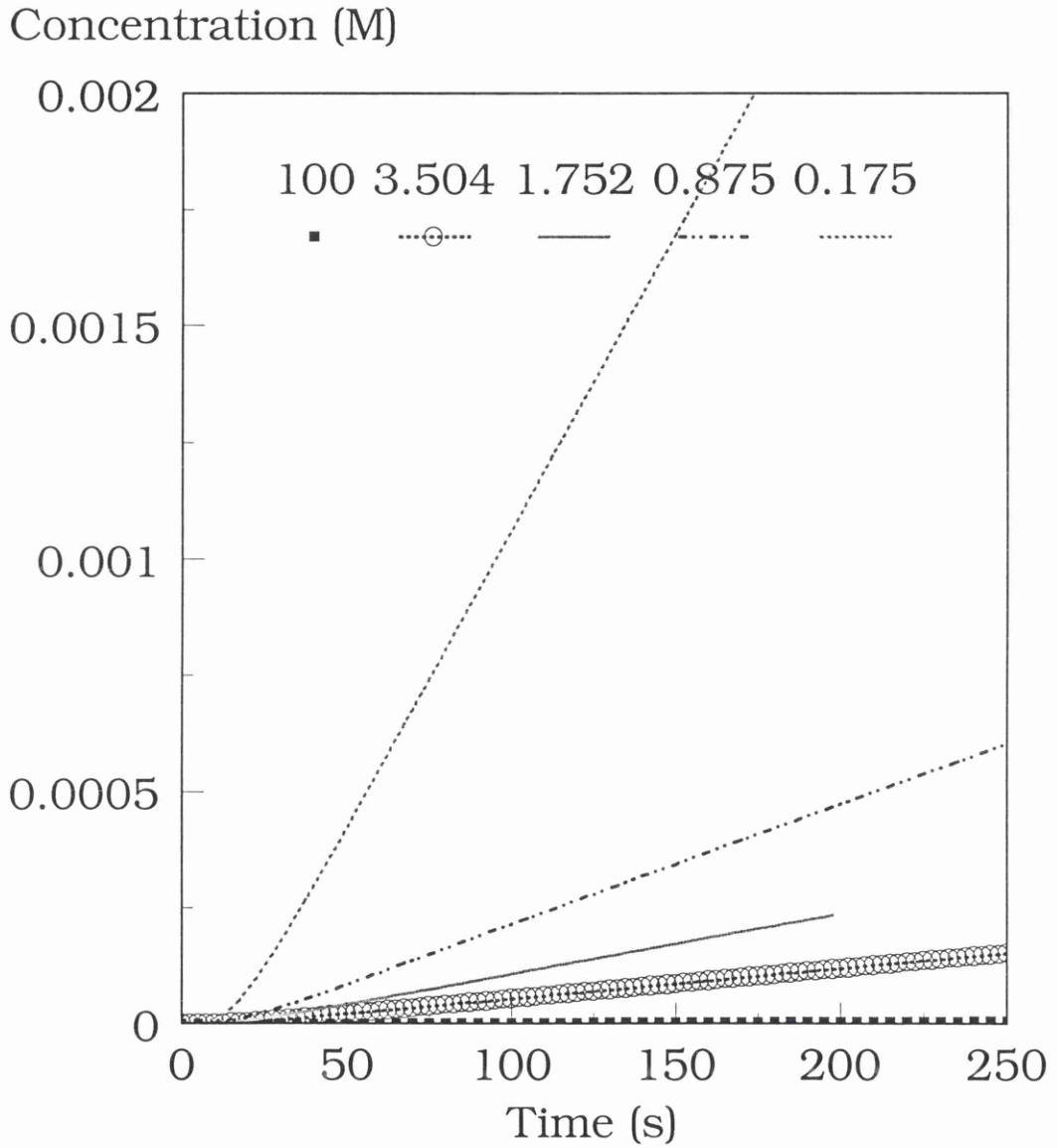


Figure 7.2 Simulated Concentration Profiles Using Various Collecting Volume Values. The model parameters are those of Table 2.1

7.1.2 Experimental Data Treatment

In using this step imposition method, the membrane experiences significant changes in concentration with time. The membrane moves from a state of initial equilibrium to a non-steady state after the imposition of the step and then, after some time to a steady state flux and (if allowed) back towards a new equilibrium condition. The analysis used by Daynes [2] and later by Crank [3], described the concentration build-up within the membrane from the moment of the step to the steady state. In this instance there is a uniform concentration distribution through the membrane but the two surface concentrations are different. In the initial non-steady state period the concentration within the membrane can be shown by Equation 7.1

$$C = C_1 + (C_2 - C_1) \frac{x}{l} + \frac{2}{\pi} \sum_{n=1}^{\infty} \frac{C_2 \cos n\pi - C_1}{n} \sin \frac{n\pi x}{l} \exp\left(-Dn^2\pi^2 t / l^2\right) + \frac{4C_0}{\pi} \sum_{m=0}^{\infty} \frac{1}{2m+1} \sin \frac{(2m+1)\pi x}{l} \exp\{-D(2m+1)^2\pi^2 t / l^2\}$$

Equation 7.1

where C_1 is the concentration at the external face ($x=0$), C_2 the concentration at the internal face ($x=l$), C_0 is the initial uniform membrane concentration, l is the membrane thickness and D is the diffusion coefficient.

As time tends towards infinity the exponential terms disappear to leave a linear concentration distribution. The rate at which the permeant material emerges (from unit area, A) at the face

is given by

$$Q = -D \left(\frac{\partial C}{\partial x} \right)_{x=l} \quad \text{Equation 7.2}$$

By integrating this with respect to time we can obtain the total quantity of the permeant material, Q_t which has passed through the membrane in time, t .

$$Q_t = D(C_1 - C_2) \frac{t}{l} + \frac{2l}{\pi^2} \sum_1^{\infty} \frac{C_1 \cos n\pi - C_2}{n^2} \left\{ 1 - \exp\left(-Dn^2\pi^2 t/l^2\right) \right\} \\ + \frac{4C_0 l}{\pi^2} \sum_{m=0}^{\infty} \frac{1}{(2m+1)^2} \left\{ 1 - \exp(-D(2m+1)^2\pi^2 t/l^2) \right\} \quad \text{Equation 7.3}$$

By experimental arrangement C_0 and C_2 are equal to zero (both pure water and assuming infinite bath conditions) and so we find

$$\frac{Q_t}{lC_1} = \frac{Dt}{l^2} - \frac{1}{6} - \frac{2}{\pi^2} \sum_1^{\infty} \frac{(-1)^n}{n^2} \exp(-Dn^2\pi^2 t/l^2) \quad \text{Equation 7.4}$$

as $t \rightarrow \infty$ this simplifies to

$$Q_t = \frac{DC_1}{l} \left(t - \frac{l^2}{6D} \right) \quad \text{Equation 7.5}$$

for unit area, this line will have an intercept (τ) on the time axis given by

$$\tau = \frac{l^2}{6D} \quad \text{Equation 7.6}$$

If from our experiment we now plot Q versus time, the steady state region of the plot will have a slope which will be equal to

$$\bar{m} = \frac{DA\Delta\bar{c}}{l} \quad \text{Equation 7.7}$$

where $\Delta\bar{c}$ is the concentration distribution within the membrane. From this slope the steady state flow (J) is

$$J = \frac{D\Delta\bar{c}}{l} = P\Delta c \quad \text{Equation 7.8}$$

where

$$P = \frac{D\Delta\bar{c}/\Delta c}{l} \quad \text{and } \Delta\bar{c}/\Delta c \text{ is the distribution coefficient } \alpha.$$

It then becomes simply a matter of accurately knowing the value of the collecting volume in order to perform such an operation, the measured concentration in the collecting volume being

$$C = \frac{Q_t}{V} \quad \text{Equation 7.9}$$

7.2 System Validation

The work of Daynes showed the empirical relationship (Equation 7.6) between the test membrane thickness and the diffusion coefficient of the permeant species under investigation. Having performed a series of rigorous tests and calibrations on the measurement systems (described in Chapter 6) it was necessary to prove that the simplest membrane based law was indeed applicable and measurable with this current device. To this end a short series of test experiments were performed.

7.2.1 Test of Daynes ($l^2 / 6D$) Law

By taking a series of otherwise identical membrane samples but with varying thickness values, tests were performed to determine the experimental timelag values obtained and the calculated values for the diffusion coefficient of a permeant material. The permeant used for these tests was a solution of

potassium chloride (0.1M). This was chosen for two main reasons (a) it could be measured easily at low concentration by conductimetric methods and (b) the knowledge that it would be a 'fast' permeant would severely test the performance of the measurement system.

7.2.2 Preparation of Membranes

The membrane chosen for this test was a regenerated cellulose acetate 'Visking' dialysis membrane. This membrane had a lack of carboxyl groups and hence had little or no fixed charge and therefore had negligible ion-exchange properties and the swelling effects associated with these materials[4]. Several squares, approximately 25x25mm were cut from one large piece of dialysis tubing. The square sections were placed in distilled water for 2 days with constant stirring, the water being changed at regular intervals during this soaking stage. Each individual section was then labelled and placed in a small sealed vessel with ultra high quality water.

Before being placed into the measurement cell each membrane section was blotted briefly in fibre free tissue to remove excess water from the surfaces. At this point the membrane thickness was measured between two previously measured microscope cover slips using a Mitutoyo digital micrometer. The membrane sections were then placed in the cell holder and the collecting volume flushed and then filled with degassed

distilled water. The solution flow loop with distilled water was started and left for 15 minutes to ensure the membrane was fully wetted and at equilibrium.

7.2.3 Experimental Procedure

For every new test experiment the collecting volume was flushed and filled with distilled water. The solutions used for the concentration step were distilled water and potassium chloride (0.108M). The automated data collection system ensured that an initial equilibrium condition was established before the imposed concentration step. At the end of every experiment the membrane sections were washed several times with distilled water and left soaking for two days in regularly changed distilled water. This entire procedure was repeated several times for each membrane section and covering a range of membrane thicknesses.

7.2.4 Results and Discussion

From the experiments described above, it was clear that membrane thickness did indeed play an important role in the overall response of the system. Some examples of the results obtained are shown in Figures 7.3 to 7.5 for three membranes of different thickness and the data extracted from these shown in Tables 7.1 to 7.3. For the three different thickness values (0.0149, 0.0303 and 0.0453 cm) the mean values for the timelags (τ) obtained were 11.22, 46.98 and 102.84 seconds

respectively.

On examination of the thickness (l^2) ratios between the 0.0149 & 0.0303cm and the 0.0149 & 0.0453cm membrane sections and using the 11.22 second timelag as a reference, the calculated values for the 0.0303 and 0.0453cm membranes were found to be 46.39 and 103.71 seconds respectively. Additionally, if a mean value for the calculated diffusion coefficient (obtained from all of the test experiments) was taken ($3.29 \times 10^{-6} \text{ cm}^2\text{s}^{-1}$) then by substitution the calculated timelag values were found to be 11.22, 46.41 and 103.73 seconds.

Based upon these values and using the 0.0149cm membrane as an internal standard the experimental timelags obtained varied from the calculated values by +1.25% for the 0.0303cm and -0.91% for the 0.0453cm membrane. From these figures, it was clear to see that the experimental determination of membrane timelags and the associated diffusion coefficients using this measurement system was easily attainable to within $\pm 2\%$. This was in effect the experimental error in the measurement of the membrane thickness but membrane heterogeneity must also be borne in mind.

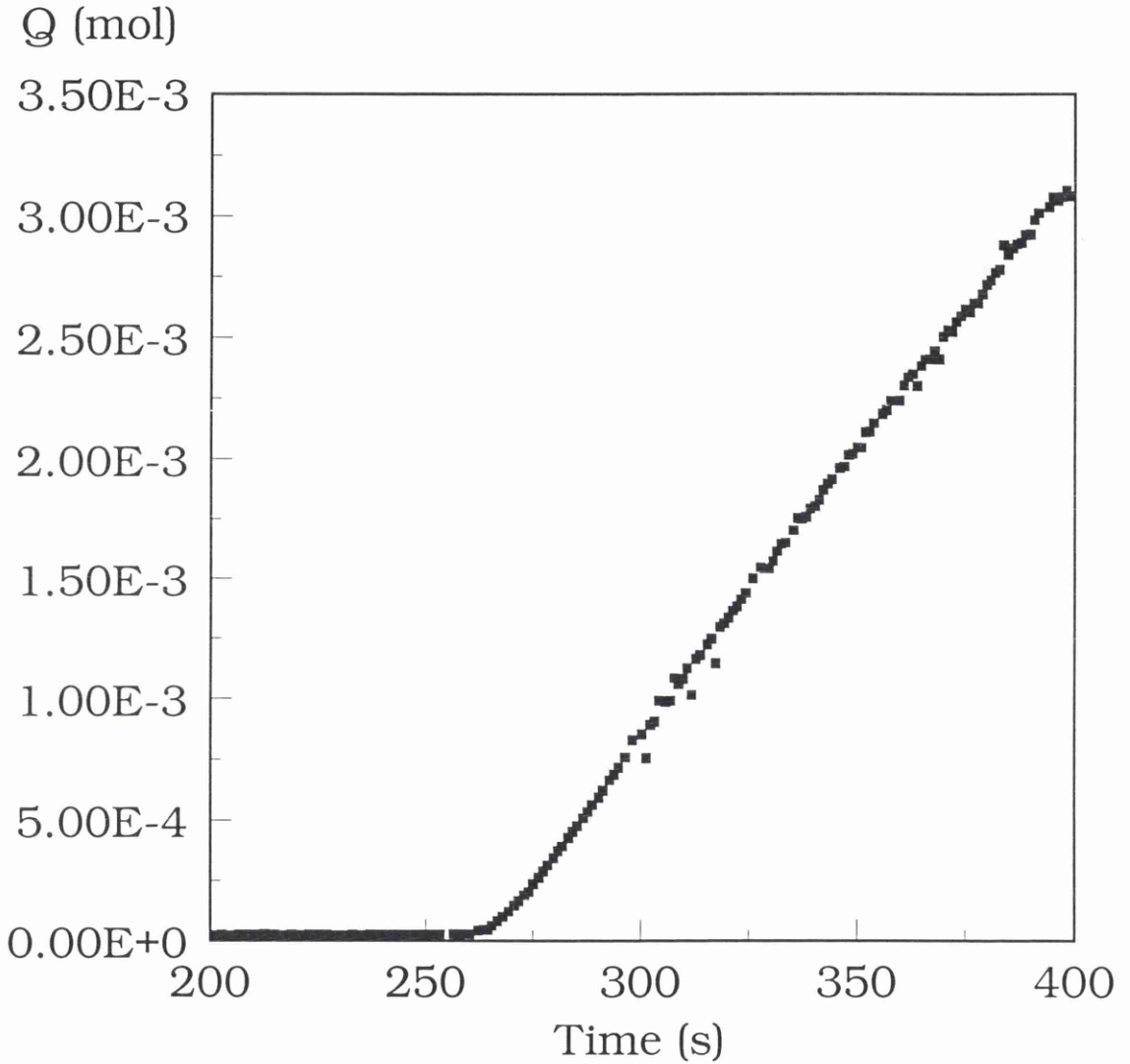


Figure 7.3 Timelag Experiment with Visking Dialysis Membrane of Thickness 0.0149cm. The Concentration Step was Imposed at 255 seconds. The Resultant τ value was 11.28 seconds.

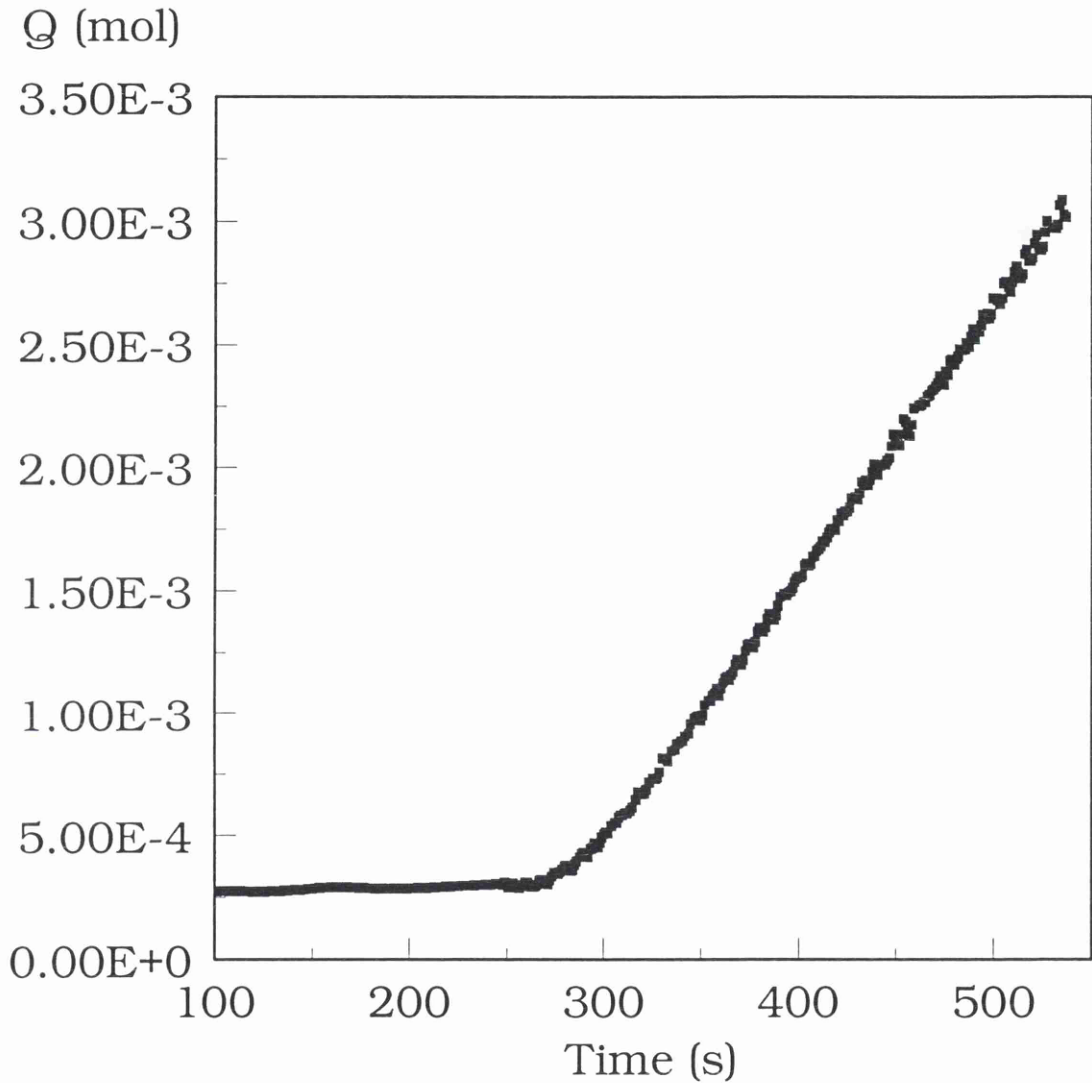


Figure 7.4 Timelag Experiment with Visking Dialysis Membrane of Thickness 0.0303cm. The Concentration Step was Imposed at 244 seconds. The Resultant τ value was 46.5 seconds.

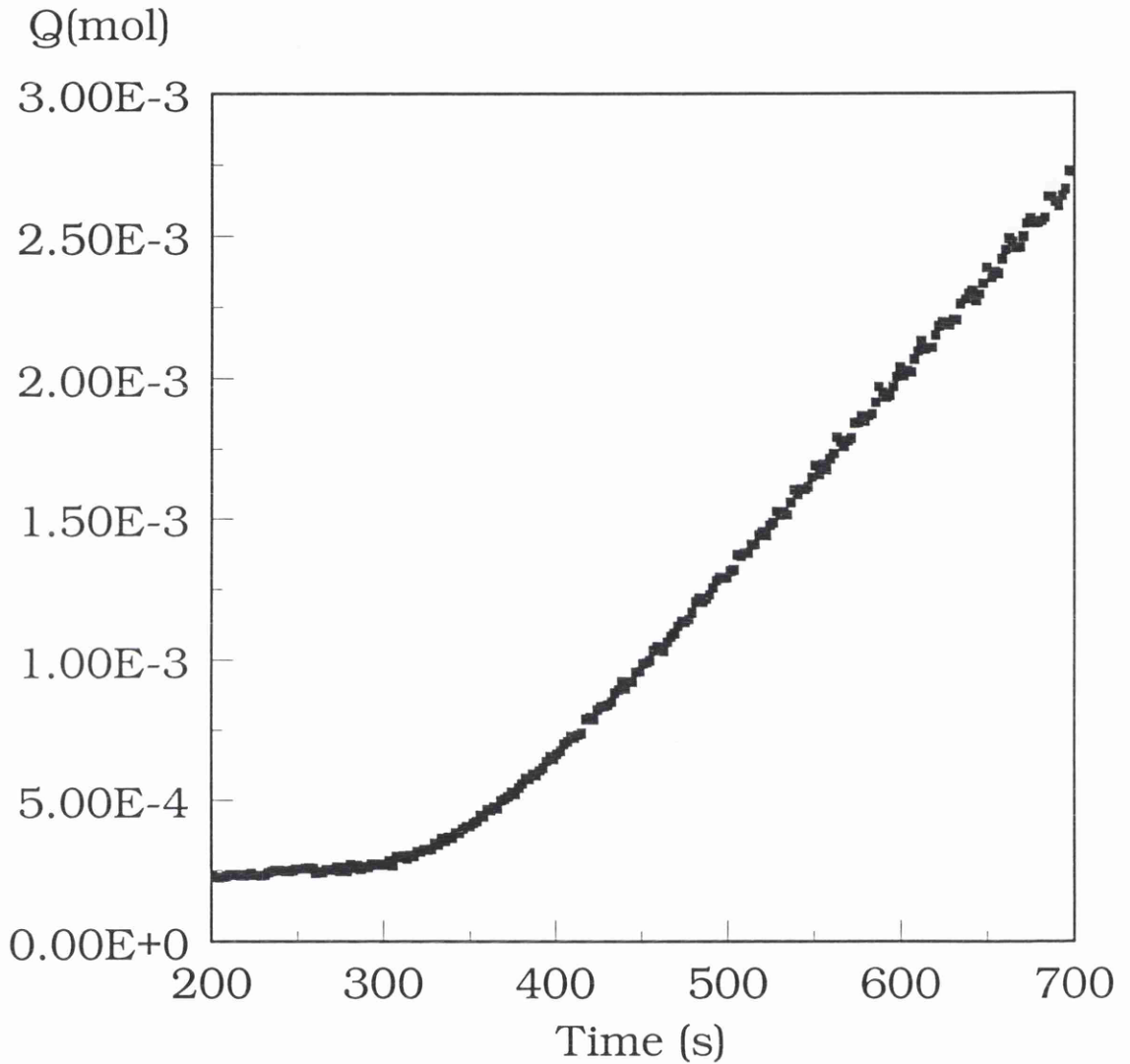


Figure 7.5 Timelag Experiment with Visking Dialysis Membrane of Thickness 0.0453cm. The Concentration Step was Imposed at 251 seconds. The Resultant τ value was 102.5 seconds.

Run #	Timelag (s)	Diffusion Coefficient (cm^2s^{-1})	Experimental Permeability ($\text{cm}\cdot\text{s}^{-1}$)	Distribution Coefficient
1	11.2	3.30×10^{-6}	2.46×10^{-5}	0.2
2	11.19	3.30×10^{-6}	2.46×10^{-5}	0.2
3	11.28	3.28×10^{-6}	2.40×10^{-5}	0.19
4	11.23	3.29×10^{-6}	2.43×10^{-5}	0.19

Table 7.1 Experimental Results for Visking Membrane of thickness 0.0149cm

Run #	Timelag (s)	Diffusion Coefficient (cm^2s^{-1})	Experimental Permeability ($\text{cm}\cdot\text{s}^{-1}$)	Distribution Coefficient
1	41.94	3.64×10^{-6}	1.11×10^{-5}	0.17
2	49.52	3.09×10^{-6}	1.08×10^{-5}	0.19
3	49.49	3.09×10^{-6}	1.08×10^{-5}	0.18

Table 7.2 Experimental Results for Visking Membrane of thickness 0.0303cm

Run #	Timelag (s)	Diffusion Coefficient (cm^2s^{-1})	Experimental Permeability ($\text{cm}\cdot\text{s}^{-1}$)	Distribution Coefficient
1	102.15	3.35×10^{-6}	6.99×10^{-6}	0.17
2	103.53	3.33×10^{-6}	6.93×10^{-6}	0.17
3	102.7	3.30×10^{-6}	6.82×10^{-6}	0.16

Table 7.3 Experimental Results for Visking Membrane of thickness 0.0453cm

7.3 Results and Discussion of Membranes Investigated

In this section the results obtained with the measurement equipment will be shown and discussed for a variety of different membrane systems. These involve both timelag and oscillator experiments and make use of the data analysis methods described earlier.

7.3.1 Anodic Alumina Membranes

In this section the results from timelag experiments with anodic alumina membranes will be shown and discussed. A series of anodic alumina membranes identical to those described earlier in Chapter 5 (Gas System) were used here for solution based studies. To recapitulate, these consisted of 'support' structures of varying thickness onto which active layers of different thickness were placed.

Unlike in the gas system, there was a hydration process that resulted in some 'swelling' or gel formation within the porous structure of these membranes[5]. To minimise any dynamic effects during experiments all membranes were pre-soaked in distilled water overnight.

As in the gas experiments, the effect of thickness and the presence of an active layer on the liquid permeation rates was to be investigated. Due to the combination of extremely thin porous membranes and the choice of potassium chloride solution as a permeant, the expected overall speed of these experiments would push the system towards its limits. It

should be emphasised that it is believed that currently no other system exists where such measurements could be considered.

Anodic alumina 'support' structures with a nominal pore size of approximately 70nm were produced in two thicknesses, 48 μ m(SAA1) and 80 μ m(SAA2). In addition two samples were produced, identical to (SAA1) to which a layer (nominal pore size 20nm) was added of thickness 9 μ m(LAA1) and 22 μ m(LAA2). Each of these membranes were tested repeatedly for their response to an imposed concentration step (0.1M KCl) versus distilled water in the collecting volume. Examples of the resultant experiments are shown in Figures 7.6 to 7.9. The slopes obtained from these plots gave a direct measurement of the permeability and from the timelag values an estimate of the diffusion coefficient as described in Section 7.1.2. The data obtained from these plots are summarised in Table 7.4.

The interest of this current work was to try and obtain information relating to the active layer contribution to transport and separation. With a knowledge of the contribution from the support and that of the composite membrane it was possible to calculate and resolve the effect of the active layer in isolation. As in the gas system it was possible to obtain permeability data for the active layer alone from the relationship

$$\frac{1}{P_{\text{layer}}} = \frac{1}{P_{\text{Composite}}} - \frac{1}{P_{\text{Support}}} \quad \text{Equation 5.18}$$

In the case of the liquid based system it was also (practically) possible to ascertain information regarding the timelag of the active layer in isolation. It has been shown using Network Thermodynamics for modelling membrane processes that the timelag value of the active layer in isolation can be calculated as described in Equation 7.10 [6].

$$\sqrt{\tau_{ab}} = \sqrt{\tau_a} + \sqrt{\tau_b} \quad \text{Equation 7.10}$$

It is believed that this current work has for the first time made this practically possible to observe.

By using the timelag value for the support (SAA1) as the backing layer contribution, the calculated timelag for the active layers in membranes (LAA1 and LAA2) were found to 0.13 and 0.74 seconds respectively. Information relating to the active layers are shown in Table 7.5. It is obvious that the potential errors involved with such small values could be large but based upon a comparison with the thickness ratio (l^2) of the two active layers and using the larger (more reliable) timelag value as a reference, the predicted timelag for the $9\mu\text{m}$ layer was 0.124 seconds. Although great care is necessary when evaluating such data the magnitudes of the values obtained appear to be within reason (better than 10% accuracy) when compared to the predicted values when using the thickness (l^2) ratios for the layers.

In terms of the effect the active layer had on the permeability values, the normalised values (P^*) for both active layer samples (LAA1 & LAA2) reduced the original (backing layer) values by approximately half. As a comparison, the same active layer samples when tested with the gas system reduced the original permeability on average by nearly 90%. This suggests that the hydration of these anodic alumina membranes may have caused some (unknown) structural change to the pore.

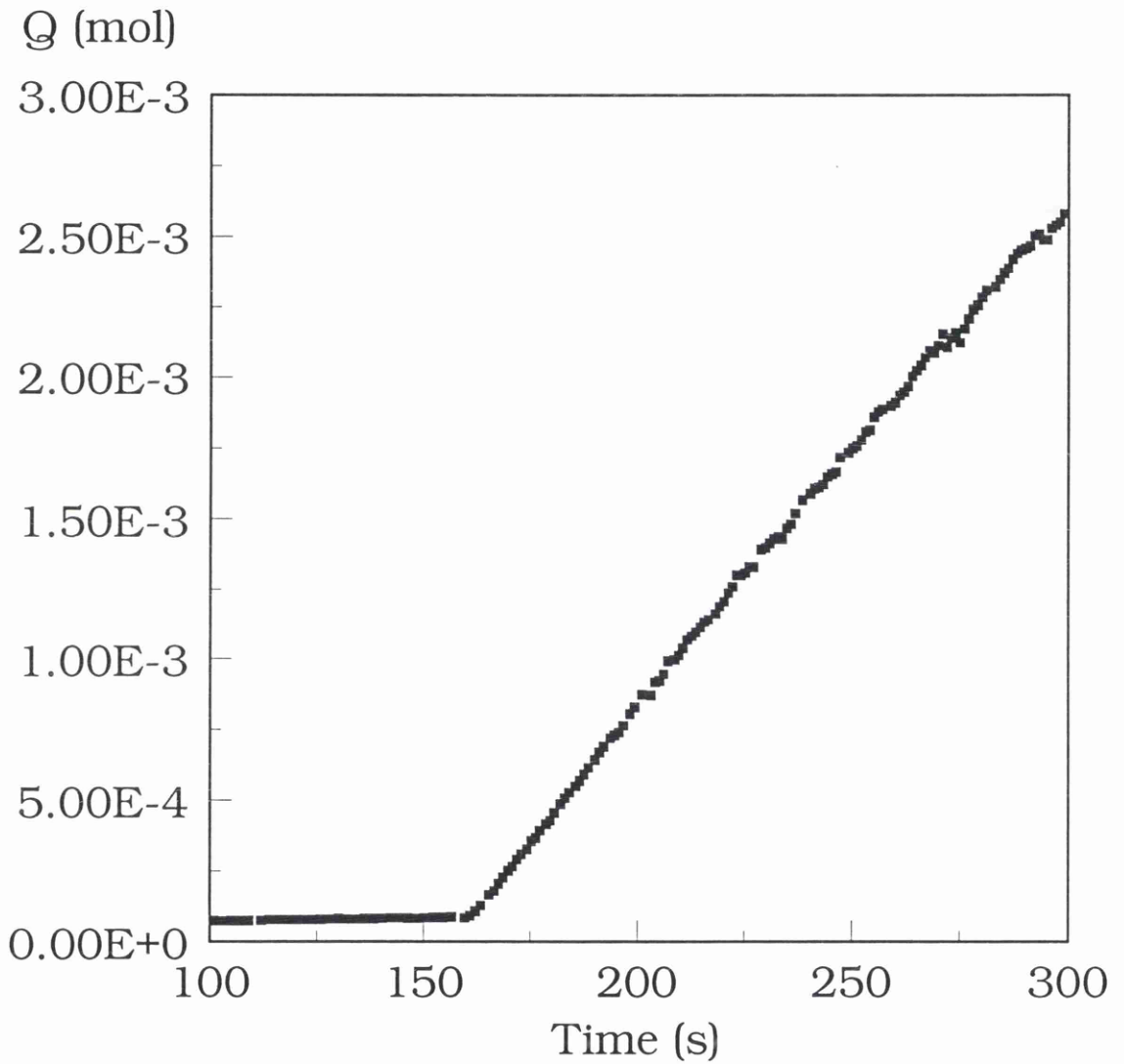


Figure 7.6 Timelag Experiment with a Symmetrical Anodic Alumina Support ($48 \mu\text{m}$ thick). The concentration step (0.1M KCl) was Imposed at 159 seconds and the resultant τ value was found to be 2.68 seconds.

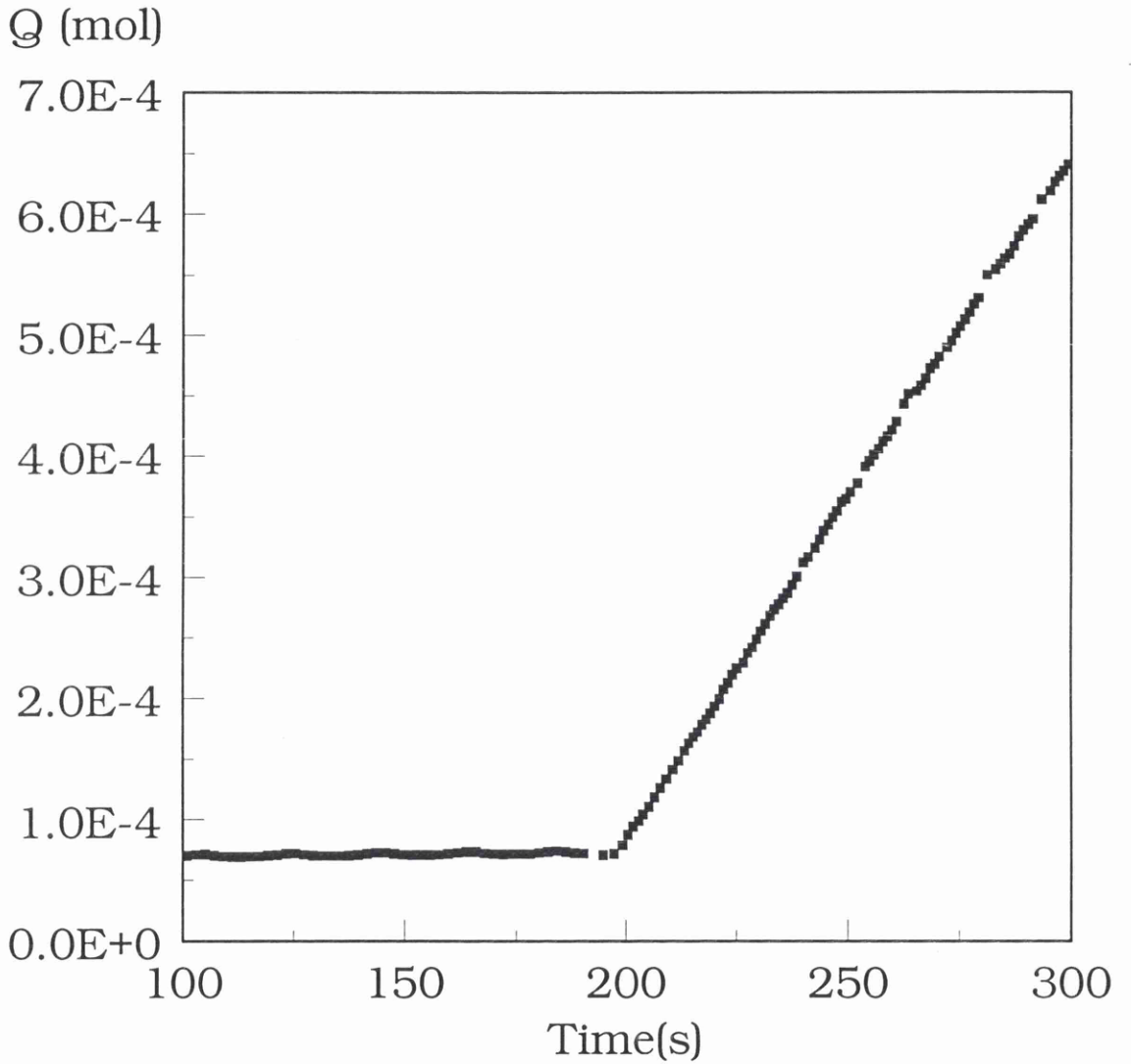


Figure 7.7 Timelag Experiment with a Symmetrical Anodic Alumina Membrane ($80\ \mu\text{m}$ thick). The concentration step (0.1M KCl) was imposed at 192.8 seconds and the resultant τ value was found to be 5.97 seconds.

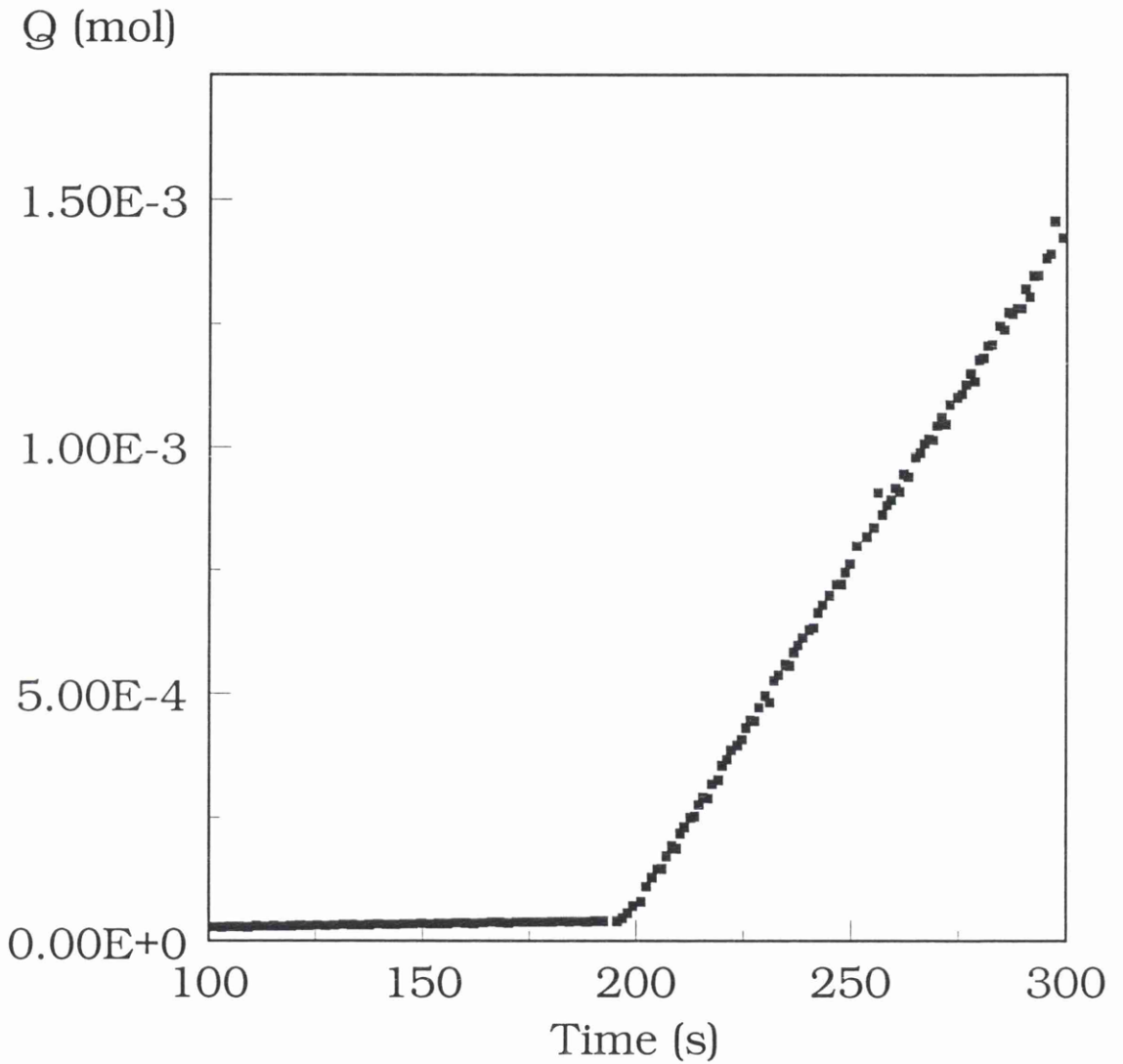


Figure 7.8 Timelag Experiment with an Asymmetrical Anodic Alumina Membrane ($48\ \mu\text{m}$ base with $9\ \mu\text{m}$ Active Layer). The concentration step (0.1M KCl) was Imposed at 194.8 seconds and the resultant τ value was found to be 3.42s.

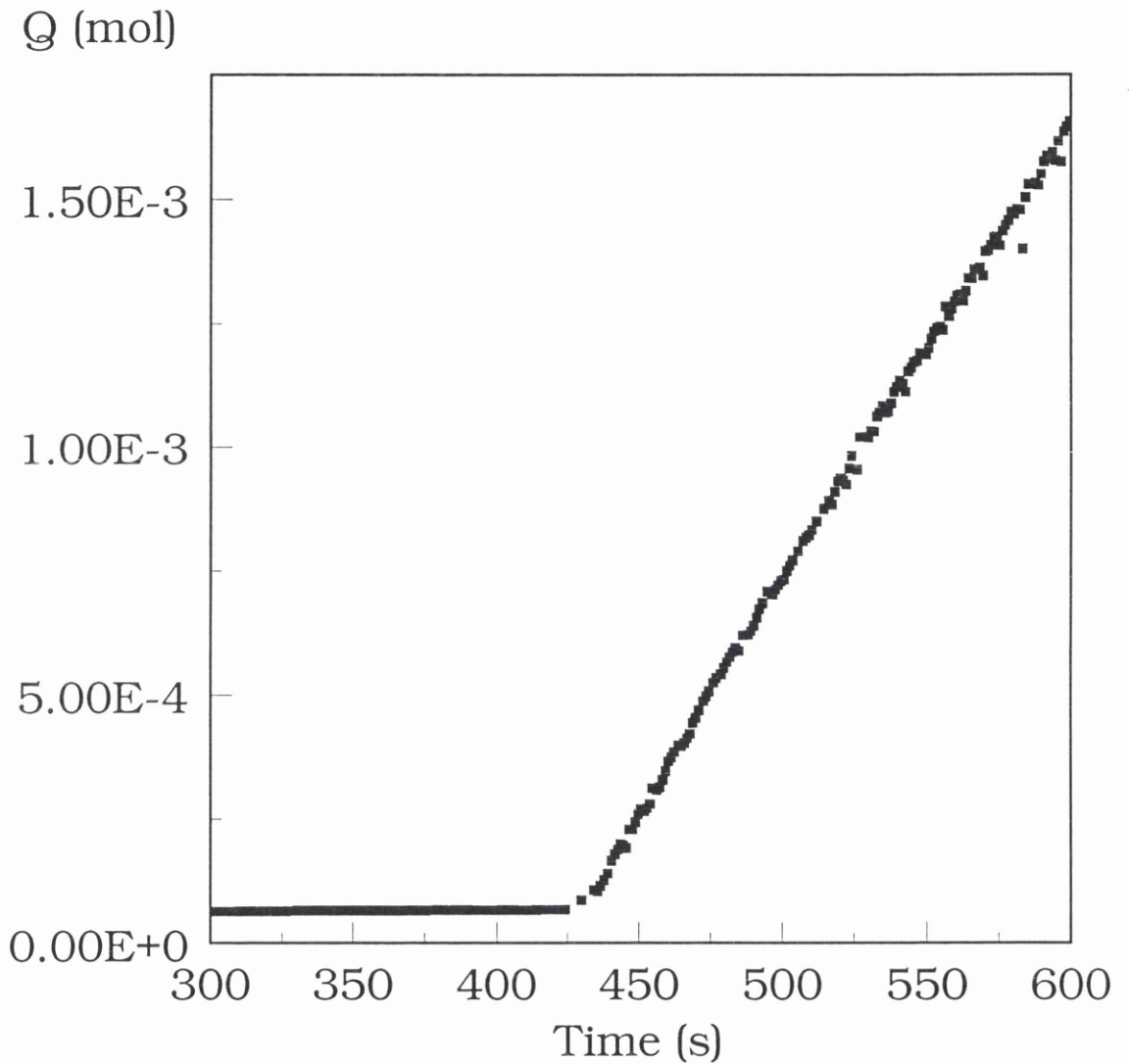


Figure 7.9 Timelag Experiment with an Asymmetrical Anodic Alumina Membrane ($48\ \mu\text{m}$ base with $22\ \mu\text{m}$ Active Layer). The concentration step (0.1M KCl) was Imposed at 426.6 seconds and the resultant τ value was found to be 5.56s

Membrane	Thickness (μm)	Mean Timelag (s)	Diffusion Coefficient (cm^2s^{-1})	Mean Permeability ($\text{cm}\cdot\text{s}^{-1}$)
SAA1	48	2.25	1.71×10^{-6}	1.93×10^{-5}
SAA2	80	6.1	1.81×10^{-6}	5.70×10^{-6}
LAA1	48/9	3.47	-	1.36×10^{-5}
LAA2	48/22	5.57	-	1.15×10^{-5}

Table 7.4 Data obtained from Timelag Experiments using Anodic Alumina Membranes. Concentration step was KCl (0.1M) versus distilled water. For bilayer systems the layer thickness is shown last.

Membrane	Layer Thickness (μm)	Timelag (s)	Diffusion Coefficient (cm^2s^{-1})	Mean Permeability ($\text{cm}\cdot\text{s}^{-1}$)	$P \times l$
LAA1	9	0.13	1.04×10^{-6}	4.66×10^{-5}	4.19×10^{-8}
LAA2	22	0.74	1.09×10^{-6}	2.35×10^{-5}	5.16×10^{-8}

Table 7.5 Calculated Data for the Active Layer Properties of Anodic Alumina Membranes.

7.3.2 Ceramic Disc Membranes

This type of ceramic membrane is being used more routinely than the anodic alumina membranes described above which are used in only specialised (niche) applications. The structure of these membranes is radically different from the anodic alumina membranes, above. The membranes used here were described and used earlier for the study of gas permeation (Section 5.4.2). The range of such membranes is limited mainly to the oxides of a few elements, Al, Ti, Zr, Si but these are being successfully exploited commercially. An example of one such membrane used here is shown in Plate 7.1.

As before, experiments were performed on both the supports and the composite membranes with a variety of layer thicknesses. The timelag experiments for three supports and the composite membrane (ZrO_2) are shown in Figures 7.10 to 7.13 and the data obtained summarised in Tables 7.6 and 7.7.

The properties of the active layer alone were calculated using Equation 5.18 and 7.10 as described in Section 7.3.1 above. From this analysis the active layer properties are shown in Table 7.8. Examination of the normalised permeabilities (P^*l) obtained showed almost a ninety fold reduction due to the presence of the thin zirconia layer.

Analysis of the timelag values in Table 7.6 showed a larger spread than had been found in previous experiments. The

values of the diffusion coefficients for the KCl solution (0.1M) were also significantly different from those obtained for other membranes investigated ($1.8-1.9 \times 10^{-5} \text{ cm}^2\text{s}^{-1}$). These values are very similar to the free solution values of KCl at these concentrations [7] so either there was effectively no resistance to flow across the membrane or some other factor was introducing an error. It has been shown by Barrer, Barrie and Rodgers [8] that the contribution of flow towards the 'clamped' edges of a test membrane can cause errors in the estimation of the diffusion coefficient from this timelag method. It was also shown that the 'edge effect' was negligible if the thickness to area ratio was much less than 0.2. All of the ceramic 'disc' membranes prepared here were of 22 mm diameter and with various thickness values.

By a simple calculation of the areas involved, 85% of the total membrane area for these discs was not in direct contact with the external solutions that defined the boundary conditions. It was also clear that the thickness of the 'supports' used in these tests made the contribution due to this edge effect to be far from negligible (for 0.199 cm support the (l/a) ratio was 0.349). The type of membrane used in Barrer's tests were the dense polymer type and it would seem reasonable to assume that this edge effect would be significantly more pronounced with these current porous ceramics.

This essentially means that the diffusion coefficient values obtained for this membrane type by the timelag method must be considerably in error. No attempt has been made here to investigate or quantify this error. This was considered not within the basic remit of the work and only this particular set of membranes suffered from the edge effect to such an extent. All other membrane types studied here were found to have (l/a) values of between 0.01 (anodic alumina) to 0.07 (the thickest Visking membrane).

Plate 7.1



Cross-sectional View SEM Photograph of a Ceramic Disc Ultrafiltration Membrane. The example shown had a Silica Active layer on an α -Alumina Support. (Courtesy of ENSC Montpellier)

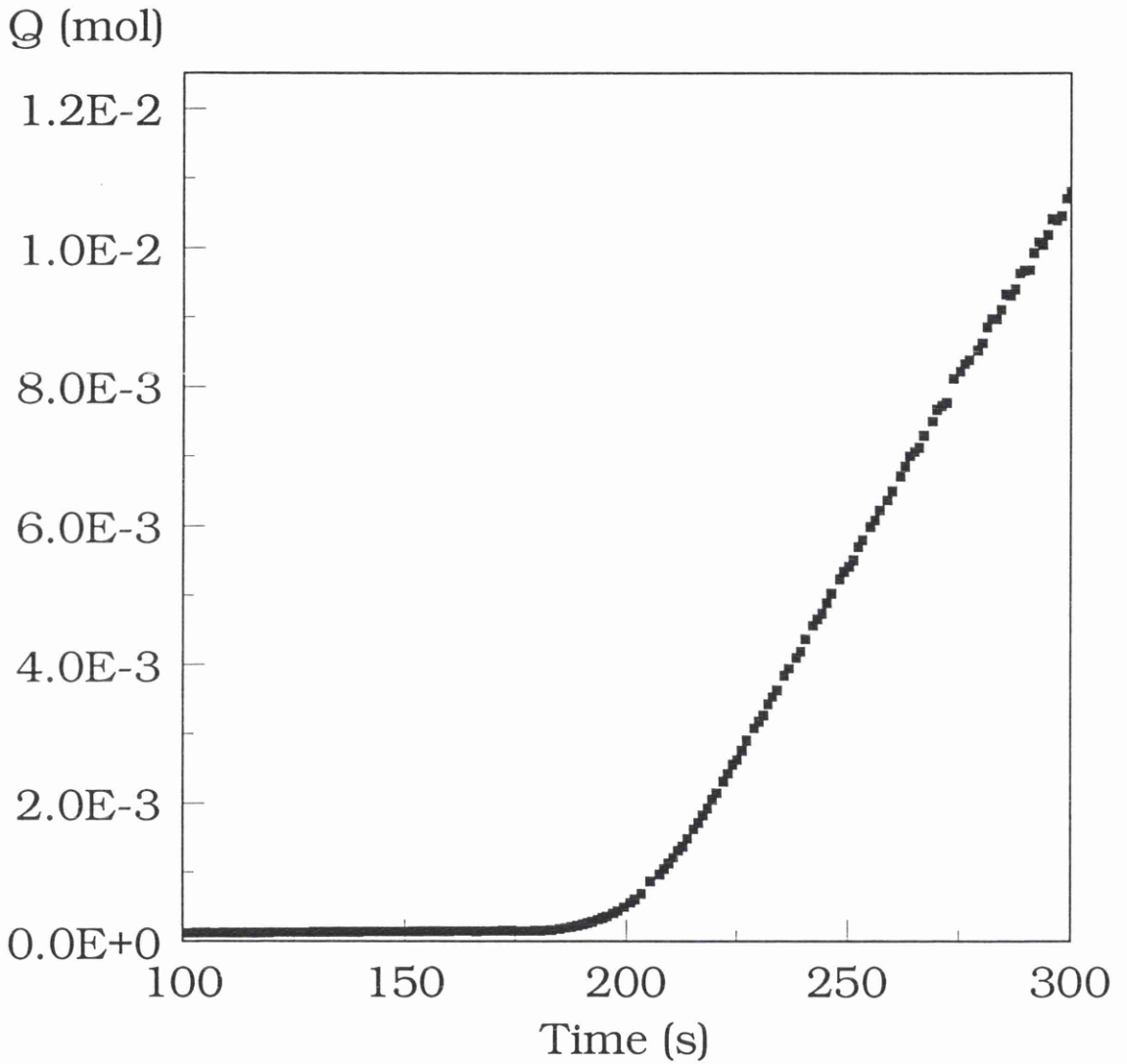


Figure 7.10 Time lag Experiment with Ceramic (Alumina) Support Disc of 0.0611 cm Thickness. The concentration step (0.1M KCl) was Imposed at 144.1 seconds and the resultant τ value was 34.55 s.

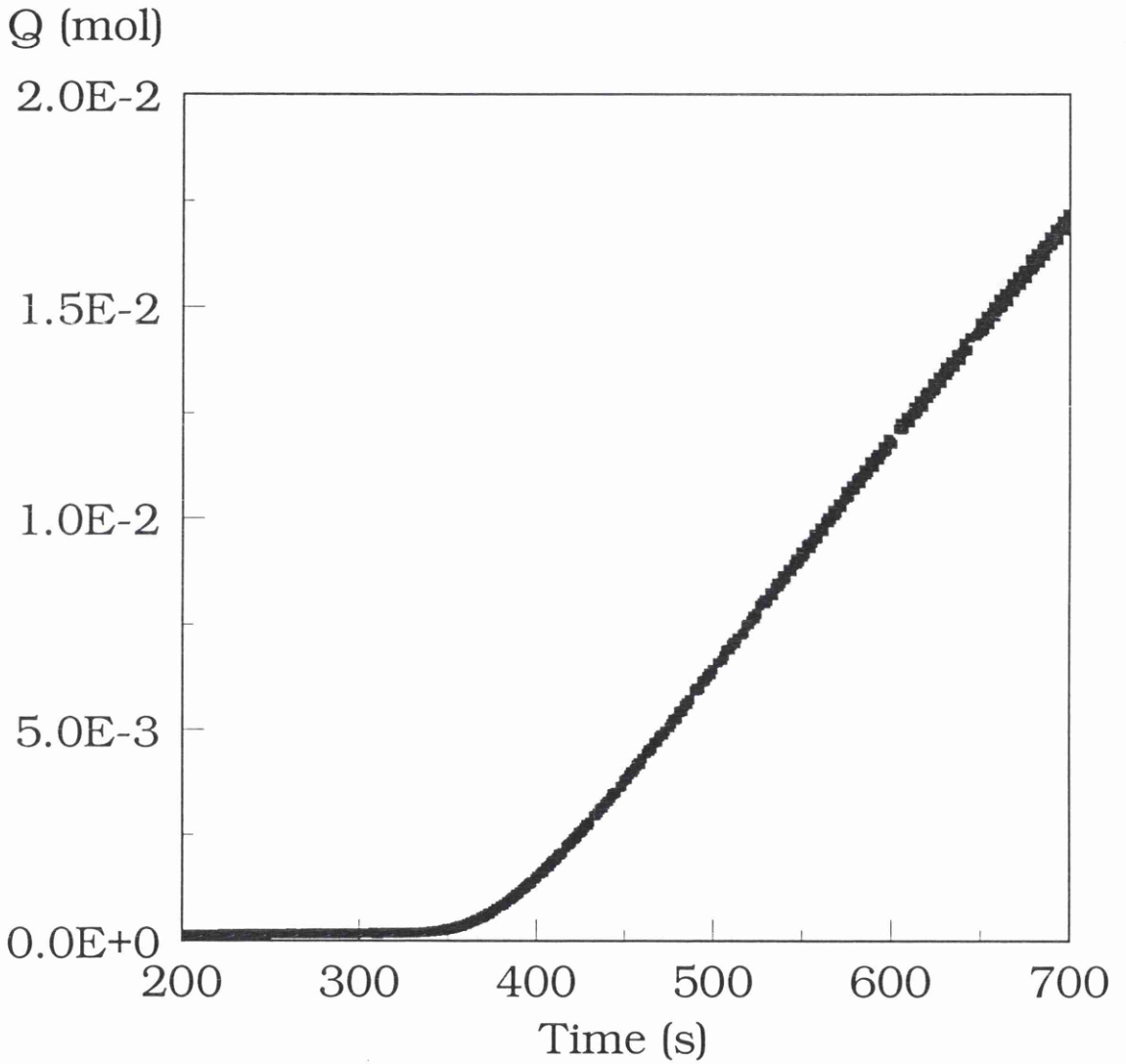


Figure 7.11 Time lag Experiment with Ceramic (Alumina) Support Disc of 0.0936cm Thickness. The concentration step(0.1M KCl) was Imposed at 302.7 s and the resultant τ value was 81.07 seconds.

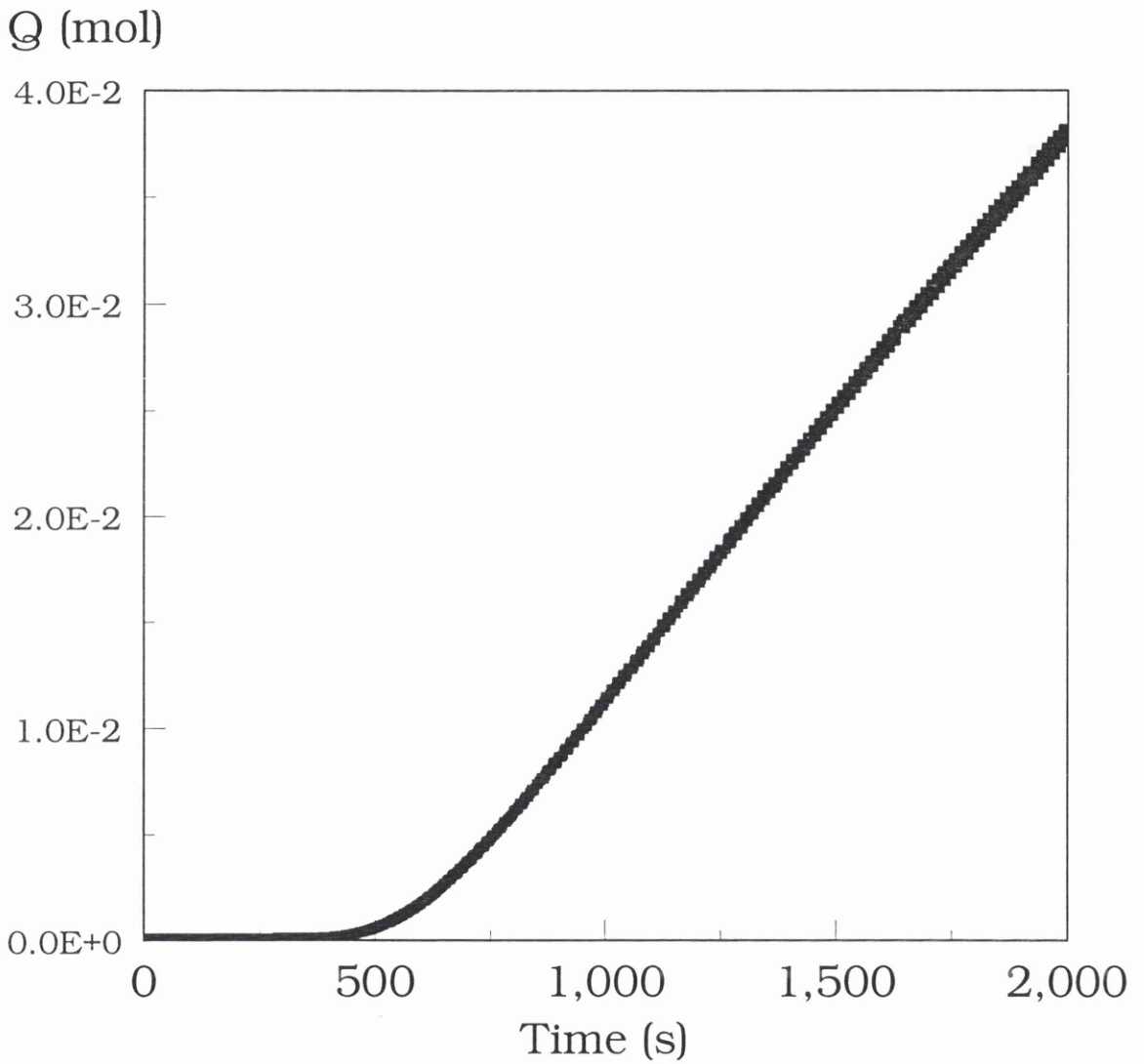


Figure 7.12 Time lag Experiment with Ceramic (Alumina) Support Disc of 0.199cm Thickness. The concentration step(0.1M KCl) was Imposed at 256.1 s and the resultant τ value was 337.72 s.

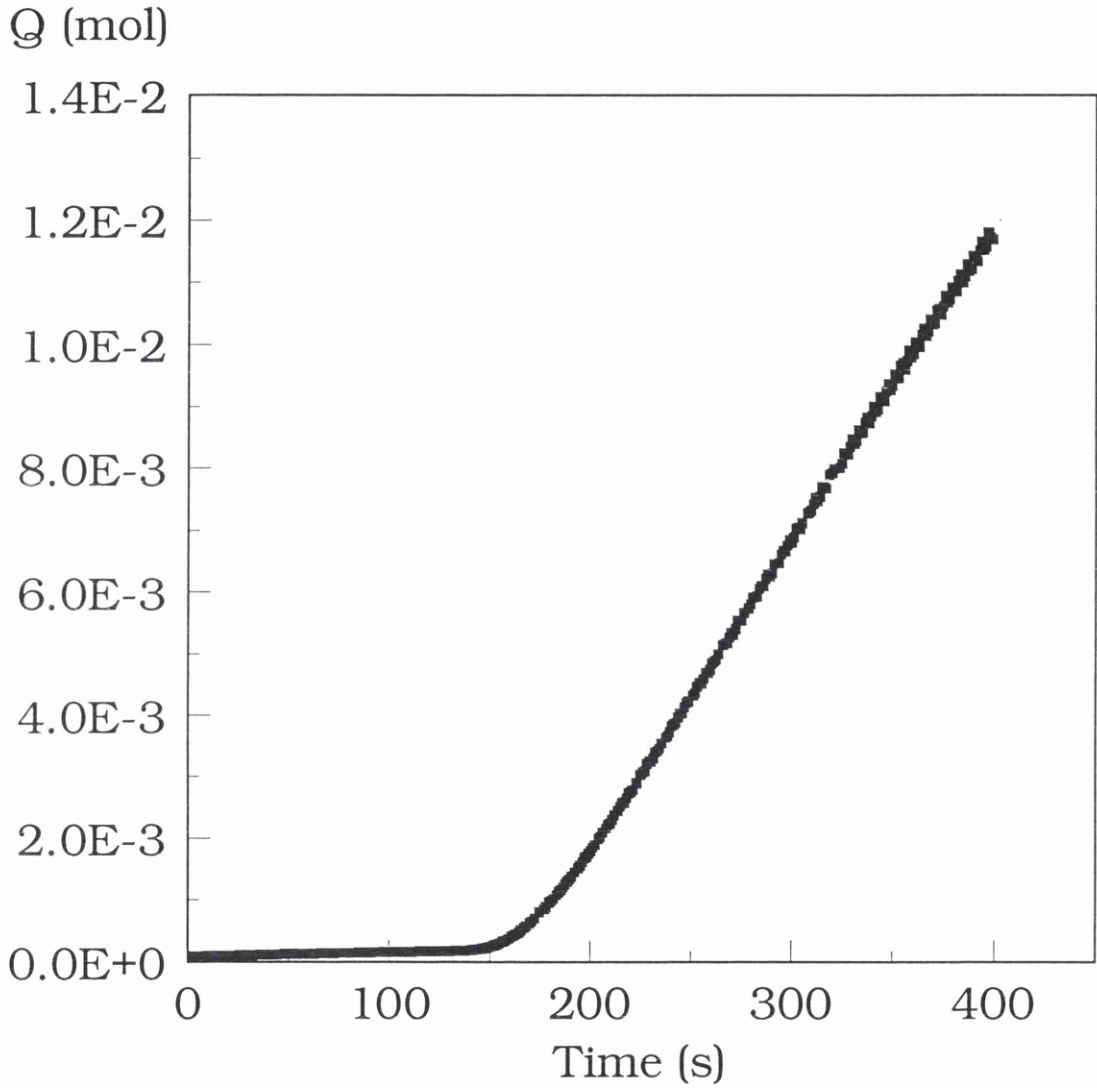


Figure 7.13 Time lag Experiment with Ceramic Membrane. The (Alumina) Support was 0.0648cm Thick and the Active Layer (Zirconia) was 4.2 μ m thick. The concentration step(0.1M KCl) was Imposed at 123.7 s and the resultant t value was 46.07 seconds.

Membrane	Thickness (cm)	Mean Exptl. Timelag (s)	Predicted Timelag (s)	% Difference
MSup	0.0611	32.35	-	-
MSup2	0.0936	80.61	75.92	5.82
MSup3	0.199	336.72	364.37	-7.58

Table 7.6 Comparison of Actual Experimental Timelag Values with Predicted values based on the thickness ratios for Ceramic Disc Membranes.

Membrane	Thickness (cm)	Calc. Diffusion Coefficient (cm^2s^{-1})	Mean Permeability ($\text{cm}\cdot\text{s}^{-1}$)	Distribution Coefficient
MSup	0.0611	1.92×10^{-5}	8.412×10^{-5}	0.469
MSup2	0.0936	1.81×10^{-5}	5.343×10^{-5}	0.485
MSup3	0.199	1.96×10^{-5}	2.657×10^{-5}	0.475
MZr1	0.064/4.2 μm	-	5.088×10^{-5}	-

Table 7.7 Data obtained from Timelag experiments with Ceramic Disc membranes.

	Layer Thickness (μm)	Layer Timelag (s)	Permeability ($\text{cm}\cdot\text{s}^{-1}$)	Perm. x Thickness	Distribution Coefficient
MZr1	4.2	0.43	1.343×10^{-4}	5.64×10^{-8}	0.825

Table 7.8 Calculated Data for a Zirconia Active Layer on an Alumina Support.

7.3.3 Tubular Ceramic Nanofiltration Membranes

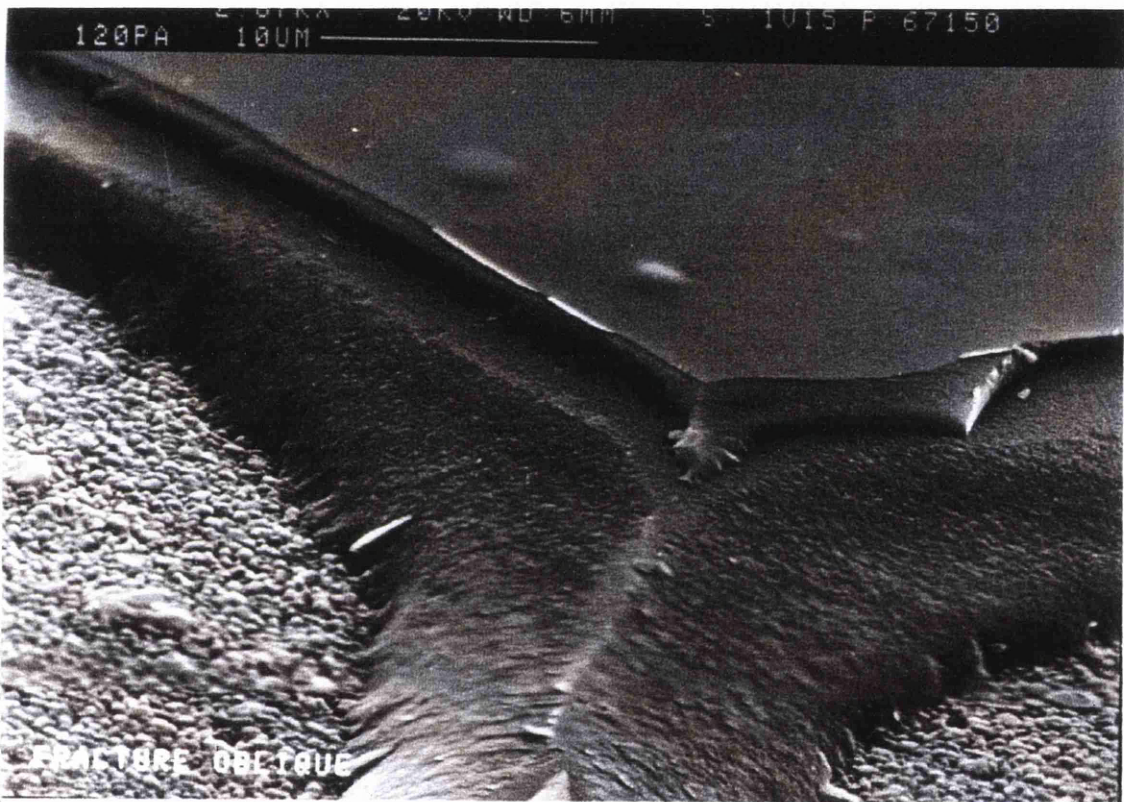
It is this format, be it a single tube or multi channel module that will be the format of choice for the future use of commercial ceramic membranes. Like any other type of membrane, a variety of properties particularly variable pore sizes are available. The membrane used for these tests was the same as described earlier in Section 5.4.3 (Gas System) and had an active layer with a nominal pore size of 5nm, an example of this membrane structure is shown in Plate 7.2. The tubular format required to be housed in a different manner from the planar membranes so far discussed. The main difference in this holder was the much larger internal volume required. This may cause some difficulty due to dilution, in measurement sensitivity for some permeant materials. The tests undertaken here again used KCl (0.1M) and so in this particular case did not represent a problem. As with the other membrane systems, experiments were performed on both the support structure alone and the composite membrane. This allowed the contribution of the support to be determined and therefore the influence of the active layer alone to be calculated.

The experimental data for the support and the composite membrane are given in Table 7.9 and shown in Figures 7.14 and 7.15. The calculated data for the active layer alone are

given in Table 7.10. The support medium of this tubular membrane showed a very free flow, the permeability value being $2.28 \times 10^{-3} \text{ cms}^{-1}$. In direct comparison the presence of the thin nanofiltration layer ($2\mu\text{m}$) caused a very substantial decrease in the overall permeability (P_{ab}), reducing in value to 2.25×10^{-5} . When the two values were normalised to take account of the thickness of the two component parts (P^*l) the reduction per unit length is of the order of 85,000 times less than the support. There is also a corresponding decrease in the calculated diffusion coefficient of the layer to 2.61×10^{-11} .

With this type of membrane having caused such a large difference between the timelag of the coated and untreated support we can with confidence believe the extracted timelag and diffusion coefficient values for these thin layers (Table 7.10). It was encouraging also that in these tests, electrolyte solutions were used. For other (slower) permeant materials this timescale should only increase allowing for even greater confidence in both the experimental and calculated results.

Plate 7.2



SEM Photograph of the Structure of a Ceramic Nanofiltration Membrane. The support structure was α -alumina and the thin active layer was of γ -alumina (Courtesy of ENSC Montpellier)

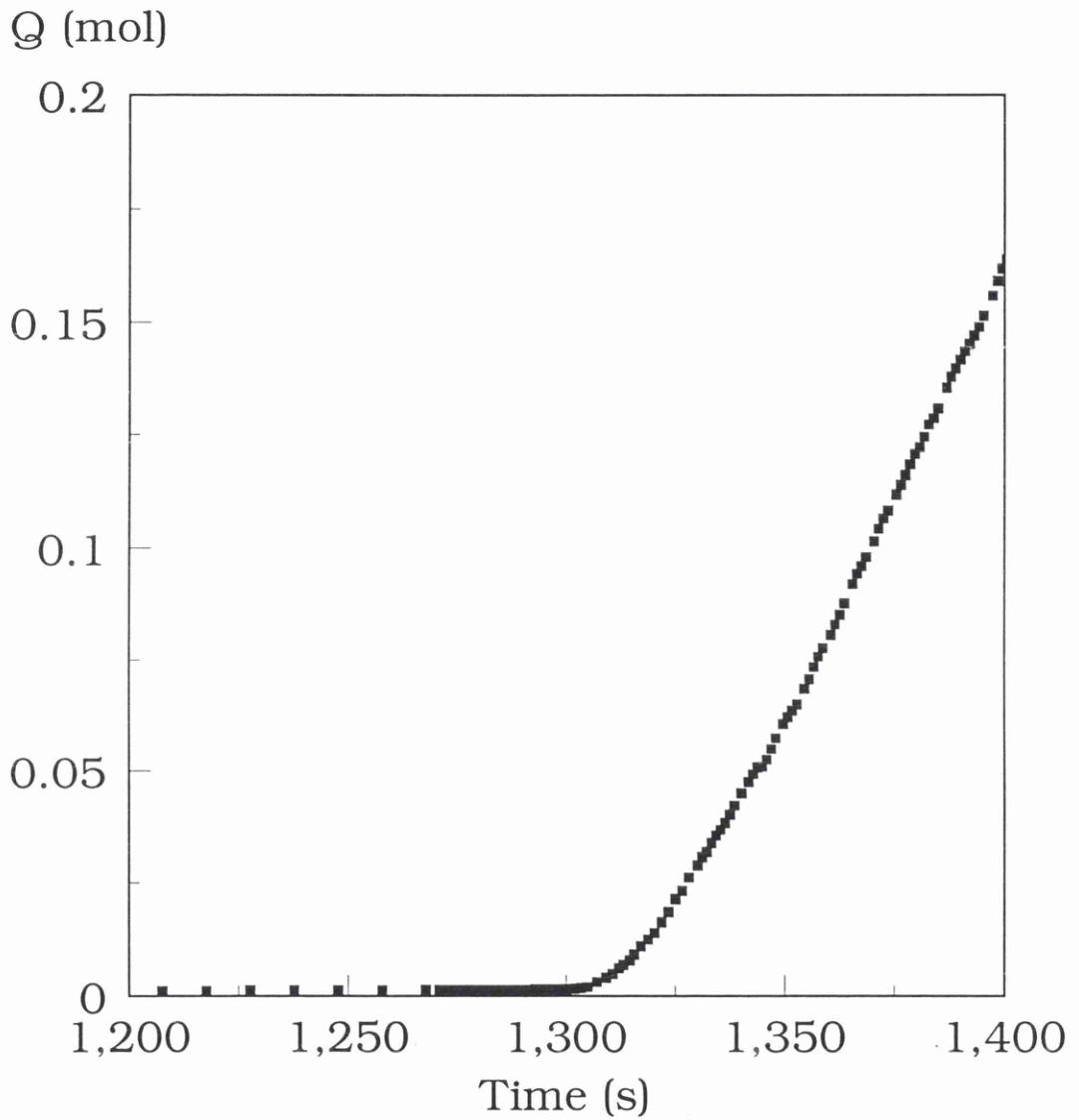


Figure 7.14 Timelag Experiment with a Tubular Support of 0.168cm thickness. The concentration step (0.1M KCl) was Imposed at 1270.1 seconds and the resultant τ was 49.71s.

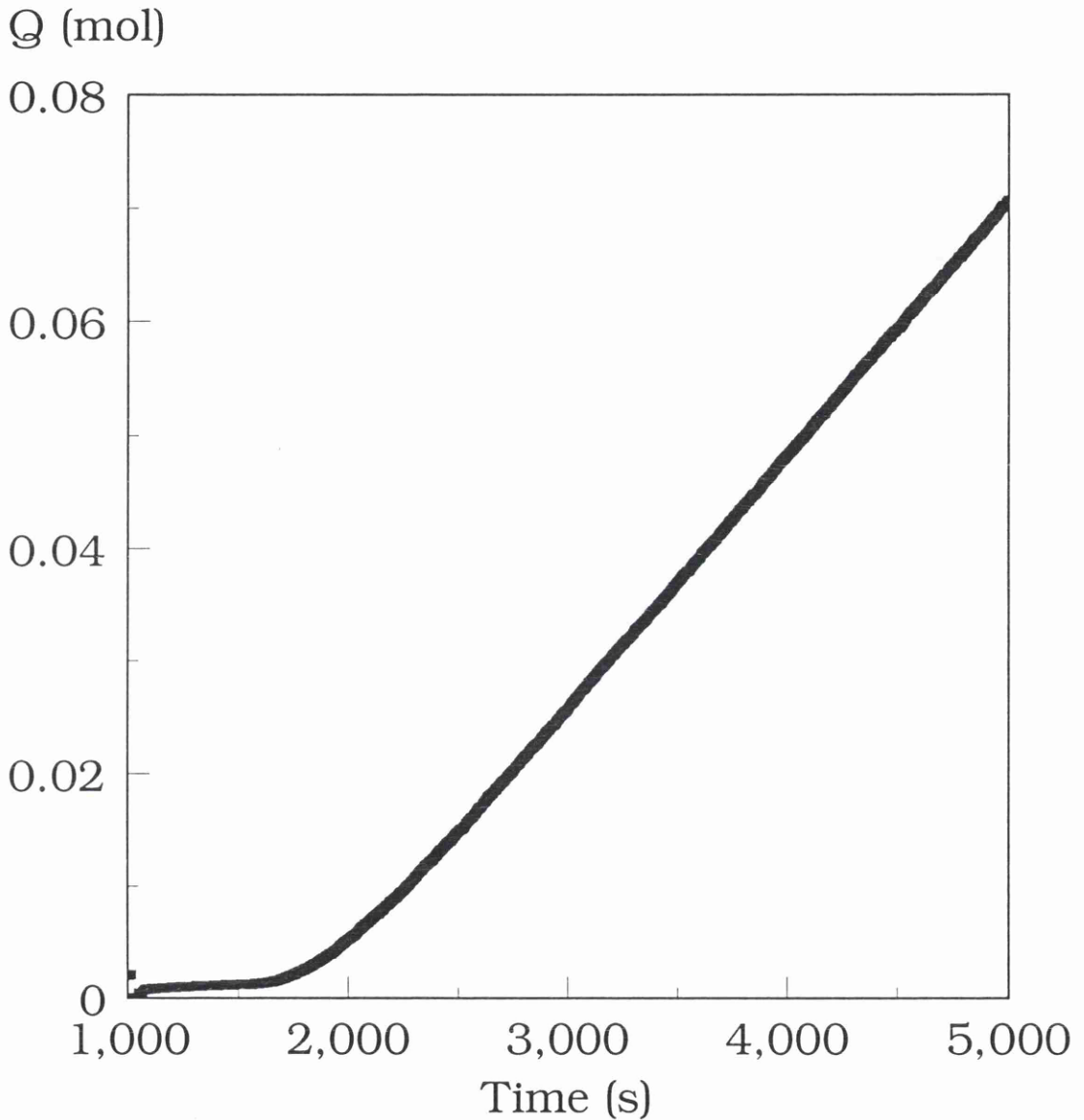


Figure 7.15 Timelag Experiment with a Tubular Membrane Support thickness was 0.1778cm and the Active Layer(γ -alumina) 2 μm . The concentration step (0.1M KCl) was Imposed at 1390.8 seconds and the resultant τ was 545.19s.

	Timelag (s)	Diffusion Coeff. (cm ² s ⁻¹)	Permeability (cms ⁻¹)	Pxl
Support TS1	50.83	2.61x10 ⁻⁵	2.28x10 ⁻³	3.84x10 ⁻⁴
Membrane TLa1	550.78	-	2.25x10 ⁻⁵	-

Table 7.9 Experimental data for tubular support (TS1), 0.168cm thickness and Tubular ceramic nanofiltration membrane (TLa1), 0.177cm/2μm

Layer	Timelag (s)	Permeability (cm s ⁻¹)	P x l	Diffusion Coeff. (cm ² s ⁻¹)	Distribution Coefficient
	255.46	2.28x10 ⁻⁵	4.52x10 ⁻⁹	2.61x10 ⁻¹¹	22.21

Table 7.10 Calculated data for Active layer of Tubular membrane (TLa1) with layer thickness 2μm.

7.3.4 Oscillator Experiments

Using the systems designed and developed in this current work ceramic membrane permeabilities and diffusion coefficients have been determined. This new automated technique has allowed for the first time the rapid and repeated determination of these membrane parameters completely automatically.

A consecutive series of timelag experiments were performed in which concentration square waves were imposed at one exposed face (as previously) but with the lower concentration of the oscillator being equal to that initially in the collecting volume, normally zero. By applying such conditions, the accumulation of permeant material in the collecting volume followed a rising 'staircase' concentration pattern.

The initial experiments chosen were to investigate the permeability of potassium chloride through Whatman Anopore™ alumina 0.2μm (homogeneous) and 0.02μm (bilayer with 0.2μm backing) membranes. The experimental data treatment was identical to that described in Section 7.1.2 but the slopes were combined as described in Chapter 2. i.e. (slope B- slope C).

The processed data obtained are shown in Table 7.11 and a portion of the experimental data is shown in Figure 7.16. From these the power and ease of the system is somewhat self

evident. For nine concentration waves (each of 100s period) eighteen separate permeabilities were obtained with a standard deviation of less than 3%. These combined slopes gave a permeability (P_{ab}) of $7.23 \times 10^{-5} \text{ cm.s}^{-1}$. The experimental timelag values obtained were $4.38\text{s} \pm 0.37\text{s}$ for the backing layer ($0.2\mu\text{m}$ support) and $5.06 \pm 0.48\text{s}$ for the bilayer ($0.02\mu\text{m}$) membrane. Obviously, such short timelag values must be treated with great care but the overall system results were excellent. These particular membranes were of low scientific interest but served their purpose of proving the validity and scope of the oscillator methodology.

This technique has been applied to a range of both homogeneous and bilayer membrane systems to determine explicitly the permeabilities and diffusion coefficients in the active layers.

For the anodic alumina membrane samples (Section 7.3.1) oscillator experiments were performed, the data obtained are shown in Table 7.12. and an experimental wave in Figure 7.17. Direct comparison between the multiple estimation of the oscillator to the single timelag experiments showed the calculated layer permeability in this case (oscillator) to be lower, $1.26 \times 10^{-5} \text{ cms}^{-1}$ (c.f. 2.35×10^{-5}) and the normalised value (P_{xl}) proportionately lower also at 2.77×10^{-8} (c.f. 5.16×10^{-8}).

Similarly, oscillator experiments were performed on a range of sol-gel type membranes (Section 7.3.2) for comparison against the single timelag parameters obtained. A summarised version of this data is shown in Table 7.13 and one example of the experimental output is shown in Figure 7.18.

The zirconia sol-gel membrane (MZr1) was found to have a slightly higher calculated layer permeability when compared to the single timelag data. The difference between the two systems being about 4%. Although this difference is not vast the (hopefully) more accurate data from the oscillator allows for greater confidence in determination of permeabilities and diffusion coefficients. It may also be the case that such a difference would prevent distinguishing between two different systems of similar properties.

Oscillator Cycle #	Slope B (x10 ⁵)	Slope C (x10 ⁶)	Slope (B-C) (x10 ⁵)	Oscillator Cycle #	Slope B (x10 ⁵)	Slope C (x10 ⁵)	Slope (B-C) (x10 ⁵)
1	7.381	-0.663	7.447	10	6.18	-1.068	7.248
2	6.803	-1.591	6.962	11	6.273	-1.08	7.353
3	7.005	-3.294	7.334	12	6.061	-1.297	7.358
4	6.676	-4.436	7.119	13	6.202	-1.158	7.36
5	6.751	-5.314	7.282	14	5.68	-1.216	6.896
6	6.558	-6.332	7.191	15	5.478	-1.521	6.999
7	6.71	-7.093	7.419	16	5.743	-1.635	7.378
8	6.422	-7.517	7.174	17	5.677	-1.387	7.064
9	6.503	-9.006	7.464	18	5.673	-1.481	7.154

Mean Slope 7.233×10^{-5}
 $\pm 1.76 \times 10^{-6}$

Tale 7.11 Oscillator Data for a Whatman Anopore™ 0.02μm Pore Size Bilayer Membrane.

Oscillations were between distilled water and 0.1M KCl solutions. The switch period used was 100 seconds.

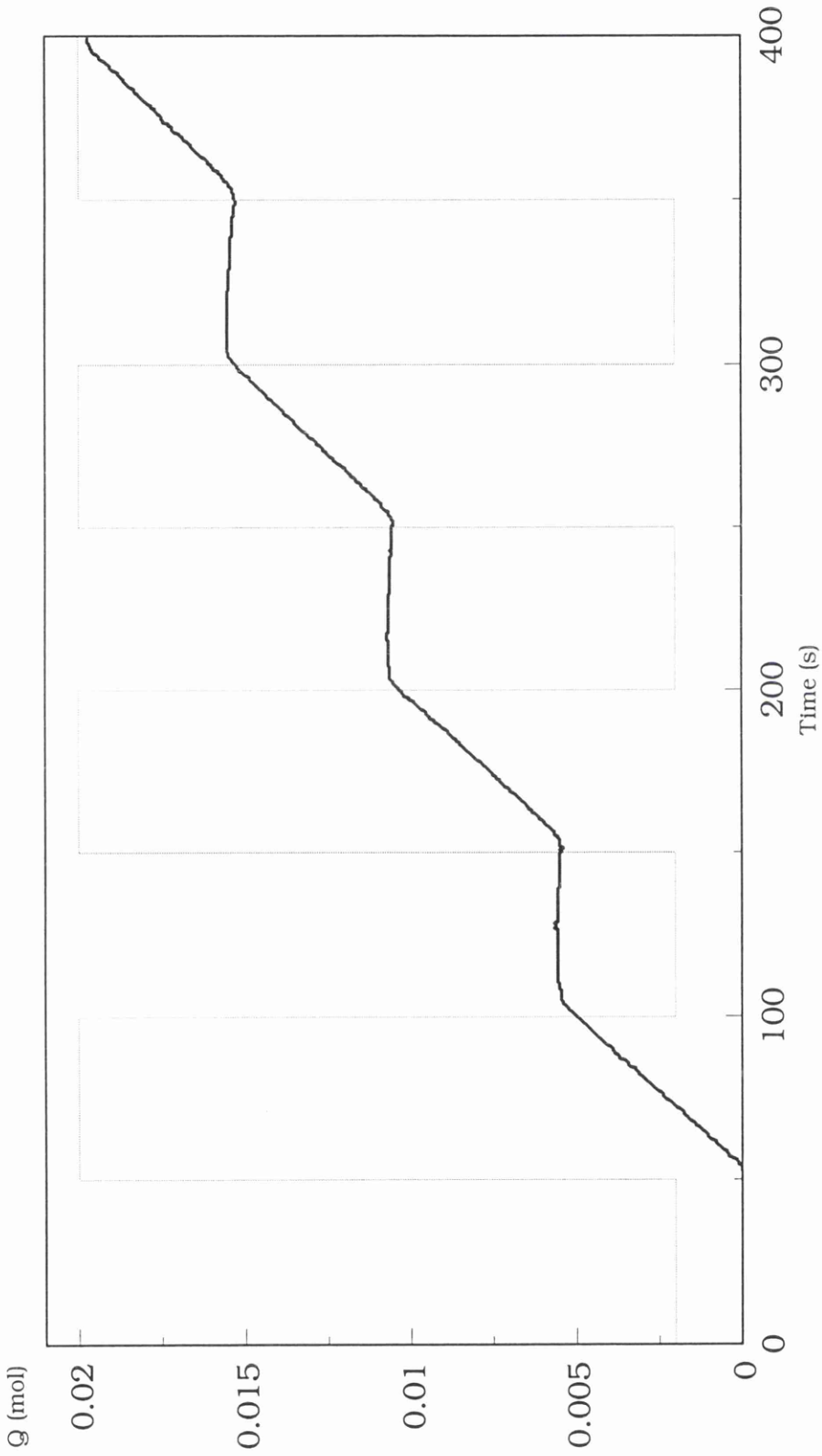


Figure 7.16 Portion of the emergent wave from a stepped oscillator experiment with a Whatman Anopore™ 0.02 μ m pore size bilayer membrane. Oscillation was between 0.1M KCl and water, the switch period used was 100 seconds.

Oscillator Cycle #	Slope B ($\times 10^6$)	Slope C ($\times 10^7$)	Slope (B-C) ($\times 10^6$)	Timelag (s)
1	8.306	0.414	8.264	3.91
2	8.198	3.497	7.848	4.15
3	7.424	-1.165	7.541	4.25
4	7.217	-2.182	7.435	4.3
5	6.702	-2.751	6.997	4.18

Mean $7.617 \times 10^{-6} \pm 4.7 \times 10^{-7}$

Table 7.12 Oscillator Experimental Results from Anodic Alumina Bilayer sample LAA2 (48/22 μm). Oscillation was between distilled water and 0.1M KCl and the Switch Period was 100 seconds.

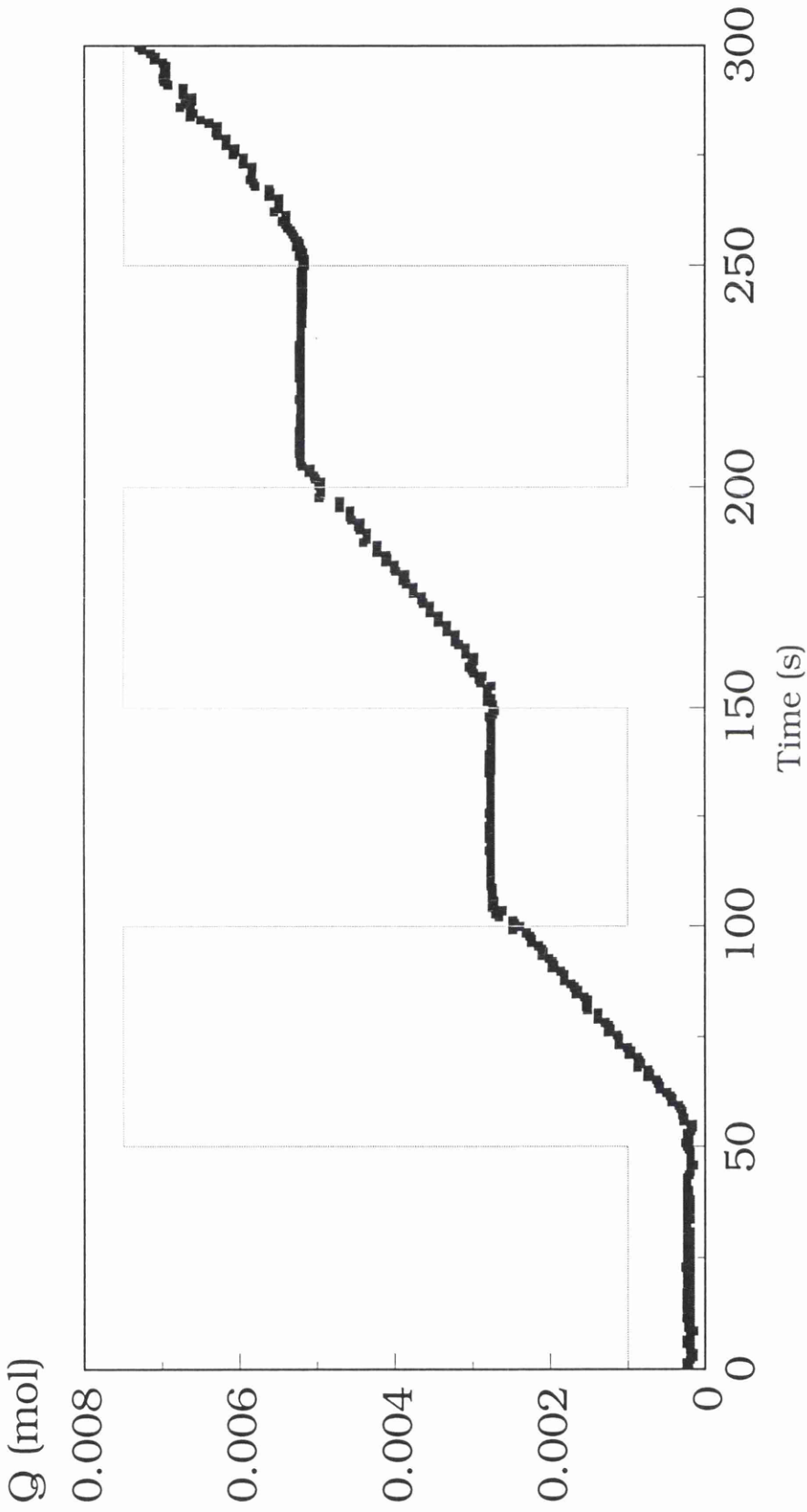


Figure 7.17 Portion of the emergent wave from a stepped oscillator experiment with the anodic alumina bilayer membrane (LAA2). Oscillation was between 0.1M KCl and water, the switch period used was 100 seconds.

Layer Thickness (μm)	Layer Timelag (s)	Layer Diffusion Coefficient (cm^2s^{-1})	Permeability ($\text{cm}\cdot\text{s}^{-1}$)	Perm. x Thickness	Distribution Coefficient
MZr1 4.2	0.44	6.69×10^{-8}	1.403×10^{-4}	5.89×10^{-8}	0.88
MTY1 4.1	0.1	2.77×10^{-7}	6.015×10^{-4}	2.47×10^{-7}	0.889
MA11 10	1.69	9.87×10^{-8}	8.031×10^{-5}	8.031×10^{-8}	0.813
MS11 6.5	0.8	8.78×10^{-8}	8.896×10^{-5}	5.782×10^{-8}	0.658

Table 7.13 Active Layer Data Calculated from Oscillator Experiments on Ceramic Membranes with Different Active Layer Materials.

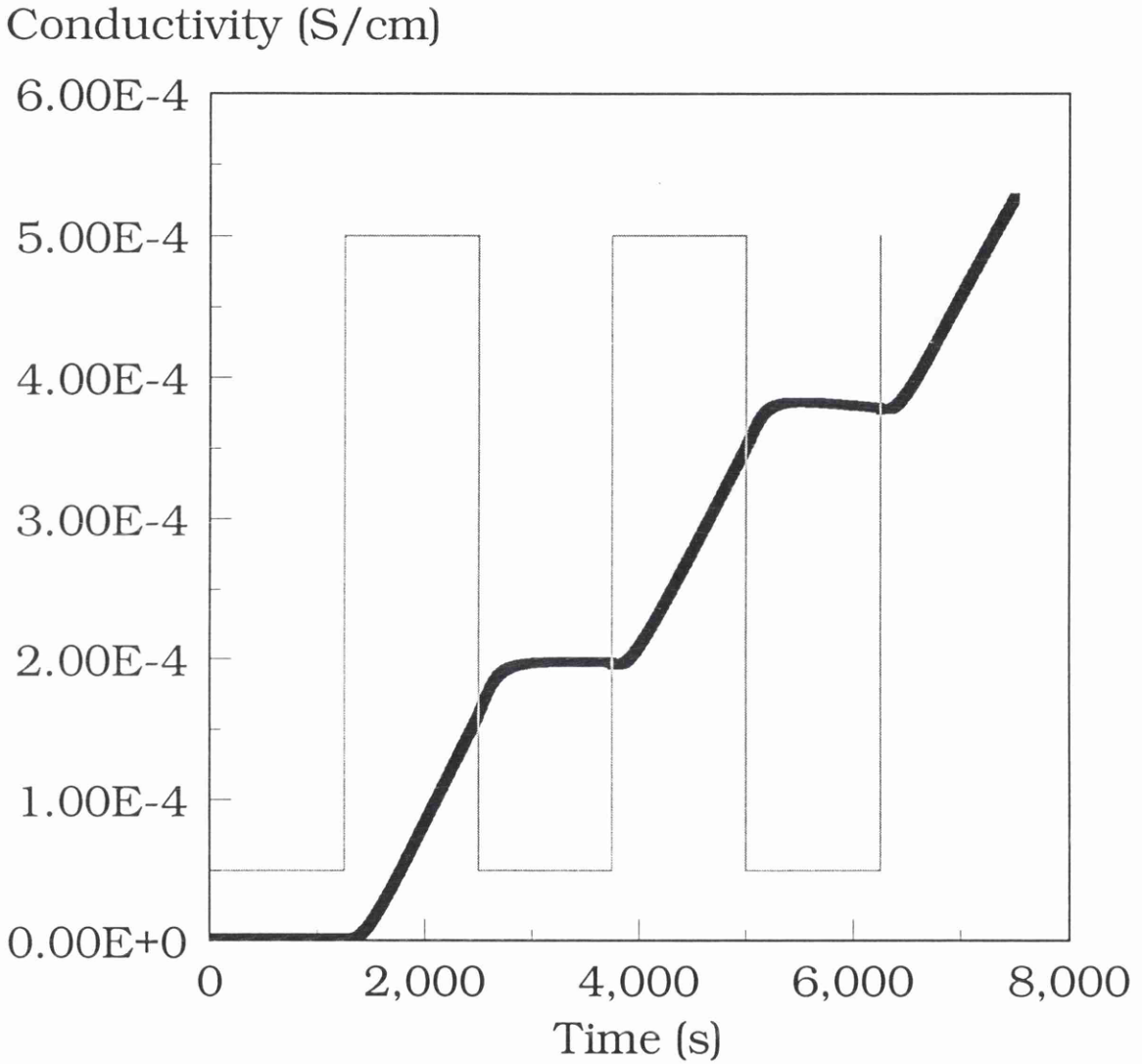
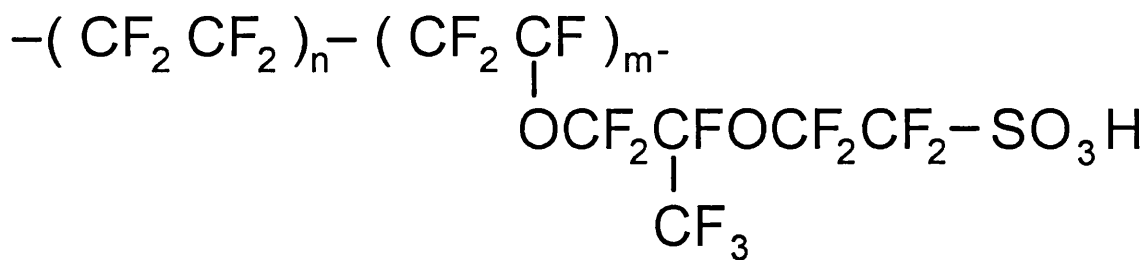


Figure 7.18 Experimental Emergent Wave from an Oscillator Experiment with a Ceramic Bilayer Membrane. The Titania active Layer(4.1 μ m) was supported by a 0.0965cm alumina support.

7.3.5 Charged Membranes

In addition to the interest in 'porous' membrane systems described in this thesis, there are of course many other types of membranes with fascinating properties, one such group being charged membranes. Some investigations on this type of membrane were performed, in particular, the effects of electrolyte transport through these charged membranes was investigated. In this instance an ion-exchange membrane, a NAFION 117 membrane (DuPont Chemicals Inc.) was chosen for investigation. This NAFION perfluorosulphonic acid membrane is used extensively in harsh chemical environments due to its high resistance to chemical attack, even in extreme conditions such as in chlor-alkali electrode cells. The structure is shown schematically below.



NAFION 117 membrane structure

This 'inertness' has not prevented research on ways of modifying these membranes to make them even more functional by chemically grafting different agents onto their surfaces such as crown ethers for potential alkali metal separations.[9] [10].

It has been shown, that the timelag method employed here will

allow for the estimation of permeability and diffusion coefficient within a single experiment. In the case of electrolyte permeation in these charged systems the relationship between these parameters becomes highly concentration dependant. This is due to the development of the Donnan potential [11] and the Donnan equilibrium that is established between the membrane matrix and the bulk solution interface. This is shown diagrammatically for an cation exchange membrane, as in the case of NAFION, in Figure 7.19. Earlier work by Paterson & Doran [12] on such systems showed that it was possible to estimate for an 'unknown' membrane, the nature of the charge and the salt uptake of the 'unknown' membrane. From Figure 7.19 it is clear that solution based anions, co-ions, will be repelled from the membrane matrix due to the small negative charge that exists within the membrane. From this, it is also clear that the exchanger will strongly favour the counter-ion (solution based cations) by electrostatic interactions. The extent of this co-ion exclusion will be valency dependant with higher valency co-ions being excluded more strongly.

In all experiments performed in this study the same co-ion (Cl⁻) was used when changing the counter ion form of the membrane matrix (H⁺, K⁺, Ca⁺⁺). This was achieved by bathing the membrane sections in 2 Molar solutions of the relevant

chloride salts for 24 hours with constant stirring. After this soaking period the cut membrane sections were washed several times with distilled water and then soaked for 2 days with constant stirring in distilled water that was refreshed at regular intervals. At the end of this procedure the membrane matrix would be in the desired ionic form (H^+ , K^+ , Ca^{++}) but free from any excess of electrolyte within the matrix.

In order for equilibrium to exist between the electrolyte in solution $A_{v_A}^{z_A} B_{v_B}^{z_B}$ and a cation exchange membrane (in the A-form)

$$a_A^{v_A} a_B^{v_B} = \bar{a}_A^{v_A} \bar{a}_B^{v_B} \quad \text{Equation 7.11}$$

where a_A and a_B represent the ion activities in solution and \bar{a}_A and \bar{a}_B represent the ion activities within the membrane matrix with v_A and v_B being the electrolytic stoichiometric coefficients.

If a solution has a molar concentration, c_s then the Donnan relationship dictates that the concentration within the membrane \bar{c}_s is given by

$$\bar{c}_s = K^{\frac{1}{v_B}} \left(C_s \gamma_{\pm} \right)^{\frac{v}{v_B}} \quad \text{Equation 7.12}$$

where γ_{\pm} is the mean ion activity coefficient, $v = v_A + v_B$ and the term K

$$K = v_A^{v_A} / \left[X^{v_A} (\bar{\gamma}_{\pm})^v \right] \quad \text{Equation 7.13}$$

where $X = |z_x| \bar{c}_x / |z_A|$ where \bar{c}_x is the concentration of fixed

charges within the membrane matrix. From equations 7.12

and 7.13 it is clear that the distribution coefficient α will not

be constant within charged membranes.

To test the response of the Donnan relationship 7.11 we will compare the steady state flows for two different salt concentrations. The concentrations chosen were 0.1M and 0.05M. Under these conditions it was expected to maintain near constant values for the term, K , this makes the estimation from the flux ratios much more reasonable.

$$\begin{aligned} Q_{(0.1)} / Q_{(0.05)} &= \bar{c}_{S(0.1)} / \bar{c}_{S(0.05)} \\ &= \left[(\gamma_{\pm} * 0.1) / (\gamma_{\pm} * 0.05) \right]^{\frac{v_A + v_B}{v_B}} \quad \text{Equation 7.14} \end{aligned}$$

A series of timelag experiments were performed using 0.1 and 0.05 molar solutions of HCl, KCl and CaCl₂ with membranes in the H⁺, K⁺ and Ca⁺⁺ forms. One such example is shown in Figure 7.20 and the steady state flux comparisons are shown in Figures 7.21 to 7.23.

The mean activity coefficients were calculated using an extended form of the Debye-Huckel equation [13] (Davies equation [14]) and these calculated values are shown in Table 7.14. The resulting data obtained from the steady state flux comparisons agreed very well with the predicted (ideal) values, these are shown in Table 7.15, the data taken from this table shows the accuracy of this analysis method to be excellent. The experimental flux ratios obtained were -3.7% of the predicted value for the potassium form, +2.9% for the hydrogen form and -4.5% for the calcium form of the exchange membrane. The order of the permeabilities obtained being

$\text{Ca}^{++} > \text{H}^+ > \text{K}^+$.

From the timelag data obtained the estimated diffusion coefficients were found to be 6.31×10^{-7} , 4.58×10^{-7} and $4.19 \times 10^{-7} \text{ cm}^2\text{s}^{-1}$ for the HCl, KCl and CaCl_2 solutions (0.1M) respectively, a different order than for the permeability data.

These diffusion coefficient values are all of similar magnitude, unlike the obtained permeability values. This narrower range in the data was more as expected as the diffusion of electrolyte will be determined mainly by concentration and the diffusion coefficient of the co-ion present [15], in each case here this was chloride ion. Donnan exclusion is unique to electrolyte transport through charged membranes (or sorbants) and it is clear that the system is very capable of monitoring such effects accurately.

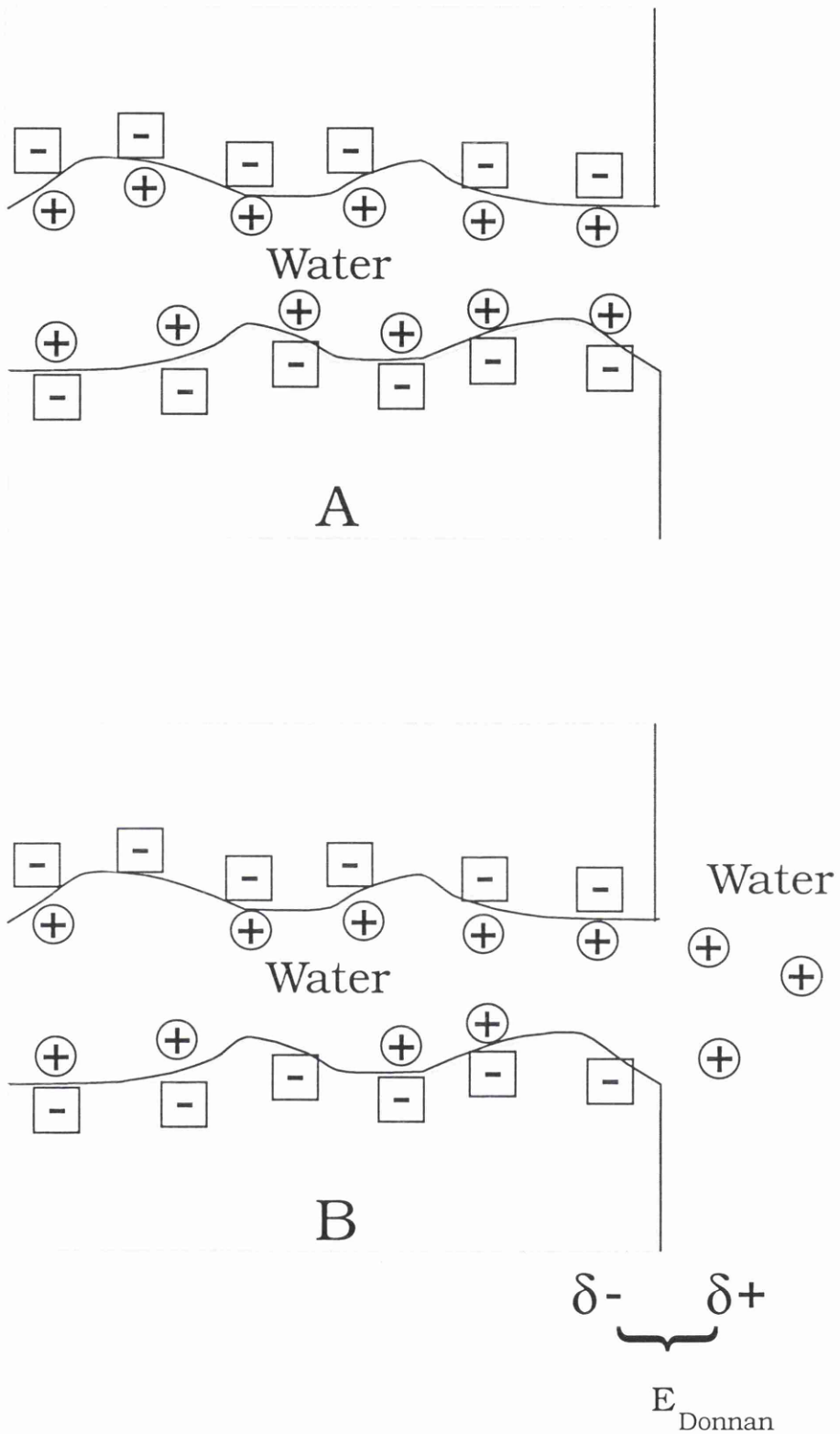


Figure 7.19 Schematic of the Development of a Donnan Potential within a pore at an ion-exchanger/water interface.

In (A) the dry (bound water) case is shown and in (B) the effect due to immersion into water.

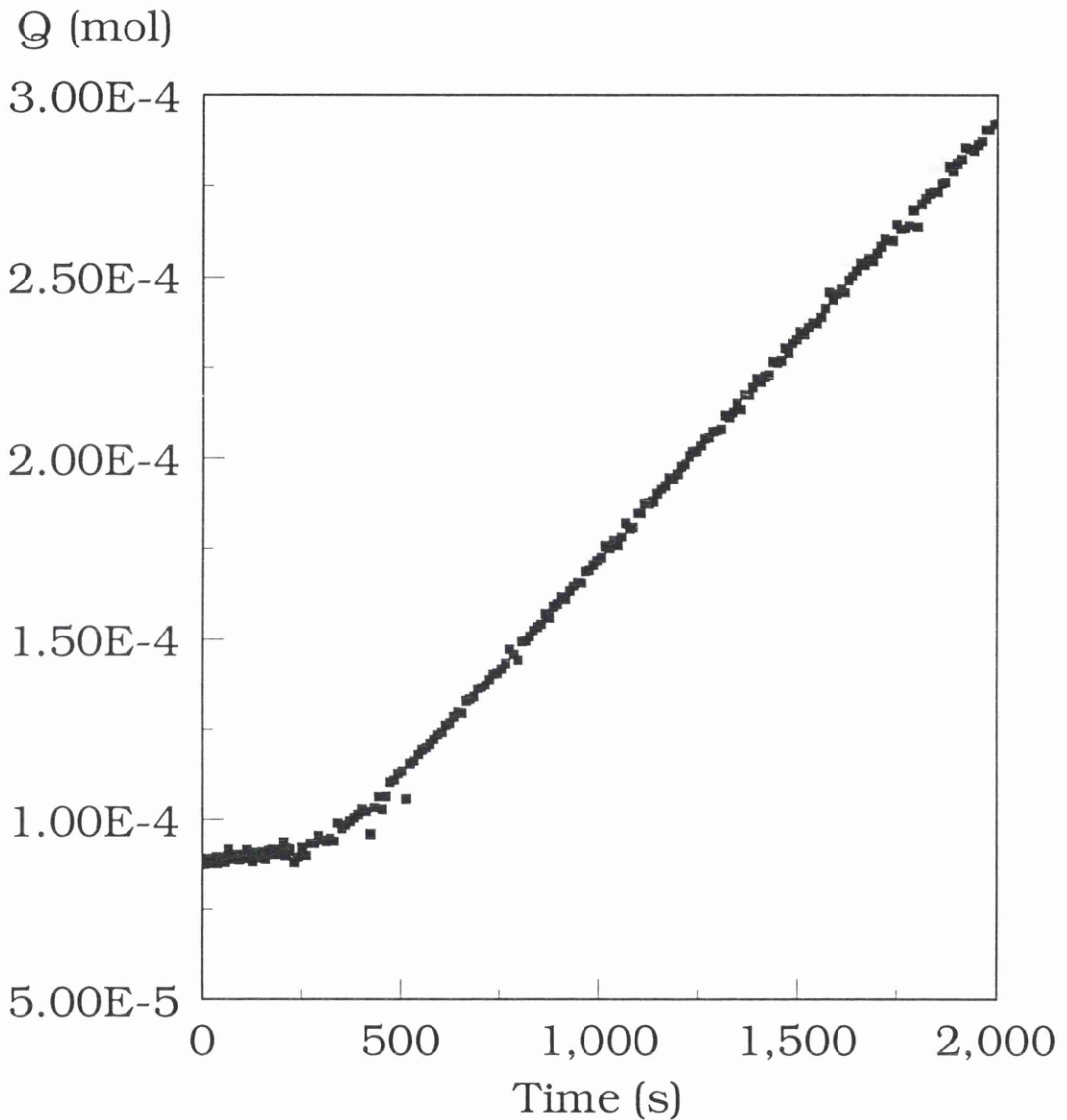


Figure 7.20 An timelag experiment for a NAFION membrane in the Potassium form of thickness 0.0189cm. The Imposed step (0.1078M KCl) occurred at 165.3 seconds. The resultant τ was 129.8 s

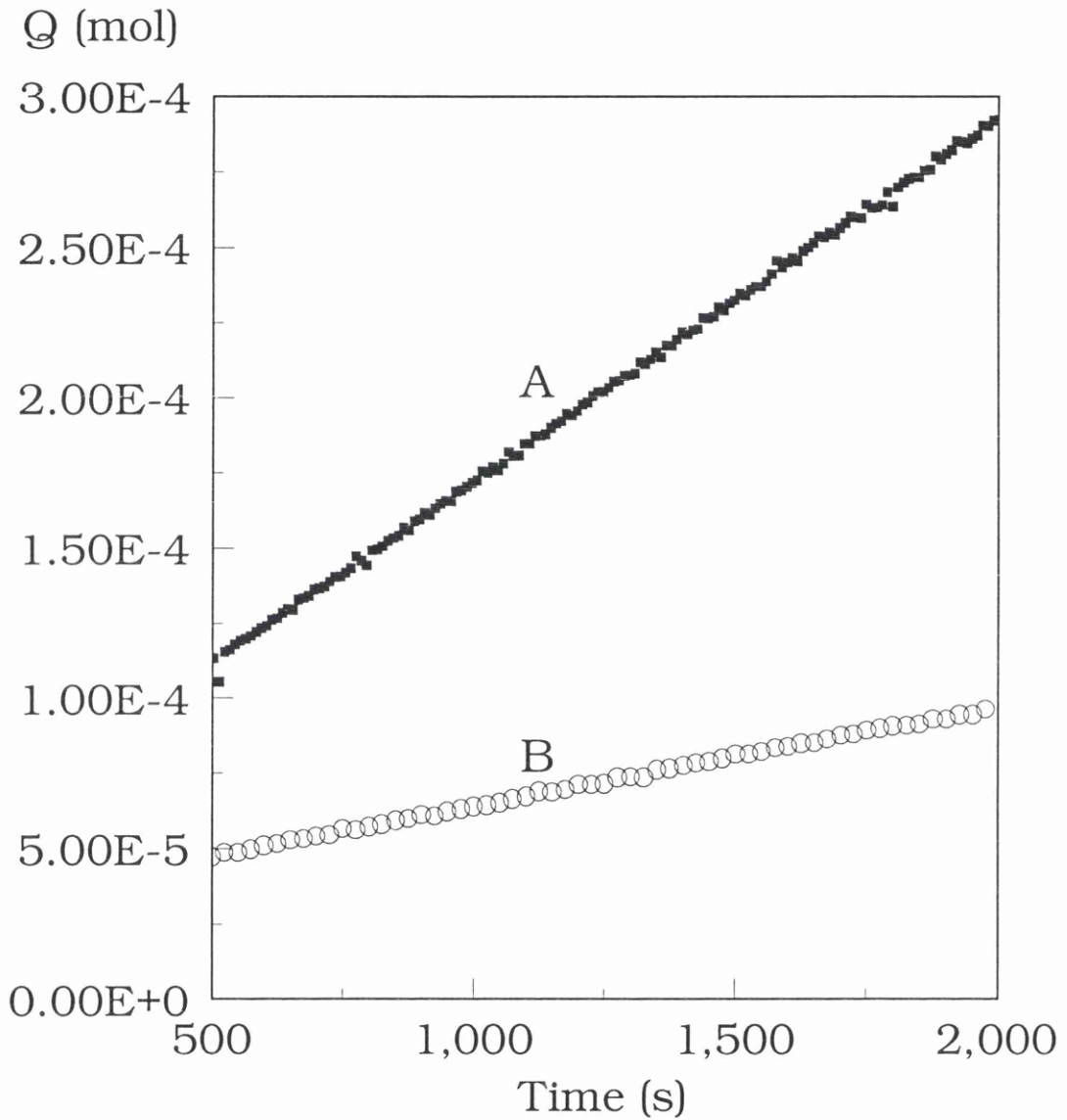


Figure 7.21 Steady State profiles for a NAFION membrane in the Potassium form. Plot A was for a 0.1078M KCl and plot B a 0.0501M KCl Imposed step. The ratio of the two slopes was 3.67, the ideal Donnan value being 3.79.

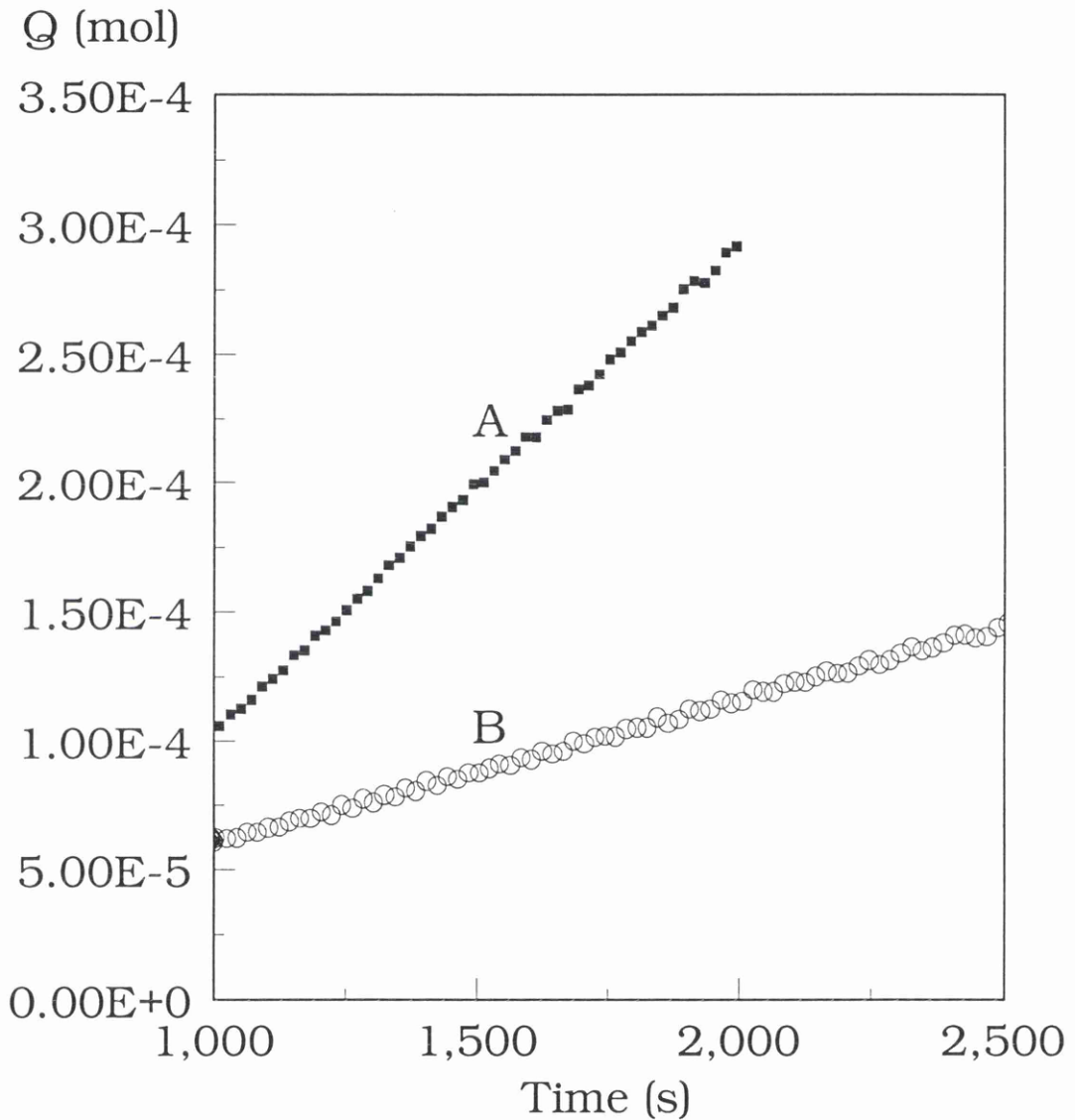


Figure 7.22 Steady State profiles for a NAFION membrane in the hydrogen form. Plot A was for a 0.1013M HCl and plot B a 0.0532M HCl Imposed step. The ratio of the two slopes was 3.42, the ideal Donnan value being 3.31.

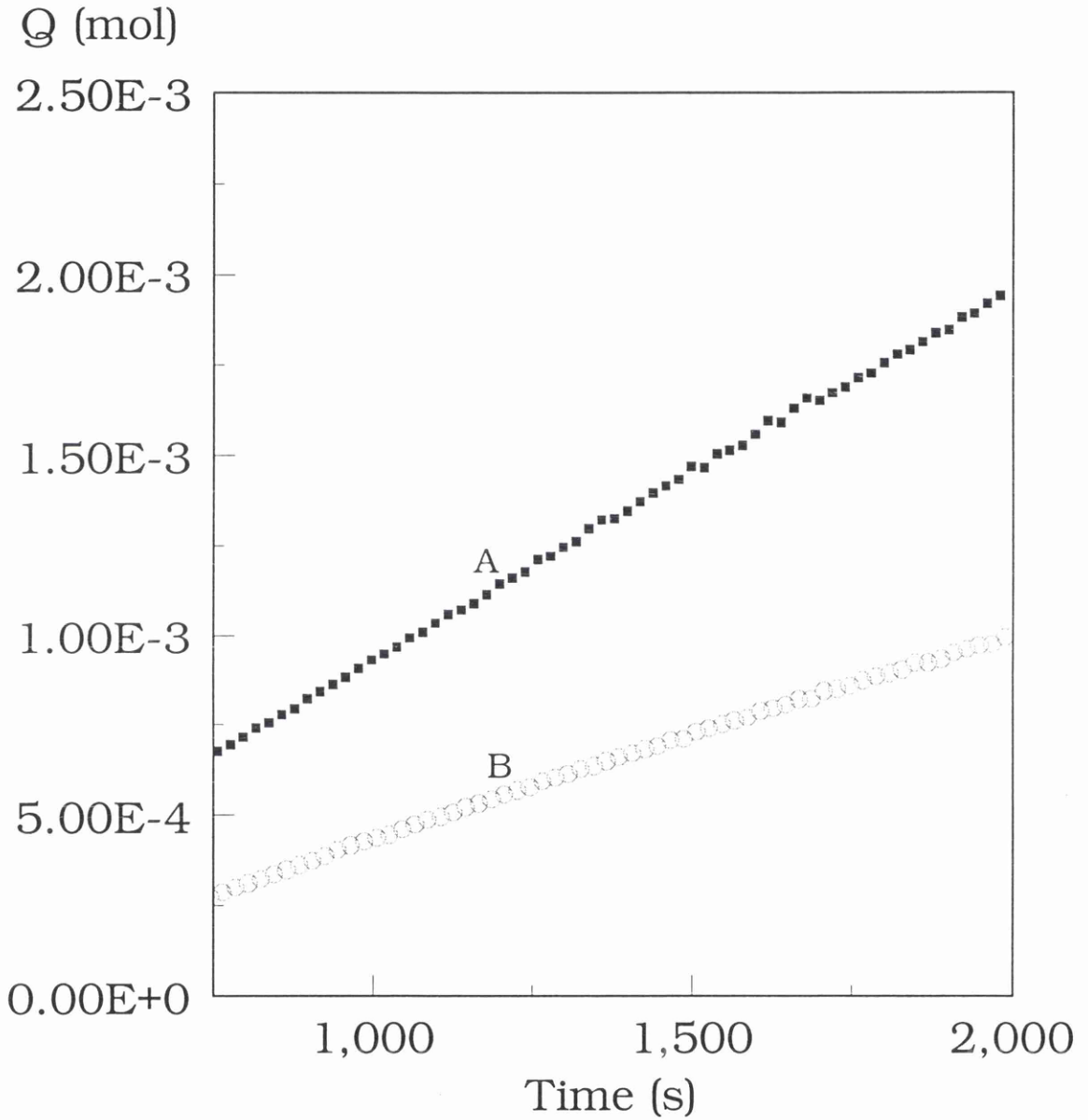


Figure 7.23 Steady State profiles for a NAFION membrane in the calcium form. Plot A was for a 0.1001M CaCl_2 and plot B a 0.0500M CaCl_2 Imposed step. The ratio of the two slopes was 2.55, the ideal Donnan value being 2.659.

Salt	Conc. (Molar)	Ionic Strength ⁽¹⁾	Activity Coefficient ⁽²⁾
KCl	0.1078	0.1078	0.7808
	0.0576	0.0576	0.8215
HCl	0.1013	0.1013	0.7843
	0.0532	0.0532	0.8208
CaCl ₂	0.1	0.2502	0.7426
	0.0501	0.1119	0.7728

Table 7.14 Calculated Values of Ionic Strength and Mean Ionic Activity Coefficients used in the Donnan Exclusion Tests.

$$^{(1)} I = \frac{1}{2} \sum c_i z_i^2$$

$$^{(2)} -\log \gamma_{\pm} = \frac{1}{2} \left(\frac{\sqrt{I}}{\sqrt{I+1}} - 0.3I \right)$$

Salt	Permeability (0.1M)	Permeability (0.05M)	Experimental Flux Ratio	Calculated ⁽³⁾ Flux Ratio	% Difference
KCl	1.19x10 ⁻⁷	3.26x10 ⁻⁸	3.65	3.79	-3.77
HCl	1.90x10 ⁻⁷	5.57x10 ⁻⁸	3.41	3.31	2.96
CaCl ₂	1.57x10 ⁻⁶	6.19x10 ⁻⁷	2.54	2.66	-4.51

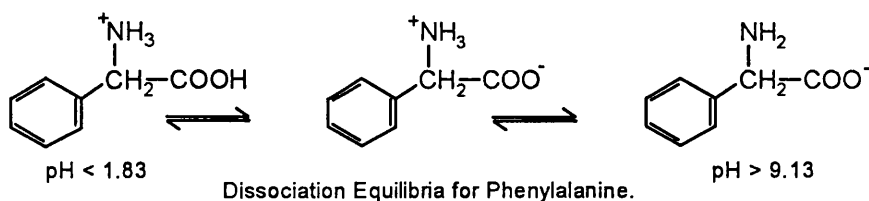
Table 7.15 Experimental Results Obtained from the Donnan Exclusion Tests with NAFION 117 ion-exchange membranes.

⁽³⁾ Calculated using Equation 7.14

7.3.6 Enhanced Transport

Using the same type of ion-exchange membrane, NAFION 117, some experiments were performed to investigate the possibility of observing 'facilitated' or enhanced transport behaviour. The test permeant material chosen for these experiments was the amino acid phenylalanine(Phe). This material was chosen due to some ongoing collaborative research with the University of Rouen investigating the activity of α -alanine transport across hollow fibre ion-exchange membranes. In these current experiments the detection was by the spectrophotometric method described earlier (Sections 6.2.2.3 & 6.3.3).

Phenylalanine being an amino acid has two discrete functional groups, one carboxylate and one amine group. The roles played by these groups are determined mainly by the pH of the supporting solvent system and the effect this has on the protonation/deprotonation of these functional groups. This is the thermodynamic process of dissociation for the ionisable groups within the phenylalanine structure (pK_{a1} & pK_{a2}) shown below. For phenylalanine these have values of $pK_{a1} = 1.83$ and $pK_{a2} = 9.13$ and $pI = 5.48$ [16]. From this equilibrium, it was clear that the solvent pH would determine the effective charge on the molecule and this we might expect to significantly effect the transport rate through the charged membrane matrix.



Membranes were prepared in the hydrogen and sodium forms by cycling the membrane sections in 1M HCl and NaOH for four hours at a time (3 to 4 cycles) and finally in one of these solutions to obtain the desired H⁺ or Na⁺ form. The membrane sections were then washed free of any excess material and stored in distilled water.

Measurements of the swelling effects caused in the membrane by changes in the ionic form were monitored. In comparison to the dry mass and dimensions the hydrogen form was found to have swollen by 15.1%. In the case of the sodium form this figure was 10.3% and for the ammonium form this was 7.3%. The ion-exchange capacity was found to be 0.91 milli-equivalents per gram (by neutralisation titration of the hydroxide loaded material.)

The experiments, both single timelags and multiple oscillators, were performed using distilled water / 0.05M Phenylalanine as the concentration step against distilled water initially in the collecting volume.

The experimental data obtained from the timelag experiments are shown in Figures 7.24 and 7.25 for 0.05M and 0.01M phenylalanine respectively. The relative slopes (permeabilities)

of the H^+ : Na^+ ionic forms for 0.05M and 0.01M Phenylalanine were 3.53 and 8.16 respectively, Table 7.16.

Oscillator experiments were also carried out, these allowed the possibility of several estimations under identical experimental conditions. The resulting data for the H^+ and Na^+ forms with 0.05M Phe versus distilled water are shown in Figure 7.26 with the extracted data shown in Tables 7.17 and 7.18. Based only on the final concentration values observed at the end of these oscillator experiments the ratio for the H^+ : Na^+ flow was 3.97 (c.f 3.53 for single timelag). As observed with both type of experiment the difference in the permeabilities between the ionic forms was a factor of approximately four, far in excess of the 5% difference in thickness between the two ionic states of the membrane matrix. The obtained oscillator data shows that the ratio of the permeabilities to be 4.25. Clearly the ease and benefit of the oscillator system is shown by the data in Tables 7.17 & 7.18. From these experiments the permeabilities were found to be $1.44 \times 10^{-6} \pm 5.7 \times 10^{-8}$ for the H^+ form and $3.38 \times 10^{-7} \pm 2.39 \times 10^{-8}$ for the Na^+ form and all data was obtained by just two experiments.

One possible explanation for this enhanced permeability in the hydrogen form was due to the internal hydrogen ion concentration. The concentration of H^+ ion was determined at 0.91 milliequivalents per gram, this equated to an H^+

concentration of approximately 1.5 Molar internally for the given membrane sections. This meant the localised pH within the membrane matrix was much lower than was needed to push the dissociation equilibria fully to the $R'-NH_2-COO^-$ form. If in this ionised state the (Phe) molecule entered the matrix of the membrane it would almost certainly be repelled back into the bulk solution. If however some small quantity were to penetrate the matrix it may be repelled by each fixed (negative) charge through the membrane and expelled at the collecting volume face. If such a mechanism were established it would be reasonable to assume that this would act as a driving force in addition to the concentration difference across the membrane and hence result in an 'enhanced' transfer rate of material.

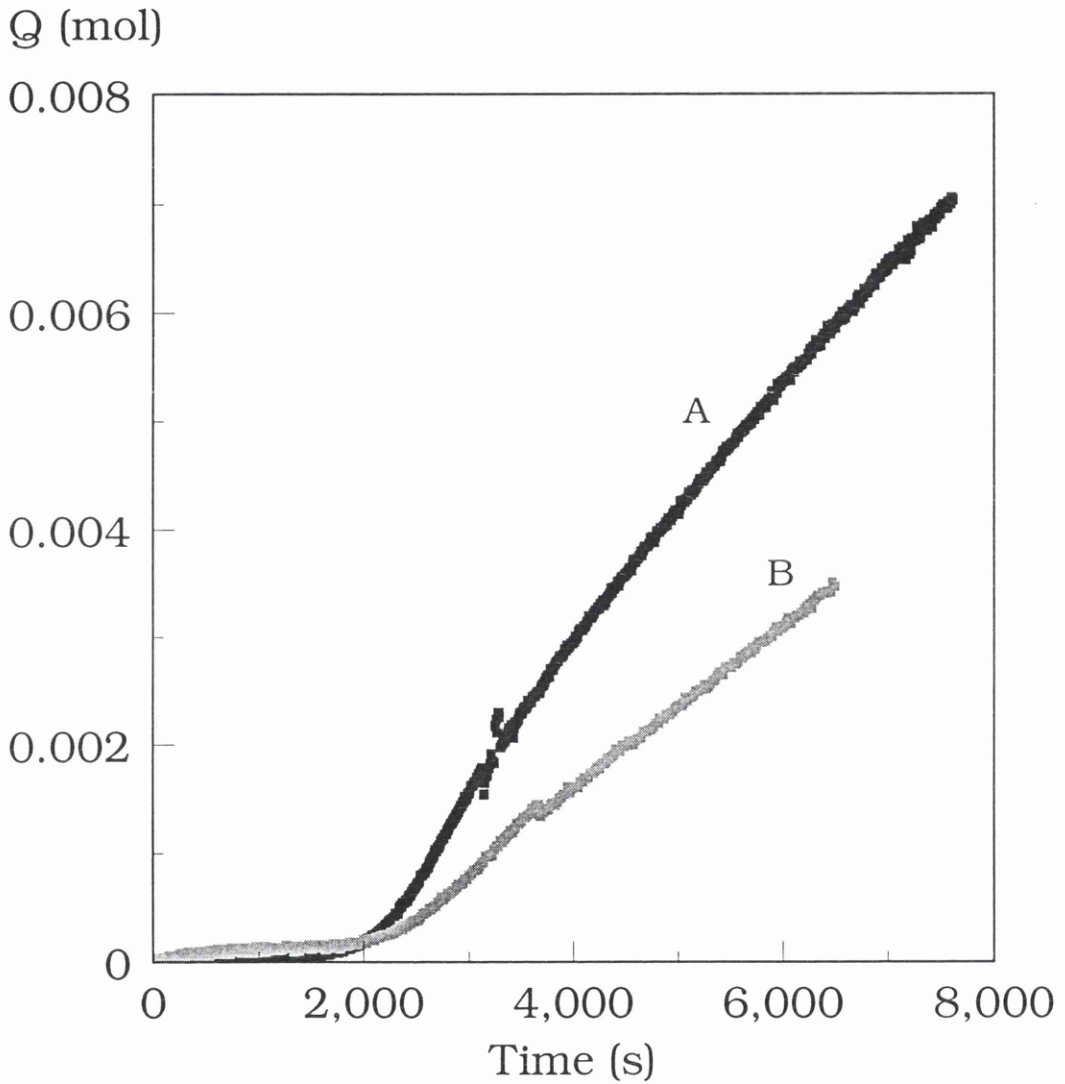


Figure 7.24 Timelag plots for 0.05M (A) and 0.01M (B) Phenylalanine solutions through a NAFION ion exchange membrane in the hydrogen form.

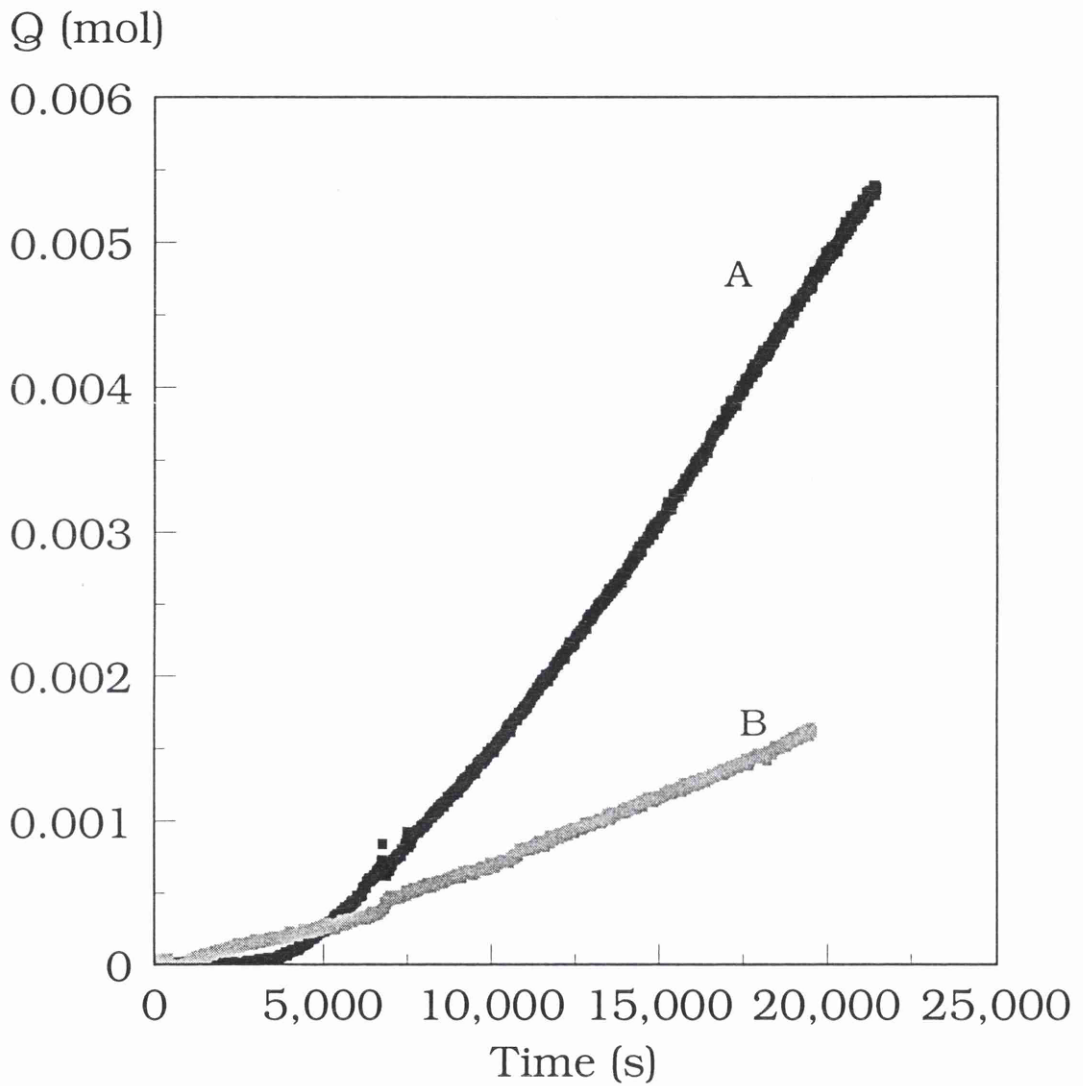


Figure 7.25 Timelag plots for 0.05M (A) and 0.01M (B) Phenylalanine solutions through a NAFION ion exchange membrane in the sodium form.

Phe Conc. (Molar)	Ionic Form		
	H ⁺ Permeability	Na ⁺ Permeability	Permeability Ratio
0.05	1.29x10 ⁻⁶	3.65x10 ⁻⁷	3.53
0.01	7.47x10 ⁻⁷	9.15x10 ⁻⁸	8.16

Table 7.16 Experimental Data from Enhanced Transport tests using NAFION 117 and Phenylalanine.

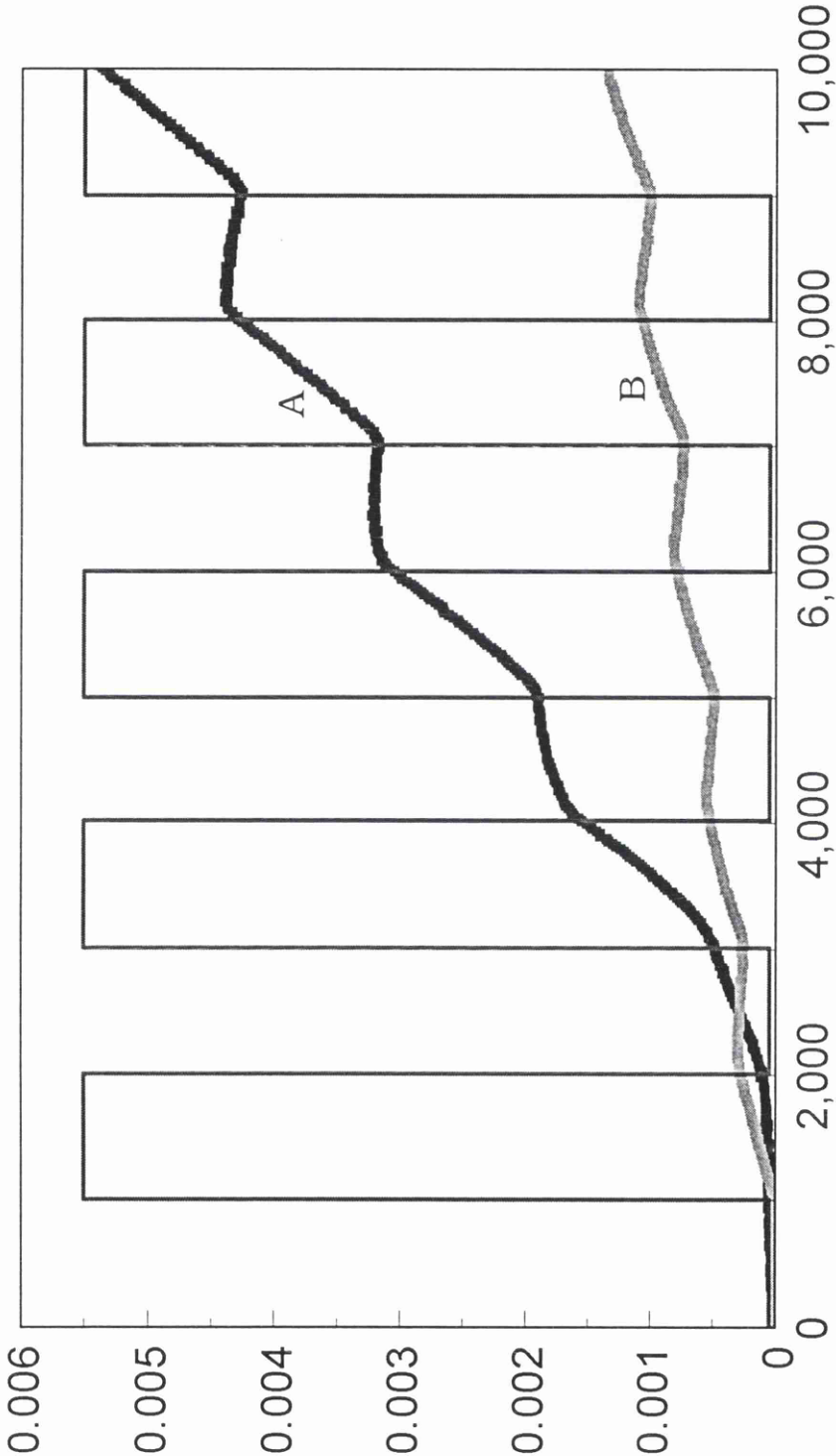


Figure 7.26 Comparison between a NAFION membrane in the hydrogen(A) and sodium(B) forms with Phenylalanine (0.05M) / Distilled water used for the concentration square wave against distilled water initially in the collecting volume. The concentration was measured using the UV/Visible system at 254.9nm.

Slope B ($\times 10^6$)	Slope C ($\times 10^7$)	Slope (B - C) ($\times 10^6$)
1.374	-1.04	1.478
1.257	-1.978	1.456
1.187	-3.168	1.504
1.059	-2.965	1.355
1.116	-3.568	1.473
0.977	-4.673	1.444
0.944	-4.233	1.367
Mean =		1.439 ± 0.06

Table 7.17 Data from an Oscillator Experiment with NAFION in the H^+ Form with 0.05M Phe as the Concentration Step. The square wave period used was 2000 s.

Slope B ($\times 10^7$)	Slope C ($\times 10^8$)	Slope (B - C) ($\times 10^7$)
2.691	-4.47	3.138
2.519	-8.86	3.405
2.645	-6.258	3.27
2.635	-10.7	3.705
Mean =		3.379 ± 0.24

Table 7.18 Data from an Oscillator Experiment with NAFION in the Na^+ Form with 0.05M Phe as the Concentration Step. The square wave period used was 2000 s.

7.3.7 Coupled Flows

Earlier (Section 3.4.1) a possible method for the investigation of mixed or coupled systems was mentioned. Here, one example of the possible use of such a system is shown. Using the U.V/Visible spectrometry as the detection method a simple two component system was investigated.

The system chosen was a phenylalanine/ sodium citrate mixture. These two compounds are commonly found together in soft drinks and other foodstuffs, phenylalanine being the major constituent of the artificial sweetener Nutrasweet™ and the citrate being used in flavouring. The U.V-Visible spectra of these materials are shown in Figure 7.27. the peak maxima being sufficiently well separated to make the determination relatively simple.

The membrane system used for the test was NAFION 117, in the hydrogen form. From the other studies using this membrane, it was expected that the timebase of the experiments would minimise errors in the collected data.

The rates of the two components were determined in isolation and then together to ascertain if any coupling (positive or negative) was detectable. In order to maintain comparable concentration driving forces the individual component systems were tested using 0.025M solutions. The test mixture had a 50:50 mix ratio with each component having a concentration

of 0.025M in the final mix volume.

The individual permeation results for the phenylalanine and sodium citrate are shown in Figures 7.28 and 7.29 respectively with the combined (mixture) data being shown in Figure 7.30.

By examination of these experimental runs it was clear that an effect was observable. The phenylalanine permeation appeared effectively unaltered by the presence of citrate. The reverse was not true however as the citrate permeation rate was substantially reduced (by a factor close to 10) by the presence of the phenylalanine.

Due to time restraints no further investigation of this or other coupled/mixed systems were investigated. It does clearly show that the measurement system developed in this current work has both the power and flexibility to look at a great variety of different membrane systems and mechanisms.

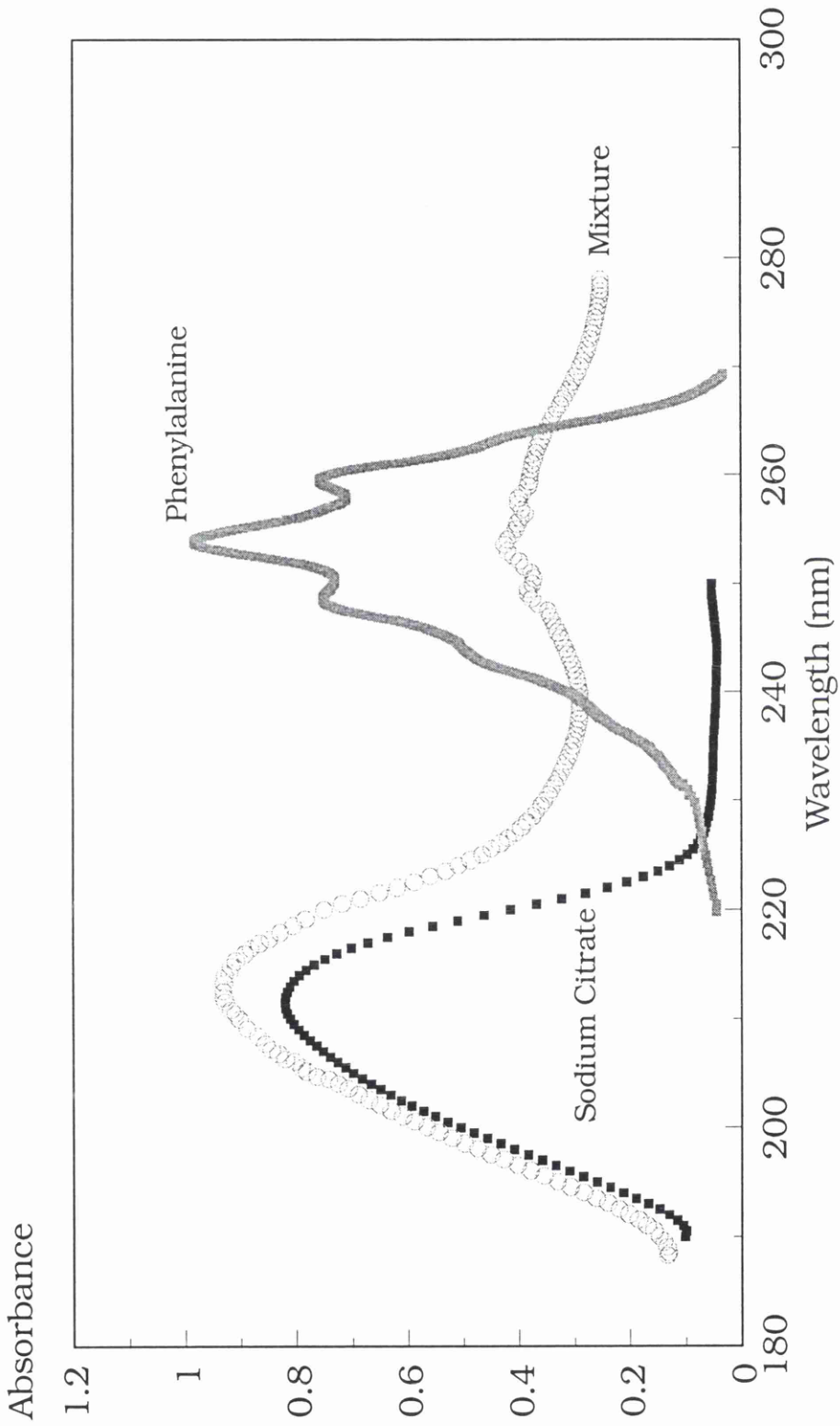


Figure 7.27 The U.V/Visible Spectra for Phenylalanine and Sodium Citrate Solutions

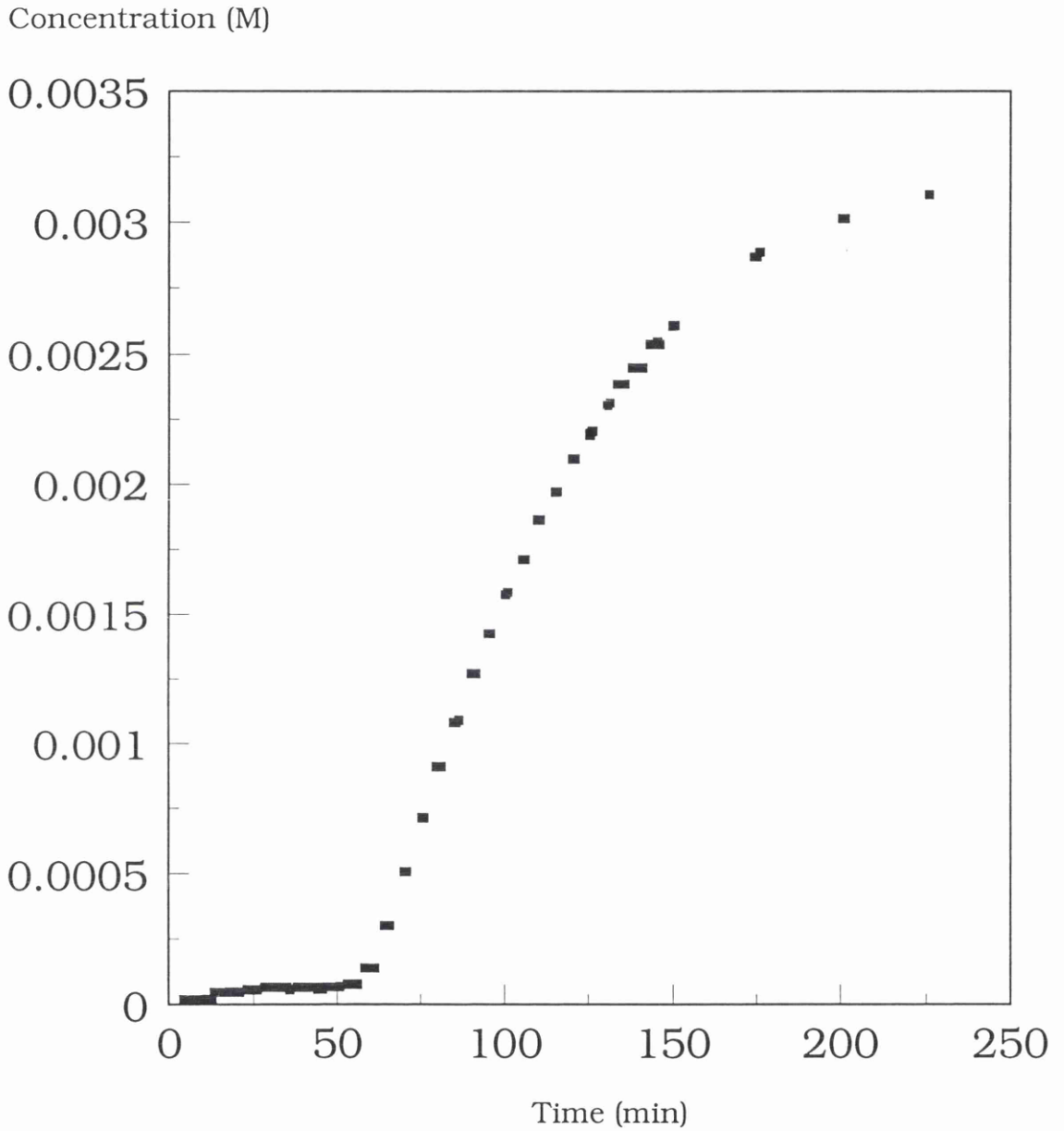


Figure 7.28 Permeation Data for a Phenylalanine Solution through a NAFION membrane in the Hydrogen form. The detection method was UV/Visible Spectrometry @ 254.9nm.

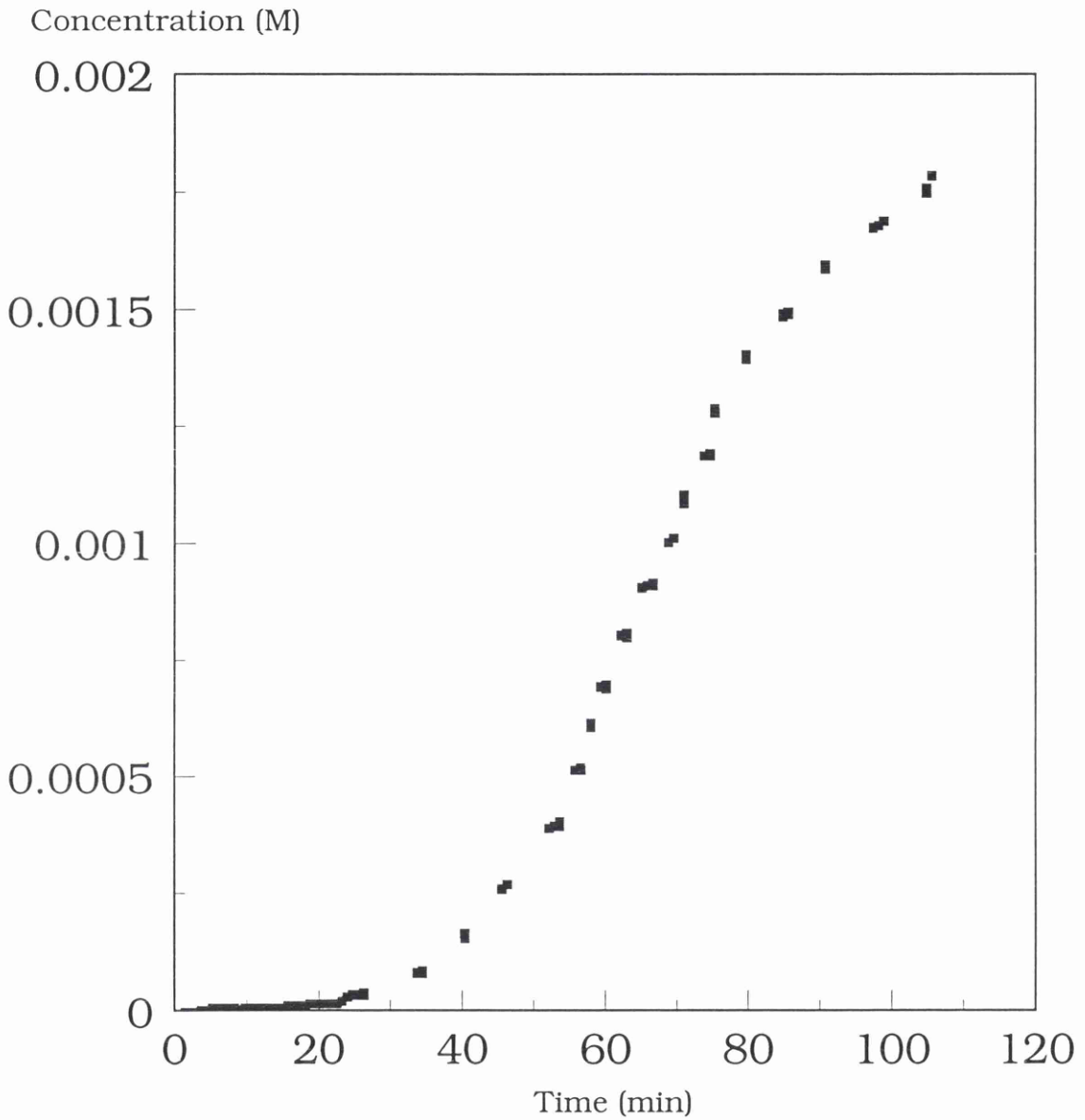


Figure 7.29 Permeation Data for a tri-Sodium Citrate Solution through a NAFION membrane in the Hydrogen form. The detection method was UV/Visible Spectrometry @ 214nm.

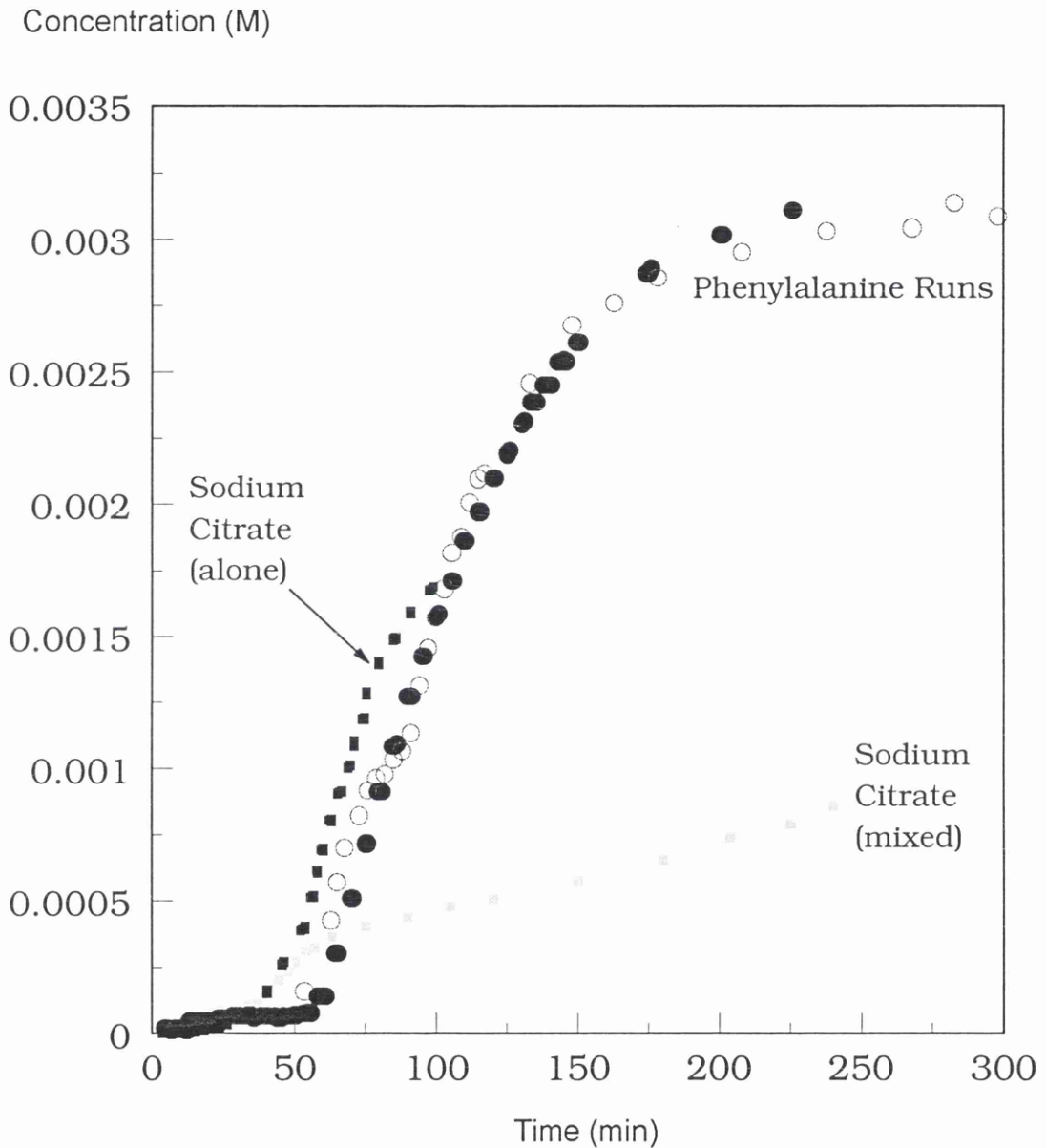


Figure 7.30 Permeation Data for a Phenylalanine /tri-Sodium Citrate mixture through a NAFION membrane in the Hydrogen form. The detection method was UV/Visible Spectrometry scanning 190-280nm.

7.4 Conclusions and Future Research

The original aim of this work was to attempt to design and construct a system that would allow for the routine measurement of transport parameters involved in membrane processes and separations. It was also originally envisaged that only liquid based systems would be investigated.

It very quickly became apparent that the level of automation / data collection required was considerable, but not prohibitive. With the rapid growth in power and availability of (inexpensive) desktop computer systems the original objective was made a much more realistic proposition.

The systems that have been described in this work (gas and liquid based) have shown themselves to be excellent in respect to both their ease of operation and the quality of the data generated.

The work described herein is effectively the justification of the quality and relative ease with which these systems can produce reliable and reproducible information, for now the really exciting science still awaits.

For what is believed to be the first time, investigation of the properties of the active layers in multilayer (ceramic) membranes has become possible in situ. Additionally, the classical membrane transport analysis is available but with the added benefits from the automated data collection and processing routines.

The extent of future research is huge for such systems, some possible

examples are given here.

(a) investigation of effects due to surface charge/pH . This could have important repercussions with regard to anti-fouling membrane systems, optimising transmembrane fluxes and other process parameters.

(b) measurement of the effects induced by surface modification such as chemical grafting (permanent or otherwise) of 'functional' groups onto existing membrane substrates. Some preliminary work in this area has already been performed but has not been included here [17,18].

(c) possible testing method for medical/pharmaceutical purposes such as the transport rates across medical prosthetic devices and time delivery systems. Some preliminary studies have also been made in this area with respect to hydrogel membranes for time release systems.

With the ever widening use and scope of membrane processes in both industry and at research level the usefulness of such systems would appear invaluable, be it for quality control purposes or in leading edge investigation. Funds for the possible commercial exploitation of the ideas and designs discussed in this work were made available by the Department of Trade and Industry (SMART Award) for the development of a commercial prototype. To this date however, due to various factors, no further progress on the production of a commercially available system has been made.

7.5 References

- [1] Doran, P., Ph.D Thesis, University of Glasgow, 1985
- [2] Daynes H. A., The Process of Diffusion Through a Rubber Membrane, Proc. Roy. Soc. Series A, 97, 286, (1920)
- [3] Crank J., The Mathematics of Diffusion, Clarendon Press, Oxford, England, 1959, p49-52.
- [4] Helfferich F., Ion Exchange, McGraw-Hill Series in Advanced Chemistry, 1962, Section 5.2 p100-125.
- [5] Itaya, K., Sugawara, S., Arai, K. and Saito, S., Properties of Porous Anodic Aluminium Oxide Films as Membranes, Journal of Chemical Engineering of Japan, Vol. 17, Nos. 5, 1984, 514-520
- [6] Paterson R., Interpretation of Timelag Experiments for Multilayer Membranes, Proceedings of ICOM '93, Hiedelberg, Germany.
- [7] Stokes R. H., Integral Diffusion Coefficients of Potassium Chloride Solutions for Calibration of Diaphragm Cells., J. Amer. Chem. Soc., 73, (1951), 3527
- [8] Barrier R. M., Barrie J. A. and Rodgers M, G., Permeation Through a Membrane With Mixed Boundary Conditions, Trans. Faraday Soc.,58, 1962, 2437
- [9] Hayashita T., Lee J.C., Bartsch R. A., Transport of alkali metals cations through monoazacrown ether modified Nafion™ 117 membrane, J.Mem. Sci., 116 (1996) 243-251.
- [10] Gebel G., Aldebert P. and Pineri M., Structure and Related Properties of Solution-Cast Perfluorosulphonated Ionomer Films,

Macromolecules, 1987, 20, 1425-1428.

- [11] Donnan F. G., Theory of Membrane Equilibria and Membrane Potentials in the Presence of Non-Dialysing Electrolytes, Z. Electrochem., 17, 572 (1911)
- [12] Paterson R. and Doran P., A Spray Technique for the Determination of Membrane Diffusion and Distribution Coefficients by the timelag Method, J. Mem. Sci., 26, (1986), 289-301.
- [13] Debye P. and Huckel E., Phys. Z., A Theory for Electrolytes (1923), 185
- [14] Davies C. W., The Extent of Dissociation of Salts in Water: Part VIII: An Equation for the Mean Ionic Activity Coefficient of an Electrolyte in Water., J. Chem. Soc. (1938), 2093
- [15] Helfferich F., Ion Exchange, McGraw-Hill Series in Advanced Chemistry, 1962, p355
- [16] Handbook of Chemistry and Physics, CRC Press Inc., USA, 75th Edition, 1994.
- [17] Ohya, H., Paterson, R., Nomura, T., McFadzean, S., Suzuki, T. and Kogure, M., Properties of New Inorganic Membranes Prepared by Metal Alkoxide Methods: Part I: A New Permselective Cation Exchange Membrane Based on Si/Ta Oxides. J. Mem. Sci., 105, 1995, 103-112
- [18] Ohya, H., Paterson, R., Nomura, T., McFadzean, S., Suzuki, T. and Kogure, M., Properties of New Inorganic Membranes Prepared

by Metal Alkoxide Methods: Part II: New Inorganic-Organic Anion Exchange Membranes Prepared by the Modified Metal Alkoxide Methods with Silane Coupling Agents., J. Mem. Sci., 126, 1995, 161-169

Annex 1

Preparation of Anodic Alumina Membranes

- 1.1 Introduction
- 1.2 Anodisation System
- 1.3 Preparation of Anodic Alumina Films
- 1.4 Electrochemical Treatments
- 1.5 References

1 Preparation of Anodic Alumina Membranes

1.1 Introduction

It has long been observed that when aluminium oxidizes, on its surface the resulting structure of the oxide is rather unique in having cylindrical pores normal to the film surface [1]. With this present implementation, the anodising voltage used controls the pore size and pore density, whereas the thickness is determined by the total amount of charge transferred. The ability to design porous films of pre-determined morphology makes the anodic alumina films potentially well-suited for use as porous membranes. Researchers have turned this unique phenomenon into a method for the synthesis of controlled membrane morphology [2-9].

A major problem with this technique, however, is that the porous anodic alumina film layer adheres extremely strongly to the aluminium substrate (anode) with the pore base closed by an oxide barrier layer which is also very difficult to remove. In order to create 'through' pores it is necessary to detach the film from its aluminium substrate and to remove the barrier layer [6].

Normally, anodic alumina films are released from the aluminium substrate by chemical attack, either by dissolution of the residual aluminium or by dissolution of the barrier layer film of alumina [2,3, 5,6,8,9]. Both methods, and in particular the second, can lead to significant enlargement of the pores due to partial dissolution of the pore walls.

Furneaux *et al* [5,6,9] described a method to separate the anodic alumina film and perforate the barrier layer by progressively reducing the anodising voltage to a very low value in order to reduce the barrier layer thickness and subsequently by chemical attack of the aluminium to detach the anodic alumina film. The membranes produced by this method had an asymmetric morphology with larger pores interconnected with smaller pores at the interface originally adjacent to the aluminium. Membranes produced by such methods are however, limited to a lower pore size limit (>15 nm) due to chemical dissolution. Paterson *et al* [10] and Mardilovich *et al* [11, 12] have developed methods in which a very large voltage pulse is applied for a very short time to the aluminium anode at the end of the anodisation, this removed the barrier layer and separated the membrane instantly. By this method the barrier film of anodic alumina was completely removed and all pores were opened.

The great advantage of this new method is that it is electrical and so fully quantifiable and does not involve (dissolving) chemicals which need to be applied carefully and removed quickly to prevent damage or even total dissolution of the membrane.

1.2 Anodisation System

An automated anodisation system has been developed (earlier). This system enabled the production of anodic alumina films to be fully controlled. It was designed to apply precise voltages for precise times and to record and monitor current/voltage curves as a function of time

during the anodisation. Using this system it was possible to obtain extremely reproducible membranes. A schematic representation of the system is shown in Figure A1.1. The system was controlled by an IBM PC computer and a Buchler programmable power supply (1000 VDC and 400 mA)

The anodisation cell (Figure A1.2) consisted of a metallic container coated with a chemically resistant insulating varnish to isolate the electrolyte solution and to prevent electrical leakage. The volume of electrolyte solution used in the cell was approximately 2 litres. A refrigerant thermostated bath (Grant LTD-20) was filled with distilled water which circulated through the walls of the anodisation bath and was used to control the temperature during the anodisation (usually maintained at 10 °C).

A circulation pump of PTFE was designed and constructed to stir the electrolyte solution. The temperature difference between the distilled water in the refrigerated circulator bath and the electrolyte solution was never more than 0.1°C. Two electrode holders also constructed from PTFE were used to support a platinum mesh cathode (10x10 cm) and an aluminium anode. Typically an aluminium electrode was (5 x 5 cm with approximately 8 cm² of exposed area). The distance between the platinum mesh cathode and the aluminium sample was typically 2.5 cm.

1.3 Preparation of Anodic Films

Anodic alumina membranes were prepared by anodisation of

aluminium foil, purity 99.999% and 70 μm thick supplied by Johnson Matthey, Materials Technology, UK. The aluminium foil was first degreased in a Soxhlet apparatus using boiling 1,1,1-tri-chloro-ethane for 30 minutes, then cleaned ultrasonically three times with fresh propanol-2-ol and finally washed in distilled water. To prepare membranes with precisely defined geometries the aluminium was coated with a photoresist (OFPR-800 positive resist, viscosity 20.0 ± 15 cps, acquired from Dynachem Corporation, UK) and was then exposed with UV light using a mask of the desired geometry.

To assist the adhesion of the photoresist on the aluminium surface a very thin layer of anodic alumina was created using an applied voltage of 40 V for 2 min. The electrolyte used was oxalic acid 3% w/w and the process was performed at room temperature. The alumina coated electrode layer was then washed with distilled water and dried at 140 $^{\circ}\text{C}$ for 30 minutes.

A few drops of photoresist solution was placed in the centre of the aluminium surface, which was then centrifuged at 1500 rpm for 10 seconds and then dried at 70 $^{\circ}\text{C}$ for 20 minutes. A thin uniform coating of photoresist was obtained by this method.

The exposed sheet was then developed in a solution of tetramethyl ammonium hydroxide (TBAH 1.2%, from Dynachem Corporation, UK) for 2 minutes. It was then washed in distilled water and baked at 80, 100, 120 and 140 $^{\circ}\text{C}$ for 20 minutes at each temperature. After, this drying stage the rear of the aluminium was protected by a latex. At

this stage only the area selected for membrane production was exposed. To re-establish electrical contact and initiate the production of a uniform anodic film layer, the initial thin layer of oxide, created to assist the coating of photoresist, was removed by dissolution using a solution of (20 g CrO_3 , 35 ml H_3PO_4 88% w/w, made up to 1.0 litre with distilled water) at 90 °C for 2 minutes.

Finally, the aluminium was washed in distilled water and mounted on its Teflon holder to be anodised. The anodisation process was performed in oxalic acid solution 3% w/w, at 10 °C under constant voltage conditions (the larger the voltage the larger in pore diameter). Oxalic acid was chosen as an electrolyte because it permits anodisation at lower voltages with sufficient current flow. Additionally, the pore and cell diameters are smaller for films formed in oxalic acid than for those formed in phosphoric acid.

1.4 Electrochemical Treatment

Conventionally the film produced by the anodisation of an aluminium sample is removed either by the dissolution of the remaining metal / barrier layer [5] or by reversing the polarity of the electrodes at the final stage of anodisation [13]. In this method developed, the aluminium substrate was removed from the alumina layer by an electrochemical treatment.

For this propose a power supply, capable of producing a voltage pulse up to 150 V and at a current up to 15A was constructed. In this current technique, the anodic film produced together with its

aluminium substrate was dipped in a mixture of perchloric acid (70 ml; 72% w/w) and acetic anhydride (130 ml 98%, d=1.08 g/ml) and a voltage 15 V greater than the final voltage of anodisation was applied for 1-3 seconds. It was found that the alumina film was separated from the aluminium substrate immediately. This process of separation also removed the barrier layer at the same time and is shown in Figure A1.3. The film was then washed in distilled water and allowed to dry at room temperature. Figure A1.4 shows a flow-chart of the preparation process.

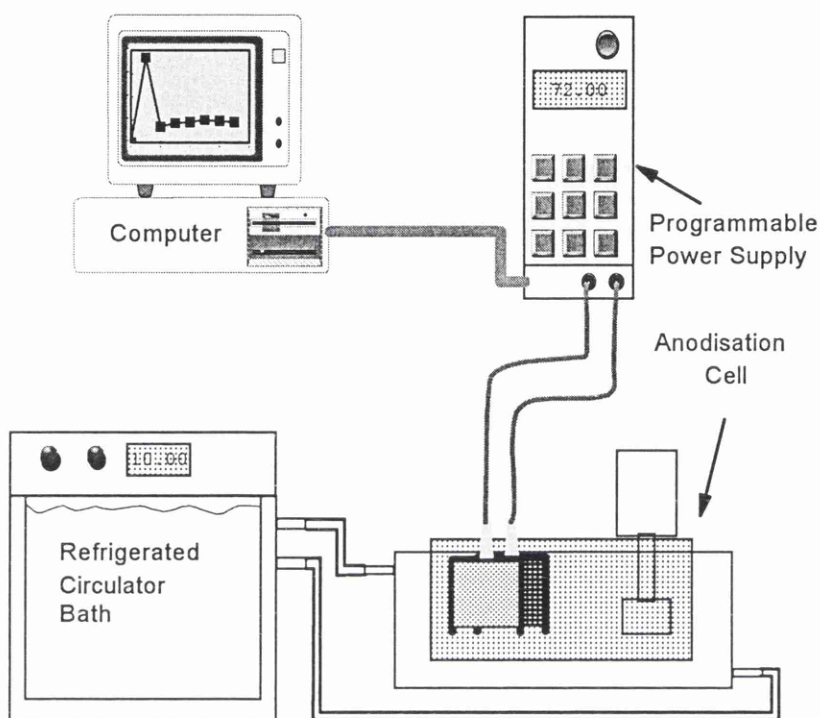
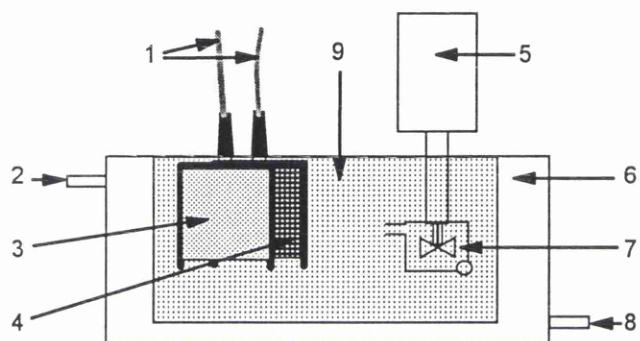


Figure A1.1 Schematic Representation of the Anodisation System



1 Electrode Connections
2 Thermostat Water Outlet
3 Aluminium Anode
4 Platinum Mesh Cathode

5 Stirring Motor
6 Electrolysis Bath
7 Circulating Pump (PTFE)
8 Thermostat Water Inlet (10 C)
9 Electrolyte Solution

Figure A1.2 Schematic Representation of the Anodisation Cell

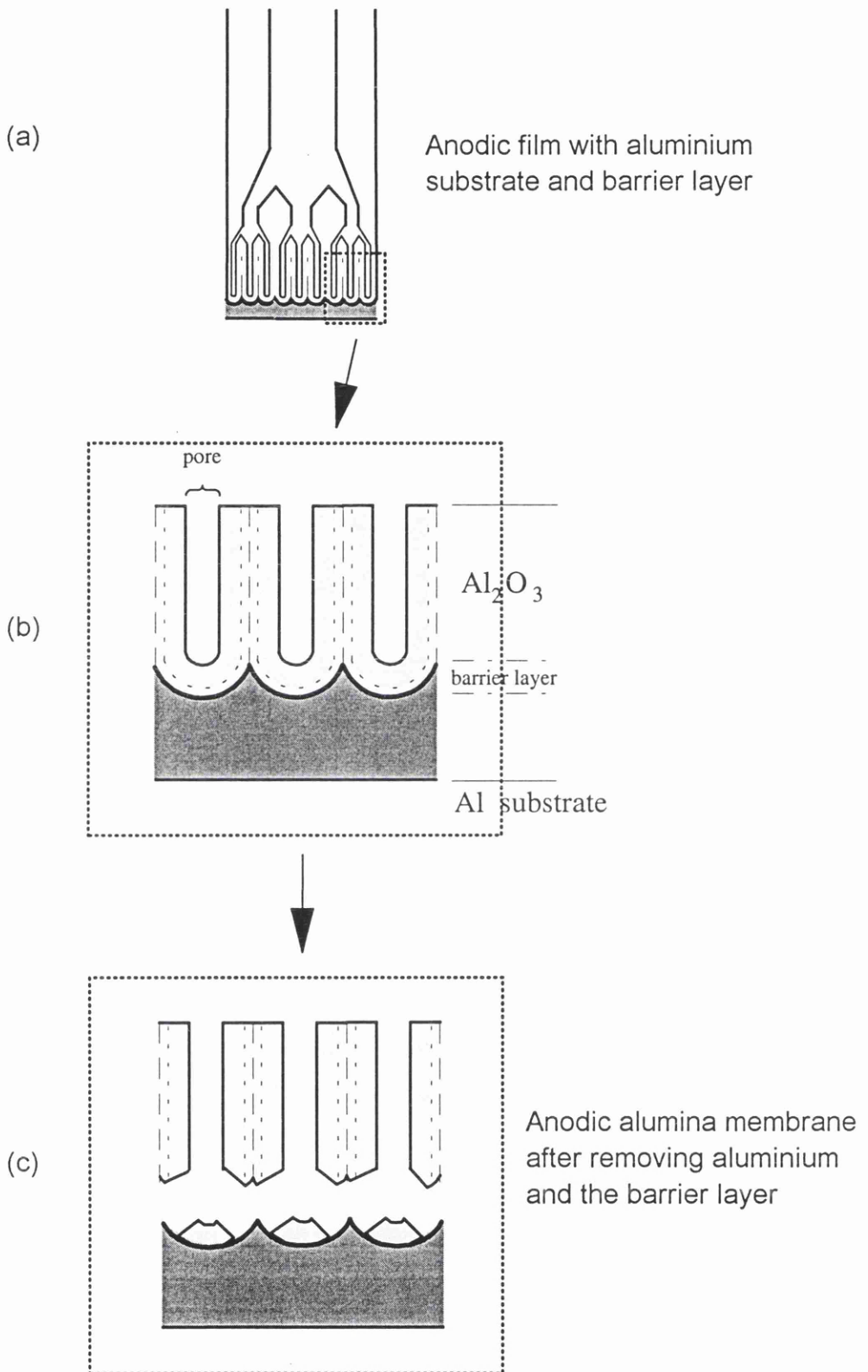


Figure A1.3 Representation of an anodic alumina film with (a) asymmetric pore structure created by reduction of the anodisation voltage, a cross-sectional view (b) anodic film with an impermeable barrier layer and aluminium substrate still in place. (c) the barrier layer and aluminium have been removed and a porous anodic alumina membrane is produced.

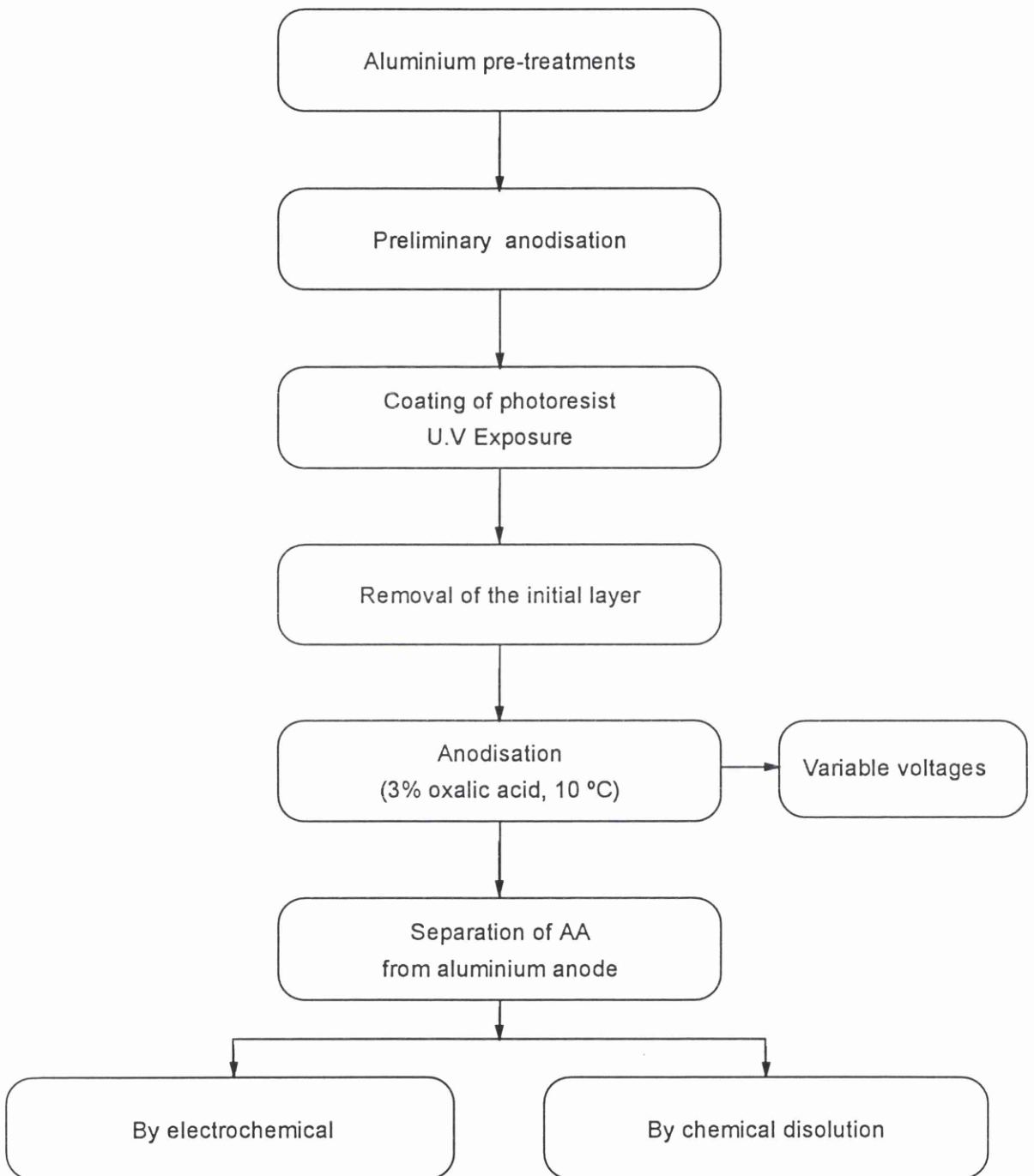


Figure A1.4 Flow-chart for the preparation of anodic alumina films

1.5 References

- [1] Hoar, T. P. and N. F. Mott, Mechanism for the formation of porous anodic oxide films on aluminium, *J. Phys. Chem. Solids*, 9 (1959) 97-99.
- [2] Smith, A. W., Process for producing an anodic aluminum oxide membrane. U.S. Patent 3,850,762 (1974)
- [3] Smith, A. W., Porous anodic aluminum oxide membrane, *J. Electrochem. Soc.*, 120(8)(1973) 1068-69.
- [4] G. E. Thompson, R. C. Furneaux, G. C. Wood, H. A. Richardson and J. S. Goode, Nucleation and growth of porous anodic films on aluminum, *Nature*, 272 (1978) 433-35.
- [5] R. C. Furneaux, W. R. Rigby, and A. P. Davidson, Porous films and method of forming them, EP 0,178,831 A1 (1986); US Pat. 4,687,551 (1987).
- [6] R. C. Furneaux, W. R. Rigby, and A. P. Davidson, The formation of controlled porosity membranes from anodically oxidized aluminum, *Nature*, 337 (1989) 147.
- [7] G. E. Thompson and G. C. Wood, Porous anodic film formation on aluminium, *Nature*, 290 (1981) 230.
- [8] Anotec Separations. Anopore-A new inorganic membrane unique in the world of microfiltration. Brochure, Whatman International Ltd., Maidstone, UK.
- [9] R. C. Furneaux, R. W. Philpott and D. M. Jenkins, Controlled pore-size membranes produced by anodizing aluminium,

Proceedings of the First International Conference on Inorganic Membranes, Montpellier, 1989, 47-53.

- [10] R. Paterson, P. P. Mardilovich, A. N. Govyadinov, N. I. Mazurenko, Permeable anodic alumina film, UK Patent WO 9534371, Dec, 1995.
- [11] P. P. Mardilovich, A. N. Govyadinov, N. I. Mukhurov, A. M. Rzhetskii, and R. Paterson, New and modified anodic alumina membranes. Part. I. Thermotreatment of anodic alumina membranes, J. Mem. Sci., 98 (1995) 131.
- [12] P. P. Mardilovich, A. N. Govyadinov, N. I. Mazurenko, and R. Paterson, New and modified anodic alumina membranes. Part. II. Comparison of solubility of amorphous (normal) and polycrystalline anodic alumina membranes, J. Mem. Sci., 98 (1995) 143.
- [13] K. K. Wada, K. N. Baba, S. Ono, T. Yoshino, Porous aluminum oxide film and method of forming of the same, US Pat. 5,061,544 (1991).

